



The University of
Nottingham

UNITED KINGDOM • CHINA • MALAYSIA

Supercapacitors with Neutral Aqueous Electrolytes

By

Jung Hoon Chae, MSc, BEng

Thesis submitted to the University of Nottingham for the
degree of Doctor of Philosophy

Department of Chemical and Environmental Engineering
The University of Nottingham

July 2014

ABSTRACT

Fossil fuels, which are the main energy sources of the current world, are running low and alternative ways of generating and storing different types of energies are becoming daunting missions. Renewable energy is very attractive because the source of the energy is often free and also environmentally friendly. The key issue to utilise the renewable energies in sustainable manner is how effectively store the energies and provide them on demand. Therefore, the significance of the energy storage devices has been widely recognised in recent time.

Electrochemical capacitors (ECs), which are also commonly known as supercapacitors, are a type of the energy storage devices and the ECs are widely used as a back-up power boosting device to the batteries. Due to EC's low energy characteristics (typically, lower than 5 Wh/kg), their applications are limited. Therefore, main aim of this study is to enhance the energy characteristics of the ECs.

In particular, aqueous ECs were examined due to a number of advantages offered by the water-based system. It was found that neutral aqueous electrolytes can expand the operating voltage close to 2 V (aqueous ECs commonly operate within 1 V) with advanced designs and hence result in remarkably higher energy. Moreover, the optimum condition of the neutral aqueous electrolytes was investigated by examining the effect of ion size, concentration and temperature. One of the main disadvantages of using the aqueous electrolytes in low temperatures was successfully resolved by using concentrated electrolytes (freezing point depressed up to $-20\text{ }^{\circ}\text{C}$). MnO_2 with carbon materials were also used to construct asymmetrical ECs.

The highest specific energy (Wh/kg) of the neutral aqueous ECs was achieved at 20 Wh/kg using unequal electrode design. This result is very much comparable to the Pb-acid battery. Based on the obtained data, larger scale (thicker and bigger electrode films) of the prototype ECs were constructed and their results correspond well with the results obtained from the smaller ECs.

The data of the neutral aqueous ECs, which is contained in this thesis, suggest that the water-based ECs have a remarkable market potential.

AFFIRMATION

The work presented in this thesis is original and solely the work of the author and it has not been published or submitted elsewhere except for the following publications.

Chae, J. H., Ng, K. C. and Chen, G. Z., *Nanostructured materials for the construction of asymmetrical supercapacitors*. Proceedings of the Institution of Mechanical Engineers, Part A: Journal of Power and Energy, 2010. **224**(4): p. 479-503.

Chae, J. H., Zhou, X. and Chen, G. Z., *From Electrochemical Capacitors to Supercapatteries*. Green, 2012. **2**(1): p. 41-54.

Chae, J. H., Chen, G. Z., *1.9 V aqueous carbon-carbon supercapacitors with unequal electrode capacitances*, *Electrochimica Acta*, 2012, **86**: p. 248-254

Chae, J. H., Chen, G. Z., *Influences of ions and temperature on performance of carbon nano-particulates in supercapacitors with neutral aqueous electrolytes*, *Journal of Particuology*, 2013, <http://dx.doi.org/10.1016/j.partic.2013.02.008>

ACKNOWLEDGEMENT

Foremost, I would like to express my sincere gratitude to my supervisor Prof. George Zheng Chen for his continuous support, patience, motivation, enthusiasm and immense knowledge during my Ph.D study. I cannot imagine having a better advisor and mentor for my Ph.D study.

Besides my supervisor, I would like to thank my thesis committee: Prof. Robert Slade and Prof. Wim Thielemans for their encouragement, insightful comments and constructive suggestions.

My sincere thanks also go to E.ON not only for their financial support during my research, but also their constructive and positive feedbacks on regular basis. I am particularly grateful to Dr. Stuart Norman for his comments.

I also want to thank previous and current members of the electrochemical technology group in the University of Nottingham for their support: Dr. Chuang Peng, Dr. Daniel Jewell, Dr. Kok Chiang Ng, Dr. Ann Zhang, Dr. Jun Jin, Dr. Han Wang, Dr. Xiaohang Zhou, Dr. Di Hu, Dr. Denys Gromadskyi, Dr. Linpo Yu, Mr. Gwangjun Kim, Mr. Ebenezer Igunnu, Mrs Guan Li, Miss Happiness Ijije, Mr. Anthony Stevenson, Mr. Ossama Al-Juboori, Mrs. Nowar Al-Shara.

Last but not the least, I would like to thank my parents Min-Seok Chae and So-Young Kim, for their unconditional love and spiritual support throughout all times.

TABLE OF CONTENTS

ACKNOWLEDGEMENT	I
ABSTRACT	II
AFFIRMATION	III
TABLE OF CONTENTS	IV
1. INTRODUCTION	1
2. LITERATURE LIVIEW	3
2.1. ENERGY STORAGE MECHANISMS OF ECs	3
2.1.1. ELECTRIC DOUBLE LAYER CAPACITANCE	3
2.1.2. PSEUDO-CAPACITANCE	5
2.1.3. MIXED MECHANISM	7
2.1.4. BAND THEORY	10
2.2. RECENT TECHNICAL DEVELOPMENTS	12
2.2.1. MATERIAL INVESTIGATIONS	13
2.2.2. ADVANCED CELL DESIGNS	24
2.2.3. STRUCTURAL STUDY	35
2.2.4. EFFECT OF ELECTROLYTES	37
2.3. TECHNICAL BARRIERS OF AQUEOUS ECs	40
2.3.1. NARROW OPERATING VOLTAGES	40
2.3.2. SELF-DISCHARGE	41
2.3.3. NARROW OPERATING TEMPERATURE	44
2.3.4. LIMITED CYCLE LIFE	45

2.3.5. CORROSION AND INTERNAL RESISTANCE	46
2.4. CURRENT STATUS OF AQUEOUS ECs	49
References	52
3. METHODOLOGY	79
3.1. THCHNIQUES FOR STRUCTURAL STUDIES	80
3.1.1. SCANNING ELECTRON MICROSCOPY (SEM)	80
3.1.2. ENERGY DISPERSIVE X-RAY SPECTROSCOPY (EDX)	82
3.1.3. TRANSMISSION ELECTRON MICROSCOPY (TEM)	83
3.1.4. X-RAY DIFFRACTION (XRD)	86
3.2. TECHNIQUES FOR ELECTROCHEMICAL ANALYSIS	88
3.2.1. CYCLIC VOLTAMMETRY (CV)	88
3.2.2. GALVANOSTATIC CHARGE-DISCHARGE	91
3.2.3. AC IMPEDANCE SPECTROSCOPY	93
References	95
4. NEUTRAL AQUEOUS ELECTROLYTES	98
4.1. STUDY OF AQUEOUS ELECTROLYTES	99
4.1.1. ACIDIC, NEUTRAL AND BASIC AQUEOUS ELECTROLYTES	99
4.1.2. EFFECT OF IONIC SIZE, CONCENTRATION AND TEMPERATURE.....	102

References	126
5. NEUTRAL AQUEOUS CARBON ECs	135
5.1. SPECIFIC CAPACITANCE OF CARBON MATERIALS	136
5.1.1. EXAMINATION OF DIFFERENT CARBON MATERIALS	136
5.2. CABOT MONARCH 1300 PIGMENT BLACK (CMPB)	140
5.2.1. ELECTROCHEMICAL ANALYSIS OF CMPB	140
5.2.2. ADVANCED DESIGN FOR HIGHER OPERATING VOLTAGE	146
5.3. ACTIVATED CARBON #1 (AC #1)	156
5.3.1. ELECTROCHEMICAL ANALYSIS OF AC #1	157
5.3.2. EFFECT OF POTENTIAL GRADIENTS ON CYCLIC STABILITY	164
5.4. ENERGY CAPACITY OF NEUTRAL AQUEOUS ECs	170
References	172
6. MnO₂-CARBON ASYMMETRICAL ECs	181
6.1. ACID TREATED CNTS	182
6.1.1. BRIEF DESCRIPTION OF ACID TREATMENT	182
6.1.2. DISCUSSION OF PRE-TREATED CNTs	184
6.2. MnO ₂ /CNTs COMPOSITE	187
6.2.1. MATERIAL SYNTHESIS	187
6.2.2. X-ray diffraction (XRD)	188

6.2.3. EM ANALYSIS (SEM, TEM)	190
6.2.3.1. SEM DATA	190
6.2.3.2. TEM DATA	193
6.2.4. ELECTROCHEMICAL PROPERTY OF MnO ₂ /CNTs	195
6.2.4.1. ELECTROCHEMICAL ANALYSIS OF MnO ₂ /CNTs	196
6.2.4.2. ELECTROCHEMICAL ANALYSIS OF MnO ₂ /CNTs + ELECTRONIC CONDUCTOR	199
6.2.5. CONSTRUCTION OF ASYMMETRICAL ECs	202
6.2.5.1. MnO ₂ /CNTs + CNT MIXTURE AS A POSITIVE ELECTRODE	203
6.2.5.2. RATE PERFORMANCE OF THE ASYMMETRICAL EC	205
6.2.5.3. DETERMINATION OF THE OPERATING VOLTAGE	206
6.2.5.4. LONG-TERM CYCLIC STABILITY OF THE ASYMMETRICAL EC	211
6.2.5.5. EVALUATION OF THE ASYMMETRICAL EC	213
References	214
7. BIPOLAR STACK	220
7.1. EFFECTIVE DESIGN OF BIPOLAR STACK	221

7.2. SYMMETRICAL STACK (EQUAL CAPACITANCE)	223
7.3. ASYMMETRICAL STACK (UNEQUAL CAPACITANCE)	225
7.4. BIPOLAR STACK (PSEUDO-CAPACITANCE)	227
7.4.1. CONDUCTING CARBON PLATES	228
7.4.2. SCALE UP SYNTHESIS OF ELECTRODE MATERIALS	233
7.4.3. CONSTRUCTION OF THE 10 CELL-STACK	235
7.4.4. ELECTROCHEMICAL PERFORMANCE OF THE STACK	239
7.5. EVALUATION	244
References	245
8. CONCLUSIONS AND FUTURE WORK	248
8.1. CONCLUSIONS	248
8.1.1. NEUTRAL AQUEOUS ELECTROLYTES	248
8.1.2. SIZE EFFECT OF IONS	249
8.1.3. EFFECT OF ION CONCENTRATION AND TEMPERATURE	250
8.1.4. FREEZING POINT DEPRESSION	250
8.1.5. ADVANCED DESIGN OF CARBON-CARBON ECs	251

8.1.6. MnO ₂ /CNTs COMPOSITE AND ITS MIXTURE	252
8.1.7. CONSTRUCTION OF ASYMMETRICAL ECs	252
8.1.8. SCALE-UP	253
8.2. FUTURE WORK	254
8.2.1. FULL UTILISATION OF POTENTIAL WINDOWS	254
8.2.2. NOTICEABLE INCREASE IN CHARGE-TRANSFER RESISTANCE	255
8.2.3. ELECTRODE MATERIALS AND COMPOSITES ...	255
8.2.4. VARIOUS METHODS OF ELECTRODE FILM FABRICATIONS	256
8.2.5. BINDER EFFECT	257
8.2.6. SELF-DISCHARGE TEST	257
8.2.7. CONSTRUCTION OF STACKED ASYMMETRICAL ECs	258
8.2.8. FURTHER SCALE UP (30 cm X 20 cm)	258

CHAPTER 1 INTRODUCTION

The enormous technical developments and rapid changes in life patterns made in the recent decades have largely been attributed to the exploitation of contemporary forms of energy sources, i.e. fossil fuels. However, their finite availability and significantly high environmental impacts have aroused concerns and spurred research to find alternative energy sources, i.e. solar and wind energy. However, it is crucial to find more efficient ways to store these types of energy effectively because they are often intermittent in nature. Accordingly, significant roles of energy storage devices have been recognised.

Recent developments of batteries and fuel cells as energy storage devices have been proven to be very promising, but their poor power characteristics and cycling stability hinder their wider applications. Conversely, conventional capacitors display great output pulsed power, but disappointing energy characteristics. Electrochemical capacitors (ECs), which are also known as supercapacitors, bridge the crucial performance disparity between fuel cells or batteries with high energy capacities and the traditional capacitor's power capability. Although, the latest ECs shows significantly improved energy characteristics, the devices are still used as a complementary to batteries in most applications due to the mentioned drawbacks of the capacitors. Therefore, further improvements in energy characteristics are essential for better market perspective of the ECs.

Most commercial ECs are based on organic electrolytes due to a higher operating voltage compared to the aqueous one. However, one of the main

focuses of this thesis is to develop the aqueous ECs which can perform comparably to the organic ECs. Although aqueous electrolytes offer a number of benefits (detailed explanation can be found in Chapter 4), the narrow operating voltage of the aqueous ECs has been problematic for a further development. However, this thesis suggests that the aqueous ECs have a great potential with a number of advantages relative to the organic ones.

Another main focus of this thesis is to develop ECs which display comparable energy characteristics of some batteries, i.e. Pb-acid battery. To achieve this goal, two different strategies were adopted. Firstly, capacitance of the ECs was improved and this was done by investigating different materials, synthesis methods and optimum conditions of the neutral aqueous electrolytes (Chapter 5 and 6). Secondly, the relatively small operating voltage of the aqueous system was also expanded and this was done by adopting advanced designs (unequal electrode capacitance using same electrode material (Chapter 5), asymmetrical design using different electrode materials (Chapter 6)), using neutral aqueous electrolytes (Chapter 4) and stabilising the ECs with a constant voltage holding process (Chapter 5). Based on the experimental data obtained, three stacked ECs were constructed (Chapter 7). The experimental results will be presented along with the literature review of the latest development in this research area (Chapter 2). Brief summary of the experimental findings will be provided at the last part of the thesis with future works (Chapter 8).

CHAPTER 2 LITERATURE REVIEW

2.1. ENERGY STORAGE MECHANISMS OF ECs

The main topic of this thesis is electrochemical capacitors (ECs). These devices involve various electrode materials showing different charge storage mechanisms, namely electric double layer capacitance, pseudo-capacitance and the supercapattery mechanism, which shows combined characteristics of the former two mechanisms. Therefore, it is important to first understand these types of charge storage mechanisms. More thorough explanations in terms of electrochemical principles and theories can be found in the literature [1-8], but the following four sub-sections provide a brief introduction.

2.1.1 ELECTRIC DOUBLE LAYER CAPACITANCE

Energy storage in the electrical double layer capacitor (EDLC) mainly relies on charge separation at the interface between the electrolyte and an inert electrode such as that made from activated carbon. The charging and discharging processes in an EDLC ideally involves no electron transfer across the electric double layer at the electrode/electrolyte interface, and are said to be non-Faradaic in nature. The storage is largely electrostatic without any chemical changes inside the solid phase of the electrode and, due to this reason, EDLCs have a remarkably long cycle life [1].

Figure 2.1 illustrates the displaced ions in the electrolyte in the interconnected pores of the electrode and the balancing charges (for example an excess of electrons or holes) on the wall surfaces of the pores that are present inside, and formed between the packed high surface area particles (e.g. activated carbon). The capacitance is dependent primarily on the ion-accessible surface area (the active area in the pores where the double layer is formed) that is a function of the pore geometry, sizes and distribution in the materials utilised as the electrodes. For a given area, the true capacitance of the electrode/electrolyte double layer is determined by the electrode material and the nature of the electrolyte, but is typically in the range of 10-40 $\mu\text{F}/\text{cm}^2$ [1]. Thus, it can be estimated that for a material with a specific surface area of 100 m^2/g , the specific capacitance is 10-40 F/g if the whole surface area is fully utilised. It is worth noting that many activated carbons can possess very high specific areas e.g. 1000-2000 m^2/g , but exhibit specific capacitances of less than 100 F/g [7]. The cause of the relatively small capacitances is largely because many of the micropores are inaccessible to the ions. Another general concern is that when the pore volume and hence the specific area increase in a material, the electrical conductivity and mechanical strength of the material will inevitably decrease, both of which would contribute to inferior performance in ECs.

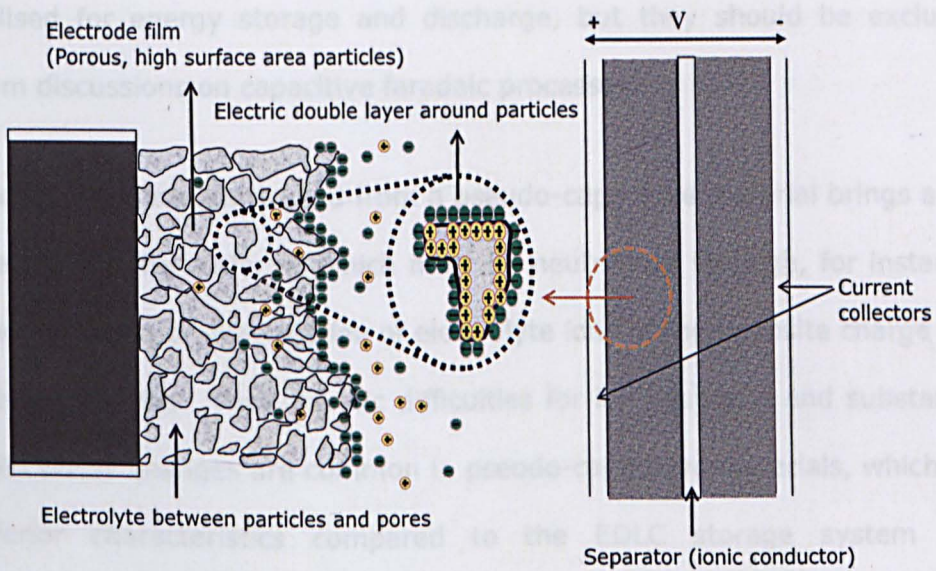


Figure 2.1 Schematic representation of an electrical double layer capacitor (EDLC) with packed conductive and inert high surface area particles as the electrodes; Ionic conductor, through which ions can travel, should allow ion exchange, but has to be an electronic insulator

2.1.2. PSEUDO-CAPACITANCE

The mechanism for charge storage in pseudo-capacitive materials differs from the case of the electric double layer. It involves electron transfer reactions i.e. reduction or oxidation (redox reaction) that occur within the electrode materials. Such changes are also referred to as faradaic reactions (or processes). It is necessary to point out that not all faradaic processes can contribute to pseudo-capacitive characteristics in terms of the relationship between current and voltage (for a cell) or potential (for an electrode). For example, the electron transfer reactions in a fuel cell or an electroplating bath are also faradaic in nature, but the respective current-voltage relations in these electrochemical devices differ significantly from those in capacitors. Such non-capacitive faradaic processes may also be

utilised for energy storage and discharge, but they should be excluded from discussions on capacitive faradaic processes.

The electron transfer to and from a pseudo-capacitive material brings a net charge into the material, which must be neutralised through, for instance, the ingress or intercalation of electrolyte ions of the opposite charge into the solid phase. Thus, kinetic difficulties for ion transport and substantial solid phase changes are common in pseudo-capacitive materials, which are inferior characteristics compared to the EDLC storage system [1]. Nonetheless, later in this chapter it will be illustrated that these drawbacks can be overcome by using advanced nanocomposites.

The maximum capacitance achievable using pseudo-capacitive materials has been observed to be remarkably higher than capacitors using solely the electric double layer, sometimes up to about 100 times larger [6, 7]. This is also related to the fact that pseudo-capacitive materials are often nanostructured with a large surface area, which can contribute to the capacitance in terms of providing a great surface area for the electric double layer and the utilisation of the redox active material. Figure 2.2 illustrates the charging-discharging mechanisms in terms of ion intercalation and depletion which take place within the active pseudo-capacitive materials. When the specific material on the positive electrode is being charged, it loses electrons and positive charges are left in the electrode materials. Consequently, an electric field exists, causing either or both of the inward movement of the anions and outward movement of the cations in the electrolyte contained in the pores of the active material to attain electro-neutrality in the electrode. The opposite process occurs when the electrode is being discharged [4]. Accordingly, for pseudo-capacitive materials, because ion intercalation starts at the interface between the

material (often particulates) and the electrolyte, the morphology of the material is as important as in the case of the electric double layer.

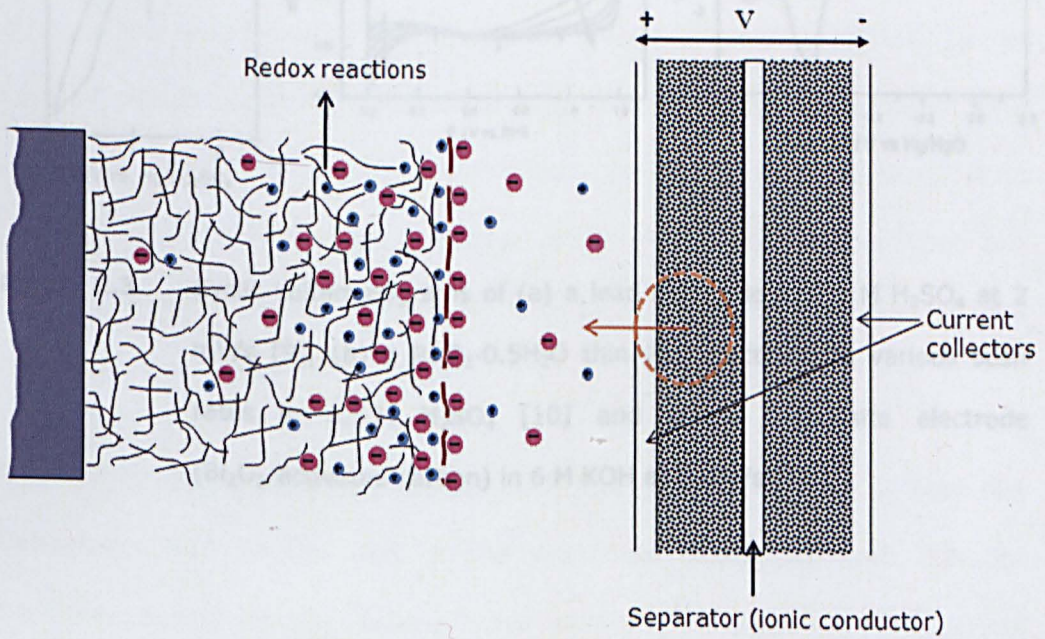


Figure 2.2 Schematic illustration of the charge storage process in a pseudo-capacitive material, highlighting the intercalation of ions (anions in this case) into the material to neutralise the positive charges in the material resulting from oxidation (removal of electrons).

2.1.3. MIXED MECHANISM

In this part, a mixed behaviour of electric double layer and pseudo-capacitance is introduced in comparison with the aforementioned two mechanisms.

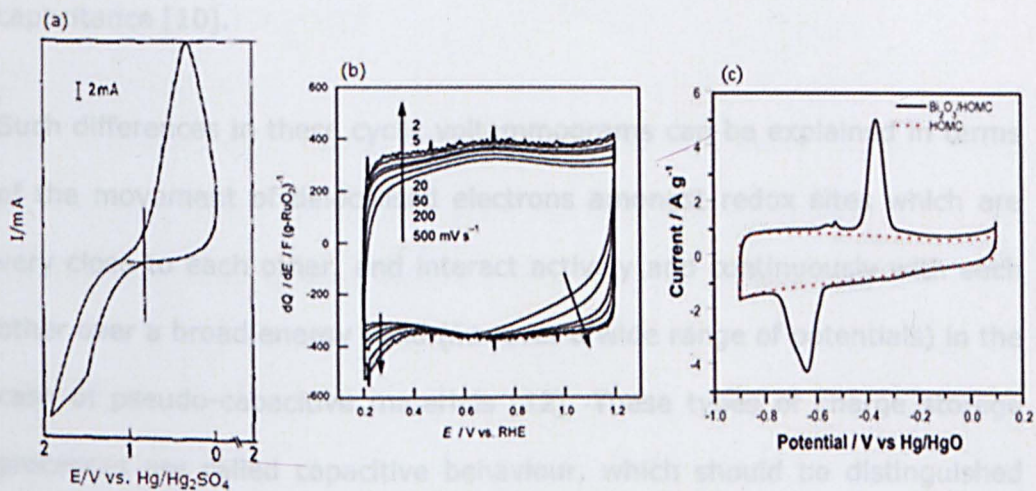


Figure 2.3 Cyclic voltammograms of (a) a lead electrode in 0.1 M H₂SO₄ at 2 mV/s [9], (b) a RuO₂·0.5H₂O thin film electrode at various scan rates in 0.5 M H₂SO₄ [10] and (c) a composite electrode (Bi₂O₃/activated carbon) in 6 M KOH at 5 mV/s [11].

Figure 2.3 (a) shows the localised electron transfer in the redox processes of a lead electrode in the H₂SO₄ electrolyte. Due to the significantly similar energy states between the localised redox active sites, the transfer of electrons to or from these sites occurs at potentials very close to each other, which leads to the narrow peak-shaped CV [9]. This type of potential-current plot is the same as that observed in tests of electrode materials for batteries.

Figure 2.3 (b) shows CVs obtained from a RuO₂ electrode material in 0.5 M H₂SO₄. The continuous transfer of electrons over the relatively wider potential range is due to the formation of a broad range or band of energy states in this pseudo-capacitive material. This results in the constant current observed over the given potential window and hence the rectangular CV shape, similar to that obtained from double-layer

capacitance [10].

Such differences in these cyclic voltammograms can be explained in terms of the movement of delocalised electrons amongst redox sites which are very close to each other, and interact actively and continuously with each other over a broad energy band (*i.e.* over a wide range of potentials) in the case of pseudo-capacitive materials [12]. These types of charge storage processes are called capacitive behaviour, which should be distinguished from battery-like behaviour. However, mixed forms of the two types are also observed in many cases, leading to the growing interest in the composite materials.

The CV in Figure 2.3 (c) shows both the capacitive and battery-like behaviours due to the use of the materials displaying both pseudo-capacitance and electric double layer capacitance together. The carbon material contributes to form the rectangular CV over a wide range of potentials and the current peaks can be attributed to localised electron transfer from/to Bi_2O_3 . Recently, this type of charge storage mechanism has been referred as capattery (capacitor + battery) behaviour [13]. There has been an urgent demand for the development of new energy storage devices with the capacity (specific energy, Wh/kg, or energy density, Wh/L) and power capability matching those of batteries and conventional ECs, respectively. In response to this demand which goes beyond the original purpose of ECs, a new concept of supercapattery (supercapacitor + battery) has come to light, taking advantage of the charge storage mechanisms of both batteries and ECs to gain improved performance. The construction and configuration of a supercapattery may follow a number of routes, but the key factor is that the device does not need to behave like a capacitor, although it is capable of that [13].

2.1.4. BAND THEORY

The Faradaic charge-storage mechanism is perhaps best described using band theory. Figure 2.4 illustrates the distribution of energy states in three different materials, namely metals, semiconductors and insulators.

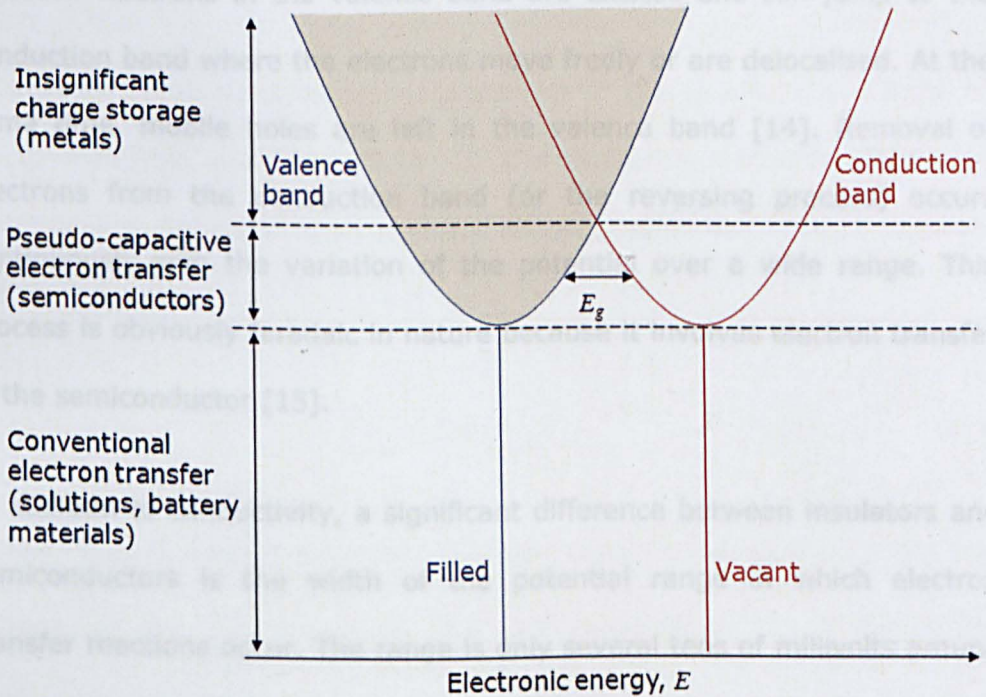


Figure 2.4 Illustration of the band theory with regards to different materials; namely metals, semiconductors and insulators [14]

The metal shows completely overlapped electron energy states which enable free electron mobility in response to an electrical field. Consequently, charge storage cannot occur in any fixed energy state (or geometric location) and no capacitance can be achieved. Conversely, insulators have a large energy gap between the filled valence and vacant conduction bands, which corresponds to a fixed amount of energy required

for electron transfer [14]. However, some insulating materials may have molecules or ions which can be oxidised at relatively low potentials, e.g. iron in ferrocene or lead in PbSO_4 [9].

For semiconductors, the energy gap, E_g , between the valence and conduction bands is not very large. Thus, when the applied potential is in the appropriate range (often wider than several hundreds of millivolts), the localised electrons in the valence band are excited and can jump to the conduction band where the electrons move freely or are delocalised. At the same time, mobile holes are left in the valence band [14]. Removal of electrons from the conduction band (or the reversing process) occurs continuously with the variation of the potential over a wide range. This process is obviously faradaic in nature because it involves electron transfer in the semiconductor [15].

In addition to conductivity, a significant difference between insulators and semiconductors is the width of the potential range in which electron transfer reactions occur. The range is only several tens of millivolts around the redox potential for insulators but is at least several hundreds millivolts for semiconductors. More importantly, when the potential is increased linearly with time, electron transfer proceeds in the same manner, leading to a constant current. This kind of charge accumulation is responsible for the rectangular cyclic voltammograms observed for many transition metal oxides and conducting polymers [14, 16]. Because the potential-independent current is the same as that from a capacitor in response to a linear voltage variation, it is termed pseudo-capacitive current to highlight the faradaic and capacitive nature.

2.2. RECENT TECHNICAL DEVELOPMENTS

One of the intrinsic properties of ECs is their ability to provide superior pulsed power, whereas the energy density characteristics of the devices are generally poor. Accordingly, the main focus in this research area has shifted to boost their energy characteristics, which are still significantly inferior to those of batteries, and this corresponds well with the aim of this thesis. There are two direct ways to achieve this goal. As the energy capacity of the ECs increases proportionally to the specific capacitance of active materials and the square of the operating voltages shown as equation 2.1, the main focus of many recent studies has been to enhance both values.

$$E_{total} = \frac{1}{2} \times C_{cell} \times U_{max}^2 \quad (2.1)$$

where, E_{total} is energy capacity, C_{cell} cell capacitance, and U_{max} the cell voltage of the EC. However, the cell capacitance (C_{cell}) should be distinguished from the material capacitance (C_M). When normalised against the mass of active materials, most of the specific capacitance values (F/g) reported in the literature regarding material investigations refer to material capacitances (C_M). For a symmetrical EC, the relationship between C_{cell} and C_M is

$$C_{cell} = \frac{1}{4} \times C_M \quad (2.2)$$

The C_M value of ECs is given by

$$C_M = C_{dl} + C_{\Phi} \quad (2.3)$$

Where, C_{dl} is contribution from the electrical double-layer capacitance and C_{Φ} from the pseudo-capacitance. For most pseudo-capacitive materials, $C_{\Phi} \gg C_{dl}$.

In the following sections, the latest technical developments of ECs are reviewed in relation to materials (increase in material capacitance) and cell design improvements (increase of operating voltage of ECs) to enhance the energy capacity. Most of capacitance values dealt with in material investigations (Chapter 2.2.1) are material capacitances (C_M), whilst the capacitance values used for the calculation of the energy capacity of ECs in Chapter 2.2.2 are cell capacitance (C_{cell}). These two terms should be distinguished according to Equation 2.2. It is important to carefully define the capacitance value, otherwise, these two terms can often cause confusion when calculating the energy capacity of ECs, and there would be a misleading energy value that is often four times higher [17].

2.2.1. MATERIAL INVESTIGATIONS

Different electrode materials for ECs possess distinctive properties and important factors to consider when selecting electrode materials are their specific capacitance (F/g) and geometric capacitance (F/cm²), which directly indicate the amount of charge stored either on the surface (electric double layer capacitance) or within the bulk of the material (pseudo-capacitance). Material investigation is particularly important because the capacitance values vary depending on the materials used. Therefore, it is

crucial to find advanced materials with high specific capacitance to achieve higher specific energy. Materials of high specific surface areas, such as those used in EDLCs, store charges at the solid/electrolyte interfaces which are two-dimensional in nature. The semiconductor-type pseudo-capacitive materials can undergo reversible redox reactions not only at the surface but also in the bulk of the material with accompanying adsorption and intercalation of ions, including protons, from the electrolyte. Such a charge storage mechanism is three-dimensional and hence much higher in capacity measured at the same mass or volume.

- Non-composite materials

Table 2.1 shows the reported specific capacitance values and potential windows of various capacitive materials. The charge storage in the carbon materials mentioned in Table 2.1 takes advantage of mainly the electric double layer capacitance which is non-faradaic in nature (see the previous section). The benefits of using carbon materials are their superior cycling (charge-discharge) stabilities, due to their chemical and electrochemical stabilities and remarkably fast responses owing to their largely electrostatic charging mechanism. For these reasons, carbon materials are widely used in industry. However, their relatively poor capacitance values (only 10 - 20 % of the theoretically predicted capacitance value) due to the presence of inaccessible micropores and hence ineffective electrolyte impregnation within the structure of the active material, prevent these ECs from showing higher energy characteristics [18]. Similarly, carbon nanotubes (CNTs) do not display satisfactory capacitance values (normally less than 20 F/g) unless they are paired with other pseudo-capacitive materials.

Table 2.1. Specific capacitance of different electrode materials

	Electrode material	Electrolyte	Potential windows (E/V)	Specific capacitance (F/g)	
EDLC	Carbon black [15]	KOH	-	95	
	Activated carbon [19]	0.1 M K ₂ SO ₄	-1.1 to 0 V vs. Ag/AgCl	95	
	Activated carbon [20]	0.5 M Na ₂ SO ₄	-1.1 to 0.85 V vs. NHE	135	
	Aerogel carbon [15]	KOH	-	140	
	Carbon cloth [15]	KOH	-	200	
	Nanotextured carbon [20]	1 M H ₂ SO ₄	0 to 0.8 V Vs. NHE	244	
	CNTs [21]	2 M KCl	-0.1 to 0.9 V vs. Ag/AgCl	39	
	Graphene [22]	30 wt% KOH	0 to 1 V -	205	
Pseudo-Capacitance	Metal oxides	MnO ₂ [16]	2 M KCl	-0.1 to 0.9 V vs. Ag/AgCl	214
		MnO ₂ [8]	0.1 M Na ₂ SO ₄	-	1380
		SnO ₂ [23]	1 M H ₂ SO ₄	-0.2 to 0.8 V vs. SCE	96.6
		RuO ₂ [24]	0.5 M H ₂ SO ₄	0 to 1 V -	720
		Fe ₃ O ₄ [25]	0.25 M Na ₂ S ₂ O ₃	-0.9 to -0.1 V vs. SCE	210
		WO ₃ [26]	0.5 M H ₂ SO ₄	-0.6 to 0.2 V vs. Ag/AgCl	290
		Bi ₂ O ₃ [27]	1 M NaOH	-0.8 to 0 V vs. SCE	98
		MoO ₂ [28]	1 M H ₂ SO ₄	-0.3 to 0.4 V Vs. Ag/AgCl	140
		V ₂ O ₅ [29]	2 M KCl	0 to 0.8 V Vs. SCE	350
	Metal Nitrides	VN [30]	6 M KOH	-	1340
		MO ₂ N [31]	0.5 M H ₂ SO ₄	0 to 0.7 V Vs. RHE	-
	Conducting polymers	PANI [32]	3 M KCl	-	240
		PANI [33]	1 M H ₂ SO ₄	0 to 0.7 V vs. SCE	775
		PPY [32]	3 M KCl	-	530
		PPY [34]	1 M KCl	-0.4 to 0.6 V Vs. SCE	480
		PEDOT [32]	3 M KCl	-	92
		PTH [35]	1M LiPF ₆	-1 to 1 V -	134

CNTs: carbon nanotubes, Ppy: polypyrrole, PANI: polyaniline, PEDOT: poly 3 4-ethylenedioxythiophene, PTH: Polythiophene

The semiconductor-type materials in Table 2.1 are capable of exhibiting pseudo-capacitance. As the specific capacitances obtained from pseudo-capacitive materials are much higher than those of carbon materials, they are often chosen to achieve a higher specific energy in ECs. Nonetheless, carbon materials, which are still dominantly used as the negative electrodes, have always been known to be very stable within the negative potential regions towards hydrogen evolution in neutral aqueous electrolytes [36, 37]. Accordingly, more investigations have been carried out to find possible positive electrodes for ECs. However, a few pseudo-capacitive materials such as Fe_2O_3 , WO_3 and Bi_2O_3 show promising results as possible candidates for use as negative electrodes [11, 25, 26]. In particular, the maximum negative potential of Fe_2O_3 is around -0.9 V and this value is quite comparable to that of the carbon materials [25]. Moreover, its higher specific capacitance value, above 200 F/g, would be advantageous in terms of the achievable energy capacity of the EC relative to the carbon negative electrode. Nevertheless, more investigations are certainly required to find ideal negative electrode materials.

Although it is an innate property of materials displaying different degrees of charge storage, the capacitance values can be modified through different techniques. There have been a number of studies to increase the specific capacitance of materials, for instance, by decreasing the particle size, which means shorter intercalation distances in the case of Li-ion batteries [18]. The charge storage effectiveness is also highly relevant to the total surface area of the active material that is accessible by the ions. The addition of some surfactants to active carbons can result in enhanced effective surface area, and an improvement in the specific capacitance of up to 60% was reported [38, 39]. Correspondingly, a 40% decrease in capacitance was reported, with a 50 % reduction of the surface area [40].

More recently, increasing attention has been shifted towards nanostructured pseudo-capacitive materials where the effective surface area can be maximised. A large number of studies in the literature have reported the remarkable effect of nanostructured materials. For example, the nanocrystalline vanadium nitride (VN) has resulted in a specific capacitance of 1,340 F/g at a scan rate of 2 mV/s [30]. Nanometre scale MnO₂ and RuO₂ films were investigated and the specific capacitances of both materials were around 1,300 F/g [8, 41]. It is worthy of noting that one of the highest reported capacitance values (840 F/g) in this research area was obtained using hydrated ruthenium oxide (RuO₂) [42]. The material displays near-ideal capacitive behaviour (rectangular shape and mirror images of CV) with reasonable charge-discharge cycling performance. It was identified that the reason for the extremely high specific capacitance of this metal oxide is its highly reversible redox transitions based on high proton ionic conductivity [1, 43]. However, relatively low electronic conductivity (89 S cm⁻¹) [44] of the hydrated material has been identified as a major intrinsic drawback to achieve high power ECs. More importantly, the cost of the noble metal discourages wide commercial applications. Recently, a new technique for mass production of hydrated RuO₂ nanofibre has been successfully developed by using highly conducting fibre mats (288 S cm⁻¹) and the specific capacitance value reached up to 886.9 F/g [44].

Alternatively, other materials such as manganese oxides (MnO₂) and conducting polymers, which are relatively cheaper, have been widely investigated and many promising results have been reported. Remarkable capacitance improvement in MnO₂ has been attained by the addition of conducting carbons, which were 40 nm in size, in the reactor for the synthesis of α -MnO₂·nH₂O powder [45]. The added nanometre-scale carbon

brought about the positive effect of an expanded active area for faradaic reactions [45]. As a result, the method was suggested as a way to improve the kinetic reversibility and hence increase capacitance. Nevertheless, the resistive nature of metal oxides and the poor mechanical strength of conducting polymers do not encourage these materials to be utilised as electrode materials on their own.

Accordingly, the research focus shifts to combining electrically conductive nanostructures (CNTs, graphene) with pseudo-capacitive materials in order to obtain both good electronic and ionic conductivities. Although the pseudo-capacitive materials exhibit, generally speaking, higher specific capacitance values than those of EDLC materials, their poor cycling stabilities and slow response due to redox reactions and resistance are not advantageous when employing these materials for the electrodes of ECs. When used as positive electrode materials, these pseudo-capacitive materials lose electrons during charging (oxidation), causing the anions in solution to intercalate into the electrode to maintain electro-neutrality. Consequently, partial depletion of the anions starts occurring near the electrode surface and a diffusion process throughout the bulk electrolyte takes place due to the resulting concentration gradients. However, ion intercalation and depletion within the electrode materials and electrolytes can lead to strain variation at microscopic levels, which can accumulate into fatigue degradation of the materials after repeated charge-discharge cycles [18]. This is a particularly significant drawback. Because ion movements into and from the pseudo-capacitive materials are inevitable during charging and discharging, the cycle stability of supercapacitors is often compromised.

- *Composite materials*

Advanced synthesis methods utilising different carbon materials such as activated carbon, CNTs or graphene in producing composite materials have been suggested as a good solution to solve the problems as mentioned above in using EDLC or pseudo-capacitive materials alone [25, 26, 33, 43, 46-48].

Regarding composites with activated carbon, two earlier papers reported that deposition of a thin film of RuO_2 onto the carbon results in a superior material in terms of capacitance while decreasing the degradation level of RuO_2 [49, 50]. However, these papers also reported that as the film thickness increases, the conductivity decreases dramatically. This is likely due to the disadvantages of structural formation using the activated carbon. Also, nano-sized powders tend to agglomerate into larger-size particles during the process, which cancels part of the nanometre-scale benefits. Conversely, CNTs and graphene boost the construction of three dimensional structures and these structures are more beneficial to attain a superior conductivity for both electrons (through carbon structures) and ions (through the liquid electrolyte contained in the carbon structures) than those of the activated carbons.

The thin pseudo-capacitive material coated on the carbon material possesses a large surface area, which means a short time for ion intercalation and depletion. These structural features were indeed recently confirmed to be beneficial in improving the storage capacity in terms of mass, and rate performances of charge-discharge [51]. Furthermore, conducting polymers by nature have very poor mechanical strengths and susceptible to decay after repeated inward and outward movements of ions during charging-discharging cycles. This weakness is, however, almost

absent in conducting polymers that are nanostructured into composites with CNTs which have superior mechanical properties [4, 52, 53]. It has been reported that CNTs can have a tensile strength up to 63 GPa, and a Young's modulus as high as 1 TPa [54]. The excellent elasticity of CNTs has been well demonstrated by buckled tubes under stress being able to return to their original shape after the release of the stress [55]. These are among the unique features which differentiate CNTs from the conventional carbon fibres. The electronic properties of CNTs are also excellent and are even comparable to high quality crystal graphite and in some cases to copper [56-59]. This feature is ideal to compensate the low electronic conductivity of metal oxides [16, 17, 47, 60, 61]. In addition to their exceptional mechanical and electronic properties, CNTs can be packed into unique three dimensional porous structures, which lead to them becoming exceptional materials when combined with other active materials.

The images given in Figure 2.5 describe the process of synthesising CNTs composites with different pseudo-capacitive materials. Their excellent electronic conductivity and high surface areas have naturally boosted the research activities on these materials since the late 1990s [62, 63]. However, as illustrated in Figure 2.5 (a), the contact resistance between the active electrode materials and the current collectors has been pointed out as a possible reason for their occasionally unsatisfactory performance [50, 64].

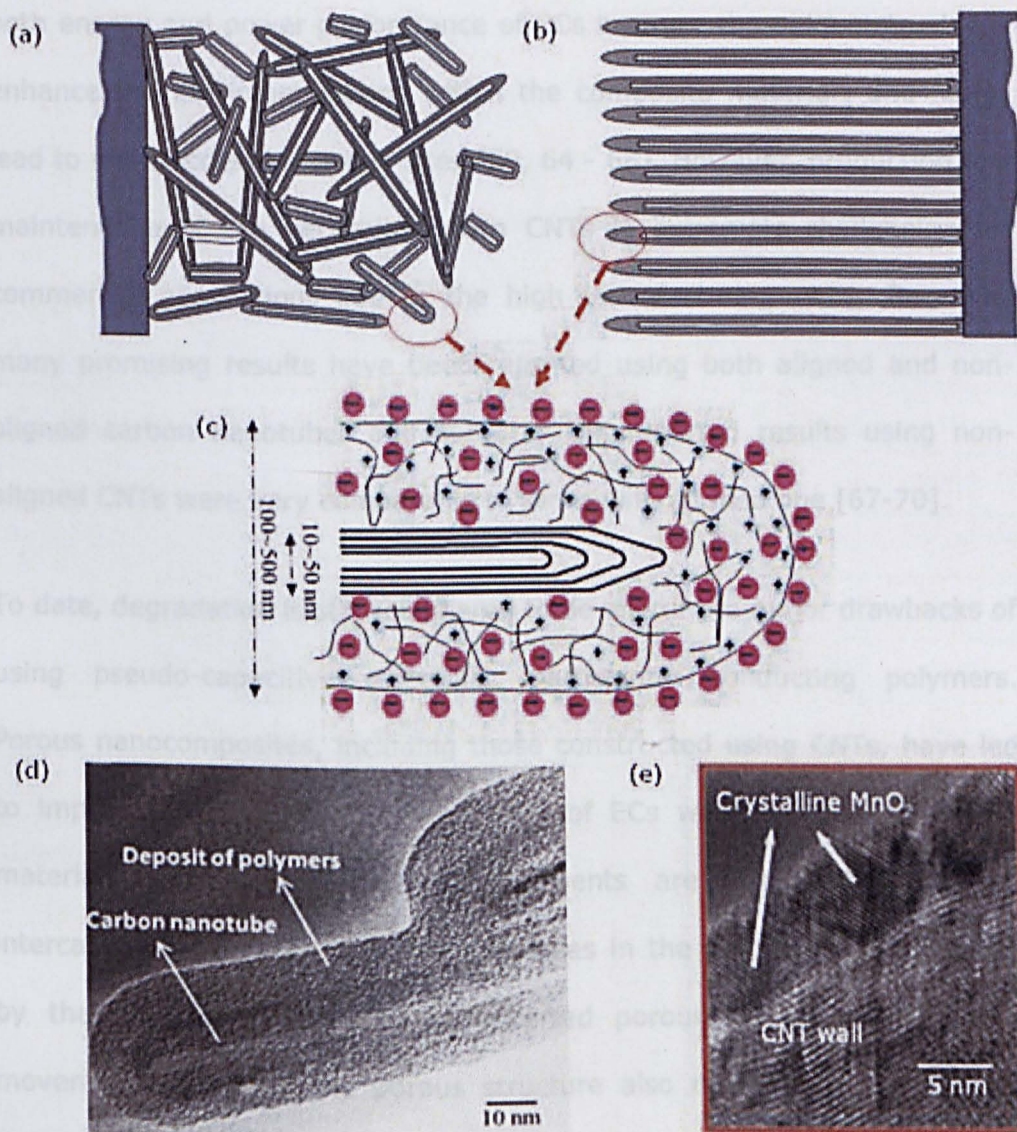


Figure 2.5 Description of utilising carbon nanotubes for synthesising composite materials; (a) Synthesis with non-aligned carbon nanotubes, (b) Synthesis with aligned carbon nanotubes, (c) Magnified image of a carbon nanotube composite, (d) TEM image of conducting polymer/CNTs composite, (e) TEM image of metal oxide/CNTs composite [14]

Accordingly, utilisation of aligned CNTs directly grown on to the metal substrate to minimise the contact resistance, as depicted in Figure 2.5 (b), has been suggested. This method seems to show better results in terms of

both energy and power performance of ECs because the unique structures enhance the ion intercalations within the composite materials and hence lead to more accessible active sites [50, 64 - 66]. However, production and maintenance of the vertically grown CNTs is extremely challenging for commercial applications due to the high manufacturing costs. Recently, many promising results have been reported using both aligned and non-aligned carbon nanotubes and some of the reported results using non-aligned CNTs were very comparable to those with aligned one [67-70].

To date, degradation is still considered to be one of the major drawbacks of using pseudo-capacitive materials, particularly conducting polymers. Porous nanocomposites, including those constructed using CNTs, have led to improvements in the specific power of ECs when used as electrode materials [60, 71-76]. The improvements are largely because ion intercalation and de-intercalation processes in the electrodes are boosted by the presence of the CNTs supported porous structure. The facile movement of ions in the porous structure also means a lower internal stress inside these nanocomposites during repeated charge-discharge cycles. In other words, the kinetic difficulty shown in conventional pseudo-capacitive materials can be resolved to a greater degree in the CNTs nanocomposites [53]. Following this understanding, nanocomposites of CNTs and conducting polymers shown in figure 2.5 (d) have been actively examined. It has been found that the addition of 1 wt.% CNTs increases the mechanical properties of the polymer (polystyrene) by around 40% in terms of elastic stiffness and 25% in terms of the tensile strength [77, 78]. As for the electronic properties of the nanocomposites, it has been reported that the nanocomposite polyaniline (PANI) and CNTs shows significantly lower electronic resistance than that of pure PANI [76] as evidenced by the absence of electrostatic charging on the CNTs/PANI composites under the

scanning electron microscope [79].

Table 2.2. Composite materials for electrode of ECs

	Electrode material	Electrolyte	Potential windows (E/V)	Specific capacitance (F/g)
Composite materials	MnO ₂ /AC [39]	1 M Na ₂ SO ₄	0 to 0.8 V vs. Hg/Hg ₂ SO ₄	115
	CO ₂ SnO ₄ /AC [80]	1 M KCl	-0.2 to 0.8 V -	285.3
	RuO ₂ /carbon black [49]	0.5 M H ₂ SO ₄	0 to 1 V vs. Ag/AgCl	647
	RuO ₂ /carbon aerogel [50]	-	-	200
	RuO ₂ /carbon nanofibre [43]	2 M H ₂ SO ₄	0 to 0.9 V -	840
	CO(OH) ₂ /TiO ₂ [81]	6 M KOH	-	229
	MnO ₂ /CNTs [82]	1 M Na ₂ SO ₄	-0.1 to 0.9 V vs. SCE	944
	RuO ₂ /CNTs [68]	0.1 M Na ₂ SO ₄	0 to 1 V vs. SCE	597
	PANI/CNTs [53]	0.5 M H ₂ SO ₄	-0.2 to 1.2 V vs. SCE	500
	SnO ₂ /graphene [47]	1 M H ₂ SO ₄	0 to 1 V -	43.4
	MnO ₂ /graphene [83]	1 M Na ₂ SO ₄	0 to 1 V vs. SCE	216
	ZnO/graphene [47]	1 M KCl	-0.5 to 0.5 V vs. SCE	11.3
	PANI/graphene [84]	2 M H ₂ SO ₄	-0.2 to 0.8 V vs. Ag/AgCl	480
	PANI/SnO ₂ [23]	1 M H ₂ SO ₄	-0.2 to 0.8 V vs. SCE	305.3
	NiO/MnO ₂ [85]	6 M KOH	-0.8 to 0.8 V vs. SCE	453
PANI/RuO ₂ [86]	-	-	1210	

In addition to CNTs, there have also been a number of investigations on using different nanotube materials to build nanocomposites. For example, utilisation of TiO₂ nanotubes to make nanocomposites has been studied and the results are promising [81, 87]. Nevertheless, the electronic conductivity of inorganic nanotubes is usually significantly lower than that of CNTs although some exceptional claims have been reported [88]. There

could be other benefits resulting from using inorganic nanotubes whose functionalities differ significantly from those of CNTs. On the other hand, further modification of the CNTs themselves may also lead to capacitance gains. It was reported that activated CNTs showed 3 times higher surface area and 1.5 times more pore volume than the normal CNTs [89]. Specific capacitance values from various nanocomposites coupled with different carbon materials are shown in Table 2.2.

One of the latest research interests is graphene, which is one of the most popularly investigated carbon materials both for synthesising composites [22, 46, 83, 84, 90, 91] and on its own in many recent cases [22, 36, 92-94]. Since the first graphene-based supercapacitor was reported in 2006 [92], and for a similar reason to CNTs, graphenes have gained fast growing attention as a potential candidate for advanced ECs due to their very promising characteristics of chemical stability [95], high electrical conductivity [46, 96], relatively large surface area [47, 92] and mechanical strength [97].

2.2.2. ADVANCED CELL DESIGNS

In the previous sections, different electrode materials and various composites were discussed in terms of their reported capacitance values. In addition, the latest research focus in terms of materials and their synthetic methods was also reviewed. Investigations on electrode materials are one of a number of approaches to increase the overall energy capacity of ECs. Although the material investigations are undoubtedly effective and a direct way to enhance the energy characteristics of ECs, continuous effort to optimise the cell performance in terms of the operating voltage is also

crucial. However, relatively fewer investigations on this effective method have been undertaken in comparison to the material studies. In this section, different configurations and designs of ECs are examined, which is another approach for increasing the energy capacity of ECs according to Equation 2.1. Before the latest methods and results from the different works in the literatures are introduced, the fundamentals of cell performance should be explained briefly.

- Cell designs with electrodes of unequal capacitances

A cell capacitance in the case of a single-cell supercapacitor is governed by either the positive or negative electrode displaying a lower capacitance value according to the equation 2.4.

$$\frac{1}{C_{\text{cell}}} = \frac{1}{C_p} + \frac{1}{C_N} \quad (2.4)$$

Where, C_{cell} is the overall cell capacitance, C_p and C_N are the positive and negative electrode capacitances respectively.

The maximum cell capacitance can be obtained by adjusting the ratio of the positive and negative electrode capacitance at 1:1. In symmetrical ECs, which use the same material and capacitance (capacitance ratio is 1:1) on both electrodes, this maximum cell capacitance can be achieved according to the equation 2.4. It should be pointed out that the cell capacitance (C_{cell}) becomes half the positive (C_p) or negative (C_N) electrode capacitances when the two capacitors (positive and negative electrodes) are connected

in series e.g. voltage becomes double. For the asymmetrical ECs, in which different materials are used on the positive and negative electrodes (different specific capacitances (F/g) between the two electrodes), the optimum loading ratio on the positive and negative electrodes can be calculated from the ratio of the specific capacitances of the two electrode materials.

From Equation 2.1 ($E = \frac{1}{2} CV^2$), maximising the cell-specific capacitance value would always help achieve the maximum energy capacity of ECs. However, little was reported on the cell voltage, which is another factor in Equation 2.1, being a function of the electrode capacitance. Recently, some workers suggested that the operating voltage of ECs is adjustable by controlling the electrode capacitances of the positive and negative electrodes [98, 99] and their observations showed that the operating voltage of the ECs may not always be an independent variable, and this can be explained using Equations 2.5 and 2.6.

$$Q = C_p U_p = C_N U_N \Rightarrow U_N = \frac{U_p C_p}{C_N} \quad (2.5)$$

$$U = U_p + U_N = U_p \left(1 + \frac{C_p}{C_N}\right) \quad (2.6)$$

where Q is the amount of charge on each electrode, C_p and C_N are the positive and negative electrode capacitances, U_p and U_N are the working

potential ranges of the positive and negative electrodes respectively and U is the operating cell voltage. According to Equation 2.1, increasing the cell voltage is more advantageous to increase the total energy capacity of ECs, even if the cell specific capacitance may be sacrificed to some degree according to Equation 2.4. Indeed, one of the latest results has successfully enhanced the overall energy capacity of ECs up to 72.6 % using the abovementioned approach [99]. However, this method was only applied to asymmetrical ECs, likely due to their wider adjustable operating voltage compared to the symmetrical ones. However, in Chapter 5 of this thesis, it will be shown that this approach can also be applied to ECs with the same electrode materials, and the results are promising.

- Asymmetrical designs

Traditionally, ECs had a symmetrical structure and were mainly based on carbon materials. Although ECs in aqueous electrolytes offer many advantages over ionic liquids or other organic electrolytes, most of the carbon-based symmetrical ECs are based on the latter electrolytes because symmetrical ECs in aqueous electrolytes usually operate within a voltage range about 1 V [100-102] and this is a fatal disadvantage for the development of aqueous ECs with a higher energy capacity (this is also disadvantageous in terms of power). Recently (before 2011), a few workers in the literature reported the successful expansion of the cell voltage of symmetrical ECs using various materials [19, 20, 103] and the highest reported voltage of a single cell was 1.6 V using a carbon material in neutral aqueous electrolytes. One of the main difficulties involved in increasing the working voltage in the symmetrical designs is

their positive potential limit resulting from the oxidations of either or both of electrode material and electrolyte, although the negative potential limit can be more negative due to the remarkable hydrogen overpotential of carbon materials [104]. In comparison, the asymmetrical design can increase the operating voltage by utilising two different potential ranges from different positive and negative electrode materials. One of the best results is 2.2 V in neutral aqueous electrolytes, but the capacitance retention after a number of cycles was very poor [98]. Accordingly, the maximum operating voltage of the asymmetrical ECs in aqueous electrolytes seems to be restricted to within 2 V voltage range [16, 98]. Many different materials for the negative electrode have been reported such as WO_3 [26], LiMn_2O_4 [105], Fe_3O_4 [25, 106] and SnO_2 [17], but carbon materials seem to be ideal for attaining wider potential windows due to their high hydrogen overpotential in the negative potential region.

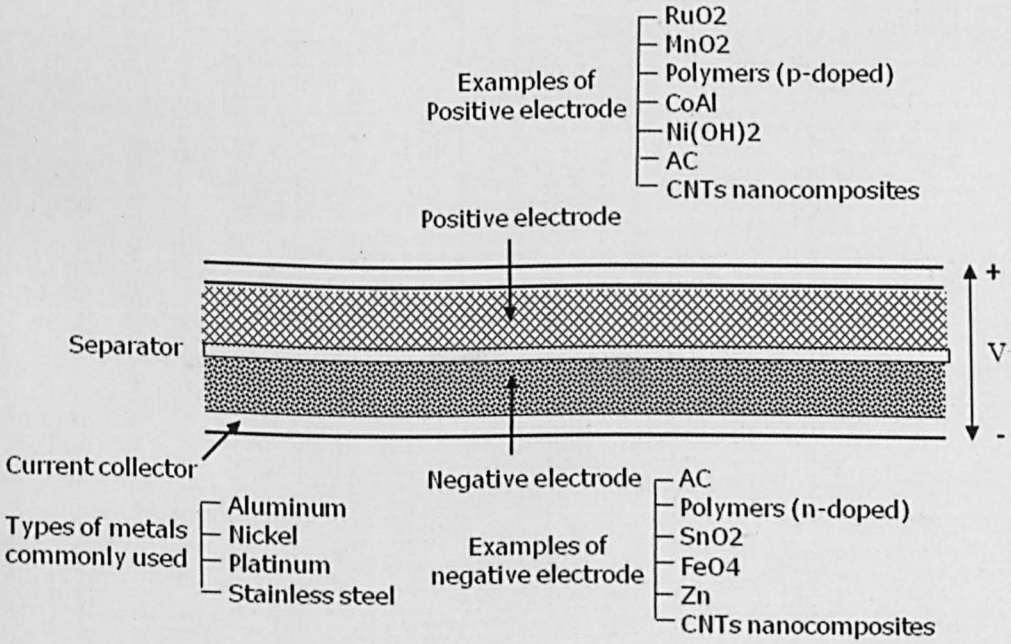


Figure 2.6 Schematic illustration of an asymmetrical supercapacitor

Figure 2.6 illustrates the schematic of the asymmetrical ECs whose positive and negative electrodes may be made from an appropriate pair of the materials listed. In terms of the positive electrode materials, popular materials such as MnO_2 and different conducting polymers display potential windows of around 1 V [45, 56, 61, 82, 101, 102]. Although the asymmetrical design can attain a window of up to 2 V, which is significantly higher than the symmetrical designs, their operating voltages are still lower than those of the commercial ECs using organic solvents. However, the higher specific capacitance and the significant increase in operating voltage shown by the aqueous ECs would result in comparable and even higher energy capacity in many cases, relative to commercial ECs (5 – 8 Wh/kg). In summary, the latest results using different designs and configurations are presented in Table 2.3.

Table 2.3. The characteristics of different supercapacitor devices [18, 19, 53, 98-100, 102, 103, 107, 108]

	Negative electrode materials	Positive electrode materials	Electrolytes	U (V)	Specific Energy (Wh/kg)
Symmetrical ECs	MnO ₂	MnO ₂	0.1 M Na ₂ SO ₄	1	-
	ZnO/carbon	ZnO/carbon	6 M KOH	1	-
	AC	AC	0.5 M Na ₂ SO ₄	1.6	10.0
	Ru _{0.7} Sn _{0.3} O ₂	Ru _{0.7} Sn _{0.3} O ₂	1 M KOH	1.45	21.0
Asymmetrical ECs	Fe ₃ O ₄	MnO ₂	0.1 M K ₂ SO ₄	1.8	21.5
	AC	MnO ₂	0.1 M K ₂ SO ₄	2.2	17.3
	SnO ₂ /CNTs	MnO ₂ /CNTs	3 M KCl	1.7	20.3
	AC	MnO ₂ /CNTs	0.5 M Na ₂ SO ₄	2	13.9
	AC	PANI/CNTs	1 M HCl	1.65	14.3
	AC	Zn	6 M KOH	1.4	-
	AC	RuO ₂ /TiO ₂	1 M KOH	1.4	5.7

As reported in 1999, the first asymmetrical system, which exceeded 10 Wh/kg in specific energy, was a combination of a titanate positive electrode with an activated carbon negative electrode [109]. The research on asymmetrical ECs to date can be classified into three major categories. The first type has pseudo-capacitive metal oxide or conducting polymer as the positive electrode and a double layer carbon material as the negative electrode [71, 72]. The second category adopts the lithium-insertion electrode as the positive electrode and carbon as the negative. The last type, which is a relatively new approach, combines two different pseudo-capacitive materials or nanocomposites as the positive and negative electrodes. One of the nanocomposites, *i.e.* CNT/SnO₂, has been utilised as a negative electrode in asymmetrical ECs. It exhibited a high overpotential against hydrogen evolution, and its effect on widening the voltage window was comparable to that of the activated carbon [112-114]. Consequently, the asymmetrical ECs with a CNT/SnO₂ negative electrode achieved cell voltages up to 1.7 V and specific energy of 20.3 Wh/kg at a mass-normalised current of 0.25 A/g in aqueous electrolytes [115]. (Note that the unit, A/g, is described as "current density" in the literature, which is obviously incorrect) Of course, the increased specific energy is also partly due to the CNTs being able to, in general, further increase the capacitance of the nanocomposite, as explained in the previous sections [116].

Various metal oxides and conducting polymers have been studied as the positive electrode in ECs, such as nickel hydroxide [72, 117, 118], manganese dioxide [112-114], polyaniline [119], Co-Al double hydroxide [120] and modified activated carbon in some cases [121]. These materials can further extend the potential limit of the positive electrode, and hence

the cell voltage. In other words, these materials are chosen because they have a higher overpotential for the oxygen evolution than a carbon positive electrode. MnO_2 is one of the most investigated materials for positive electrodes because it is more economic than RuO_2 but displays almost comparable performance. The combination of MnO_2 and carbon as the positive and negative electrodes respectively has resulted in a cell voltage of 2.0 V in aqueous electrolytes due to their overpotentials for O_2 and H_2 evolution, respectively. Besides that, the highly porous carbon negative electrode can promote the utilisation of nascent hydrogen to gain added charging-discharging capacities [104]. Non-faradaic lithium-inserted electrodes, which should be distinguished to Li-ion batteries, with a capacitive carbon electrode, have also been investigated, leading to specific energy of over 15 Wh/kg at 3.8 V operating voltage (although this value is not based on an aqueous electrolyte, which is the main focus in this thesis, it is worthy of mentioning) [122, 123].

Conducting polymers have been considered as promising materials for ECs, given their good electrical conductivity and the available delocalised electrons in their structures. Pairing conducting polymers effectively (p-dopable and n-dopable polymers as positive and negative electrodes, respectively) [124] has resulted in excellent capacitance and specific energy [125, 126]. Replacement of activated carbon with n-dopable polymers as the negative electrode [127, 128] has been proven to show superior results due to the high conductivity of the n-doped form on top of their high pseudo-capacitance [129]. It has been reported that the achievable specific energy and power are 18.0 Wh/kg and 1.25 kW/kg respectively, operating at a cell voltage of 1.6 V [119]. The specific energy in such an asymmetrical system was improved by a factor of about 5 times in comparison with that of a symmetrical PANI-based capacitor using

different electrolytes [72, 130].

The total energy, which is the most important parameter that ECs strive to achieve, can be calculated using Equation 2.1 [112, 113, 115].

In simple electrical terms, the power output (P) from an energy device is proportional to both current (I) and voltage (V), i.e. $P = I \times V = V^2/R$ where R is the resistance of the whole circuit. However, as the voltage of an EC decreases continuously during discharging, so does the power output. Thus, ECs are usually evaluated against their maximum power output in relation to the maximum cell voltage (V) and the internal resistance or the equivalent series resistance (ESR). For comparison between different materials, the concept of maximum specific power (P_{\max}) has been proposed and can be calculated using Equation 2.7 [3, 115, 131, 132].

$$P_{\max} = \frac{V_{\max}^2}{4 \times ESR \times M} \quad (2.7)$$

Where M is the mass of the active materials on both of the positive and negative electrode, neglecting the weight of the current collector.

It should be pointed out that Equation 2.5 has been derived for symmetrical ECs in which the material mass is the same on both the positive and negative electrodes. However, asymmetrical ECs have different materials with different specific capacitances on each electrode. To construct the asymmetrical EC with equal electrode capacitance, the

positive and negative electrodes must differ in mass. Alternatively, the asymmetrical EC may be constructed with the same mass on both electrodes, but different electrode capacitances. In both cases, Equation 2.7 may still be applied to give the equivalent maximum specific power for comparison with symmetrical ECs. When different electrode masses are used, M in Equation 2.7 is the sum of the two electrode masses. Table 2.3 summarises data from the literature as derived from Equation 2.1 for various aqueous asymmetrical ECs.

- Designs of thicker electrode films

Advanced configurations of ECs are not necessarily limited to increasing their operating voltages. By designing electrodes to allow the loading of more active material with minimum impact on electron and/or ion transfer, enhancement of the cell performance in terms of overall energy capacity can be expected. One good example of this is to produce a thicker film of the active material attached to the electrode substrate (current collector). By examining the properties of different materials, the specific capacitance value (F/g) is evaluated as described in the previous section, and the utilisation of active materials is the key to improvement. Electrode capacitance, which is defined as capacitance per unit area (F/cm²), is also of great significance when the overall capacitance of the ECs is under consideration. Most of the metal oxides and conducting polymers show a higher resistivity compared to the carbon materials which are widely used for the construction of EDLCs. Thus, thicker films of pseudo-capacitive materials often lead to a significant decrease in both the material utilisation and current response, since only the surface of the film takes part in the

charge storage process, at least for the most part. A number of researchers have reported promising results in terms of the specific capacitance (F/g) by using noticeably thin electrode films [29, 69, 133-135]. However, there have been a number of publications focusing on capacitance relative to geometric area as a function of the thicknesses of films, and some studies have suggested that the charge storage process may occur within the bulk of the film material rather than only on the limited surface area. It was revealed that the electrode capacitance (F/cm²) increased linearly with increasing the loading on the electrode (thickness of the film) up to certain thickness [23, 136]. This linear relationship has also been observed by the present author. Using activated carbon (CMPB), the geometric capacitance increased linearly with the additional loading and the value reached up to 10 F/cm² after a thorough wetting process.

2.2.3. STRUCTURAL STUDY

Structural investigations of the film materials on the electrode are of great significance for developing ECs. Different effects on capacitance or operating voltages are expected from the various film structural elements including particle sizes, pore size distributions and surface functionalities. Producing smaller particles (nano-scale in many cases) in the film materials has been commonly believed as one of the direct ways to increase the specific capacitance value (F/g), mainly owing to the shorter intercalation distance for ions. In addition, smaller particles have a larger surface area and can accommodate more active sites effectively. Indeed, there are a number of publications claiming how effective this method could be on both the double layer and pseudo-capacitance [42, 137, 138]. However, it was also observed in these early studies that the specific capacitance values

only increased up to a certain level beyond which a further decrease in the particle size was not always accompanied by enhanced specific capacitance. This is largely attributed to the pores between the small particles becoming too narrow for ions to travel through. Consequently, attention has been shifted to the pore structure of the film materials. Conventionally, it was accepted that larger pores within the film structure would be more advantageous due to the greater kinetics of ions (less resistance), compared to materials with smaller pores and this was proven in several studies [139-142]. However, this may not always be the case based on the latest studies in the literature, in which the ion desolvation theory has been suggested [38, 137, 143, 144]. According to these studies, the specific capacitance reached the maximum value where the average pore sizes were around 0.7 nm and the ions were still accessible to the pores by either partially or fully removing their hydrated shell. Another study suggested that pores may be accessible to ions as long as the pore size is greater than 0.6 nm, but this would have a significant effect on charge-discharge rate due to the slow ion diffusion rate [37].

Moreover, the pore structures are strongly correlated with hydrogen adsorption which is directly related to the magnitude of the applied overpotential, especially in the case of the carbon-based electrode films [106, 145, 146]. In the carbon studied, hydrogen intercalation is mainly established within micropores and hence the use of carbon materials with smaller pore is more advantageous for hydrogen trapping and hence leads to a higher overpotential for hydrogen gas formation. For example, finely processed activated carbon would be more advantageous than CNTs in general, due to a higher hydrogen overpotential. This is one of the reasons why activated carbons are widely used as the negative electrode in asymmetrical ECs to take advantage of the high hydrogen overpotential of

carbon, in order to avoid water electrolysis at the highest operating voltages.

Lastly, surface functionalities also show a great influence on the performance of the film materials. There have been many investigations on the effect of oxygen-containing surface functional groups, especially on carbon materials such as activated carbon and CNTs [142, 147, 148]. As mentioned previously, the specific capacitance of the carbon-based materials is considerably lower than that of pseudo-capacitive materials in which the charge storage processes are mainly based on Faradaic redox reactions. Enriching the oxygen-containing surface groups on the carbon materials has been rigorously investigated in order to increase their specific and geometric capacitance values, since the charge storage mechanisms of the oxygen-rich functional groups are faradaic in nature and hence enhanced capacitance values are expected with long life spans (carbon-based ECs). One of the highest values reported using this method with carbon materials was 370 F/g in 3 M KOH [147]. However, oxygen groups also show drawbacks in terms of the long term performance of the ECs. It has been claimed that the surface functionalities may result in significant leakage of current and a high internal resistance. Accordingly, this can lead to the poor cycling stability and power characteristics [1, 149-151].

2.2.4. EFFECT OF ELECTROLYTES

Electrolytes are another important element in determining the performance of ECs. Since one of the main topics in this thesis is the use of neutral aqueous electrolytes, some relevant results reported in the literature regarding these electrolytes are discussed in this section.

The difference in the pH value in aqueous electrolytes is one of the most significant factors determining the performance of the ECs, in terms of both specific capacitance and operating voltage. Generally speaking, higher capacitance values have been observed with either acidic or basic electrolytes due to the higher transport kinetics of H^+ and OH^- ions [14, 19]. However, it has been suggested that neutral aqueous electrolytes are more advantageous in that they exploit wider potential windows with carbon materials due to a high hydrogen overpotential [19, 20]. Accordingly, the latest research focus on aqueous ECs has been shifted to neutral aqueous electrolytes.

There have been a number of studies on the effect of ion size on electrode capacitance in aqueous electrolytes. It is well known that smaller ions are more advantageous for achieving higher capacitance values due to greater diffusion and migration rates [152, 153]. However, recent studies have suggested that ion size changes in the aqueous electrolytes due to their hydration by water molecules. Regarding cations, crystal ionic radii (non-hydrated ion size) and hydrated ionic radii should be distinguished and the performance of ECs seems to be governed by hydrated ion sizes [153-155]. In these studies, smaller hydrated cations have shown higher capacitances and better rate performance (low ionic resistance).

The importance of selecting appropriate anions becomes more significant especially when designing ECs with a carbon negative electrode to operate with higher operating voltages. As discussed, the oxidation of the electrolyte is more problematic in aqueous ECs than the reduction of electrolyte owing to high hydrogen overpotential. Cl^- is a widely used anion and shows excellent solubility in water compared to, for example, SO_4^{2-} . However, the oxidation potential for the conversion of chloride ion to

chlorine gas on the positive electrode has been identified, and this is from 0.6 to 0.8 V vs. Ag/AgCl [156, 157]. Thus, this anion may not be suitable for applications where high operating voltages are used [158].

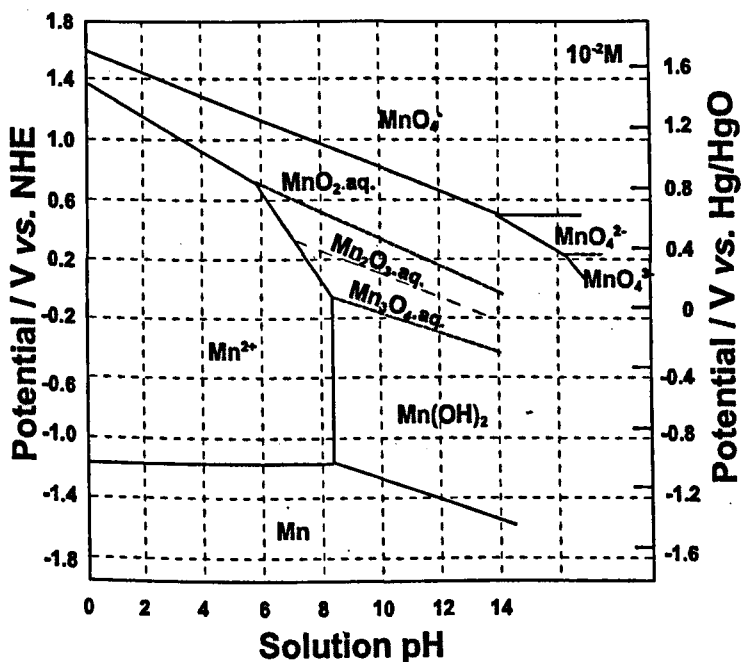


Figure 2.7 Potential-pH diagram of manganese in aqueous solution at 25°C [159]

Although many studies have been focused on carbon materials, which are dominantly governed by electric double layer capacitance, there is evidence that pseudo-capacitive materials are also hugely influenced by the nature of aqueous electrolytes. One good example is MnO₂, which is one of the most widely used positive electrode materials; it exhibits relatively rectangular CVs because it is a semiconductor in neutral aqueous electrolytes. However, battery-like behaviour (indicated by a bell-shaped CV) is observed in alkaline solutions because in an alkaline solution, MnO₂ is reduced to Mn(OH)₂ which is a poor conductor (insulator) [160]. The

reason for the formation of the insulating $\text{Mn}(\text{OH})_2$ is mainly to do with the solubility of MnOOH which becomes significant in concentrated alkaline electrolytes [161, 162]. The dissolved $\text{Mn}(\text{III})$ species in turn undergo a reduction process to form $\text{Mn}(\text{II})$ species at sufficiently low voltages and eventually turn into the insoluble $\text{Mn}(\text{OH})_2$ by combining with OH^- ions [12, 160, 163-165]. Accordingly, MnO_2 materials are not ideal for ECs using alkaline electrolytes. However, non-capacitive behaviour found in insulating materials, such as $\text{Mn}(\text{OH})_2$ in alkaline electrolytes, can be utilised in batteries for energy storage.

2.3. TECHNICAL BARRIERS OF AQUEOUS ECs

Aqueous ECs have a few intrinsic disadvantages compared to ECs that use other electrolytes. In the following sub-sections, the main drawbacks of aqueous ECs are identified and recent efforts made to overcome these technical obstacles are also discussed.

2.3.1. NARROW OPERATING VOLTAGES

Due to the thermodynamic limitations of water, it seems that a narrow operating voltage of aqueous ECs is inevitable. It was commonly believed that aqueous ECs were only able to perform with a voltage window about 1 V due to water decomposition. However, recent studies have suggested that advanced cell configurations and designs can resolve the problem significantly. Difference in the maximum voltages between the ECs using aqueous (around 2 V) and organic electrolytes (2.5 – 2.7 V) has narrowed. Most of the latest technical developments and ideas to increase the

operating voltage of ECs have already been thoroughly explained in Section 2.2.2 of this chapter and thus are not discussed in detail here. Nonetheless, the main technical obstacles limiting further increases in the voltage of aqueous ECs shall be reviewed here. Since carbon materials are widely used as a negative electrode material, showing excellent high hydrogen overpotential in the negative potential region, the reduction of hydrogen cations (hydrogen gas evolution) at the negative electrode seems to be a minor issue in the use of aqueous ECs.

Therefore, the chemical and electrochemical durability of aqueous electrolytes towards oxidation on the positive electrode remains one of the main issues in aqueous ECs. The oxidation problem at the positive electrode limits the operating voltage of aqueous ECs and this limitation should be resolved in order to further increase the operating voltage [19]. Nonetheless, the operating voltage of aqueous ECs has rapidly increased due to recent technical developments. These are mainly owing to advanced cell configurations such as asymmetrical design and unequalisation (unbalanced instead of unequalisation is also a widely used term) of electrode capacitances [101]. The maximum potential window width of electrolytes and materials can be more completely utilised by adopting the abovementioned approaches.

2.3.2. SELF-DISCHARGE

Like other electrochemical energy storage devices, aqueous ECs experience so-called self-discharge after they are fully-charged because the charged state possesses a higher free energy compared to the discharged state [1]. After charging, a decline in the voltage under open circuit conditions

contributes to the degradation of performance characteristics, such as the power and energy densities of the EC [1]. Significant self-discharge in an open circuit state may introduce unpredictability and unreliability in energy storage devices, especially when used for critical applications [5, 84]. The self-discharge issue has been identified for a long time and a relatively large amount of research has been undertaken to understand the mechanism.

For carbon-based EDLCs, the self-discharge characteristics may be influenced by the surface functionalities, which contribute to the charge storage process by redox reactions, on the active materials. It has been reported that the degree to which oxygen is retained, through physical adsorption or acidic functionalisation on the surface of carbon, may influence the rate of self-discharge in EDLCs [1, 166]. Moreover, a high concentration of surface complexes could increase the rate of self-discharge, suggesting an electro-catalytic role of the complexes on the oxidation or reduction of carbon [167-169]. Indeed, a lower leakage current was reported when these surface functional groups were removed from the carbon through special heat treatment in non-reactive environments [166, 168].

In comparison, the fundamentals of self-discharge processes within pseudo-capacitive materials differ from those materials displaying double-layer capacitance (mainly carbon materials). This is because the charge transfer process in the pseudo-capacitive materials is faradaic in nature as discussed earlier, and involves various oxidation states which may correspond to different solid phases [170]. For these materials, a gradient of oxidation state can exist from the outer surface into the bulk [1]. Thus, the potential decline of an apparently fully charged pseudo-capacitive

electrode with time can be caused by a diffusion- and migration controlled mechanism, resulting in the relaxation of the oxidation state gradient. Such a self-discharge mechanism would be quickened in the presence of conducting materials such as graphite and with a greater surface area [171]. Greater numbers of active sites, due to an increased surface area, were believed to facilitate a faster self-discharge [171].

There has been another approach towards investigating the self-discharge process, and this work dealt with the shift of the Nernst potentials of water decomposition. It was claimed that undesirable electrolyte decomposition might occur on the electrode surface due to the change in the water decomposition potentials, resulting from dissolved H_2 and O_2 . This possibly accelerates the self-discharge of the overall system when in an open-circuit [172].

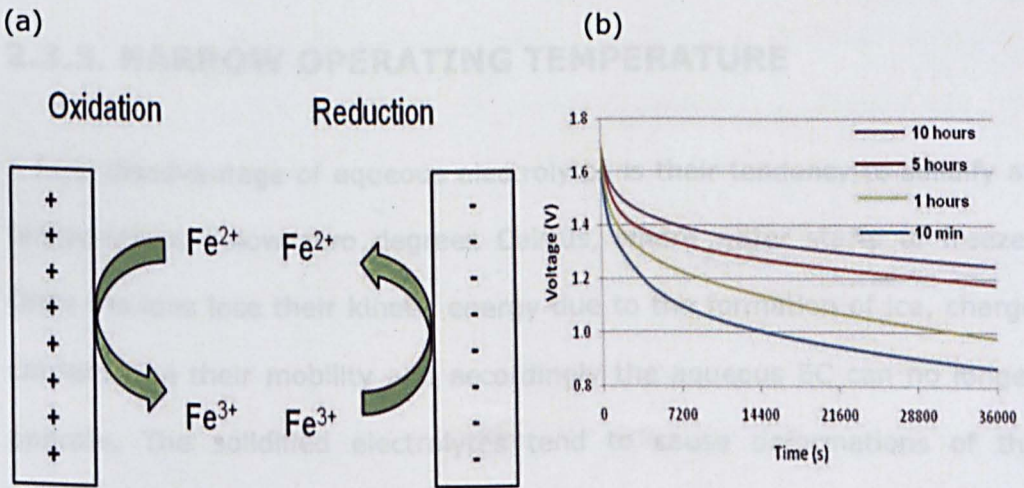


Figure 2.8 (a) Possible effects of the Fe^{3+} and Fe^{2+} ions as impurities on self-discharge. (b) Different self-discharge profiles of a carbon-carbon symmetrical supercapacitor with aqueous electrolyte (0.3 M K_2SO_4) as recorded upon the application of different charging times (at a constant cell voltage of 1.7 V) from 10 minutes to 10 hours.

Metallic impurities in an electrolyte also show a significant influence on the self-discharge process [173-175]. In particular, the ions of Fe have been reported to show a greater effect on self-discharge rates than other common metallic impurities, due to a shuttle redox reaction in which the Fe^{2+} ion is oxidised to the Fe^{3+} ion on the positive electrode, and the Fe^{3+} ion is reduced to the Fe^{2+} ion on the negative electrode, as illustrated in Figure 2.8 (a) [174]. Lately, the effect of charge redistribution on the self-discharge profile of a porous carbon electrode (EDLC) was investigated [176-178]. The use of a high-surface-area activated carbon means that the electrode has pores of different sizes, from macro to micro level. Thus, electrode charge-discharge processes cannot proceed evenly along the pore wall and this causes a potential gradient along the carbon structures. Faster self-discharge is observed with a higher potential gradient and this result is shown in Figure 2.8 (b).

2.3.3. NARROW OPERATING TEMPERATURE

A fatal disadvantage of aqueous electrolytes is their tendency to solidify at temperatures below zero degrees Celsius, where water starts to freeze. Once the ions lose their kinetic energy due to the formation of ice, charge carriers lose their mobility and accordingly the aqueous EC can no longer operate. The solidified electrolytes tend to cause deformations of the electrode materials and these may cause permanent damage to the aqueous EC after the electrolytes return to the liquid phase again. Although the use of salts in electrolytes will lower the freezing temperature below 0 °C to some degree (freezing temperature depression), the ECs containing aqueous electrolytes do not seem to be suitable for applications at very low temperatures. Some experimental work has been carried out in the present

work regarding the freezing point depression of different electrolytes, and these results can be found in Chapter 4.1.2 in this thesis.

2.3.4. LIMITED CYCLE LIFE

Based on the findings of this literature review, the asymmetrical design of aqueous ECs is very likely to be an attractive way to achieve a higher energy storage capacity. However, the utilisation of asymmetrical aqueous ECs for commercial purposes has rarely been reported up to now. There are still many technical barriers to be overcome which limits their applications in industry.

One technical barrier is the low cycling performance due to redox reactions, which is the core mechanism behind the pseudo-capacitance phenomenon. MnO_2 is one of the most studied pseudo-capacitive transition metal oxides as the positive electrode material in asymmetrical ECs. However, based on many studies in the literature, its charging/discharging stability has not been tested to the same cycle life of EDLCs based on activated carbons (>100,000 cycles [19]). It has been reported that the MnO_2 -activated carbon asymmetrical system displays a cell voltage of up to 2.2 V at constant 1.2 kW/kg specific power. The cell has been tested over 10,000 charging-discharging cycles, but only 55% of the cell's initial specific energy remains after cycling [114]. Decreasing the maximum cell voltage from 2.2 to 1.5 V, which would result in lower energy and power densities, improved the retention of the initial specific energy to 77% after 23,000 cycles. Although much effort has been put into this research area to overcome the cycling limitations, many studies have not been able to address the degradation issues and have only reported from a few hundred

to less than 5,000 cycles [112-114, 127, 132, 179, 180].

Overcharging of the ECs also limits their cycle lives [1]. This occurs when the cell voltage exceeds the thermodynamic or, in practice, the kinetic limits for decomposition of the electrolytes in the ECs. One of the more common mistakes made while operating ECs is when too high a charging rate is applied. This would lead to the current component passing in parallel with the faradaic charging process causing the decomposition of the electrolyte in the EC, forming H_2 and O_2 in the case of aqueous electrolytes. Thus, a control mechanism needs to be in place to ensure that ECs are not overcharged or over-discharged when used in the circuit.

2.3.5. CORROSION AND INTERNAL RESISTANCE

Another common problem associated with the long-term cycling performance of aqueous asymmetrical ECs is corrosion and the consequent increase in the resistance of some metal-based current collectors. Corrosion can lead to the formation of non-conducting oxides on the surface of current collectors made from *e.g.* stainless steel [114], besides introducing contaminants to the electrolyte. More severe corrosion could also lead to cracking of the metal current collectors.

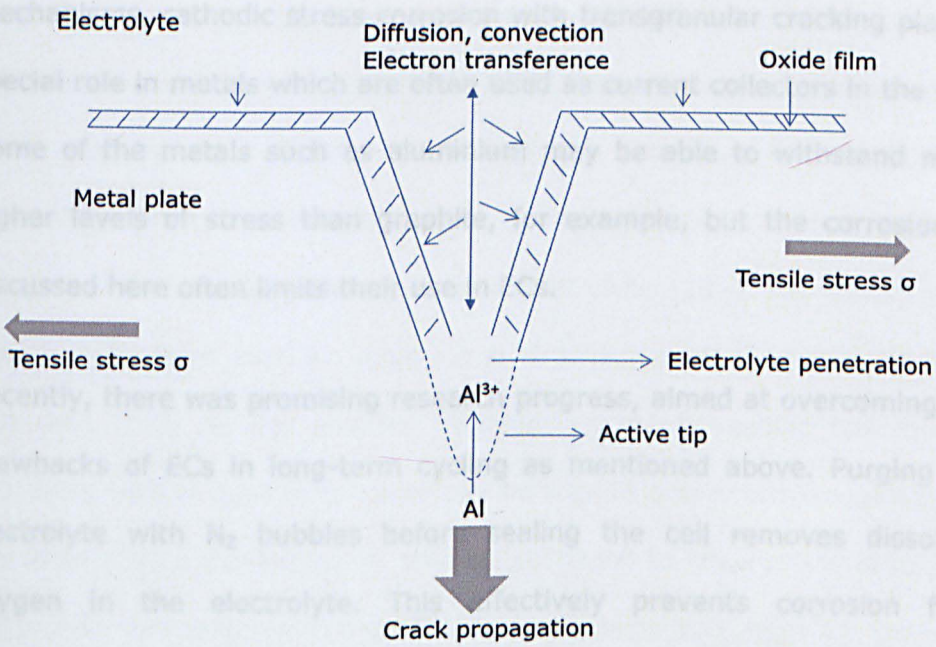


Figure 2.9 Modelling of stress corrosion crack propagation in an aluminium metal plate serving as a current collector or bipolar plate.

Figure 2.9 shows schematically one of the many possible scenarios leading to electrode cracking in ECs. There are two types of stress corrosion cracking in metals. The first type is called 'cathodic stress corrosion cracking' where the formation of atomic hydrogen plays a decisive role. These hydrogen atoms can easily enter some metal substrates, *e.g.* steel, to form metal hydrides. When hydride formation proceeds to a certain degree, the dislocation movement in the metal is blocked and the metal becomes locally brittle. Cracking of the metal can then take place above a critical stress level. The second type is called 'anodic stress corrosion cracking' where a dissolution process causes the crack formation and progression. Often, the crack forms at an incipient corrosion pit and the progress of corrosion involves alternating phases of crack propagation and broadening through dissolution of the metal. Localised embrittlement of the metal can occur ahead of the crack tip. Between the two cracking

mechanisms, cathodic stress corrosion with transgranular cracking plays a special role in metals which are often used as current collectors in the ECs. Some of the metals such as aluminium may be able to withstand much higher levels of stress than graphite, for example, but the corrosion as discussed here often limits their use in ECs.

Recently, there was promising research progress, aimed at overcoming the drawbacks of ECs in long-term cycling as mentioned above. Purging the electrolyte with N₂ bubbles before sealing the cell removes dissolved oxygen in the electrolyte. This effectively prevents corrosion from progressing to a significant degree. The system shows a surprisingly better performance, maintaining 93% of initial specific energy after 60,000 cycles (53 % of initial specific energy without N₂ bubble treatment over 50,000 cycles). Moreover, after the cycling, the internal resistance was only increased by 28 %, which is remarkably lower compared to the value of 167 % showed in the same system without N₂ bubble treatment [20]. The experiment has shown even more surprising results after 195,000 cycles, where the capacitance lost was only 12.5% and the equivalent series resistance (ESR) of the aqueous asymmetrical EC only increased by 27 % [20], which is noticeably lower than previous results from other workers in the literature [112].

There are still ample possibilities to improve ECs. For example, the aforementioned correlation between current collector corrosion and increased ESR in aqueous ECs following a large number of cycles deserves much more research effort. However, corrosion seems to be much less of a concern in ECs with an organic electrolyte whose ESR could be less than 1 Ω/cm^2 [181, 182] even after a large number of repeated cycles. The role of dissolved oxygen in corrosion of current collector materials (e.g. AISI

304L stainless steel) has also been reported [183] and can be addressed fairly well by the N_2 gas treatment of the electrolyte as mentioned above [20]. Alternatively, coating of the current collectors with nickel can effectively prevent corrosion when strong alkaline solutions such as potassium hydroxide are used as the electrolyte [184]. For strong acid-based electrolytes such as sulphuric acid, which is often used in aqueous ECs with RuO_2 as the positive electrode material, coating the current collectors with a layer of graphite can be a good preventative approach to corrosion [185]. Obviously, by limiting corrosion to the current collectors, electrolyte contamination and internal resistance can both be lowered, which in turn leads to an improved cycle life of aqueous ECs. To minimise the corrosion problem, titanium metal substrates are used as a current collector in many studies – titanium is one of the most resistant metals to corrosion.

2.4. CURRENT STATUS OF AQUEOUS ECs

EDLCs display kinetically and thermodynamically high reversibility in charging-discharging processes. They usually have the same carbon material on both the positive and negative electrodes, and are thus termed to be symmetrical. Also, because of the electrostatic mechanism for charge storage, these systems have a longer cycle life with great stability. However, the low specific energy of EDLCs due to a relatively narrow voltage window has always been an issue when it comes to commercialisation of the technology. This is because both the specific energy and power of the device increase proportionally with the square of the voltage. Similarly, the cell voltage is the crucial factor that has

determined the relatively low specific power in fuel cells and some rechargeable batteries, and hinders their wider application despite their remarkably high specific energy [186-188].

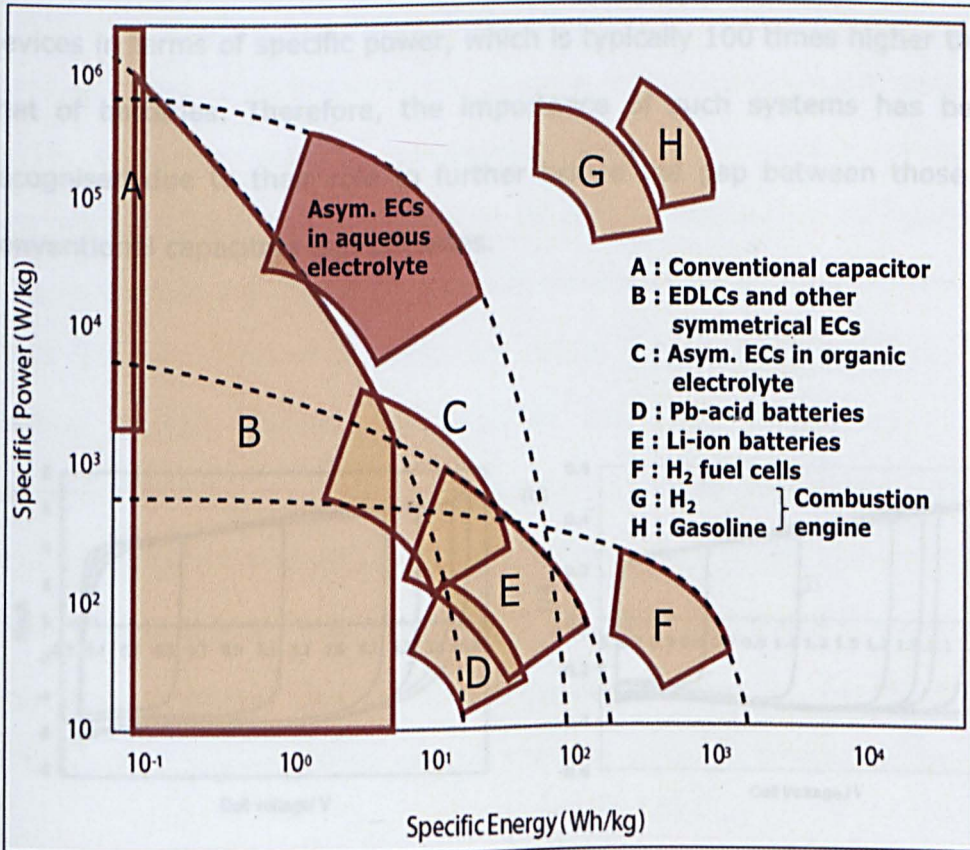


Figure 2.10 Ragone plots of various electrochemical and internal combustion power devices. [3, 5, 61] (The data of aqueous asymmetrical ECs are based on electrode mass)

The concept of neutral aqueous ECs has been suggested to overcome the shortcomings of the narrow voltage window and the consequent low specific energy and power observed using conventional aqueous ECs. Figure 2.10 shows the specific power-energy region occupied by asymmetrical ECs with neutral aqueous electrolytes, as compared to other

power devices. Up until now, although these asymmetrical devices still show a relatively lower level of specific energy as compared to batteries, an improvement in terms of their specific energy can be observed when compared to EDLCs or the other first generation variants of aqueous ECs. Moreover, they have been proven to be one of the best energy storage devices in terms of specific power, which is typically 100 times higher than that of batteries. Therefore, the importance of such systems has been recognised due to their role to further bridge the gap between those of conventional capacitors and batteries.

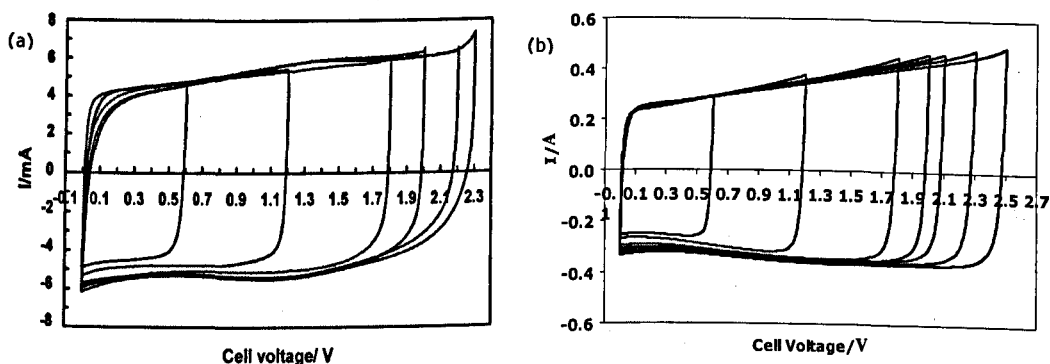


Figure 2.11 Cyclic voltammograms of (a) an aqueous asymmetrical AC-MnO₂ supercapacitor in 2 M KNO₃ reaching a cell voltage of 2.3 V without showing signs of water decomposition at a scan rate of 10 mV/s [111], and (b) a commercial symmetrical supercapacitor with carbon electrodes and an organic electrolyte with a cell limit of 2.5 V at a scan rate of 20 mV/s.

Organic electrolyte-based ECs show higher specific energy in comparison with the aqueous-based systems due to the former having wider operating voltages. However, they exhibit lower specific powers and capacitances due

to the low mobility of large ions in the organic electrolyte. Besides that, there are other problems associated with the organic electrolyte, such as high handling costs, safety issues, and environmental impact [6, 7].

Figure 2.11 demonstrates the rapid development of ECs using neutral aqueous electrolytes. The figure shows examples of cyclic voltammograms obtained using a laboratory-scale aqueous asymmetrical supercapacitor [111], achieving voltages comparable to a commercially available symmetrical carbon supercapacitor in an organic electrolyte. By selecting suitable positive and negative materials the drawback associated with the small voltage window of aqueous cells, which is limited to 1.23 V, can be avoided. Voltage windows as large as 2.2 V were achieved in an asymmetrical AC-MnO₂ (MnO₂ type: α -MnO₂·nH₂O) supercapacitor without signs of water decomposition (at 2.3 V, indication of faradaic reaction, water decomposition, was observed) [111], giving a specific energy as large as 21.0 Wh/kg. This is greater than that reported for a symmetrical carbon-carbon supercapacitor of 17-18 Wh/kg using an organic electrolyte [3].

References

1. Conway, B. E., *Electrochemical supercapacitors: scientific fundamentals and technological applications*. 1999: Springer. US. New York
2. Frackowiak, E. and Béguin, F., *Carbon materials for the electrochemical storage of energy in capacitors*. Carbon, 2001. **39**(6): p. 937-950.

3. Kötzt, R. and Carlen, M., *Principles and applications of electrochemical capacitors*. *Electrochim. Acta*, 2000. **45**(15-16): p. 2483-2498.
4. Peng, C., Zhang, S., Juwell, D and Chen, G. Z, *Carbon nanotube and conducting polymer composites for supercapacitors*. *Prog. Nat. Sci.*, 2008. **18**(7): p. 777-788.
5. Simon, P. and Gogotsi, Y., *Materials for electrochemical capacitors*. *Nat. Mater.*, 2008. **7**(11): p. 845-854.
6. Zhang, L. L. and Zhao, X. S., *Carbon-based materials as supercapacitor electrodes*. *Chem. Soc. Rev.*, 2009, **38**: p. 2520 - 2531
7. Simon, P. and Burke, A., *Nanostructured carbon; Double-layer capacitance and more*. *Electrochem. Soc. Interface*, 2008, **17**: p. 38 - 43.
8. Toupin, M., Brousse, T. and Bélanger, D., *Charge storage mechanism of MnO₂ electrode used in aqueous electrochemical capacitor*. *Chem. Mater.*, 2004. **16**(16): p. 3184-3190.
9. Vinod, M. P., Vijayamohanan, K. and Joshi, S. N., *Effect of silicate and phosphate additives on the kinetics of the oxygen evolution reaction in valve-regulated lead/acid batteries*. *J. Power Sources*, 1998. **70**(1): p. 103-105.
10. Sugimoto, W., Yokoshima K., Murakami Y. and Takasu Y., *Charge storage mechanism of nanostructured anhydrous and hydrous ruthenium-based oxides*. *Electrochim. Acta*, 2006. **52**(4): p. 1742-1748.

11. Yuan, D., Zheng, J., Kristian, N., Wang, Y. and Wang, X., *Bi₂O₃ deposited on highly ordered mesoporous carbon for supercapacitors*. *Electrochem. Commun.*, 2009. **11**(2): p. 313-317.
12. Zhang, L. L., Wei, T., Wang, W. and Zhao, X. S., *Manganese oxide-carbon composite as supercapacitor electrode materials*. *Microporous Mesoporous Mater.*, 2009. **123**(1-3): p. 260-267.
13. Faulkner, L. R. and Bard, A. J., *Electrochemical Methods: Fundamentals and Applications*. 2001: John Wiley & Sons. New York
14. Zhang, S. W. and Chen, G. Z., *Manganese oxide based materials for supercapacitors*. *Energ. Mater.: Mater. Sci. Eng. Energ. Syst.*, 2008. **3**(3): p. 186-200.
15. Burke, A., *Ultracapacitors: why, how, and where is the technology*. *J. Power Sources*, 2000. **91**(1): p. 37-50.
16. Brousse, T., Taberna P-L., Crosniera, O., Dugasa, R., Guillemeta, P., Scudellera, Y., Zhoud, Y., Favierd, F., Bélangerc, D. and Simon, P., *Long-term cycling behavior of asymmetric activated carbon/MnO₂ aqueous electrochemical supercapacitor*. *J. Power Sources*, 2007. **173**(1): p. 633-641.
17. Ng, K. C., Zhang, S. Peng, C. and Chen, G. Z., *Individual and Bipolarly Stacked Asymmetrical Aqueous Supercapacitors of CNTs/SnO and CNTs/MnO Nanocomposites*. *J. Electrochem. Soc.*, 2009. **156**: p. A846-A853.
18. Aricò, A. S., Bruce, P., Scrosati, B., Tarascon, J. M. and Schalkwijk, W. V., *Nanostructured materials for advanced energy conversion and storage devices*. *Nat. Mater.s*, 2005. **4**: p. 366-377.

19. Demarconnay, L., Raymundo-Pinero, E. and Béguin, F., *A symmetric carbon/carbon supercapacitor operating at 1.6 V by using a neutral aqueous solution*. *Electrochem. Commun.*, 2010. **12**(10): p. 1275-1278.
20. Bichat, M. P., Raymundo-Piero, E. and Béguin, F., *High voltage supercapacitor built with seaweed carbons in neutral aqueous electrolyte*. *Carbon*, 2010, **48**(15), p. 4351-4361.
21. Jin, X., Zhou, W., Zhang, S. and Chen, G. Z., *Nanoscale Microelectrochemical Cells on Carbon Nanotubes*. *Small*, 2007. **3**(9): p. 1513-1517.
22. Wang, Y., Shi, Z., Huang, Y., Ma, Y., Wang, C., Chen, M. and Chen, Y., *Supercapacitor Devices Based on Graphene Materials*. *J. Phys. Chem. C*, 2009. **113**(30): p. 13103-13107.
23. Hu, Z. A., Xie, Y. L., Wang, Y. X., Mo, L. P., Yang, Y. Y. and Zhang, Z. Y., *Polyaniline/SnO₂ nanocomposite for supercapacitor applications*. *Mater. Chem. Phys.*, 2009. **114**(2-3): p. 990-995.
24. Zheng, J. P. and Jow, T. R., *A New Charge Storage Mechanism for Electrochemical Capacitors*. *J. Electrochem. Soc.*, 1995. **142**(1): p. L6-L8.
25. Nagarajan, N. and Zhitomirsky, I., *Cathodic electro synthesis of iron oxide films for electrochemical supercapacitors*. *J. Appl. Electrochem.*, 2006. **36**(12): p. 1399-1405.
26. Chang, K. H., Hu, C. C., Huang, C. M., Liu, Y. L. and Chang, C. I., *Microwave-assisted hydrothermal synthesis of crystalline WO₃-*

- $WO_3 \cdot 0.5 H_2O$ mixtures for pseudocapacitors of the asymmetric type. J. Power Sources, 2011. **196**: p. 2387-2392.
27. Gujar, T. P., Shinde, V. R., Lokhande, C. D. and Han S. H., *Electrosynthesis of Bi_2O_3 thin films and their use in electrochemical supercapacitors*. J. Power Sources, 2006. **161**(2): p. 1479-1485.
28. Rajeswari, J., Kishore, P. S., Viswanathan, B. and Varadarajan, T. K., *One-dimensional MoO_2 nanorods for supercapacitor applications*. Electrochem. Commun., 2009. **11**(3): p. 572-575.
29. Lee, H. Y. and Goodenough, J. B., *Ideal supercapacitor behavior of amorphous $V_2O_5 \cdot nH_2O$ in potassium chloride (KCl) aqueous solution*. J. Solid State Chem., 1999. **148**(1): p. 81-84.
30. Choi, D., Blomgren, G. E. and Kumta, P. N., *Fast and Reversible Surface Redox Reaction in Nanocrystalline Vanadium Nitride Supercapacitors*. Adv. Mater., 2006. **18**(9): p. 1178-1178.
31. Liu, T. C., Pell, W. G., Conway, B. E. and Roberson, S. L., *Behavior of molybdenum nitrides as materials for electrochemical capacitors*. J. Electrochem. Soc., 1998. **145**: p. 1882-1888.
32. Snook, G. A. and Chen, G. Z., *The measurement of specific capacitances of conducting polymers using the quartz crystal microbalance*. J. Electroanal. Chem., 2008. **612**(1): p. 140-146.
33. Gupta, V. and Miura, N., *High performance electrochemical supercapacitor from electrochemically synthesized nanostructured polyaniline*. Mater. Lett., 2006. **60**(12): p. 1466-1469.

34. Fan, L. Z. and Maier, J., *High-performance polypyrrole electrode materials for redox supercapacitors*. *Electrochem. Commun.*, 2006. **8**(6): p. 937-940.
35. Gnanakan, S. R. P., Rajasekhar, M. and Subramania, A., *Synthesis of Polythiophene Nanoparticles by Surfactant-Assisted Dilute Polymerization Method for High Performance Redox Supercapacitors*. *Int. J. Electrochem. Sci.*, 2009. **4**: p. 1289-1301.
36. Liu, C., Yu, Z., Neff, D., Zhamu, A. and Jang, B. J., *Graphene-Based Supercapacitor with an Ultrahigh Energy Density*. *Nano Lett.*, 2010. **10**: p. 4863-4868.
37. Frackowiak, E. and Beguin, F., *Carbon materials for the electrochemical storage of energy in capacitors*. *Carbon*, 2001. **39**(6): p. 937-950.
38. Devaraj, S. and Munichandraiah, N., *High Capacitance of Electrodeposited MnO₂ by the Effect of a Surface-Active Agent*. *Electrochem. Solid-State Lett.*, 2005. **8**: p. A373-A377.
39. Devaraj, S. and Munichandraiah, N. *Electrochemical Supercapacitor Studies of Nanostructured α -MnO Synthesized by Microemulsion Method and the Effect of Annealing*. *J. Electrochem. Soc.*, 2007. **154**: p. A80-A88.
40. Brousse, T., Toupin, M., Dugas, R., Athouel, L., Crosnier, O. and Belanger, D., *Crystalline MnO₂ as Possible Alternatives to Amorphous Compounds in Electrochemical Supercapacitors*. *J. Electrochem. Soc.*, 2006. **153**: p. A2171-A2180.

41. Sugimoto, W., Iwata, H., Yasunaga, Y., Murakami, Y. and Takasu, Y., *Preparation of ruthenic acid nanosheets and utilization of its interlayer surface for electrochemical energy storage*. *Angew. Chem. Int. Ed. Engl.*, 2003. **42**(34): p. 4092-6.
42. Dmowski, W. and Egami, T., *Local atomic structure and conduction mechanism of nanocrystalline hydrous RuO₂ from X-ray scattering*. *J. Phys. Chem. B*, 2002. **106**(49): p. 12677-12683.
43. Pico, F., Ibanez, J., Lillo-Rodenas, M. A., Linares-Solano, A., Rojas R. M., Amarilla, J. M. and Rojo, J. M., *Understanding RuO₂·xH₂O/carbon nanofibre composites as supercapacitor electrodes*. *J. Power Sources*, 2008. **176**(1): p. 417-425.
44. Hyun, T. S., Tuller, H. L., Youn, D. Y., Kim, H. G. and Kim, I. D., *Facile synthesis and electrochemical properties of RuO₂ nanofibers with ionically conducting hydrous layer*. *J. Mater. Chem.*, 2010. **20**: p. 9172-9179.
45. Lee, H. Y. and Kim, S. W., *Expansion of active site area and improvement of kinetic reversibility in electrochemical pseudocapacitor electrode*. *Electrochem. Solid-State Lett.*, 2001. **4**: p. A19-A22.
46. Stankovich, S., Dikin, D. A., Piner, R. D., Kohlhaas, K. A., Kleinhammes, A., Jia, Y., Wu, Y., Nguyen, S. T. and Ruoff, R. S., *Synthesis of graphene-based nanosheets via chemical reduction of exfoliated graphite oxide*. *Carbon*, 2007. **45**(7): p. 1558-1565.

47. Zhang, Y., Li, H., Pan, L. and Sun, T. L., *Capacitive behavior of graphene-ZnO composite film for supercapacitors*. J. Electroanal. Chem., 2009. **634**(1): p. 68-71.
48. Shaijumon, M. M., Ou, F. S., Ci, L. and Ajayan, P. M., *Synthesis of hybrid nanowire arrays and their application as high power supercapacitor electrodes*. Chem. Commun., 2008: p. 2373-2375.
49. Min, M., Machida, K., Jang, J. H. and Naoi, K., *Hydrous RuO₂/Carbon Black Nanocomposites with 3D Porous Structure by Novel Incipient Wetness Method for Supercapacitors*. J. Electrochem. Soc., 2006. **153**: p. A334-A338.
50. Miller, J. M., Dunn, B., Tran, T. D. and Pekala, R. W., *Deposition of Ruthenium Nanoparticles on Carbon Aerogels for High Energy Density Supercapacitor Electrodes*. Ft. Belvoir Defense Technical Information Center, 1998
51. Frackowiak, E., Khomenko, V., Jurewicz, K., Lota, K. and Beguin, F., *Supercapacitors based on conducting polymers/nanotubes composites*. J. Power Sources, 2006. **153**(2): p. 413-418.
52. Wang, D. W., Li, F. Zhao, J., Ren, W., Chen, Z. G., Tan, J., Wu, Z. S., Gentle, I., Lu, G. Q. and Cheng, H. M., *Fabrication of graphene/polyaniline composite paper via in situ anodic electropolymerization for high-performance flexible electrode*. ACS Nano, 2009. **3**(7): p. 1745-1752.
53. Zhang, J., Kong, L. B., Wang, B., Luo, Y. C. and Kang, L., *In-situ electrochemical polymerization of multi-walled carbon*

nanotube/polyaniline composite films for electrochemical supercapacitors. Synth. Met., 2009. 159(3-4): p. 260-266.

54. Yu, M. F., Lourie, O., Dyer, M. J., Moloni, K. Kelly, T. F. and Ruoff, R. S., *Strength and breaking mechanism of multiwalled carbon nanotubes under tensile load. Science, 2000. 287(5453): p. 637-640.*
55. Poncharal, P., Wang, Z. L., Ugarte, D. and De Heer, W. A., *Electrostatic deflections and electromechanical resonances of carbon nanotubes. Science, 1999. 283(5407): p. 1513-1516.*
56. Hamada, N., Sawada, S. and Oshiyama, A., *New one-dimensional conductors: Graphitic microtubules. Phys. Rev. Lett., 1992. 68(10): p. 1579-1581.*
57. Mintmire, J. W., Dunlap, B. I. and White, C. T., *Are fullerene tubules metallic?, Phys. Rev. Lett., 1992. 68(5): p. 631-634.*
58. Saito, R., Fujita, M., Dresselhaus, G. and Dresselhaus, M. S., *Electronic structure of graphene tubules based on C₆₀. Am. J. Phys., 1992. 46(3): p. 1804-1811.*
59. Ebbesen, T. W., Lezec, H. J., Hiura, H., Bennett, J. W., Ghaemi, H. F. and Thio, T., *Electrical conductivity of individual carbon nanotubes. Nature, 1996. 382(6586): p. 54-56.*
60. Kang, Y. J., Kim, B., Chung, H. and Kim, W., *Fabrication and characterization of flexible and high capacitance supercapacitors based on MnO₂/CNT/papers. Synth. Met., 2010. 160(23-24): p. 2510-2514.*

61. Diederich, L., Barborini, E., Piseri, P., Podesta, A., Milani, P., Schneuwly, A. and Gallay, R., *Supercapacitors based on nanostructured carbon electrodes grown by cluster-beam deposition*. Appl. Phys. Lett., 1999. **75**(17): p. 2662-2664.
62. Niu, C., Sichel, E. K., Hoch, R., Moy, D. and Tennent, H., *High power electrochemical capacitors based on carbon nanotube electrodes*. Appl. Phys. Lett., 1997. **70**(11): p. 1480.
63. Yoon, B. J., Jeong, S. H., Lee, K. H., Kim, H. S., Park, C. G. and Han, J. H., *Electrical properties of electrical double layer capacitors with integrated carbon nanotube electrodes*. Chem. Phys. Lett., 2004. **388**(1-3): p. 170-174.
64. Du, C., Yeh, J. and Pan, N., *High power density supercapacitors using locally aligned carbon nanotube electrodes*. Nanotechnology, 2005. **16**: p. 350.
65. Talapatra, S., Kar, S., Pal, S. K., Vajtai, R., Ci, L., Victor, P., Shaijumon, M. M., Kaur, S., Nalamasu, O. and Ajayan, P. M., *Direct growth of aligned carbon nanotubes on bulk metals*. Nat. Nanotech., 2006. **1**(2): p. 112-116.
66. Fan, Z., Chen, J. H., Zhang, B., Liu, B., Zhong, X. X. and Kuang, Y. F., *High dispersion of $r\text{-MnO}_2$ on well-aligned carbon nanotube arrays and its application in supercapacitors*. Diamond Relat. Mater., 2008. **17**(11): p. 1943-1948.
67. Gao, F., Zhang, L. and Huang, S., *Fabrication horizontal aligned MoO_3 /single-walled carbon nanotube nanowires for electrochemical supercapacitor*. Mater. Lett., 2010. **64**(4): p. 537-540.

68. Park, J. H., Ko, J. M. and Park, O. O., *Carbon Nanotube/RuO₂ Nanocomposite Electrodes for Supercapacitors*. J. Electrochem. Soc., 2003. **150**(7): p. A864-A867.
69. Park, J. H., Park, O. O., Shin, K. H., Jin, C. S. and Kim, J. H., *An Electrochemical Capacitor Based on a Ni(OH)₂/Activated Carbon Composite Electrode*. Electrochem. Solid-State Lett., 2002. **5**(2): p. H7-H10.
70. Lota, K., Khomenko, V. and Frackowiak, E., *Capacitance properties of poly (3, 4-ethylenedioxythiophene)/carbon nanotubes composites*. J. Phys. Chem. Solids, 2004. **65**(2-3): p. 295-301.
71. Ryu, K. S., Lee, Y. G., Kim, K. M., Park, Y. J., Hong, Y. S., Wu, X., Kang, M. G., Park, N. G., Song, R. Y and Ko, J. M., *Electrochemical capacitor with chemically polymerized conducting polymer based on activated carbon as hybrid electrodes*. Synth. Met., 2005. **153**(1-3): p. 89-92.
72. Kim, J. H., Sharma, A. K. and Lee, Y. S., *Synthesis of polypyrrole and carbon nano-fiber composite for the electrode of electrochemical capacitors*. Mater. Lett., 2006. **60**(13-14): p. 1697-1701.
73. Mondal, S. K., Barai, K. and Munichandraiah, N., *High capacitance properties of polyaniline by electrochemical deposition on a porous carbon substrate*. Electrochim. Acta, 2007. **52**(9): p. 3258-3264.
74. Qian, D., Dickey, E. C., Andrews, R. and Rantell, T., *Load transfer and deformation mechanisms in carbon nanotube-polystyrene composites*. Appl. Phys. Lett., 2000. **76**: p. 2868-2890.

75. Andrews, R., Jacques, D., Qian, D. and Rantell, T., *Multiwall carbon nanotubes: synthesis and application*, *Ace. Chem. Res*, 2002. **35**: p. 1008-1017.
76. Cochet, M., Maser, W. K., Benito, A. M., Callejas, M. A., Martinez, M. T., Benoit, J. M., Schreiber, J. and Chauvet, O., *Synthesis of a new polyaniline/nanotube composite: "in-situ" polymerisation and charge transfer through site-selective interaction*. *Chem. Commun.*, 2001. **2001**(16): p. 1450-1451.
77. Lozano, K. and Barrera, E. V., *Nanofiber-reinforced thermoplastic composites. I. Thermoanalytical and mechanical analyses*. *J. Appl. Polym. Sci.*, 2001. **79**(1): p. 125-133.
78. Lozano, K., Bonilla-Rios, J. and Barrera, E. V., *A study on nanofiber-reinforced thermoplastic composites (II): Investigation of the mixing rheology and conduction properties*. *J. Appl. Polym. Sci.*, 2001. **80**(8): p. 1162-1172.
79. Malak-Polaczyk, A., Matei-Ghimbeu, C., Vix-Guterl, C. and Frackowiak, E., *Carbon/ λ -MnO₂ composites for supercapacitor electrodes*. *J. Solid State Chem.*, 2010. **183**(4): p. 969-974.
80. He, P., Chen, Y., Du, L., Chen, Y., Zhang, T., Yi, X. and Wang, W., *Co₂SnO₄/Activated Carbon Composite Materials for Supercapacitor*. *ECS Meeting Abstracts*, 2011. **1101**(6): p. 262.
81. Tao, F., Shen, Y., Liang, Y. and Li, H., *Synthesis and characterization of Co(OH)₂/TiO₂ nanotube composites as supercapacitor materials*. *J. Solid State Electrochem.*, 2007. **11**(6): p. 853-858.

82. Yan, J., Fan, Z. Wei, T. Cheng, J. Shao, B., Wang, K., Song, L. and Zhang, M., *Carbon nanotube/MnO₂ composites synthesized by microwave-assisted method for supercapacitors with high power and energy densities*. J. Power Sources, 2009. **194**(2): p. 1202-1207.
83. Chen, S., Zhu, J., Wu, X., Han, Q. and Wang, X., *Graphene Oxide-MnO₂ Nanocomposites for Supercapacitors*. ACS Nano, 2010. **4**(5): p. 2822-2830.
84. Zhang, K., Zhang, L. L., Zhao, X. S. and Wu, J., *Graphene/Polyaniline Nanofiber Composites as Supercapacitor Electrodes*. Chem. Mater., 2010. **22**(4): p. 1392-1401.
85. Liu, E. H., Li, W., Li, J., Meng, X. Y., Ding, R. and Tan, S. T., *Preparation and characterization of nanostructured NiO/MnO₂ composite electrode for electrochemical supercapacitors*. Mater. Res. Bull., 2009. **44**(5): p. 1122-1126.
86. Machida, K., Furuuchi, K., Min, M. and Naoi, K., *Mixed Proton-electron Conducting Nanocomposite Based on Hydrrous RuO₂ and Polyaniline Derivatives for Supercapacitors*. Electrochemistry-Tokyo. 2004. **72**(6): p. 402-404.
87. Wang, Y. and Zhang, X., *Enhanced Electrochemical Capacitance of NiO Loaded on TiO Nanotubes*. J. Electrochem. Soc., 2005. **152**: p. A671.
88. Liew, S. Y., Thielemans, W. and Walsh, D. A., *Electrochemical Capacitance of Nanocomposite Polypyrrole/Cellulose Films*. J. Phys. Chem. C 2010, **114**: p. 17926-17933

89. Jiang, Q., Qu, M. Z., Zhou, G. M., Zhang, B. L. and Yu. Z. L., *A study of activated carbon nanotubes as electrochemical supercapacitors electrode materials*. Mater. Lett., 2002. **57**(4): p. 988-991.
90. Cheng, Q., Tang, J., Ma, J., Zhang, H., Shinya, N. and Qin, L. C., *Graphene and nanostructured MnO₂ composite electrodes for supercapacitors*. Carbon, 2011. **49**(9): p. 2917-2925
91. Yan, J., Fan, Z., Wei, T., Qian, W., Zhang, M. and Wei, F., *Fast and reversible surface redox reaction of graphene-MnO₂ composites as supercapacitor electrodes*. Carbon, 2010. **48**(13): p. 3825-3833.
92. Stankovich, S., Dikin, D. A., Dommett, G. H. B., Kohlhaas, K. M., Zimney, E. J., Stach, E. A., Piner, R. D., Nguyen, S. T. and Ruoff, R. S., *Graphene-based composite materials*. Nature, 2006. **442**(7100): p. 282-286.
93. Stoller, M. D., Park, S., Zhu, Y., An, J. and Ruoff, S., *Graphene-based ultracapacitors*. Nano Lett., 2008. **8**(10): p. 3498-3502.
94. Vivekchand, S. R. C., Rout, C. S., Subrahmanyam, K. S., Govindaraj, A. and Rao, C. N. R., *Graphene-based electrochemical supercapacitors*. J. Chem. Sci., 2008. **120**(1): p. 9-13.
95. Geim, A. K. and Novoselov, K. S. *The rise of graphene*. Nat. Mater., 2007. **6**(3): p. 183-191.
96. Becerril, H. A., Mao, J., Liu, Z., Stoltenberg, R. M., Bao, Z. and Chen, Y., *Evaluation of solution-processed reduced graphene oxide films as transparent conductors*. ACS Nano, 2008. **2**(3): p. 463-470.

97. Dikin, D. A., Stankovich, S., Zimney, E. J., Piner, R. D., Dommett, G. H. B., Evmenenko, G., Nguyen, S. T. and Ruoff, R. S., *Preparation and characterization of graphene oxide paper*. *Nature*, 2007. **448**(7152): p. 457-460.
98. Demarconnay, L., Raymundo-Pinero, E. and Beguin, F., *Adjustment of electrodes potential window in an asymmetric carbon/MnO₂ supercapacitor*. *J. Power Sources*, 2011. **196**(1): p. 580-586.
99. Peng, C., Zhang, S., Zhou, X. and Chen, G. Z., *Unequalisation of electrode capacitances for enhanced energy capacity in asymmetrical supercapacitors*. *Energ. Environ. Sci.*, 2010. **3**(10): p. 1499-1502.
100. Cottineau, T., Toupin, M., Delahaye, T., Brousse, T. and Belanger, D., *Nanostructured transition metal oxides for aqueous hybrid electrochemical supercapacitors*. *Appl. Phys. A: Mater. Sci. Proc.*, 2006. **82**(4): p. 599-606.
101. Sivakkumar, S. R., Ko, J. M., Kim, D. Y., Kim, B. C. and Wallace, G. G., *Performance evaluation of CNT/polypyrrole/MnO₂ composite electrodes for electrochemical capacitors*. *Electrochim. Acta*, 2007. **52**(25): p. 7377-7385.
102. Wei, J., Nagarajan, N. and Zhitomirsky, I., *Manganese oxide films for electrochemical supercapacitors*. *J. Mater. Process. Technol.*, 2007. **186**(1-3): p. 356-361.
103. Yuan, C., Dou, H., Gao, B., Su, L. and Zhang, X., *High-voltage aqueous symmetric electrochemical capacitor based on*

Ru_{0.7}Sn_{0.3}O₂·nH₂O electrodes in 1 M KOH. J. Solid State Electrochem., 2008. **12**(12): p. 1645-1652.

104. Jurewicz, K., Frackowiak, E. and Béguin, F., *Towards the mechanism of electrochemical hydrogen storage in nanostructured carbon materials.* Appl. Phys. A: Mater. Sci. Process., 2004. **78**(7): p. 981-987.
105. Ma, S. B., Nam, K. W., Yoon, W. S., Yang, X. Q., Ahn, K. Y., Oh, K. H. and Kim, K. B., *A novel concept of hybrid capacitor based on manganese oxide materials.* Electrochem. Commun., 2007. **9**(12): p. 2807-2811.
106. De Koninck, M., Brousse, T. and Bélanger, D., *The electrochemical generation of ferrate at pressed iron powder electrodes: effect of various operating parameters.* Electrochim. Acta, 2003. **48**(10): p. 1425-1433.
107. Wang, Y. G., Wang, Z. D. and Xia, Y. Y., *An asymmetric supercapacitor using RuO₂/TiO₂ nanotube composite and activated carbon electrodes.* Electrochim. Acta, 2005. **50**(28): p. 5641-5646.
108. Kalpana, D., Omkumar, K. S., Kumar, S. and Renganathan, N. G., *A novel high power symmetric ZnO/carbon aerogel composite electrode for electrochemical supercapacitor.* Electrochim. Acta, 2006. **52**(3): p. 1309-1315.
109. Amatucci, G. G., Badway, F. and Du Pasquier, A., *Intercalation compounds for battery materials.* J. Electrochem. Soc., 2000. **99**: p. 344-359.

110. Hong, M. S., Lee, S. H. and Kim S. W., *Use of KCl Aqueous Electrolyte for 2 V Manganese Oxide/Activated Carbon Hybrid Capacitor*. *Electrochem. Solid-State Lett.*, 2002. **5**: p. A227.
111. Khomenko, V., Raymundo-Piñero, E. and Béguin, F., *Optimisation of an asymmetric manganese oxide/activated carbon capacitor working at 2 V in aqueous medium*. *J. Power Sources*, 2006. **153**(1): p. 183-190.
112. Brousse, T., Toupin, M. and Belanger, D., *A Hybrid Activated Carbon-Manganese Dioxide Capacitor using a Mild Aqueous Electrolyte*. *J. Electrochem. Soc.*, 2004. **151**(4): p. A614-A622.
113. Ng, K. C., Zhang, S. and Chen, G. Z., *An Asymmetrical Supercapacitor Based on CNTs/SnO₂ and CNTs/MnO₂ Nanocomposites Working at 1.7 V in Aqueous Electrolyte*. *ECS Transactions*, 2008. **16**(1): p. 153-162.
114. Fischer, A. E., Pettigrew, K. A., Rolison, D. R., Stroud, R. M. and Long, J. W., *Incorporation of Homogeneous, Nanoscale MnO₂ within Ultraporous Carbon Structures via Self-Limiting Electroless Deposition: Implications for Electrochemical Capacitors*. *Nano Lett.*, 2007. **7**(2): p. 281-286.
115. Nohara, S., Asahina, T., Wada, H., Furukawa, N., Inoue, H. Sugoh, N., Iwasaki, H. and Iwakura, C., *Hybrid capacitor with activated carbon electrode, Ni(OH)₂ electrode and polymer hydrogel electrolyte*. *J. Power Sources*, 2006. **157**(1): p. 605-609.
116. Wang, Y. G., Yu, L. and Xia, Y. Y., *Electrochemical Capacitance Performance of Hybrid Supercapacitors Based on Ni(OH)₂/Carbon*

Nanotube Composites and Activated Carbon. J. Electrochem. Soc., 2006. **153**(4): p. A743-A748.

117. Park, J. H. and Park, O. O., *Hybrid electrochemical capacitors based on polyaniline and activated carbon electrodes*. J. Power Sources, 2002. **111**(1): p. 185-190.
118. Wang, Y. G., Cheng, L. and Xia, Y. Y., *Electrochemical profile of nano-particle CoAl double hydroxide/active carbon supercapacitor using KOH electrolyte solution*. J. Power Sources, 2006. **153**(1): p. 191-196.
119. Inoue, H., Morimoto, T. and Nohara, S., *Electrochemical Characterization of a Hybrid Capacitor with Zn and Activated Carbon Electrodes*. Electrochem. Solid-State Lett., 2007. **10**: p. A261-A263.
120. Naoi, K. and Simon, P., *New Materials and New Configurations for Advanced Electrochemical Capacitors*. Interface Pennington, 2008. **17**(1): p. 34-37.
121. Burke, A., *R&D considerations for the performance and application of electrochemical capacitors*. Electrochim. Acta, 2007. **53**(3): p. 1083-1091.
122. Rudge, A., Davey, J., Raistrick, I. and Gottesfeld, S., *Conducting polymers as active materials in electrochemical capacitors*. J. Power Sources, 1994. **47**(1-2): p. 89-107.
123. Meerholz, K. and Heinze, J., *Electrochemical solution and solid-state investigations on conjugated oligomers and polymers of the a-thiophene and the p-phenylene series*. Electrochim. Acta, 1996. **41**(11-12): p. 1839-1854.

124. Fusalba, F., Mehdi, N. E., Breau, L. and Belanger, D., *Physicochemical and Electrochemical Characterization of Polycyclopenta dithiophen-4-one as an Active Electrode for Electrochemical Supercapacitors*. Chem. Mater., 1999. **11**: p. 2743-2753.
125. Di Fabio, A., Giorgi, A., Mastragostino, M. and Soavi, F., *Carbon-Poly (3-methylthiophene) Hybrid Supercapacitors*. J. Electrochem. Soc., 2001. **148**: p. A845-A850.
126. Laforgue, A., Simon, P., Fauvarque, J. F., Sarrau, J. F. and Lailier, P., *Hybrid Supercapacitors Based on Activated Carbons and Conducting Polymers*. J. Electrochem. Soc., 2001. **148**: p. A1130-A1134.
127. Mastragostino, M., Arbizzani, C. and Soavi, F., *Conducting polymers as electrode materials in supercapacitors*. Solid State Ionics, 2002. **148(3-4)**: p. 493-498.
128. Fusalba, F., Guerec, P., Villers, D. and Belanger, D., *Electrochemical Characterization of Polyaniline in Nonaqueous Electrolyte and Its Evaluation as Electrode Material for Electrochemical Supercapacitors*. J. Electrochem. Soc., 2001. **148(1)**: p. A1-A6.
129. Taberna, P. L., Chevallier, G., Simon, P., Plee, D. and Aubert, T., *Activated carbon-carbon nanotube composite porous film for supercapacitor applications*. Mater. Res. Bull., 2006. **41(3)**: p. 478-484.

130. Brousse, T. and Bélanger, D., *A Hybrid FeO-MnO Capacitor in Mild Aqueous Electrolyte*. *Electrochem. Solid-State Lett.*, 2003. **6**: p. A244.
131. Lee, S. W., Kim, J. Chen, S., Hammond, P. T. and Shao-Horn, Y., *Carbon nanotube/manganese oxide ultrathin film electrodes for electrochemical capacitors*. *ACS Nano*, 2010. **4**(7): p. 3889-3896.
132. Kim, H. K., Seong, T. Y., Lim, J. H., Cho, W. I. and Yoon, Y. S., *Electrochemical and structural properties of radio frequency sputtered cobalt oxide electrodes for thin-film supercapacitors*. *J. Power Sources*, 2001. **102**(1-2): p. 167-171.
133. Muthulakshmi, B., Kalpana, D., Pitchumani, S. and Renganathan, N.G., *Electrochemical deposition of polypyrrole for symmetric supercapacitors*. *J. Power Sources*, 2006. **158**(2): p. 1533-1537.
134. Kim, J. H., Nam, K. W., Ma, S. B. and Kim, K. B., *Fabrication and electrochemical properties of carbon nanotube film electrodes*. *Carbon*, 2006. **44**(10): p. 1963-1968.
135. Chmiola, J., Yushin, G., Dash, R. and Gogotsi, Y., *Effect of pore size and surface area of carbide derived carbons on specific capacitance*. *J. Power Sources*, 2006. **158**(1): p. 765-772.
136. Devaraj, S. and Munichandraiah, N., *Effect of crystallographic structure of MnO₂ on its electrochemical capacitance properties*. *The J. Phys. Chem. C*, 2008. **112**(11): p. 4406-4417.
137. Shi, H., *Activated carbons and double layer capacitance*. *Electrochim. Acta*, 1996. **41**(10): p. 1633-1639.

138. Qu, D. and Shi, H., *Studies of activated carbons used in double-layer capacitors*. J. Power Sources, 1998. **74**(1): p. 99-107.
139. Reddy, R. N. and Reddy, R. G., *Sol-gel MnO₂ as an electrode material for electrochemical capacitors*. J. Power Sources, 2003. **124**(1): p. 330-337.
140. Raymundo-Piñero, E., Leroux, F. and Béguin, F., *A High-Performance Carbon for Supercapacitors Obtained by Carbonization of a Seaweed Biopolymer*. Adv. Mater., 2006. **18**(14): p. 1877-1882.
141. Chmiola, J., Yushin, G., Gogotsi, Y., Portet, C., Simon, P. and Taberna, P. L., *Anomalous increase in carbon capacitance at pore sizes less than 1 nanometer*. Science, 2006. **313**(5794): p. 1760-1763.
142. Simon, P. and Gogotsi, Y., *Materials for electrochemical capacitors*. Nature Mater. 2008. **7**(11): p. 845-854.
143. Jurewicz, K., Frackowiak, E. and Béguin, F., *Enhancement of reversible hydrogen capacity into activated carbon through water electrolysis*. Electrochem. Solid-State Lett., 2001. **4**: p. A27-A29.
144. Lozano-Castelló, D., Cazorla-Amoros, D., Linares-Solano, A. and Quinn, D. F., *Micropore size distributions of activated carbons and carbon molecular sieves assessed by high-pressure methane and carbon dioxide adsorption isotherms*. J. Phys. Chem. B, 2002. **106**(36): p. 9372-9379.
145. Zhang, C., Long, D., Xing, B., Qiao, W., Zhang, R., Zhan, L., Liang, X. and Ling, L., *The superior electrochemical performance of*

- oxygen-rich activated carbons prepared from bituminous coal.* Electrochem. Commun., 2008. **10**(11): p. 1809-1811.
146. Raymundo Piñero, E., Cadek, M. and Béguin, F., *Tuning carbon materials for supercapacitors by direct pyrolysis of seaweeds.* Adv. Funct. Mater., 2009. **19**(7): p. 1032-1039.
147. Bleda-Martínez, M. J., Macia-Agullo, J. A., Lozano-Castello, D. Morallon, E., Cazorla-Amoros, D. and Linares-Solano, A., *Role of surface chemistry on electric double layer capacitance of carbon materials.* Carbon, 2005. **43**(13): p. 2677-2684.
148. Ruiz, V., Blanco, C., Raymundo-Pinero, E., Khomenko, V., Beguin, F. and Santamaria, R., *Effects of thermal treatment of activated carbon on the electrochemical behaviour in supercapacitors.* Electrochim. Acta, 2007. **52**(15): p. 4969-4973.
149. Oda, H., Yamashita, A., Minoura, S., Okamoto, M. and Morimoto, T., *Modification of the oxygen-containing functional group on activated carbon fiber in electrodes of an electric double-layer capacitor.* J. Power Sources, 2006. **158**(2): p. 1510-1516.
150. Jeong, Y. U. and Manthiram, A., *Nanocrystalline manganese oxides for electrochemical capacitors with neutral electrolytes.* J. Electrochem. Soc., 2002. **149**: p. A1419-A1422.
151. Kirk, D. W. and Graydon, J. W., *Electrochemical Double Layer Capacitance in Activated Carbon: Ion Size Effects.* 2010: ECS.
152. Qu, Q. T., et al., *Study on electrochemical performance of activated carbon in aqueous Li_2SO_4 , Na_2SO_4 and K_2SO_4 electrolytes.* Electrochem. Commun., 2008. **10**(10): p. 1652-1655.

153. Lee, H. Y. and Goodenough, J. B., *Supercapacitor behavior with KCl electrolyte*. J. Solid State Chem., 1999. **144**(1): p. 220-223.
154. Izumiya, K., Akiyama, E., Habazaki, H., Kawashima, A., Asami, K. and Hashimoto, K., *Surface activation of manganese oxide electrode for oxygen evolution from seawater*. J. Appl. Electrochem., 1997. **27**(12): p. 1362-1368.
155. Zhou, X. L., Ye, Z. G., Hua, X. Z., Zou, A. H. and Dong, Y. H., *Electrocatalytic activity and stability of Ti/IrO₂+ MnO₂ anode in 0.5 M NaCl solution*. J. Solid State Electrochem., 2010. **14**(7): p. 1213-1219.
156. Mosqueda, H. A., Crosnier, O., Athouel, L., Dandeville, Y., Scudeller, Y., Guilemet, P. and Schleich, D.M., *Electrolytes for hybrid carbon-MnO₂ electrochemical capacitors*. Electrochim. Acta, 2010. **55**(25): p. 7479-7483.
157. Messaoudi, B., Joiret, S., Keddou, M. and Takenouti, H., *Anodic behaviour of manganese in alkaline medium*. Electrochim. Acta, 2001. **46**(16): p. 2487-2498.
158. Malloy, A. P. and Donne, S. W., *Characterization of solid electrode materials using chronoamperometry: A study of the alkaline MnO₂ electrode*. J. Power Sources, 2008. **179**(1): p. 371-380.
159. Qu, D. Y., Conway, B. E., Bai, L., Zhou, Y. H. and Adams, W. A., *Role of dissolution of Mn (iii) species in discharge and recharge of chemically-modified MnO₂ battery cathode materials*. J. Appl. Electrochem., 1993. **23**(7): p. 693-706.

160. Kozawa, A., T. Kalnoki-Kis, and Yeager, J. F., *Solubilities of Mn (II) and Mn(III) ions in concentrated alkaline solutions*. J. Electrochem. Soc., 1966. **113**: p. 405-409.
161. Toupin, M., Brousse, T. and Belanger, D., *Influence of microstructure on the charge storage properties of chemically synthesized manganese dioxide*. Chem. Mater., 2002. **14**(9): p. 3946-3952.
162. Donne, S. W., Lawrance, G. A. and Swinkels, D. A. J., *Redox processes at the manganese dioxide electrode*. J. Electrochem. Soc., 1997. **144**: p. 2949-2960.
163. Yuan, A., Wang, X., Wang, Y. and Hu, J., *Textural and capacitive characteristics of MnO₂ nanocrystals derived from a novel solid-reaction route*. Electrochim. Acta, 2009. **54**(3): p. 1021-1026.
164. Pandolfo, A. G. and Hollenkamp, A. F., *Carbon properties and their role in supercapacitors*. J. Power Sources, 2006. **157**(1): p. 11-27.
165. Morimoto, T., Hiratsuka, K., Sanada, Y. and Kurihara, K., *Electric double-layer capacitor using organic electrolyte*. J. Power Sources, 1996. **60**(2): p. 239-247.
166. Yoshida, A., Tanahashi, I. and Nishino, A., *Effect of concentration of surface acidic functional groups on electric double-layer properties of activated carbon fibers*. Carbon, 1990. **28**(5): p. 611-615.
167. Hsieh, C. T. and Teng, H., *Influence of oxygen treatment on electric double-layer capacitance of activated carbon fabrics*. Carbon, 2002. **40**(5): p. 667-674.

168. Niu, J., Conway, B. E. and Pell, W. G., *Comparative studies of self-discharge by potential decay and float-current measurements at C double-layer capacitor and battery electrodes*. J. Power Sources, 2004. **135**(1): p. 332-343.
169. Skipworth, E. and Donne, S. W., *Role of graphite in self-discharge of nickel (III) oxyhydroxide*. J. Power Sources, 2007. **174**(1): p. 186-190.
170. Pillay, B. and Newman, J., *The Influence of Side Reactions on the Performance of Electrochemical Double Layer Capacitors*. J. Electrochem. Soc., 1996. **143**: p. 1806-1814.
171. Kazaryan, S. A., Kharisov, G. G., Litvinenko, S. V. and Kogan, V. I., *Self-Discharge Related to Iron Ions and its Effect on the Parameters of HES PbO₂-H₂SO₄-C Systems*. J. Electrochem. Soc., 2007. **154**: p. A751-A759.
172. Kazaryan, S. A., Litvinenko, S. V. and Kharisov, G. G., *Self-Discharge of Heterogeneous Electrochemical Supercapacitor of PbO₂H₂SO₄C Related to Manganese and Titanium Ions*. J. Electrochem. Soc., 2008. **155**(6): p. A464-A473.
173. Andreas, H. A., Lussier, K. and Oickle, A. M., *Effect of Fe-contamination on rate of self-discharge in carbon-based aqueous electrochemical capacitors*. J. Power Sources, 2009. **187**(1): p. 275-283.
174. Black, J. and Andreas, H. A., *Effects of charge redistribution on self-discharge of electrochemical capacitors*. Electrochim. Acta, 2009. **54**(13): p. 3568-3574.

175. Black, J. and Andreas, H. A., *Prediction of the self-discharge profile of an electrochemical capacitor electrode in the presence of both activation-controlled discharge and charge redistribution*. J. Power Sources, 2010. **195**(3): p. 929-935.
176. Kaus, M., Kowal, J. and Sauer, D. U., *Modelling the effects of charge redistribution during self-discharge of supercapacitors*. Electrochim. Acta, 2010. **55**: p. 7516-7523.
177. Khomenko, V., Reymundo-Pinero, E., Frackowiak, E. and Beguin, F., *High-voltage asymmetric supercapacitors operating in aqueous electrolyte*. Appl. Phys. A, 2006. **82**: p. 567-573.
178. Wang, Y. G. and Xia, Y. Y., *Hybrid aqueous energy storage cells using activated carbon and lithium-intercalated compounds. I. The C/LiMn₂O₄ system*. J. Electrochem. Soc., 2006. **153**(2): p. 450-454.
179. Taberna, P. L., Simon, P. and Fauvarque, J. F., *Electrochemical characteristics and impedance spectroscopy studies of carbon-carbon supercapacitors*. J. Electrochem. Soc., 2003. **150**: p. A292-A300.
180. Portet, C., Taberna, P. L., Simon, P. and Flahaut, E., *Modification of Al current collector/active material interface for power improvement of electrochemical capacitor electrodes*. J. Electrochem. Soc., 2006. **153**: p. A649-A653.
181. Kim, Y. P., Fregonese, M., Mazille, H., Feron, D. and Santarini, G., *Study of oxygen reduction on stainless steel surfaces and its contribution to acoustic emission recorded during corrosion processes*. Corros. Sci., 2006. **48**(12): p. 3945-3959.

182. Razoumov, S., Klementov, A., Litvinenko, S. and Beliakov, A., *Asymmetric electrochemical capacitor and method of making*. 2001, US Patent 6,222,723.
183. Nedoshivin, V. P., Stepanov, A. B., Tarasov, S. V., Varakin, I. N. and Razoumov, S. N., *Electrode and current collector for electrochemical capacitor having double electric layer and double electric layer electrochemical capacitor formed therewith*. 2006, US Patent 7,444,650.
184. Linden, D., *Handbook of batteries and fuel cells*. 1984: McGraw-Hill Book Company, New York.
185. Kordesch, K. V. and Simader, G. R., *Environmental impact of fuel cell technology*. Chem. Rev., 1995. **95**(1): p. 191-207.
186. Winter, M., Besenhard, J. O., Spahr, M. E. and Novak, P., *Insertion electrode materials for rechargeable lithium batteries*. Adv. Mater., 1998. **10**(10): p. 725-763.
187. Steele, B. C. H. and Heinzl, A., *Materials for fuel-cell technologies*. Nature, 2001. **414**(6861): p. 345-352.
188. Winter, M. and Brodd, R. J., *What are batteries, fuel cells, and supercapacitors?* Chem. Rev., 2004. **104**(10): p. 4245-4270.

CHAPTER 3 METHODOLOGY

The main aim of this thesis is to develop an optimum cell design of ECs using neutral aqueous electrolytes. One of the most important factors to consider in developing an advanced design is the electrode material. Most electrode materials used in this research are nanostructured in nature. Hence, the choice of suitable electrochemical and non-electrochemical methods to investigate their performance is highly significant. An overall description of procedures is material synthesis, general characterisations with non-electrochemical methods and electrochemical characterisations by using three- or two-electrode cells. In this chapter, material synthesis will not be discussed because detailed explanations will be presented in Chapters 6 and 7 of this thesis. Fundamentals and brief discussions of electrochemical and non-electrochemical methods for the examination of different materials in terms of their structures and performances will be discussed in this chapter.

3.1. THECHNIQUES FOR STRUCTURAL STUDIES

In the following sections, brief explanations of the equipment for chemical and structural studies will be given.

3.1.1. SCANNING ELECTRON MICROSCOPY (SEM)

A scanning electron microscope (SEM, Philips FEI XL30 FEG-ESEM) was used to investigate the surface morphology of the electrode materials, mainly for different carbons and their nanocomposites. High resolution images of the material's surface can be obtained from the SEM scanning using a high-energy beam of electrons. A schematic diagram of a SEM device can be found in Figure 3.1.

Briefly, tungsten or lanthanum hexaboride (LaB_6) are common materials used as a cathode in SEM because of their high melting point, which is crucial since the materials are superheated by an electric current up to $2700\text{ }^\circ\text{C}$, and lower vapour pressures enable it to be heated for electron emission [1]. When the instrument is initially operated, electrons are emitted from a cathode and the electron beam is focused into a very fine spot (1 to 5 nm). Then the beam passes through a pair of scanning coils in the objective lens, in which the beam is deflected over the sample surface. As the primary electrons hit the specimen, they interact with atoms from the specimen in either an elastic or inelastic way [1].

In the former scattering way, the path of the primary electron can be diverted up to 180 ° with minimal energy (velocity) loss. This event is named as 'back scattered' electron which are commonly used to evaluate the homogeneity of atom and depth profiles because the amount of the

diverted back scattered electrons increases with an increasing atomic number [2].

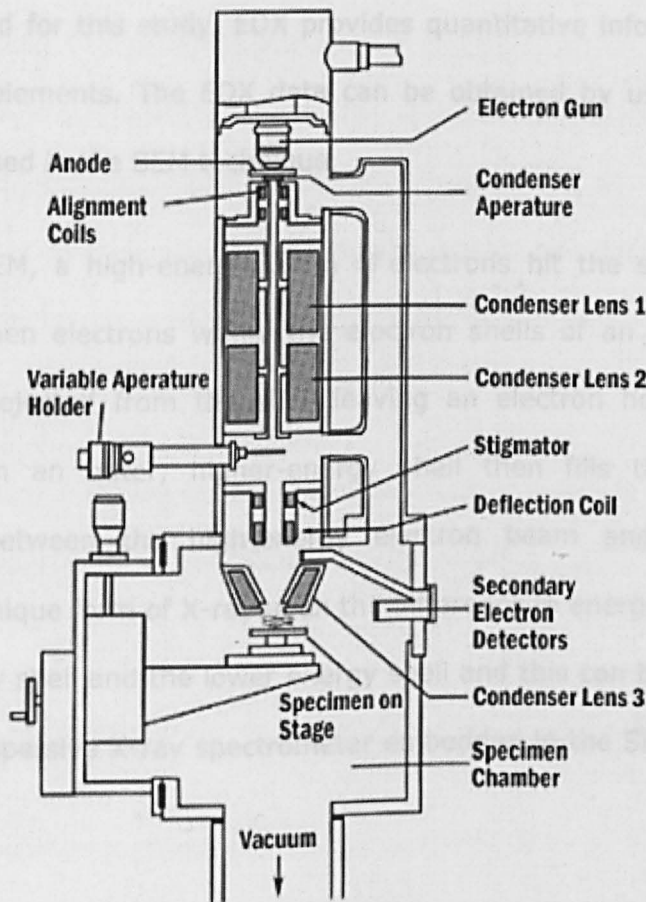


Figure 3.1 A schematic diagram of a scanning electron microscope [1]

In inelastic scattering, the primary electron goes through a direction change along with transferring energy to the specimen and hence a smaller velocity than that of initial state. In general, the energy level of electrons with this event is relatively smaller, which is in a range between 0–50 eV ($1 \text{ eV} = 1.6 \times 10^{-19} \text{ J}$ in SI unit) [3], compared to the back scattered electrons. The electrons with the inelastic scattering event (secondary-electron emission) are commonly employed for the study of surface morphology because the chance of the electron's escape from the specimen is far lower than the back scattered electrons [1].

3.1.2. ENERGY DISPERSIVE X-RAY SPECTROSCOPY (EDX)

Energy dispersive X-ray spectroscopy which is commonly known as EDX was also used for this study. EDX provides quantitative information about the surface elements. The EDX data can be obtained by using the same equipment used in the SEM technique.

Similar to SEM, a high-energy beam of electrons hit the sample on the specimen. Then electrons within the electron shells of an atom may be excited and ejected from the shell leaving an electron hole behind. An electron from an outer, higher-energy shell then fills the hole. This interaction between the high-energy electron beam and the sample generate a unique form of X-ray upon the difference in energy between the higher-energy shell and the lower energy shell and this can be detected by an energy-dispersive X-ray spectrometer embedded in the SEM instrument [4].

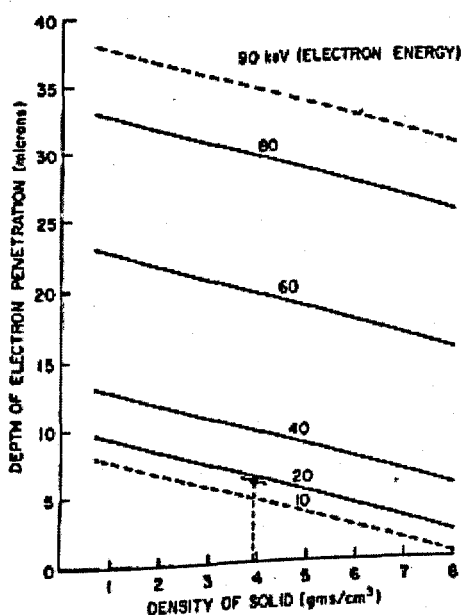


Figure 3.2 Depth of electron penetration vs. density of solid with electron energy as parameter [5]

Although EDX is commonly known to provide information on the surface elements, the definition of 'surface' using this technique should be clarified because the electron beam is, indeed, able to penetrate the material up to a certain depth. The penetration depth of electron can be determined by electron energy and density of material and this is shown in Figure 3.2. More detailed explanation can be found in literature [5, 6]. For this thesis, up to 10 keV of electron energy was chosen for the elemental analysis. It is expected up to 10 μm penetration depth using this energy range according to Figure 3.2.

The result using EDX will be presented in Chapter 5 where elemental and structural properties of cabot monarch pigment black (CMPB) are discussed.

3.1.3. TRANSMISSION ELECTRON MICROSCOPY (TEM)

Transmission electron microscopy (TEM) is widely used in material studies to investigate the internal structure of a material as well as crystal diffraction by samples. Figure 3.3 shows a schematic image of TEM and each component of the device can be found from the image.

Similar to SEM, a beam of electrons is focused onto a specimen. Through this process of TEM, an enlarged image of sample structures can be obtained. In general, TEM is able to provide images with a higher resolution than SEM (over 10 times) despite a few exceptional findings [7, 8]. This is because of the use of an electron beam possessing higher energy since the applied voltage in TEM is greater than that of SEM. For a better understanding in terms of energy between the two EM equipment, the concept of matter waves should be introduced. Before the concept of wave-particle duality in which all particles exhibit both wave and particle

properties, matter was believed to consist of localised particles. However Louis de Broglie proposed in his PhD thesis that all particles also show a wave property [9].

The above mentioned de Broglie equation can be expressed by,

$$\lambda = h/p \quad (3.1)$$

$$f = E/h \quad (3.2)$$

Where, λ is wavelength, p is the momentum, f is frequency, E is the kinetic energy and h is Planck's constant.

According to de Broglie, the frequency of matter waves is directly proportional to the total energy E (hence wavelength is inversely proportional to the total energy E). This can be applied to explain the fundamentals of both TEM and SEM. According to the de Broglie theory [9, 10], each electron within the electron beam shows both wave and particle properties and the total energy E of each electron can be determined from the applied voltage (eV). Since TEM is given greater voltage compared to SEM, the energy possessed by each electron and hence the electron beam is greater. Therefore, a higher frequency and shorter wavelength of the electron beam in TEM is observed than those of SEM [11]. This can explain the reason why higher resolution images are often achievable using TEM [12] and this feature of TEM is different from SEM.

Electrons are commonly generated in an electron microscope by a thermionic emission from a filament, which is often tungsten, or by field emission. Then, the electrons are accelerated by an electric potential and

focused by electrostatic and electromagnetic lenses onto the sample [13]. The transmitted beam contains information about electron density, phase and periodicity which are used to produce an image. Applications of TEM are often restricted because of sophisticated requirements from the specimens. In particular, the specimen for the TEM techniques should be thin enough for the electron beam to penetrate (typically, less than $0.5\ \mu\text{m}$ and more sophisticated preparation is required compared to SEM) and sufficient chemical stability and physical strength has to be provided to withstand a high vacuum atmosphere [13]. As explained previously, TEM requires a higher voltage (between 100,000 to 300,000 volts) than SEM (200 to 30,000 volts) which enables the electrons to pass through the samples [14].

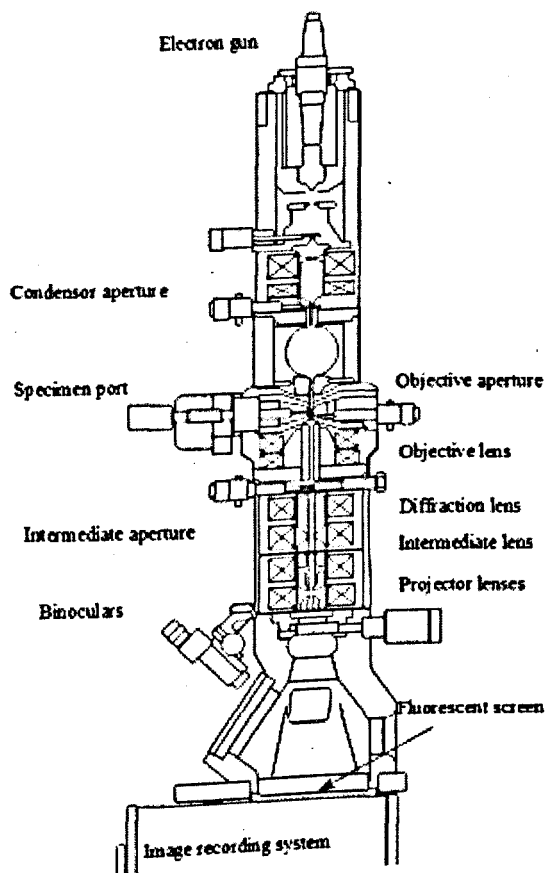


Figure 3.3 A schematic diagram of a transmission electron microscope [15]

In this thesis, the TEM technique was used to study MnO₂/CNTs binary composite (MnO₂ coating on the surface of CNTs) and the results will be presented in Chapter 6.

3.1.4. X-RAY DIFFRACTION (XRD)

The X-Ray diffraction (XRD) technique is also used in this research. Therefore, a brief discussion of the device's basic operating principle is presented in this part.

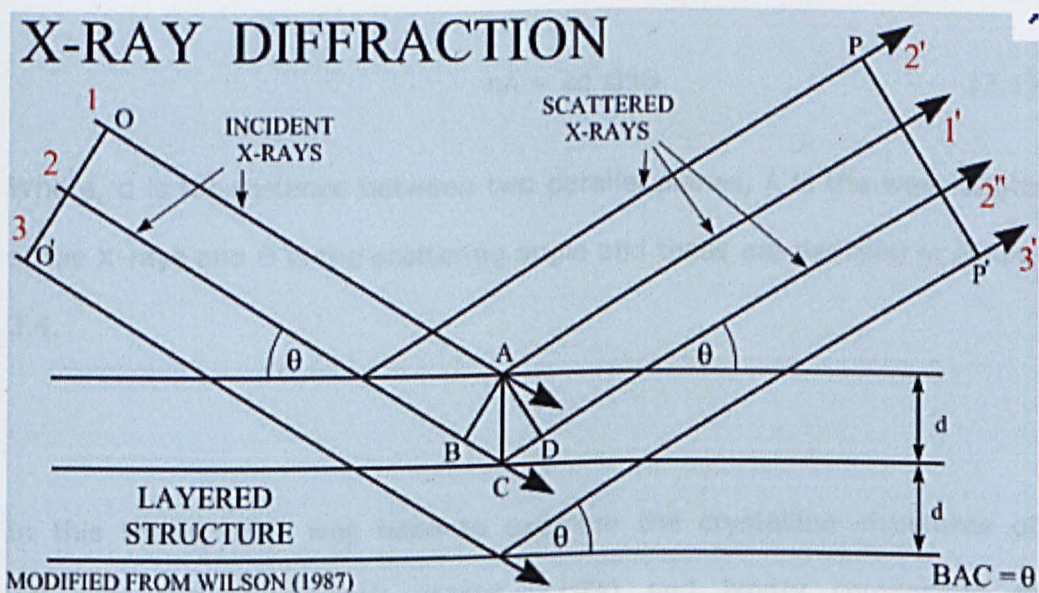


Figure 3.4 Diffraction of X-rays [16]

Figure 3.4 shows a schematic image of X-ray's diffraction patterns within a crystal structure of a material (strictly speaking, it is a scattering pattern by one particular plane orientation). X-rays are electromagnetic waves of 1-2 Ångströms in wavelength [16].

Diffraction of the X-ray occurs when the incident X-rays encounter obstacles (atoms) arranged in planes with the distance of the same magnitude. Different substances show different diffraction patterns which are shown as the scattering angle θ [17]. Depending on a material's unique crystal orientation and structure, interpretation of the different diffraction patterns (scattered X-ray patterns) of the scattered X-ray provides crystallographic information [16]. In particular, powder X-ray diffraction is a useful analytical technique to examine crystallographic structure and grain size of solid samples, and this information can be obtained using the following equation, termed Bragg's law.

$$n\lambda = 2d \sin\theta \quad (3.1)$$

Where, d is the distance between two parallel planes, λ is the wavelength of the X-rays and θ is the scattering angle and these are depicted in Figure 3.4.

In this thesis, XRD was used to examine the crystalline structures of different carbon materials (CMPB, CNTs) and binary composites of MnO_2/CNTs with different MnO_2 contents. The phases present in the samples were identified by comparing with the existing diffraction database. These results can be found in Chapter 6.

3.2. TECHNIQUES FOR ELECTROCHEMICAL ANALYSIS

For an application of ECs, different techniques for electrochemical analysis are as important as those for the structural studies to evaluate an electrochemical performance of materials. In this section, some techniques to study electrochemical properties of materials will be introduced and their principles will also be discussed briefly.

3.2.1. CYCLIC VOLTAMMETRY (CV)

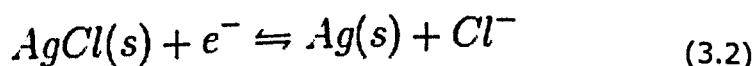
Cyclic voltammetry is one of the most widely used techniques to examine electrochemical properties of nanocomposites for ECs. The technique was employed to investigate different electrode film materials (mainly carbons and CNT composites) in this work. The results will be presented in Chapters 4-7.

In cyclic voltammetry, the current response of a working electrode is recorded upon an applied potential to the working electrode which changes with time. Using this technique, the amount of current flowing through the working and counter electrodes can be recorded as a function of the applied potential and current vs. potential plot is constructed. This is known as a 'voltammogram' [18]. The magnitude of the current response is determined by the change of concentration profiles in complex chemical reactions. Hence, redox properties of the chemicals and interfacial structures at the electrode can be determined by using this technique [19].

Although a two-electrode single cell is widely used for performance evaluation of a fully constructed EC, the standard configuration for cyclic voltammetry is the three-electrode cell in which the working electrode (WE), counter electrode (CE) and reference electrode (RE) are immersed in

an electrolyte. When electrochemical performances of various materials are evaluated using the three-electrode cell, a fabricated film is attached on the surface of the WE and this electrode is used to obtain results. However, the performance of the WE cannot be recorded without the other two electrodes because the WE on its own does not give any information, e.g. its potential relative to RE and current response. The potential of the WE is monitored with respect to the RE, so this monitored potential is not the cell value (WE vs. CE) and hence different values can be obtained by using different REs. One of the most important features of the RE is its high stability. The high stability of the electrode potential can be achieved by using a redox system with constant concentrations of each participant in the redox reaction [18, 20]. One of the widely used REs is silver/silver chloride RE (Ag/AgCl), and this RE was used for obtaining experimental data in this thesis. The Ag/AgCl RE takes advantage of the redox reaction between the silver metal (Ag) and its oxidised salt which is silver chloride (AgCl).

The redox reaction between the two forms can be expressed by,



Another electrode in the three electrode system is the CE and this electrode has to be placed in the system for the electrical current flow [19, 21] from the mentioned WE. The CE is often advised to have a much higher surface area than that of the WE and this ensures the fast enough

half-reaction at the CE so the other half reaction at the WE cannot then be limited by the CE [20, 22, 23]. Using the mentioned three electrodes, the current responses at the various potentials vs. RE can be recorded in the voltammetric analysis. A simplified configuration of this technique is shown in Figure 3.5. In this study, different carbon materials and their composites were applied to the confined area of epoxy coated graphite rods and these were used as the WE. Graphite rod was used as the CE and the Ag/AgCl couple was used as the RE.

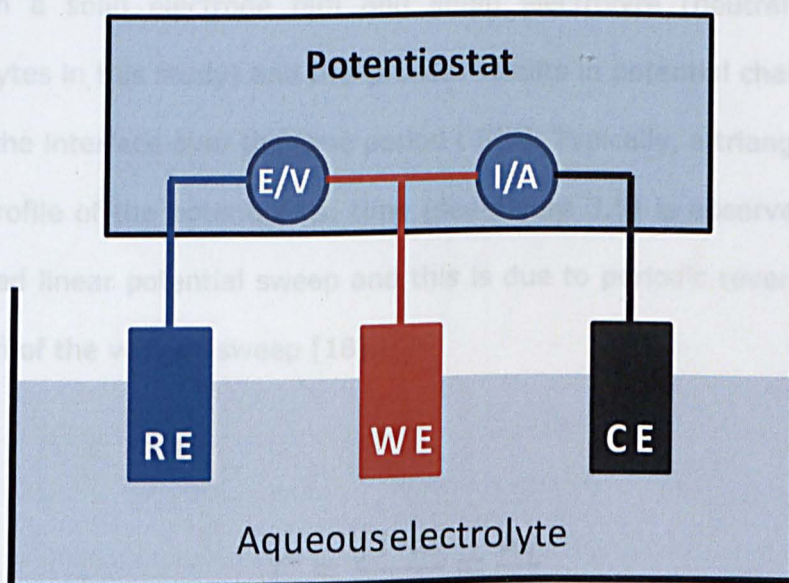


Figure 3.5 A schematic of the three-electrode system

Throughout this thesis, cyclic voltammetry was employed to evaluate materials and cells at different potentials or voltage scan rates from 5 mV/s to 500 mV/s. Important and relevant equations using CVs for this research were already discussed, mainly in Chapter 2 and in later chapters. Therefore, these will not be discussed again in this Chapter.

3.2.2. GALVANOSTATIC CHARGE-DISCHARGE

The galvanostatic charge-discharge technique is also employed to evaluate the performance of materials and cells throughout this thesis. This technique records potential responses as a function of the applied current. However, this current is not dependant on the time t (fixed current value). Using the three-electrode system, the constant current is applied across the WE and CE and the relative potential, which is monitored using the WE and RE, can be obtained. When a constant current (i) is applied over a given time period, accumulation of charges (Δq) occurs at the interface between a solid electrode film and liquid electrolyte (neutral aqueous electrolytes in this study) and this process results in potential changes (ΔV) across the interface over the time period t [24]. Typically, a triangular saw-tooth profile of the potential vs. time (see Figure 3.5) is observed upon a controlled linear potential sweep and this is due to periodic reversal of the direction of the voltage sweep [18].

$$C = \frac{\int i \cdot dt}{\Delta V} = \frac{\Delta q}{\Delta V} \quad (3.3)$$

Where, Δt is the given time to reach the particular potential and $\Delta q = \int i \cdot dt$. According to the Equation 3.3, the capacitance value C should be determined by ΔV because other two values are fixed. Therefore, it behaves closely to the ideal double-layer ECs (EDLC) in which a charge accumulation mechanism is predominantly governed by a purely electrostatic attraction (non-faradaic) and hence an ideal polarization. In such a case, ΔV increases or decreases linearly with the fixed current supply throughout the interval time Δt [20] and this behaviour is

equivalent to the very rectangular shape of CV in the cyclic voltammetry (constant current over an operating voltage) and carbon material is a good example. However, it is often observed that this is not the case, in particular utilising transition metal oxide or conducting polymers. In many cases using these materials, ΔV diverges from a linear behaviour over a time period at a fixed current. This phenomenon is depicted in Figure 3.6; (a) ideal polarisation (purely electrostatic and non-faradaic), (b) non-ideal polarisation (indication of a faradaic reaction).

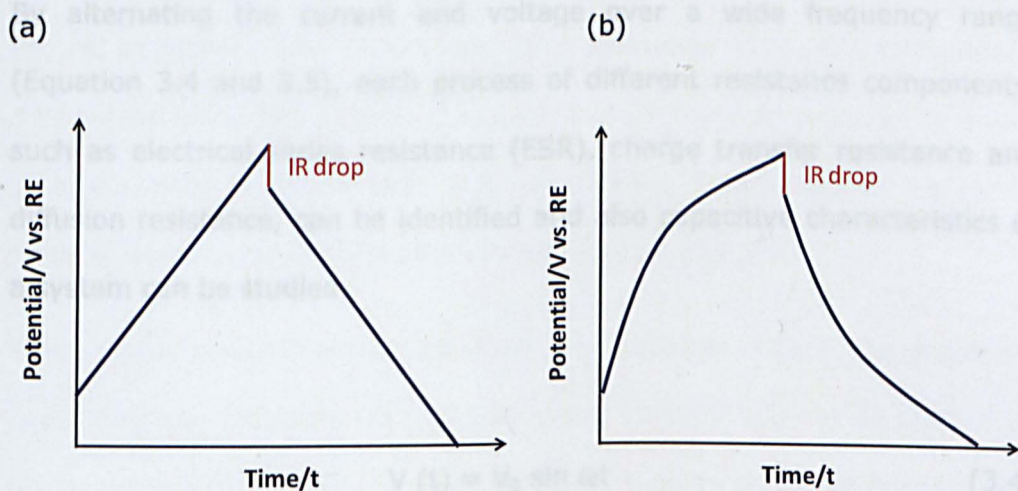


Figure 3.6 Gavanostatic charge-discharge cycle of (a) linear ΔV , (b) non-linear ΔV upon a time period t

In this study, this technique was employed to test the cycling stability of two-electrode cells. Detailed results will be provided in Chapter 5 using different carbon materials.

3.2.3. AC IMPEDANCE SPECTROSCOPY

AC impedance spectroscopy, which is also called electrochemical impedance spectroscopy (EIS), is the last electrochemical technique used in this study. EIS is a very powerful technique to investigate electrochemical systems and information different from using cyclic voltammograms and galvanostatic charge-discharge can be obtained. This tool is based on perturbation of the system upon an alternating signal of small magnitude and the measurements are obtained at the equilibrium state [24] or very slightly displacing the system from its equilibrium [25]. By alternating the current and voltage over a wide frequency range (Equation 3.4 and 3.5), each process of different resistance components, such as electrical series resistance (ESR), charge transfer resistance and diffusion resistance, can be identified and also capacitive characteristics of a system can be studied.

$$V(t) = V_0 \sin \omega t \quad (3.4)$$

$$I(t) = I_0 \sin (\omega t + \Phi) \quad (3.5)$$

where, V_0 and I_0 are voltage and current amplitude, $\omega = 2\pi f$ (frequency of rotation) and Φ is the phase angle. The phase angular (Φ) of an ideal capacitor is $\pi/2$ radians while the value of a pure resistor is 0 [24, 26].

The imaginary (Z'') and real impedance (Z') are the data obtained using AC Impedance spectroscopy. A commonly accepted and usually accurate model for the ECs is a simple combination of capacitor and resistor series circuits. As mentioned, the pure resistor has a phase angular (Φ) of 0 and hence

the real impedance of Z' is equal to resistance (R) [26]. The imaginary impedance (Z''), which is not influenced by the real impedance (Z'), can be described by following;

$$Z'' = \frac{1}{\omega C} = \frac{1}{2\pi f C} \Rightarrow C = \frac{1}{2\pi f Z''} \quad (3.6)$$

where, C is capacitance, f is frequency and Z'' is the imaginary component of the impedance. Therefore, capacitance of either a cell or material can be determined by examining the Z'' value at low frequency ranges in which the AC impedance plot shows capacitive behaviour [13]. The capacitance determined using this method is known as low frequency capacitance and it is often more accurate than the capacitance value induced by cyclic voltammetry due to the equilibrium state while measuring.

Three main components which form an electrical circuit are resistors, capacitors and inductors. In this thesis, the inductor will not be studied or discussed since the main focus of the thesis is on a capacitive behaviour of various materials. All the AC impedance plots in this thesis are presented to discuss the resistance and capacitance which is shown in the negative imaginary value; expressed by $-Z''$. Therefore, the positive imaginary region (Z'') will not be presented when AC impedance plots are discussed.

References

1. Flegler, S. L., Heckman Jr, J. W. and Klomparens, K. L. *Scanning and transmission electron microscopy: an introduction*. 1993: Oxford University Press, U.S., New York
2. Reed, S. J. B., *Electron microprobe analysis and scanning electron microscopy in geology*. 2005: Cambridge University Press, U.K., Cambridge
3. Goldstein, J., Newbury, D. E., Joy, D. C., Lyman, C. E., Echlin, P., Lifshin, E., Sawyer, L. and Michael, J. R., *Scanning electron microscopy and X-ray microanalysis*. 2003: Springer, U.S., New York
4. Kämpfe, B., Luczak, F. and Michel, B., *Energy Dispersive X-Ray Diffraction*. Part. Part. Syst. Charact., 2005: **22**(6): p. 391-396.
5. Stimler, M., *Determination of Electron-Beam Penetration in Laser Crystals*. Applied Optics, 1965: **4**(5): p. 626-628.
6. Reed, S. J. B., *Electron Microprobe Analysis*, 1993, 2nd ed. Cambridge University Press, Cambridge.
7. Zhang, X. F., *A 200 kV STEM/SEM produces 1 Å SEM resolution*. Microscopy Today, 2011: p. 26-29.
8. Asahina, S., Togashi, T., Terasaki, O., Takami, S., Adschiri, T., Shibata, M. and Erdman, N., *High-resolution low-voltage scanning electron microscope study of nanostructured materials*. Microscopy and Analysis, 2012: p. S12-S14.

9. De Broglie, L., *Recherches sur la théorie des quanta* (Researches on the quantum theory), Thesis (Paris), 1924; L. de Broglie, *Ann. Phys. (Paris)*, 1925: **3**(22).
10. De Broglie, L., *The Reinterpretation of Wave Mechanics Foundations*, *Foundation of Physics*, 1970: **1**(1): p. 5-15.
11. Resnick, R. and Eisberg, R., *Quantum Physics of Atoms, Molecules, Solids, Nuclei and Particles*, 1985, 2nd ed.: John Wiley & Sons, New York.
12. Spence, J. C. H., *High-resolution electron microscopy*. 2003: Oxford University Press, U.K., Oxford
13. Reimer, L. and Kohl, H., *Transmission electron microscopy: physics of image formation*. 2008: Springer, U.S., New York
14. Vieu, C, Carcenac, F., Pepin, A. and Chen, Y., *Electron Beam Lithography: Resolution limits and applications*, *Applied Surface Science*, 2000: **164**: p. 111-117.
15. Williams, D. B. and Carter, C. B., *Transmission electron microscopy: a textbook for materials science*. 2009: Springer, U.S., New York
16. Warren, B. E., *X-ray Diffraction*. 1990: Dover publications, US.
17. Moore, D. M. and Reynolds Jr, R. C., *X-ray diffraction and the identification and analysis of clay minerals*. 1989: Oxford University Press, U. S., New York
18. Compton, R. G. and Banks, C. E., *Understanding Voltammetry*, 2007, World Scientific Publishing Co. Pte. Ltd., Singapore

19. Vielstich, W., Lamm, A. and Gasteiger, H. A., *Handbook of fuel cells-fundamentals, Technology and applications*, 2003: Wiley, New York.
20. Bard, A. J. and Faulkner, L. R., *Electrochemical Methods: Fundamentals and Applications*, 2000, 2nd ed., Wiley, New York.
21. Kissinger, P. T. and Heineman, W. R., *Cyclic voltammetry*. *J. Chem. Educ.*, 1983. **60**(9): p. 702.
22. Kissinger, P. T. and Heineman, W. R., *Laboratory Techniques in Electroanalytical Chemistry*, 1996, 2nd ed., Marcel Dekker, Inc., New York.
23. Zoski, C. G., *Handbook of Electrochemistry.*, 2007, Elsevier Science. ISBN 0-444-51958-0, Oxford.
24. Krause, S., *Impedance methods; Encyclopedia of Electrochemistry*. 2003: Wiley-VCH.
25. Albery, W. J., Chen. Z., Horrocks, B.R., Mount, A.R., Wilson, P.J., Bloor, D., Monkman, A.T. and Elliott, C.M., *Spectroscopic and electrochemical studies of charge transfer in modified electrodes*. *Faraday Discuss. Chem. Soc.*, 1989. **88**: p. 247-259.
26. Conway, B. E., *Electrochemical supercapacitors: scientific fundamentals and technological applications (POD)*. 1999: Kluwer Academic/plenum. New York.

CHAPTER 4 NEUTRAL AQUEOUS ELECTROLYTES

Most commercial ECs are based on organic solvents because of their electrochemical stability over wider potential windows than aqueous ECs. This feature is crucial since the energy capacity of the ECs is proportional to the square of an operating voltage and the operating voltage is largely determined by chemical and electrochemical stabilities of electrode materials and electrolytes [1-3]. Generally speaking, the electrolytes rather than the electrode materials determine the operating voltage because carbon materials are normally used as an electrode and these materials demonstrate excellent chemical and electrochemical stabilities. Organic solvents show relatively good stability and they offer around 2.5 V operating voltage [4, 5]. Conversely, aqueous electrolytes show inferior chemical and electrochemical stabilities and it is commonly considered that water-based ECs are only capable of displaying an operating voltage around 1 V, which is close to their thermodynamic limit (1.23 V) [4, 6, 7]. This is the main reason to hinder their further development although the ECs with aqueous electrolytes offers a number of benefits such as their non-flammability, low toxicity and environmental impact, ease of maintenance, cost effectiveness and large specific heat capacity [2, 6]. The high heat capacity is important since high current induces a thermal effect within the system and this is directly related with the safety issue as well as the performance of the device. For these reasons, there is a great potential for the aqueous electrolytes in ECs and this has been reported in many literatures [1, 2, 8-11]. Especially, neutral aqueous electrolytes have shown many promising results owing to their wider potential windows (hydrogen overpotential which exceed the thermodynamic limit) in comparison to acidic and alkaline aqueous electrolytes [1, 2, 12, 13].

Although their electrochemical windows are still narrower than that of organic solvents, the energy capacity of the aqueous ECs would be compensated by their relatively higher specific capacitances in the aforementioned electrolytes. Generally speaking, the double layer distance 'd' between solid electrode and ions is shorter using aqueous electrolytes than organic solvents. In this chapter, the reasons of selecting neutral aqueous electrolytes for the ECs, rather than acidic or basic electrolytes, are explained by investigating their potential windows, sizes of anions and cations and effect of molar concentrations and temperatures. Previous researchers had studied one or two of these factors [14], but not yet in a comprehensive manner on the same system.

4.1. STUDY OF AQUEOUS ELECTROLYTES

4.1.1. ACIDIC, NEUTRAL AND BASIC AQUEOUS ELECTROLYTES

Traditionally, the majority of research focus in water-based ECs is based on either acidic or basic electrolytes because popular electrode materials such as carbons, manganese oxides and ruthenium oxides show higher capacitance in these electrolytes. When calculating energy capacity of ECs, the capacitance value, which differs on various conditions, is surely one of the key factors. Therefore, it is crucial to maximise the capacitance of ECs by selecting the right electrode materials and electrolytes. Conventionally, the acidic and basic electrolytes were believed to be more suitable than neutral electrolytes because they often offer higher capacitance than using carbon materials. However, it becomes more complex to choose the ideal aqueous electrolytes when considering an operating voltage which is the other key factor determining the energy capacity of ECs. Some

experimental data are presented to compare the different capacitive performances using various electrolytes.

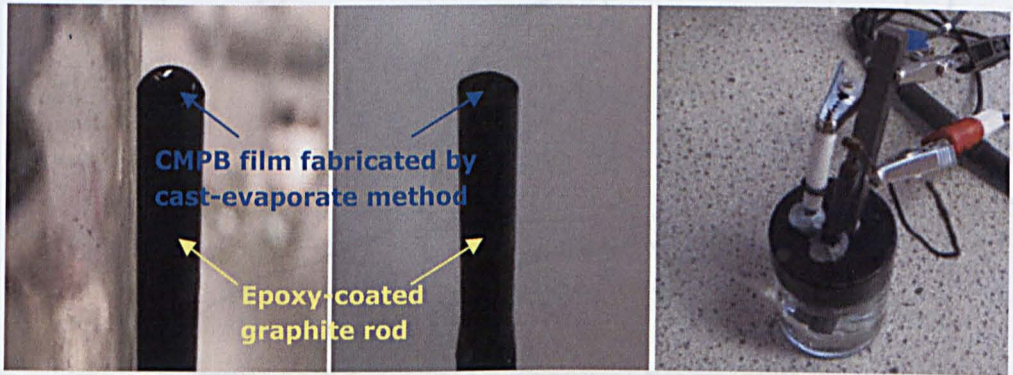


Figure 4.1 Images of cast-evaporation electrode-film preparation and the three-electrode cell for electrochemical analysis; CMPB (Cabot monarch 1300 pigment black)

Figure 4.1 shows the images of the preparation of the cast electrode on to the graphite working electrode and the three-electrode system for the material examination in terms of electrochemical methods. Briefly, Cabot monarch 1300 pigment black (CMPB) were mixed with water and 5 wt% PTFE as a binder was added into the carbon-water solution. The solution was then placed in the sonication bath for 15 minutes to disperse the carbon powder and the PTFE properly in water. After sonication, the solution is assumed to be homogeneous. The desired amounts of the solution were taken using a micropipette (50 μl in the case of Figure 4.1) and applied on to the surface of the working electrode (the working electrode should be polished and rinsed before use). After the solution had dried off, a thin CMPB electrode film was generated for the electrochemical tests.

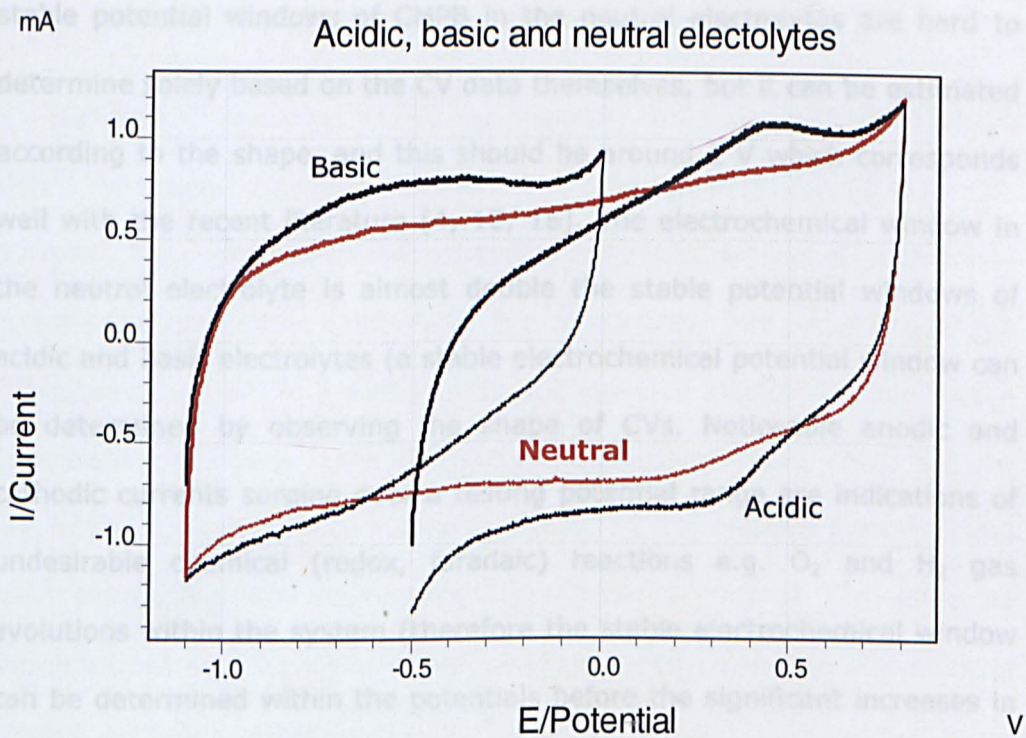


Figure 4.2 Determination of electrochemical windows (CMPB electrode in three different pH electrolytes; 3 M H_2SO_4 , 3 M KCl, 3 M NaOH)

Figure 4.2 shows a carbon film's current response over the different potential ranges in three different electrolytes. As expected, the vertical width of CVs (current response level) in acidic or basic electrolytes, which corresponds to the amount of charge 'Q' and hence capacitance, are slightly wider than that with the neutral electrolyte. This is due to the smaller sizes of ions, e.g. H^+ in acidic electrolyte and OH^- in basic electrolyte. However, their horizontal windows (potential ranges) are restricted to around 1 V and this is the reason that water-based ECs are considered to display significantly lower energy than ECs with organic electrolytes [4, 6, 15]. Conversely, the carbon electrode with neutral electrolytes shows significantly wider potential windows while its capacitance is quite comparable to the other two. The electrochemically

stable potential windows of CMPB in the neutral electrolytes are hard to determine solely based on the CV data themselves, but it can be estimated according to the shape, and this should be around 2 V which corresponds well with the recent literature [4, 12, 16]. The electrochemical window in the neutral electrolyte is almost double the stable potential windows of acidic and basic electrolytes (a stable electrochemical potential window can be determined by observing the shape of CVs. Noticeable anodic and cathodic currents surging over a testing potential range are indications of undesirable chemical (redox, faradaic) reactions e.g. O₂ and H₂ gas evolutions within the system (therefore the stable electrochemical window can be determined within the potentials before the significant increases in current). This is surely exciting because the maximum energy capacity of ECs in neutral electrolytes would be theoretically four times higher than one with acidic or basic electrolytes based on $E = 1/2 CU^2$. More accurate determinations of the potential windows and enhanced energy of the water-based systems will be discussed in Chapter 5.

4.1.2. EFFECT OF IONIC SIZE, CONCENTRATION AND TEMPERATURE

The advantages of using neutral aqueous electrolytes have been reviewed. However, there are a number of neutral aqueous electrolytes and each of them would give different results due to a number of possible combinations of anions and cations, concentrations and temperature. In this section, the results of different neutral aqueous electrolytes in terms of the hydrated ionic sizes and of concentrations and temperature will be presented.

- Study of different cations (Li^+ , Na^+ , K^+)

Li^+ , Na^+ and K^+ are most widely used cations combining with Cl^- or SO_4^{2-} anions as neutral aqueous electrolytes in this research area [8, 11, 12]. However, their effects on electrochemical behaviour are not as intensively investigated as organic electrolytes due to currently low popularity of the water-based system in industry. Although aqueous electrolytes are known to possess remarkably faster diffusivity and migration rates, which are the key factors for charge accumulation process [17-19], various performances result from using different ions and this will be investigated. This would be beneficial not only to water-based systems, but also to the ECs utilising organic solvents or ionic liquids.

To investigate the ion size effect on the capacitive behaviour of the CMPB electrode, cyclic voltammograms (CVs) were recorded in different aqueous electrolytes with either changing the cations with the same anion, or changing the anion with the same cation. To examine the cation effect, Cl^- was chosen to be the common anion due to its high solubility in water. For example the maximum solubility of K_2SO_4 in water is only around 0.6 M at room temperature [20]. The results of three different neutral electrolytes are presented in terms of their effect on current responses in Figure 4.3. It was expected that LiCl would give the highest current response due to its smallest crystal size. However, Figure 4.3 demonstrates an opposite result. For the alkali metal ions, the crystal ionic radii are K^+ (0.133 nm), Na^+ (0.095 nm) and Li^+ (0.060 nm) [21, 22, 23]. However, their hydrated radii are in the reverse order once they are dissolved in water.

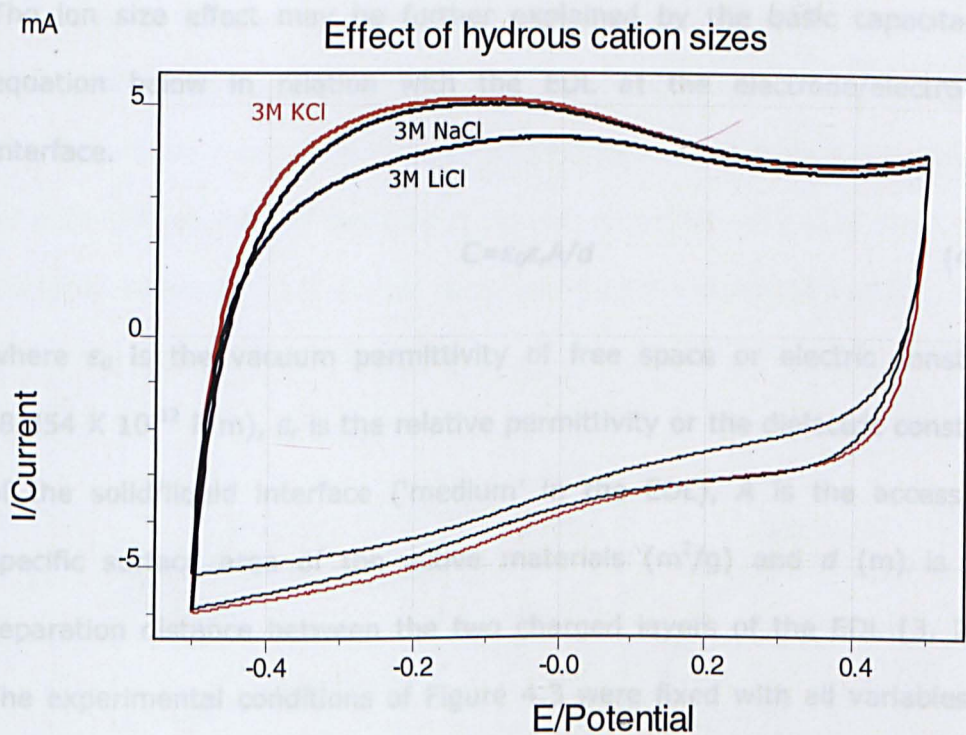


Figure 4.3 Current responses of CMPB electrode upon the potential ranges of -0.5 V to +0.5 V at 200 mV/s (3M LiCl, NaCl, KCl)

The metal ions are surrounded by hydrated shells when dissolved in water and the size of hydration radii for the alkali metal ions changes to $K^+(aq)$ (0.331 nm), $Na^+(aq)$ (0.358 nm) and $Li^+(aq)$ (0.382 nm) which is in a reverse order to that of the crystal ionic radii [21, 22, 23]. This can explain the capacitive behaviour of the CMPB in the three different electrolytes. When ions travel around in water, they travel with their hydrated shells. The actual sizes of cations when considering diffusion and migration process within electrolytes should be the hydrated ionic radius rather than the crystal ionic radius [21]. Therefore, the highest capacitance of the single electrode is observed in 3 M KCl due to $K^+(aq)$ having the smallest hydrated ionic radius.

The ion size effect may be further explained by the basic capacitance equation below in relation with the EDL at the electrode/electrolyte interface.

$$C = \epsilon_0 \epsilon_r A / d \quad (4.1)$$

where ϵ_0 is the vacuum permittivity of free space or electric constant (8.854×10^{-12} F/m), ϵ_r is the relative permittivity or the dielectric constant of the solid/liquid interface ('medium' in the EDL), A is the accessible specific surface area of the active materials (m^2/g) and d (m) is the separation distance between the two charged layers of the EDL [3, 24]. The experimental conditions of Figure 4.3 were fixed with all variables of Equation 4.1, except for d value. The smallest hydrated $\text{K}^+(\text{aq})$ cations may allow for the highest density of ions to form double layer at the solid/liquid interface and the shortest double layer distance ' d ' between negatively charged carbon and $\text{K}^+(\text{aq})$ may also contribute to the highest capacitance.

The sizes of hydrated cations are expected to influence their diffusivity and migration rate within the carbon structures [17, 18]. Accordingly, current responses of the CMPB carbon film in the three-electrode cell were examined at different scan rates from 50 to 1000 mV/s. The results are shown in Figure 4.4. Specific capacitance of the carbon electrode does not show much difference at the relatively slow scan rates (50 mV/s). However, the difference amongst the three electrolytes becomes greater as the scan rate increases and the biggest difference is observed at 1000 mV/s. This is understandable because the difference in ion sizes does not play a significant role at slow rates where the ions are provided a relatively longer time for diffusion and migration. Therefore, there is not much difference in specific capacitance between bigger and smaller cations. Conversely, the

diffusivity and migration speed play a crucial role to determine the shape of the CV at the relatively fast rates. At the extremely fast rate of 1000 mV/s, the cations are given a significantly short time scale to build a certain level of potential, so most of the charge separation occurs very near the carbon surfaces where ion can access relatively easier and this process is likely governed by the diffusion process.

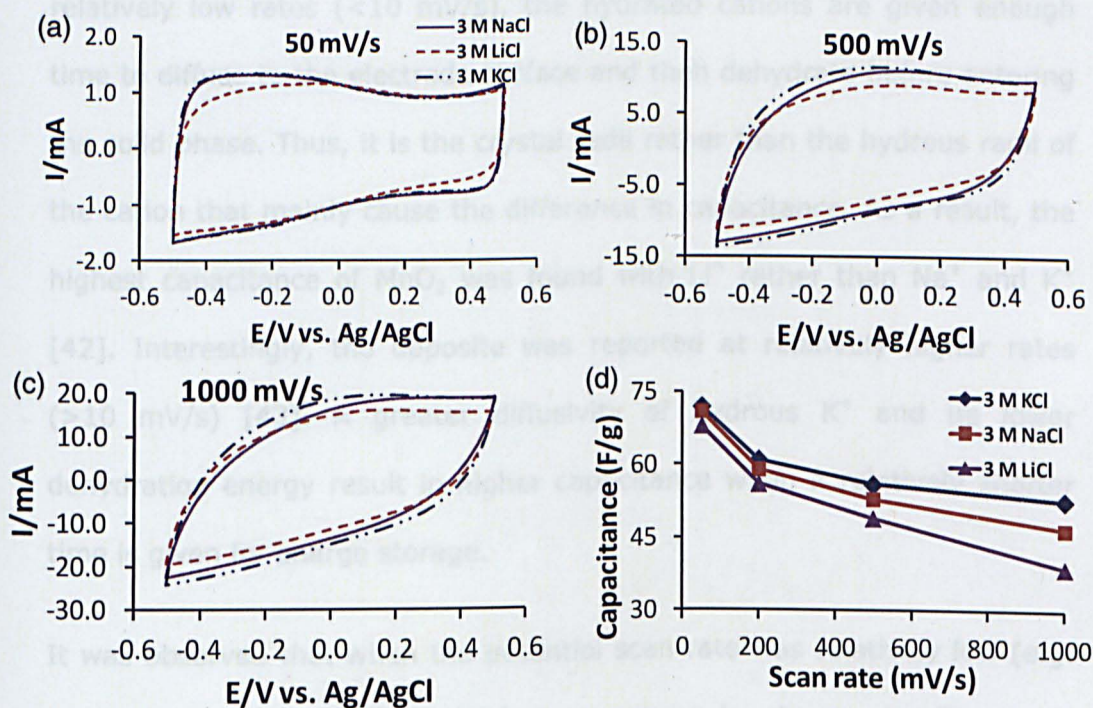


Figure 4.4 Effect of hydrated cation sizes on rate performances; (a-c) CVs of the CMPB electrode recorded at different scan rates in 3.0 M aqueous solutions of NaCl (solid line), LiCl (dashed line) and KCl (dot-dashed line). (d) Rate performance plots derived from the CVs. CMPB loading: 380 μg .

However, this trend may not be applicable to other materials showing pseudo-capacitance such as transition metal oxides (TMOs) and conducting polymers which are widely investigated for the positive electrode materials

[25-40]. Unlike carbons which offer electric double layer (EDL) capacitance, TMOs such as MnO_2 are based on the so called pseudo-capacitance resulting from redox change in the material, and the accompanying intercalation/depletion of protons and other alkali cations, e.g. Li^+ , Na^+ and K^+ . Although protons play the predominant role (>60%) [41], the alkali cations also contribute to the pseudo-capacitance. Before intercalation, the water molecules of the hydrous cations need to be removed [42]. At relatively low rates (<10 mV/s), the hydrated cations are given enough time to diffuse to the electrode surface and then dehydrate before entering the solid phase. Thus, it is the crystal radii rather than the hydrous radii of the cation that mainly cause the difference in capacitance. As a result, the highest capacitance of MnO_2 was found with Li^+ rather than Na^+ and K^+ [42]. Interestingly, the opposite was reported at relatively higher rates (>10 mV/s) [43]. A greater diffusivity of hydrous K^+ and its lower dehydration energy result in higher capacitance when a relatively shorter time is given for charge storage.

It was observed that when the potential scan rate was relatively low (e.g. 50 mV/s) the CVs exhibited satisfactory rectangular shapes, see Figure 4.4 (a), in agreement with the behaviour of a capacitor (or capacitive behaviour). In the same potential range, a lower scan rate corresponds to a longer time for both the fast (near the electrode surface and in large pores) and slow (within small pores) transport of ions which can then access (or depart from) more active sites in the carbon. This means a more complete charge accumulation (or depletion) in the electrode, and hence the more capacitive behaviour (rectangular CVs). On the contrary, increasing the scan rate shortens the time for ion transport, resulting in incomplete charge accumulation (or depletion) and hence poorer capacitive behaviour as shown by the oval CVs in Figure 4.4 (c). Nonetheless, the

other and more important cause for the fast scan distortion is the inevitable electrode and electrolyte resistance (R_{el}). When a current (I) passes through R_{el} , a potential loss occurs ($E_{loss} = IR_{el}$). This causes the actual or useful potential (E) on the electrode to be smaller than that applied externally (E_{app}), i.e. $E = E_{app} - E_{loss}$. As in any capacitor, the current increases with the scan rate and this leads to a higher potential loss and hence a smaller potential to drive the ions into or from the electrode. This also leads to incomplete charge accumulation (or depletion), and hence the distortion on the CV traces.

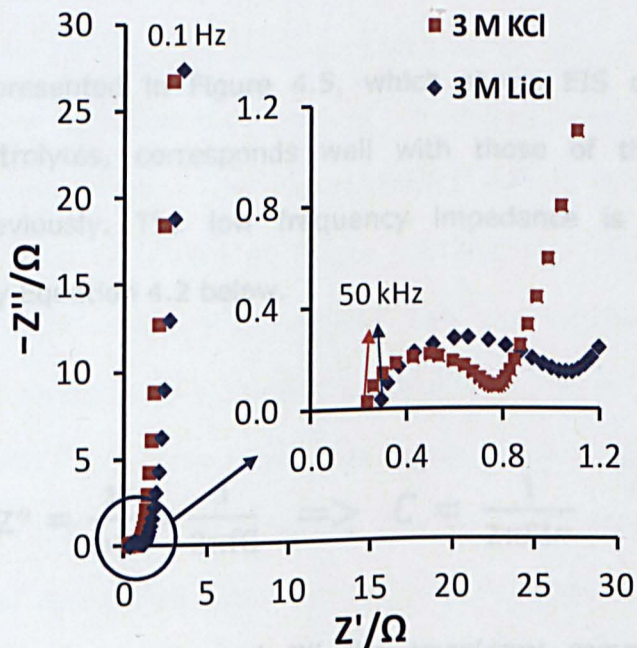


Figure 4.5 AC impedance plots of the CMPB electrode in the indicated aqueous electrolytes; bias potential 0 V vs. Ag/AgCl; CMPB loading 830 μg .

Electrochemical impedance spectrometry (EIS) is a useful technique for analysing both resistive and capacitive properties [3, 44]. It can differentiate different sources of resistance via simple graphical features on the ac impedance plot (also known as the Nyquist plot), as exemplified in

Figure 4.5. The equivalent series resistance (ESR) is the intercept of the plot at the real impedance (Z') axis, whilst the charge transfer resistance (CTR) is reflected by the radius of the semicircle at relatively high frequencies. Capacitive behaviour is featured by the nearly vertical straight line at low frequencies. Note that diffusion related impedance is usually reflected by a 45° line between the semicircle and the vertical line, but this feature is not very clear in Figure 4.5. The reason is likely that in the thin CMPB film, diffusion impedance covered a frequency range that was too narrow to be seen clearly on the impedance plots. Nevertheless, the LiCl plot in the inset of Figure 4.5 still shows a wider joining section between the semicircle and the vertical line, implying greater diffusion impedance.

The results presented in Figure 4.5, which shows EIS data with two different electrolytes, corresponds well with those of the CV results discussed previously. The low frequency impedance is correlated to capacitance by Equation 4.2 below.

$$Z'' = \frac{1}{\omega C} = \frac{1}{2\pi f C} \Rightarrow C = \frac{1}{2\pi f Z''} \quad (4.2)$$

where f is the frequency and Z'' the imaginary component of the impedance. As expected, the CMPB electrode showed lower Z'' values along the vertical section, and hence higher capacitance in KCl than in LiCl. The lowest frequency in the plot was set at 0.10 Hz which is sufficiently low to solely witness the capacitive behaviour of the carbon electrode.

As expected, in KCl the electrode shows higher capacitance than in LiCl, and this can be observed from the Z'' value at the lowest frequency. A smaller hydrated ionic size may enable the formation of a more densely

packed charge accumulation [3, 24]. The lowest frequency in the plot was set to be 100 mHz which would still be a high frequency to solely see capacitive behaviour, and so a difference in capacitance would be greater if measured at frequencies lower than 100 mHz. Regarding resistance, the carbon electrode in LiCl shows higher resistance overall, i.e. ESR, charge transfer resistance and also diffusion resistance (45° phase angle shown in the mid-frequencies). The presence of ESR is mainly due to two factors, namely electronic and ionic resistances [19]. The electronic resistance is known to be influenced by the intrinsic resistance of the carbon electrode, contact resistance between carbon particles and carbon particles to the current collectors. The ionic resistance is due to the electrolyte in both pores and bulk phases. The testing conditions for the prepared carbon electrodes were identical e.g. amount of loading, geometric area of electrode, current collector and so on. Therefore, any difference in ESR (0.23Ω and 0.29Ω) shown in Figure 4.5 is highly likely due to the difference in ionic resistances between the two cations. Hence, the hydrated ionic conductivity between the two electrolytes is $\text{KCl} > \text{LiCl}$. The larger hydrated $\text{Li}^+(\text{aq})$ (0.382 nm) may result in 20 % higher ESR than that of $\text{K}^+(\text{aq})$ (0.331 nm). As expected, there is a noticeable difference in charge transfer resistances which are indicated by semi-circles (although the shape of the plot is not a complete semi-circle due to a non-subjected inductance plot (positive Z''); these arc-shaped plot will be referred to as semi-circles throughout this thesis). The resistance is known to be related to charge transfer at the interfaces between the electrode materials and electrolytes, the current collectors and the electrode materials [3]. Therefore it is understandable to observe this resistance which may result from the possible surface group on carbon surfaces and also the possible oxide layers on the current collectors [45]. However, the significant

difference in charge transfer resistance can be explained by size difference between the hydrated $K^+(aq)$ and $Li^+(aq)$ ions entering/leaving the pores in the carbon, considering that the same metal plates and carbon electrode material were used. This resistance may be also influenced by the ionic dynamic dispersion within the pores [19]. Due to the rate of hydrated ion transport in the deeper pores, LiCl electrolyte may show higher charge transfer (ion transport) resistance. The result also demonstrates information about diffusion resistance and this is depicted as the x-axis length (z') of the 45° section of the plots. Accordingly, the size of the hydrated ions influences diffusivities of the cations ($K^+(aq) > Li^+(aq)$).

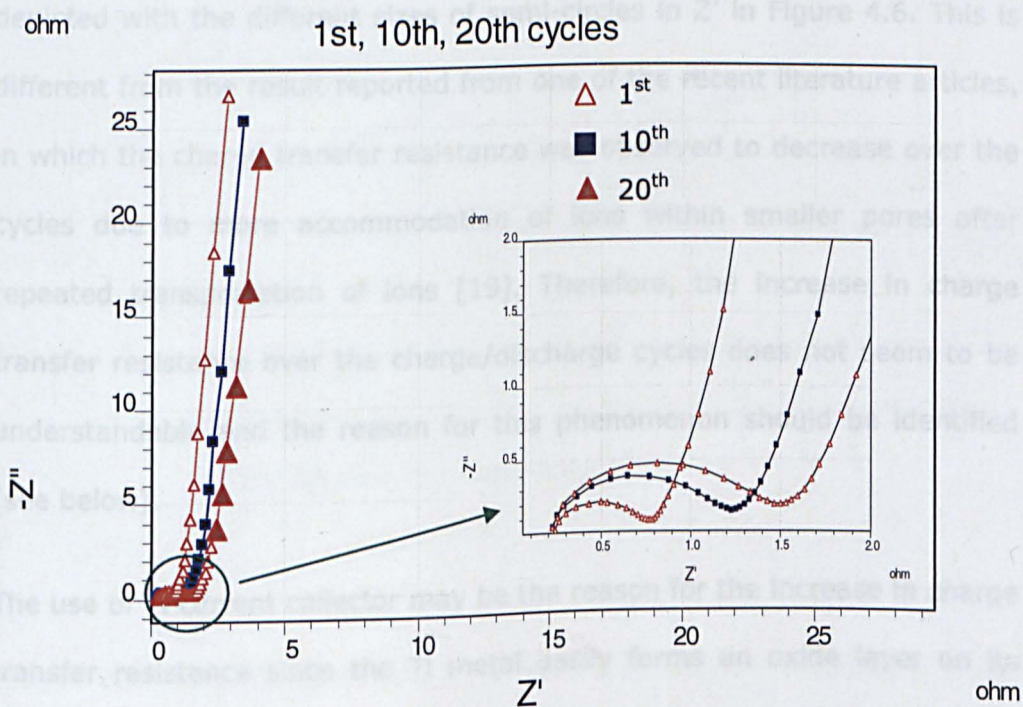


Figure 4.6 AC impedance (50 kHz to 100 mHz); 1st, 10th and 20th cycles at 0 V in 3 M KCl

Figure 4.6 presents AC impedance data after different numbers of charging-discharging cycles (1, 10 and 20) to see how the resistance and capacitance vary upon cycling. Regarding the capacitance which is mainly shown at lower frequencies, it increases with more cycles and this is evidenced by the lower imaginary impedance value ($-Z''$) with the plot of greater cycle numbers. This indicates that more active sites within the carbon structures can be accessed by ions and hence more utilisation as the cycle number increases. ESR of the constructed cell using 3 M KCl does not show much change over the cycles, indicating that there is no change of intrinsic properties in metal plates, electrode materials and electrolytes over the cycles. Different from ESR, noticeable change (significant increase) in charge transfer resistance over cycles can be observed and this is depicted with the different sizes of semi-circles in Z' in Figure 4.6. This is different from the result reported from one of the recent literature articles, in which the charge transfer resistance was observed to decrease over the cycles due to more accommodation of ions within smaller pores after repeated transportation of ions [19]. Therefore, the increase in charge transfer resistance over the charge/discharge cycles does not seem to be understandable and the reason for this phenomenon should be identified (see below).

The use of Ti current collector may be the reason for the increase in charge transfer resistance since the Ti metal easily forms an oxide layer on its surface. This feature is advantageous when using aqueous electrolytes because Ti prevents crack propagation (corrosion) by formation of these oxide layers. However, these oxide layers may increase the charge transfer resistance (electron transfer from one phase to the other) at the interface between the metal plate and the carbon electrode. Relevant experiments were carried out and the supporting evidence is presented later.

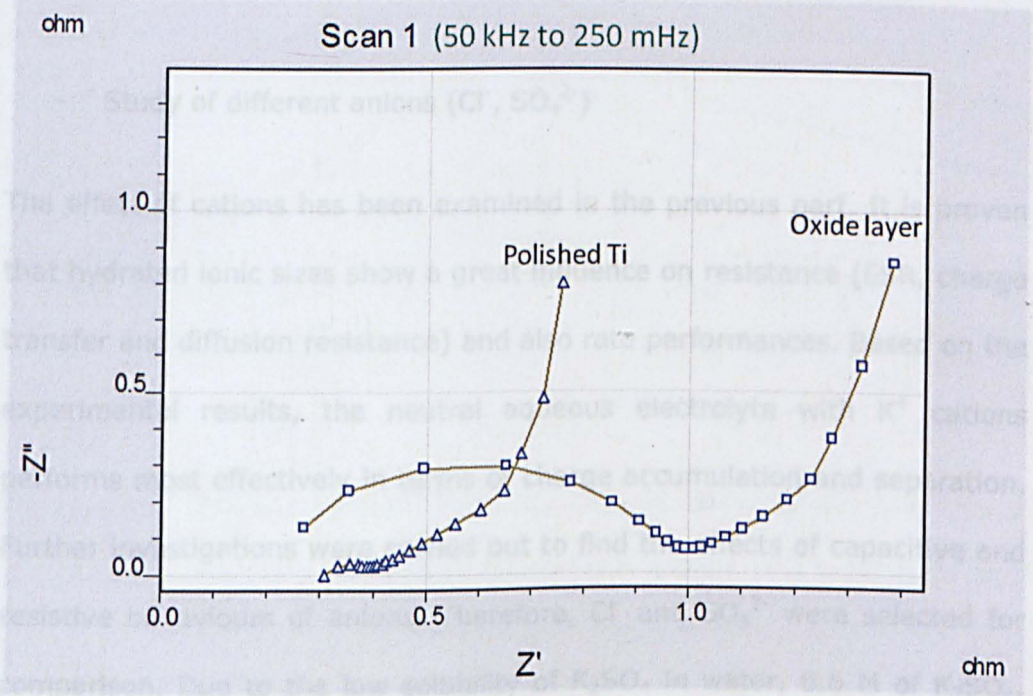
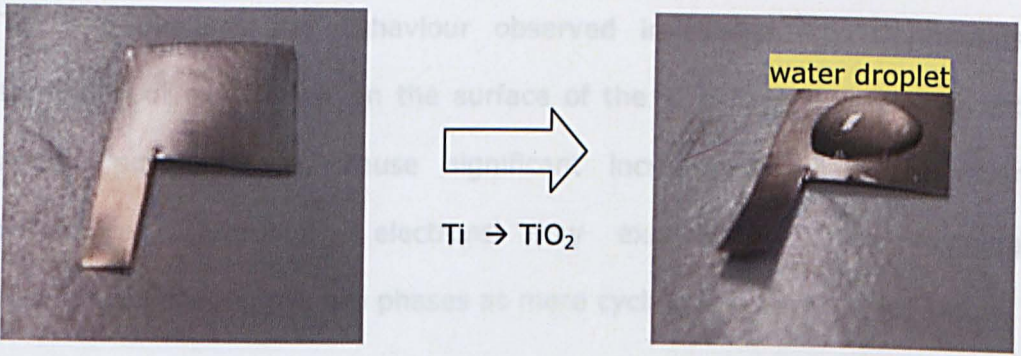


Figure 4.7 Possible effects of oxide layers on the charge transfer resistance; water droplet was placed on the surface of the Ti current collector and the EIS data demonstrate the difference

To see the effect of the oxide layers on charge transfer resistance, water drops were applied on the surface of the polished Ti metal plates and the water was dried in the oven (60°C). AC impedance results of the polished plates and the water applied plates show noticeably different sizes of semi-circles as shown in Figure 4.7. There is a dramatic increase in charge transfer resistance with the water-evaporated plates and it is observed that almost 8 times higher in charge transfer resistance relative to the polished

Ti. This explains the behaviour observed in Figure 4.6. Continuous formation of oxide layer on the surface of the Ti plates near the highest anodic potential may cause significant increase in charge transfer resistance. Accordingly, electrons may experience higher hopping resistance between the two phases as more cycling tests are carried out.

- Study of different anions (Cl^- , SO_4^{2-})

The effect of cations has been examined in the previous part. It is proven that hydrated ionic sizes show a great influence on resistance (ESR, charge transfer and diffusion resistance) and also rate performances. Based on the experimental results, the neutral aqueous electrolyte with K^+ cations performs most effectively in terms of charge accumulation and separation. Further investigations were carried out to find the effects of capacitive and resistive behaviours of anions. Therefore, Cl^- and SO_4^{2-} were selected for comparison. Due to the low solubility of K_2SO_4 in water, 0.6 M of K_2SO_4 , which is close to the highest molar concentration at room temperature, was used for the experiment. Accordingly, 1.2 M KCl was prepared to balance the different cation charge number between the two electrolytes and hence any differences in performance should be solely owing to the anions. Relevant CV traces are shown in Figure 4.8 and active material in KCl shows higher capacitances in the all tested scan rates from 50 to 500 mV/s. A relatively narrow electrochemical window (as mentioned previously, the stable electrochemical window of carbon material in neutral aqueous electrolytes can be higher than 2 V), which was 0.9 V (-0.5 to 0.4 V vs. Ag/AgCl), was applied for convenience in measurement since this was not to determine the stable electrochemical window of the electrode materials and electrolytes.

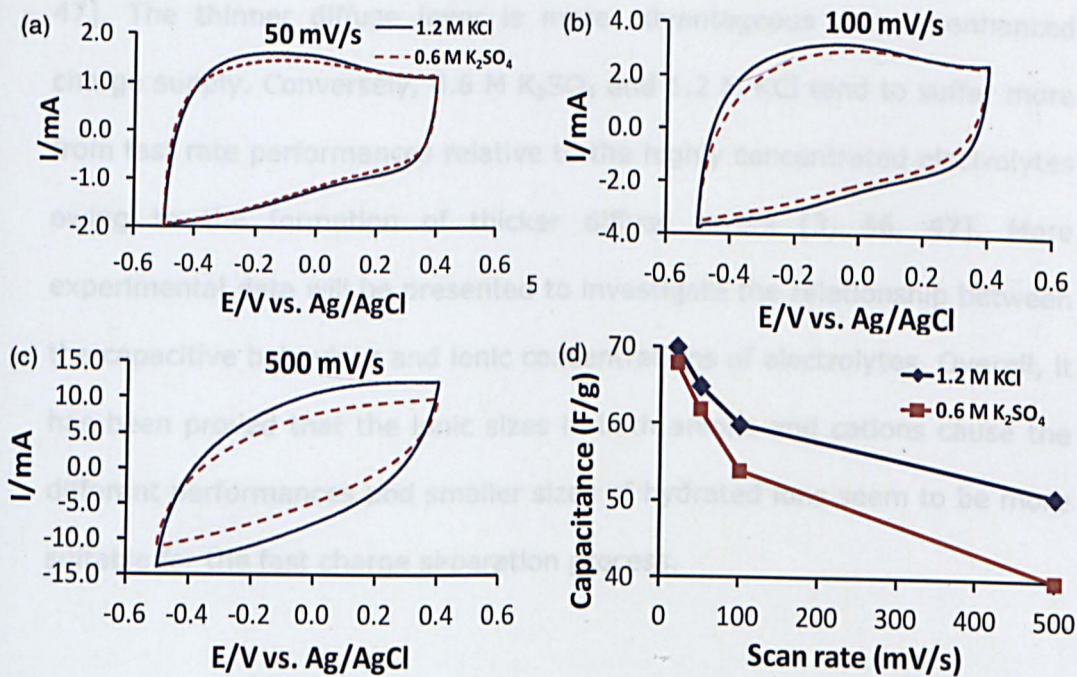


Figure 4.8 Effect of hydrated anion sizes to rate performances; (a-c) CVs of the CMPB recorded at different scan rates in 1.2 M KCl (solid line) and 0.6 M K₂SO₄ solutions. (d) Rate performance plots derived from the CVs. CMPB loading: 420 μg .

Similar to the result from cations, the size of anions also influences the material's capacitive performance. As observed in the effect of cations, different sizes between the two anions do not cause a significant change of capacitance at relatively slow rates (50 mV/s). However, the difference in capacitance between the two electrolytes gradually increases as the charging-discharging speed becomes faster and it is remarkably noticeable at the fastest rate (500 mV/s). It is worthy pointing out that the difference in rate performances due to the anions is greater than that of cations. This should be attributed to the different molar concentrations of the two experiments. Higher molar concentrations of 3 M of KCl, NaCl and LiCl may

result in relatively thinner diffuse layer within the bulk electrolyte [3, 46, 47]. The thinner diffuse layer is more advantageous due to enhanced charge supply. Conversely, 0.6 M K_2SO_4 and 1.2 M KCl tend to suffer more from fast rate performances relative to the highly concentrated electrolytes owing to the formation of thicker diffuse layers [3, 46, 47]. More experimental data will be presented to investigate the relationship between the capacitive behaviour and ionic concentrations of electrolytes. Overall, it has been proved that the ionic sizes in both anions and cations cause the different performances and smaller sizes of hydrated ions seem to be more suitable for the fast charge separation process.

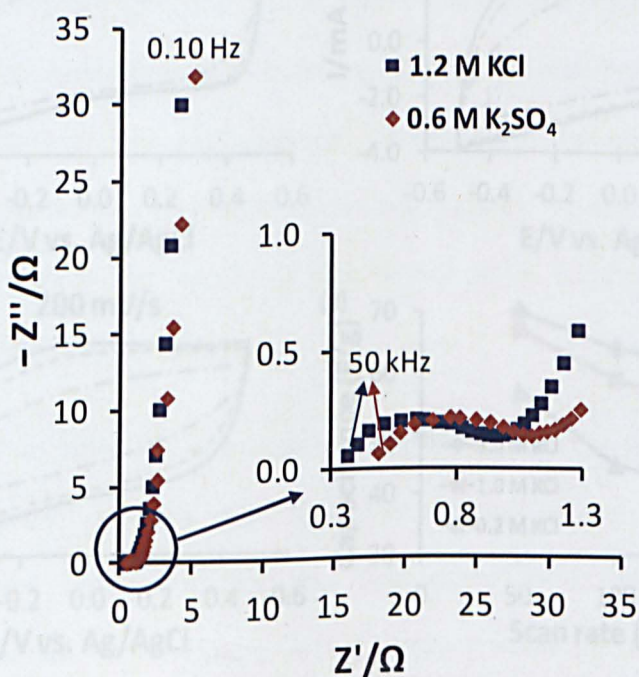


Figure 4.9 AC impedance plots recorded in the indicated electrolytes; bias potential 0 V vs. Ag/AgCl; frequency range 50 kHz to 100 mHz; CMPB loading 780 μg .

AC impedance results shown in Figure 4.9 also reveal that different anions result in distinctive ionic resistances and hence conductivities. The results show good agreement with the previous data from cations. Bigger SO_4^{2-} anions display lower capacitance and higher resistance relative to smaller Cl^- anions. This is understandable since more energy is required to move the bigger anions.

- Effect of molar concentrations and temperature

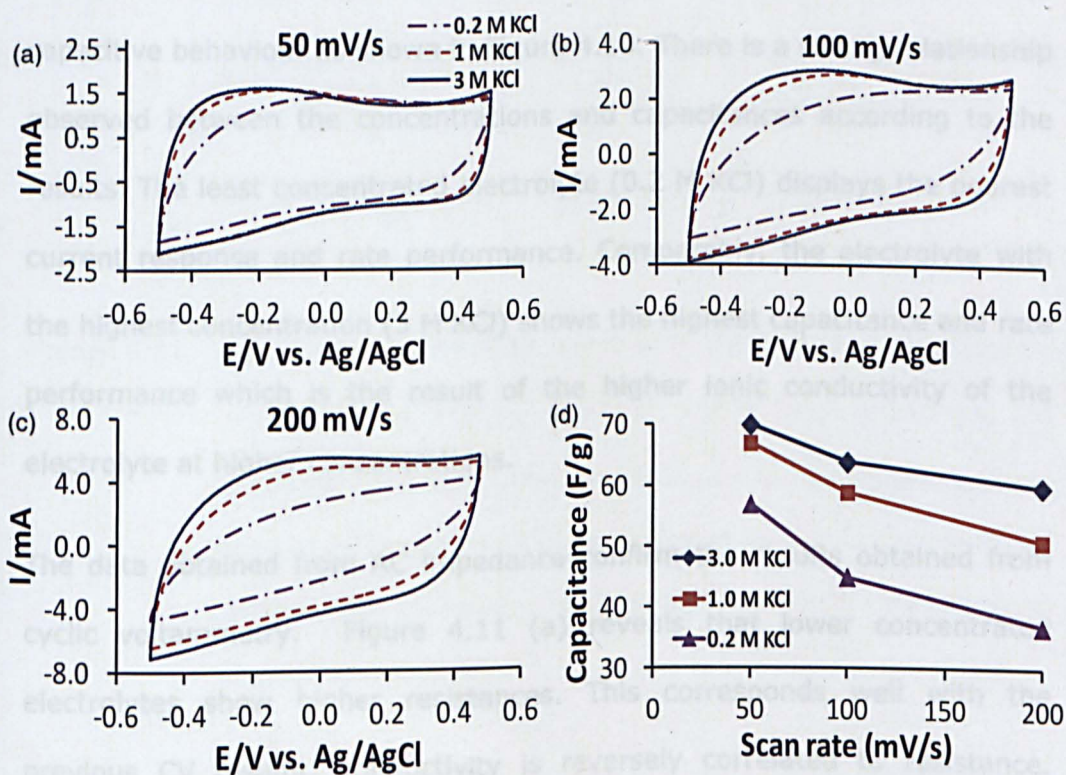


Figure 4.10 Effect of molar concentration (0.2 M, 1 M and 3 M KCl) on capacitive behaviour and rate performance; (a-c) CV traces for CMPB recorded at different scan rates in aqueous KCl solutions of the indicated concentrations. (d) Rate performance plots derived from the CV traces. CMPB loading: 400 μg .

The charge separation at the interface between fine carbon particles and electrolytes strongly depends on mass transfer, namely diffusion and migration. Migration occurs due to the potential gradient present along the depth of the porous structures in which charges cannot accumulate at the same rate because of non-uniform distribution of ionic resistance. Diffusion is a dispersion process owing to a concentration gradient, and depends on several factors e.g. concentrations and size of ions, temperature, porous structure and so on. In this section, other experimental conditions are fixed to study the concentration effect on the CMPB performance.

Different molar concentrations of the electrolyte result in differences in capacitive behaviour as shown in Figure 4.10. There is a strong relationship observed between the concentrations and capacitances according to the results. The least concentrated electrolyte (0.2 M KCl) displays the poorest current response and rate performance. Comparably, the electrolyte with the highest concentration (3 M KCl) shows the highest capacitance and rate performance which is the result of the higher ionic conductivity of the electrolyte at higher concentrations.

The data obtained from AC impedance confirm the results obtained from cyclic voltammetry. Figure 4.11 (a) reveals that lower concentrated electrolytes show higher resistances. This corresponds well with the previous CV results. Conductivity is reversely correlated to resistance. Therefore, the 3 M KCl which shows the highest ionic conductivity displays the lowest ESR. In addition, the charge transfer resistance, which is depicted by the semi circles, seems to be influenced by the concentrations. Dynamics of ions within pores may be relevant to the resistance, and both diffusion and migration within the small pores should be slower with the less concentrated electrolyte. The capacitance increase with concentration

may be explained by more ions being available in a more concentrated solution to accumulate at the CMPB/electrolyte inter-face. High concentrations of ions can also decrease the ESR, and promote dynamics of ion within the pores via both diffusion and migration.

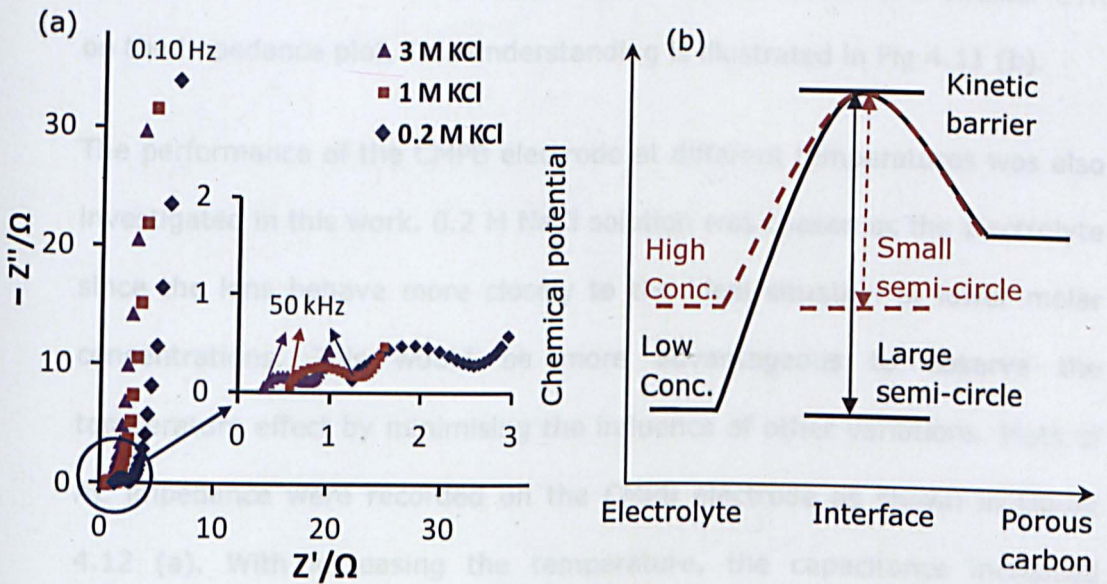


Figure 4.11 (a) AC impedance plots recorded in the indicated electrolytes. bias potential 0 V vs. Ag/AgCl; CMPB loading 780 μg , (b) schematic illustration of the kinetic barrier for ion transfer crossing the carbon/electrolyte interface in relation to high or low electrolyte concentration producing a small or large semi-circle, respectively, in the AC impedance plot.

The inset of Figure 4.11 (a) also shows that the CTR becomes smaller with increasing the ion concentration. As explained previously, because these impedance plots were measured on the same CMPB electrode, the CTR should have not been related with electron transfer at the electrode/CMPB interface but reflected the kinetic barrier to ion transfer crossing the CMPB/electrolyte interface. Considering that the ions in the pores of the

carbon had the same activity (chemical potential), and that the kinetic barrier remained unchanged, increasing the ion activity (smaller hydrated ion size, higher concentration, and/or higher temperature) would give a higher chemical potential of the ions in the electrolyte. Thus, the relative chemical potential difference between the ions in the solution and that of the kinetic barrier was reduced, which can be translated to a smaller CTR on the impedance plot. This understanding is illustrated in Fig 4.11 (b).

The performance of the CMPB electrode at different temperatures was also investigated in this work. 0.2 M NaCl solution was chosen as the electrolyte since the ions behave more closely to the ideal situation at lower molar concentrations. This would be more advantageous to observe the temperature effect by minimising the influence of other variations. Plots of AC impedance were recorded on the CMPB electrode as shown in Figure 4.12 (a). With increasing the temperature, the capacitance increased slightly, but both the ESR and CTR (inset of Figure 4.12 (a)) became noticeably smaller. The results can be seen in Figure 4.12 (a) and are summarised in Table 4.1.

Table 4.1. Temperature influence on the resistive and capacitive features of a CMPB electrode.

		0 °C	30 °C	60 °C
Resistive features (Ω)	ESR ^a	2.57	1.32	0.33
	CTR ^b	1.14	0.52	0.37
	Diffusion resistance ^c	0.73	0.26	0.28
Capacitive feature (Ω)	-Z'' at 100 mHz ^a	32.1	35.2	36.3

^a Measured directly from the impedance plots.

^b Obtained by fitting the impedance data with IviumSoft.

^c Visual estimation from the impedance plots.

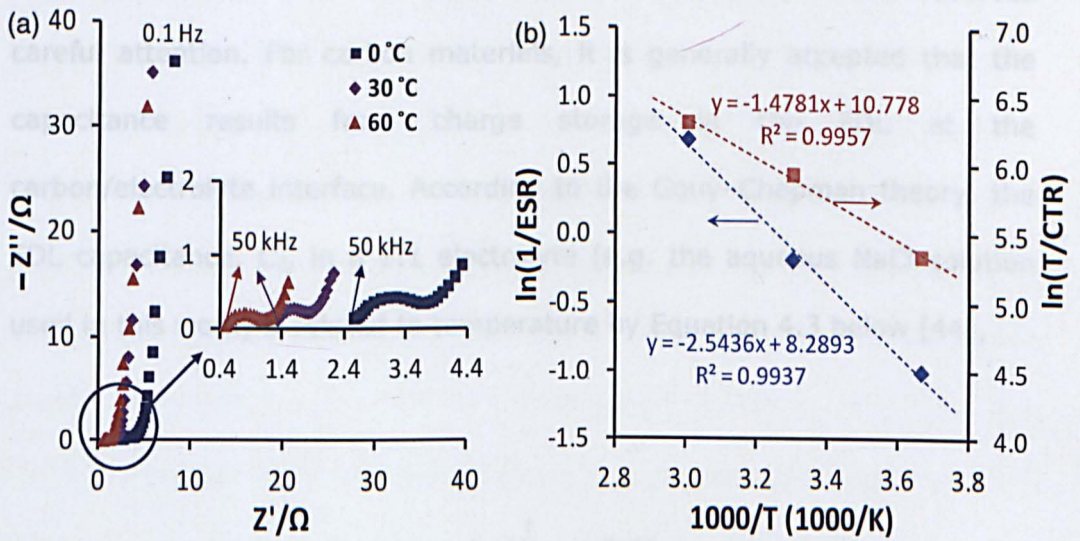


Figure 4.12 (a) AC impedance plots recorded in 0.2 M NaCl aqueous solution at the indicated temperatures; bias potential 0 V vs. Ag/AgCl; frequency range 50 kHz to 100 mHz ; CMPB loading 800 μg ; (b) variation of ESR (diamond) and CTR (square) with temperature in the form of Arrhenius (ESR) and modified Arrhenius (CTR) plots.

The smaller values of ESR and CTR are expected to have resulted from improved ion diffusivity and kinetics, respectively, at higher temperatures. To verify this expectation, Figure 4.12 (b) plots $\ln(1/ESR)$ vs. $1000/T$ [48], and $\ln(T/CTR)$ vs. $1000/T$ [49]. It can be seen that satisfactory linear correlations can be established in both cases, confirming the ESR and CTR to be related to thermally activated behaviour of ions. Apparently due to the low molar concentration, the impedance plots recorded in 0.2 M NaCl presented more visible joining sections between the semicircle and the vertical line. The ranges of Z' values in the diffusion section were visually estimated as given in Table 4.1, suggesting larger diffusion resistances at lower temperatures. However, due to the low accuracy of visual estimation,

no further effort was made to elaborate the diffusion resistance data. The capacitance increase of the CMPB electrode with temperature deserves careful attention. For carbon materials, it is generally accepted that the capacitance results from charge storage in the EDL at the carbon/electrolyte interface. According to the Gouy-Chapman theory, the EDL capacitance, C_d , in a 1:1 electrolyte (e.g. the aqueous NaCl solution used in this work) is related to temperature by Equation 4.3 below [44],

$$C_d = \left(\frac{\alpha}{T}\right)^{\frac{1}{2}} \cosh\left(\frac{\beta}{T}\right) \quad (4.3)$$

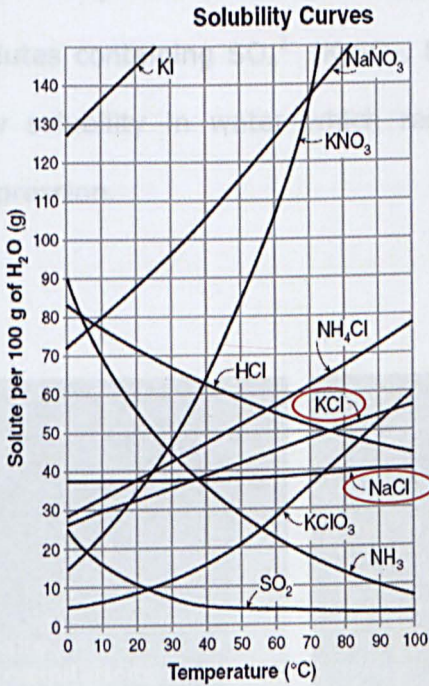
where α is a function of the concentration and the dielectric property of the electrolyte, and β depends on the electrode potential.

It is known that the dielectric constant of water decreases with increasing temperature [50], which reduces the α value. Thus, the first term in Equation 4.3 should always decrease with temperature. On the other hand, at a given electrode potential, the cosh term in Equation 4.3 also declines with increasing temperature. Thus, the observed capacitance increase with temperature in this work could have resulted from a mechanism that is different from the Gouy-Chapman theory. In fact, the capacitance increase with temperature was previously observed in carbon based supercapacitors [51, 52], although these researchers did not investigate the response of individual electrodes. Similar phenomena were also reported in ionic liquids and attributed to increased dissociation of complex ions [53]. This attribution is obviously not applicable to the 0.2 M NaCl aqueous solution in which ions should have been well dissociated. Past efforts to identify the cause for the capacitance increase with temperature were all focused on

variables related to the electrolyte, but little attention was paid to the temperature effect on the structure of the carbon materials. The CMPB is rich in micro-pores (this can be found in Chapter 5 with SEM, TEM and BET data). However, most materials do expand at higher temperatures with the expansion coefficient, γ , being positive. Specifically, different carbon structures such as diamond, graphite and CNTs were investigated by molecular dynamic simulation. The findings show that the carbon-carbon bond length expands thermally at almost the same rate ($\gamma = 6.9 \pm 0.2 \times 10^{-6} \text{K}^{-1}$) in both diamond (sp^3 bonding) and graphite (sp^2 bonding) [54]. Thus, if a portion or all of the micro-pores may open further at higher temperatures and enable access by ions, the observed larger capacitance can be accounted for. This hypothesis seems to be logical and reasonable, although further experimental investigation is needed for confirmation.

The effects of concentration and temperature on capacitive and resistive behaviours were examined. Higher concentration and temperature are more advantageous to obtain higher capacitance and lower resistance. Although aqueous electrolytes for ECs seem to be promising according to the results presented previously, there is an intrinsic disadvantage to discourage wider applications of water-based systems due to their narrow operating temperatures related to the freezing temperature of water. However, complementary studies of both temperature and concentration can effectively suppress the freezing temperature of water solution (salt + water). It was observed in this work that 5 M NaCl electrolytes successfully reduced the freezing temperature down to $-20 \text{ }^\circ\text{C}$, which shows a good agreement with the existing literature [55, 56].

(a)



(b)

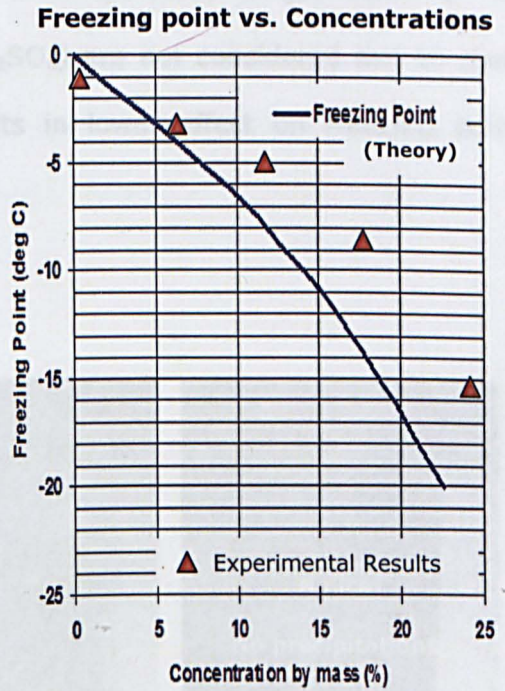


Figure 4.13 (a) Solubility plots of different solutes [55], (b) Decrease of freezing temperature upon increasing the mass concentrations of solute (salt) in water from both theoretical and experimental studies [56]

The narrow operating temperature of aqueous ECs is mainly problematic in the winter time. This problem can be resolved remarkably by taking advantage of freezing temperature depression in aqueous electrolytes. The freezing temperature of salt containing water decreases further from 0 °C as the concentration of salt in water increases and this is shown in Figure 4.13 (b). Although the KCl electrolyte shows better capacitive and resistive features than NaCl due to the smaller hydrated ion size of K⁺ than Na⁺, the NaCl electrolyte would be more suitable for the aqueous ECs operating at low temperatures (<0 °C) according to Figure 4.13 (a). The diagram shows that NaCl salts dissolve significantly more than KCl at lower temperatures. At 0 °C, maximum solubility of NaCl is about 6 M whereas KCl only

dissolves slightly higher than 3 M, and the gap of solubility between the two is expected to become bigger in temperature ranges below 0 °C. Solutes containing SO_4^{2-} (K_2SO_4 , Na_2SO_4) are not considered due to their low solubility in water which results in lower effect on freezing point depression.

Figure 4.14 shows the last image of figure 4.14. More experimental data can be found in the Table 4.2.

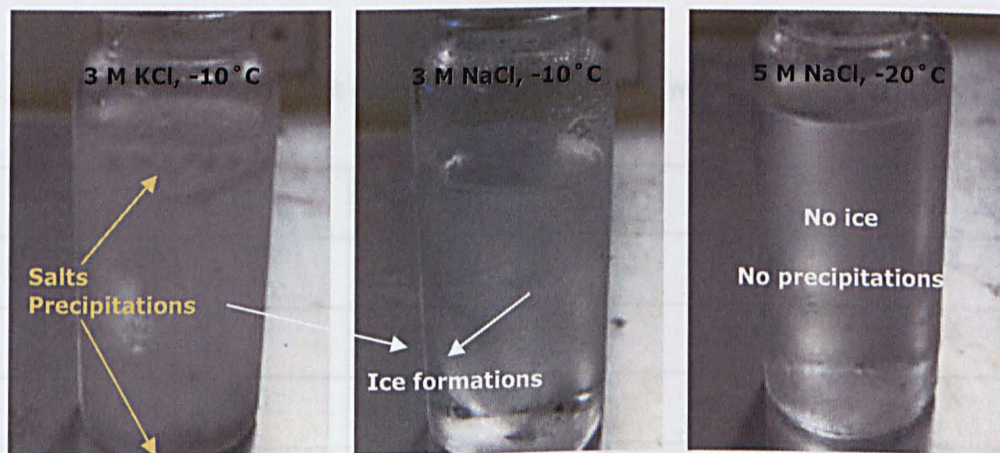


Figure 4.14 Images of different electrolytes at various temperatures

Figure 4.14 shows a few images of electrolytes at different temperatures. KCl is not an ideal electrolyte for the ECs operating at low temperature. 3 M KCl starts precipitating salt around -5 °C due to over saturation. The maximum solubility of KCl at 0 °C is slightly over 3 M and the maximum value remarkably decreases as temperature goes further below 0 °C which is described in Figure 4.13 (a). Accordingly it forms ice around -10 °C and this is significantly lower than that of theoretical value because of rapid loss of ions in the electrolyte. Conversely, 3 M NaCl does not show any precipitation at -10 °C, but it also starts forming ice. Experimentally obtained results using NaCl are plotted as red triangles along with the theoretical data [56] and this is shown in figure 4.13 (b). Theoretically, 4 M

NaCl (23 wt % by mass) should be able to reach $-20\text{ }^{\circ}\text{C}$ without phase transformation from liquid to solid. However, it started producing the ice around $-15\text{ }^{\circ}\text{C}$. This may be due to the impurities of electrolyte and dusts from the air. 5 M NaCl successfully reached down to $-20\text{ }^{\circ}\text{C}$ in liquid form and the image is shown in the last image of figure 4.14. More experimental data can be found in the Table 4.2.

Table 4.2 Freezing point depression of electrolytes with various concentrations

	$0\text{ }^{\circ}\text{C}$	$-5\text{ }^{\circ}\text{C}$	$-10\text{ }^{\circ}\text{C}$	$-15\text{ }^{\circ}\text{C}$	$-20\text{ }^{\circ}\text{C}$
0.2 M NaCl (1.2 wt%)	O	X	X	X	X
3 M KCl (22 wt %)	O	Δ	X	X	X
3 M NaCl (18 wt%)	O	O	X	X	X
4 M NaCl (24 wt%)	O	O	O	X	X
5 M NaCl (30 wt%)	O	O	O	O	O

* O: No ice formation observed
 Δ : No ice formation, but presence of precipitated salts
 X: Ice formation observed

References

1. Zhang, L. L. and Zhao, X. S., *Carbon-based materials as supercapacitor electrodes*. Chem. Soc. Rev., 2009, 38: p. 2520 – 2531
2. Simon, P. and Burke, A., *Nanostructured carbon; Double-layer capacitance and more.*, Electrochem. Soc. Interface, 2008, 17: p. 38 – 43.

3. Conway, B. E., *Electrochemical Supercapacitors: Scientific Fundamentals and Technological Applications*. 1999: Kluwer Academic/Plenum Publishers. New York.
4. Lewandowski, A., Olejniczak, A., Galinski, M. and Stepniak, I., *Performance of carbon-carbon supercapacitors based on organic, aqueous and ionic liquid electrolytes*. *J. Power Sources*, 2010. **195(17)**: p. 5814-5819.
5. Ricketts, B. W. and Ton-That, C., *Self-discharge of carbon-based supercapacitors with organic electrolytes*. *J. Power Sources*, 2000. **89(1)**: p. 64-69.
6. Burke, A., *Ultracapacitors: why, how, and where is the technology*. *J. Power Sources*, 2000. **91(1)**: p. 37-50.
7. Beck, F., Dolata, M, Grivei, E. and Probst, N., *Electrochemical supercapacitors based on industrial carbon blacks in aqueous H₂SO₄*. *J. Appl. Electrochem.*, 2001. **31(8)**: p. 845-853.
8. Hong, M. S., Lee, S. H. and Kim, S. W., *Use of KCl aqueous electrolyte for 2 V manganese oxide/activated carbon hybrid capacitor*. *Electrochem. Solid-State Lett.*, 2002. **5**: p. A227.
9. Jeong, Y. U. and Manthiram, A., *Nanocrystalline manganese oxides for electrochemical capacitors with neutral electrolytes*. *J. Electrochem. Soc.*, 2002. **149(11)**: p. A1419-A1422.
10. Long, J. W., Young, A. L. and Rolison, D. R., *Spectroelectrochemical characterization of nanostructured, mesoporous manganese oxide in aqueous electrolytes*. *J. Electrochem. Soc.*, 2003. **150(9)**: p. A1161-A1165.

11. Qu, Q., Zhang, P., Wang, B., Chen, Y., Tian, S., Wu, Y and Holze, R., *Electrochemical performance of MnO₂ nanorods in neutral aqueous electrolytes as a cathode for asymmetric supercapacitors*. *The J. Phys. Chem. C*, 2009. **113**(31): p. 14020-14027.
12. Bichat, M. P., Raymundo-Piñero, E. and Béguin, F., *High voltage supercapacitor built with seaweed carbons in neutral aqueous electrolyte*. *Carbon*, 2010. **48**(15): p. 4351-4361.
13. Khomenko, V., Raymundo-Pinero, E., Frackowiak, E. and Beguin, F., *High-voltage asymmetric supercapacitors operating in aqueous electrolyte*. *Appl. Phys. A: Mater. Sci. Proc.*, 2006. **82**(4): p. 567-573.
14. Hu, C. C. and Wang, C. C., *Effects of electrolytes and electrochemical pretreatments on the capacitive characteristics of activated carbon fabrics for supercapacitors*. *J. Power Sources*, 2004. **125**(2): p. 299-308.
15. Kötz, R. and Carlen, M., *Principles and applications of electrochemical capacitors*. *Electrochim. Acta*, 2000. **45**(15-16): p. 2483-2498.
16. Demarconnay, L., Raymundo-Pinero, E. and Béguin, F., *A symmetric carbon/carbon supercapacitor operating at 1.6 V by using a neutral aqueous solution*. *Electrochem. Commun.*, 2010. **12**(10): p. 1275-1278.
17. Lee, H. Y., Manivannan, V. and Goodenough, J. B., *Electrochemical capacitors with KCl electrolyte*. *C. R. Acad. Sci. Paris*, 1999. **2**(11-13): p. 565-577.

18. Reddy, R. N. and Reddy, R. G., *Sol-gel MnO₂ as an electrode material for electrochemical capacitors*. J. Power Sources, 2003. **124**(1): p. 330-337.
19. Qu, Q. T., Wang, B., Yang, L. C., Shi, Y., Tian, S. and Wu, Y. P. *Study on electrochemical performance of activated carbon in aqueous Li₂SO₄, Na₂SO₄ and K₂SO₄ electrolytes*. Electrochem. Commun., 2008. **10**(10): p. 1652-1655.
20. Sawamura, S., Ishigami, T., Egoshi, N., Tsuchiya, M., Taniguchi, Y. and Suzuki, K., *Effect of pressure on the solubilities of LiF, NaF, KCl, NH₄Cl, K₂SO₄, (NH₄)₂SO₄, and ZnSO₄·7H₂O in water at 298.15 K*. Int. J. High Pres. Res., 1994. **11**(6): p. 347-353.
21. Kirk, D. W. and Graydon, J. W., *Electrochemical Double Layer Capacitance in Activated Carbon: Ion Size Effects*. 2010, ECS, **25**(35): p. 163-171.
22. Eliad, L., Salitra, G., Soffer, A. and Aurbach, D. *Ion sieving effects in the electrical double layer of porous carbon electrodes: Estimating effective ion size in electrolytic solutions*. J. Phys. Chem. B, 2001. **105**(29): p. 6880-6887.
23. Conway, B. E., *Ionic hydration in chemistry and biophysics*. 1981, Elsevier Scientific Pub. Co., New York
24. Sillars, F. B., Fletcher, S.I., Mirzaeian, M. and Hall, P.J. *Variation of electrochemical capacitor performance with room temperature ionic liquid electrolyte viscosity and ion size*. PCCP, 2012. **14**(17): p. 6094-6100.

25. Toupin, M., Brousse, T. and Bélanger, D., *Charge storage mechanism of MnO₂ electrode used in aqueous electrochemical capacitor*. Chem. Mater., 2004. **16**(16): p. 3184-3190.
26. Sugimoto, W., Yokoshima K., Murakami Y. and Takasu Y., *Charge storage mechanism of nanostructured anhydrous and hydrous ruthenium-based oxides*. Electrochim. Acta, 2006. **52**(4): p. 1742-1748.
27. Yuan, D., Zheng, J., Kristian, N., Wang, Y. and Wang, X., *Bi₂O₃ deposited on highly ordered mesoporous carbon for supercapacitors*. Electrochem. Commun., 2009. **11**(2): p. 313-317.
28. Zhang, L. L., Wei, T., Wang, W. and Zhao, X. S., *Manganese oxide-carbon composite as supercapacitor electrode materials*. Microporous Mesoporous Mater., 2009. **123**(1-3): p. 260-267.
29. Ng, K. C., Zhang, S. Peng, C. and Chen, G. Z., *Individual and Bipolarly Stacked Asymmetrical Aqueous Supercapacitors of CNTs/SnO and CNTs/MnO Nanocomposites*. J. Electrochem. Soc., 2009. **156**: p. A846-A853.
30. Hu, Z. A., Xie, Y. L., Wang, Y. X., Mo, L. P., Yang, Y. Y. and Zhang, Z. Y., *Polyaniline/SnO₂ nanocomposite for supercapacitor applications*. Mater. Chem. Phys., 2009. **114**(2-3): p. 990-995.
31. Nagarajan, N. and Zhitomirsky, I., *Cathodic electrosynthesis of iron oxide films for electrochemical supercapacitors*. J. Appl. Electrochem., 2006. **36**(12): p. 1399-1405.
32. Chang, K. H., Hu, C. C., Huang, C. M., Liu, Y. L. and Chang, C. I., *Microwave-assisted hydrothermal synthesis of crystalline WO₃-WO₃·0.5 H₂O mixtures for pseudocapacitors of the asymmetric type*. J. Power Sources, 2011. **196**: p. 2387-2392.

33. Rajeswari, J., Kishore, P. S., Viswanathan, B. and Varadarajan, T. K., *One-dimensional MoO₂ nanorods for supercapacitor applications*. *Electrochem. Commun.*, 2009. **11**(3): p. 572-575.
34. Lee, H. Y. and Goodenough, J. B., *Ideal supercapacitor behavior of amorphous V₂O₅·nH₂O in potassium chloride (KCl) aqueous solution*. *J. Solid State Chem.*, 1999. **148**(1): p. 81-84.
35. Snook, G. A. and Chen, G. Z., *The measurement of specific capacitances of conducting polymers using the quartz crystal microbalance*. *J. Electroanal. Chem.*, 2008. **612**(1): p. 140-146.
36. Gupta, V. and Miura, N., *High performance electrochemical supercapacitor from electrochemically synthesized nanostructured polyaniline*. *Mater. Lett.*, 2006. **60**(12): p. 1466-1469.
37. Frackowiak, E., Khomenko, V., Jurewicz, K., Lota, K. and Beguin, F., *Supercapacitors based on conducting polymers/nanotubes composites*. *J. Power Sources*, 2006. **153**(2): p. 413-418.
38. Wang, D. W., Li, F. Zhao, J., Ren, W., Chen, Z. G., Tan, J., Wu, Z. S., Gentle, I., Lu, G. Q. and Cheng, H. M., *Fabrication of graphene/polyaniline composite paper via in situ anodic electropolymerization for high-performance flexible electrode*. *ACS Nano*, 2009. **3**(7): p. 1745-1752.
39. Fan, Z., Chen, J. H., Zhang, B., Liu, B., Zhong, X. X. and Kuang, Y. F., *High dispersion of r-MnO₂ on well-aligned carbon nanotube arrays and its application in supercapacitors*. *Diamond Relat. Mater.*, 2008. **17**(11): p. 1943-1948.
40. Qian, D., Dickey, E. C., Andrews, R. and Rantell, T., *Load transfer and deformation mechanisms in carbon nanotube-polystyrene composites*. *Appl. Phys. Lett.*, 2000. **76**: p. 2868-2890.

41. Kuo, S.-L. and Wu, N.-L., *Investigation of pseudocapacitive charge-storage reaction of $MnO_2 \cdot nH_2O$ supercapacitors in aqueous electrolytes*. J. Electrochem. Soc., 2006. **153**: p. A1317–A1324.
42. Wang, Y., Yuan, A. and Wang, X., *Pseudocapacitive behaviours of nano-structured manganese dioxide/carbon nanotubes composite electrodes in mild aqueous electrolytes: Effect of electrolytes and current collectors*. J. SolidState Electrochem., 2008. **12**: p. 1101–1107.
43. Qu, Q., Zhang, P., Wang, B., Chen, Y., Tian, S. and Wu, Y., *Electrochemical performance of MnO_2 nanorods in neutral aqueous electrolytes as a cathode for asymmetric supercapacitors*. J. Phys. Chem. C, 2009. **113**: p. 14020–14027.
44. Bard, A. J. and Faulkner, L. R., *Electrochemical Methods: Fundamentals and Applications*, 2000, 2nd ed., Wiley, New York.
45. Sivakkumar, S. R., Kim, W. J., Choi, J. A., MacFarlane, D. R., Forsyth, M. and Kim, D. W., *Electrochemical performance of polyaniline nanofibres and polyaniline/multi-walled carbon nanotube composite as an electrode material for aqueous redox supercapacitors*. J. Power Sources, 2007. **171**(2): p. 1062-1068.
46. Fischer, A. C., *Electrode dynamics*. 1996: Oxford Science publication, U.K., Oxford
47. Compton, R. G. and Sanders, G. H. W., *Electrode potentials*. 1996: Oxford University Press, U.K., Oxford
48. Baskaran, R., Selvasekarapandian, S., Kuwata, N., Kawamura, J. and Hattori, T. *Conductivity and thermal studies of blend polymer*

- electrolytes based onPVAc-PMMA*. Solid State Ionics, 2006, **177**: p. 2679–2682.
49. Malki, M. and Echegut, P. *Electrical conductivity of the CaO-SiO₂ system in the solid and the molten states*. Journal of Non-Crystalline Solids, 2003, **323**: p. 131–136.
50. Uematsu, M. and Franck, E. U. *Static dielectric constant of water and steam*. Journal of Physical and Chemical Reference Data, 1980, **9**: p. 1291–1305.
51. Gualous, H., Bouquain, D., Berthon, A. and Kauffmann, J. M. *Experimental study of supercapacitor serial resistance and capacitance variations with temperature*. J. Power Sources, 2003, **123**: p. 86–93.
52. Kotz, R., Hahn, M. and Gallay, R. *Temperature behavior and impedance fundamentals of supercapacitors*. J. Power Sources, 2006, **154**: p. 550–555.
53. Lcokett, V., Sedev, R. and Ralston, J. *Differential capacitance of the electrical double layer in imidazolium-based ionic liquids: Influence of potential, cationsize, and temperature*. J. Phys. Chem. C, 2008, **112**: p. 7486–7495.
54. Schelling, P. K. and Koblinski, P. *Thermal expansion of carbon structures*. Phys. Rev. B, 2003, **68**: p. 1–7.
55. Colin, W. E. and Glew, D. N. *Evaluation of the thermodynamic functions for aqueous sodium chloride from equilibrium and calorimetric measurements below 154 °C*. J. Phys. Ref. Data, 1985, **14** (2): p. 489 - 610

56. Bodnar, R. J., *Revised equation and table for determining the freezing point depression of H₂O-NaCl solutions*. *Geochimica. Cosmochimica. Acta*, 1993, **57**: p. 683-684

Chapter 5 NEUTRAL AQUEOUS CARBON ECs

Carbon is one of the most widely used materials in this particular subject area because of its abundance in nature, relatively low cost, chemical and electrochemical stabilities [1]. Therefore it is crucial to examine different carbon materials in terms of their specific capacitance and electrochemically stable potential windows (maximum operating voltage) to design the ECs displaying improved energy characteristics. Typically, specific energy of commercial carbon-carbon ECs using organic solvents (EDLC) is in a range of 5 to 8 Wh/kg and these designs, which can offer an operating voltage up to 2.7 V, have an innate advantage over water-based ECs. Therefore, development of the aqueous ECs which can display higher energy capacity than that of commercial ECs is a very difficult task due to aqueous electrolytes showing lower electrochemical stability than organic solvents (theoretical water decomposition voltage: 1.23 V) [1-3]. As mentioned in the previous chapter, this is one of the biggest obstacles to commercialisation of the carbon-based ECs with aqueous electrolytes although the water-based systems offer a number of benefits [2, 3]. However, this study suggests an exception. Taking advantage of the hydrogen overpotential of high specific surface carbons in aqueous electrolytes enables to extend the operating voltage window in carbon-carbon ECs. Moreover, it is proven in this study that minimising potential gradients (non-uniform charging process) along the carbon structures in the initial charging-discharging cycles shows a significant effect toward long-term cycling stabilities. Owing to the two methods mentioned, neutral aqueous carbon-carbon ECs show comparable potential windows (operating voltage) and their specific energy surpasses that of the commercial carbon-carbon ECs using organic solvents. By thoroughly examining different

carbon materials in terms of specific capacitance (F/g) and optimising cell design utilising different electrode capacitances, advanced carbon-carbon ECs containing neutral aqueous electrolytes result in remarkable improvement, displaying specific energy up to 20 Wh/kg .

5.1. SPECIFIC CAPACITANCE OF CARBON MATERIALS

5.1.1. EXAMINATION OF DIFFERENT CARBON MATERIALS

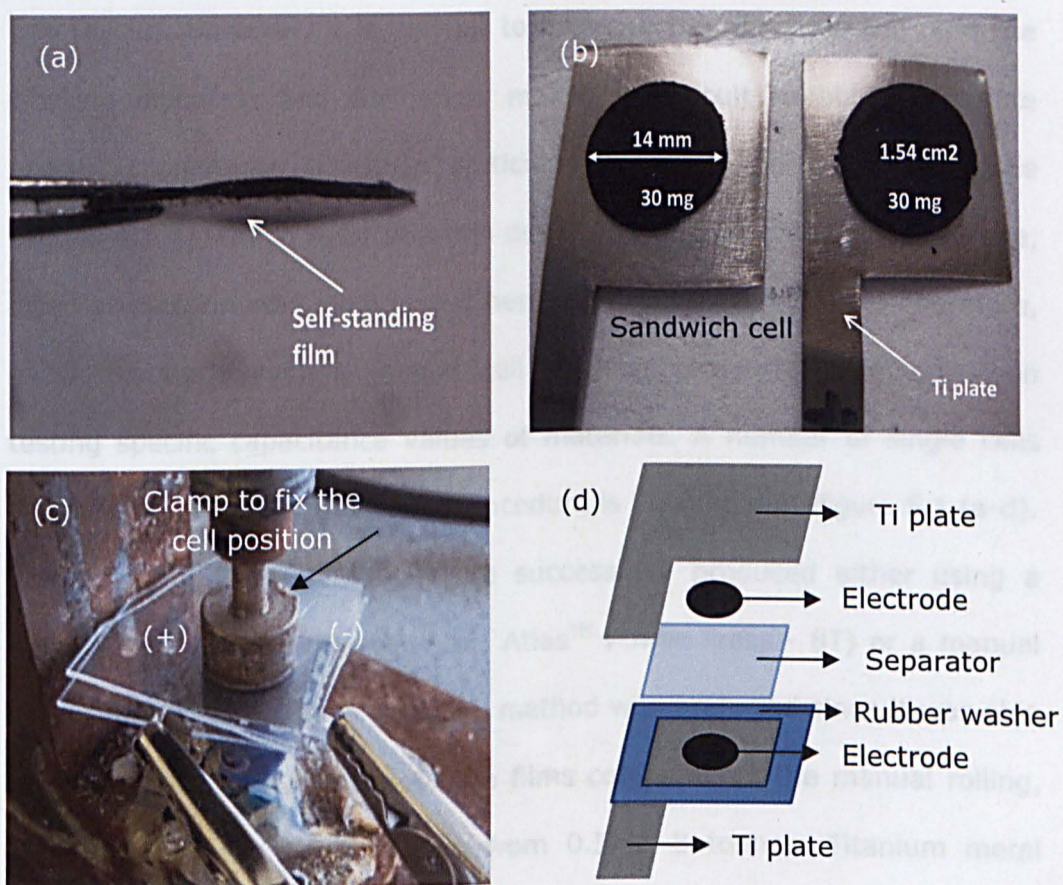
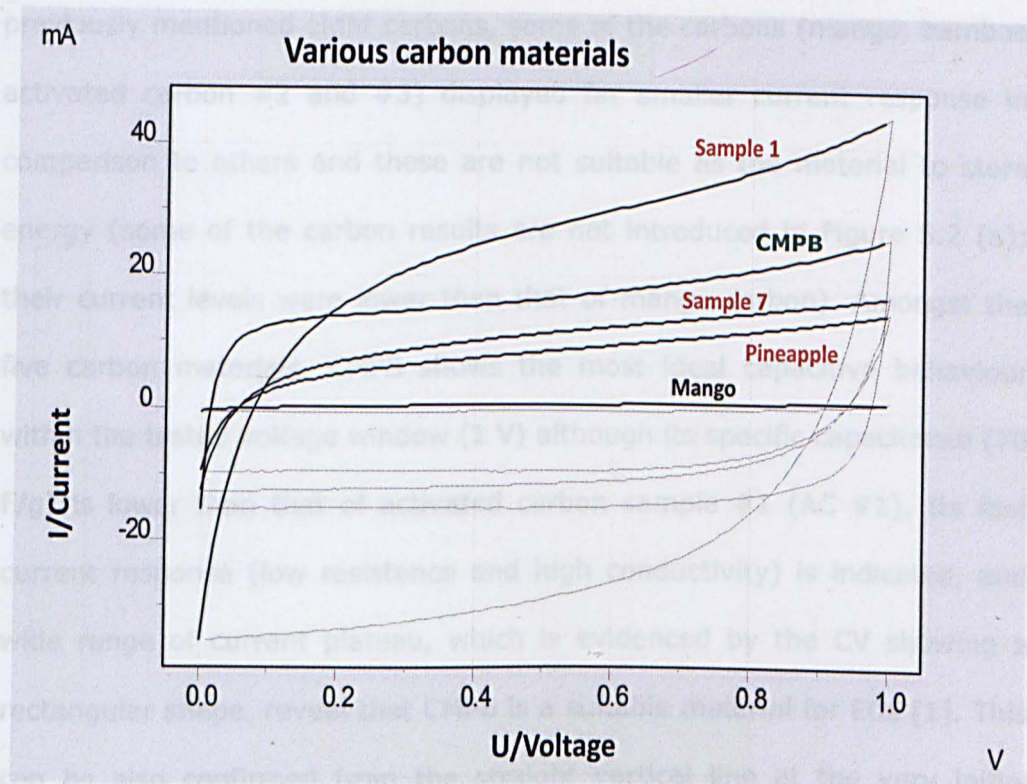


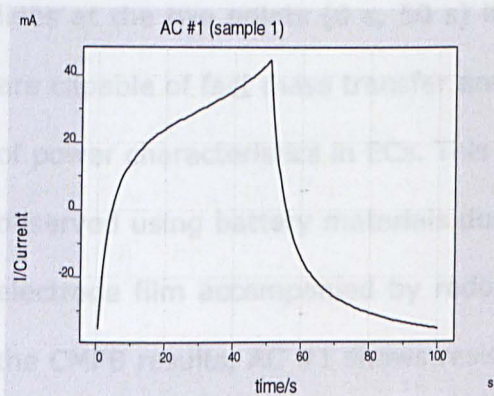
Figure 5.1 Images of carbon electrode and construction of C-C symmetrical single cell; (a) Self-standing carbon electrode by pellet press, (b) Inside image of sandwich design single cell, (c) A two-electrode test using clamp and potentiostat, (d) a schematic of a single cell construction; Separator: Whatman 597 filter paper

Eight different carbon materials, namely pineapple, mango, bamboo, activated carbon #1, #2, #3, #7 and the Cabot monarch 1300 pigment black (CMPB), were made into electrode films and their capacitive properties were evaluated to identify which was the best material for ECs displaying higher energy capacity. A three-electrode system which displays current response as a function of applied potential is a strong tool to examine electrochemical performances of various materials and this method is very widely used in electrochemistry research [4-15] (detailed explanations and its fundamental can be found in Chapter 3 and a number of case studies were carried out and the results can be found throughout this thesis). However, it is difficult to measure the exact loading onto the working electrode and this often makes it difficult to obtain accurate specific capacitance (F/g). In particular, a cast-evaporate method (see section 4.1.1), which is for thin film deposition on to the working electrode, often gives estimated loading and hence estimated capacitance. Therefore, a two-electrode system (single cell measurement) was adopted when testing specific capacitance values of materials. A number of single cells were constructed and their brief procedure is illustrated in Figure 5.1 (a-d). Self-standing electrode films were successfully produced either using a pellet press machine (Specac Ltd., Atlas™ Power Press - 8T) or a manual rolling method. The pellet pressing method was preferred since it was able to produce more uniform electrode films compared to the manual rolling, by controlling the press loading from 0.5 to 8 tonnes. Titanium metal plates were chosen as current collectors because they show high durability against corrosion in aqueous electrolytes. Before the tests, a rubber washer was placed in between the two current collectors to prevent a short circuit as well as electrolyte evaporation; this design is briefly sketched in Figure 5.1 (d).

(a)



(b)



(c)

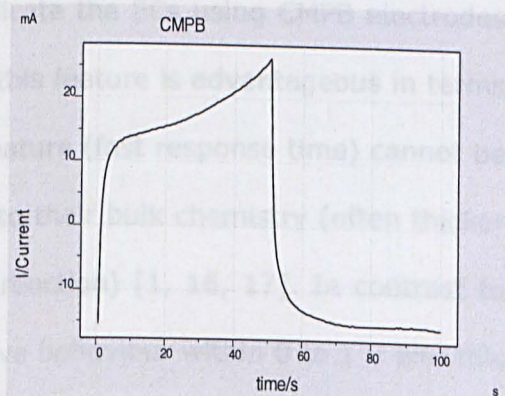


Figure 5.2 (a) CVs with different carbon materials at 20 mV/s in 0.3 mol L⁻¹ K₂SO₄, (b) Current response versus time from the CV data of AC #1 at 20 mV/s, (c) Current response versus time from the CV data of CMPB at 20 mV/s, (single cell test, 30 mg per electrode = 20 mg/cm², 5 wt % PTFE added as a binder)

Figure 5.2 (a) shows CVs of the five carbon materials. Amongst the previously mentioned eight carbons, some of the carbons (mango, bamboo, activated carbon #2 and #3) displayed far smaller current response in comparison to others and these are not suitable as the material to store energy (some of the carbon results are not introduced in Figure 5.2 (a); their current levels were lower than that of mango carbon). Amongst the five carbon materials, CMPB shows the most ideal capacitive behaviour within the tested voltage window (1 V) although its specific capacitance (70 F/g) is lower than that of activated carbon sample #1 (AC #1). Its fast current response (low resistance and high conductivity) is indicated, and wide range of current plateau, which is evidenced by the CV showing a rectangular shape, reveal that CMPB is a suitable material for ECs [1]. This can be also confirmed from the straight vertical line at the very initial stages of charging at 0 second and discharging at 50 second, which is shown in Figure 5.2 (c) (current vs. time plot). The initial vertical straight lines at the two points (0 s, 50 s) indicate the ECs using CMPB electrodes are capable of fast mass transfer and this feature is advantageous in terms of power characteristics in ECs. This feature (fast response time) cannot be observed using battery materials due to their bulk chemistry (often thicker electrode film accompanied by redox reaction) [1, 16, 17]. In contrast to the CMPB results, AC #1 shows resistive behaviour within 0 to 1 V and this is noticeable from the non-rectangular CV shown in Figure 5.2 (a). Moreover, the current response of AC #1 (response time of the material) is not as fast as that of CMPB shown in Figure 4.2 (b). This result indicates that there is a higher resistance within the material. Firstly, electronic conductivity of the carbon may be lower than CMPB. Secondly, mass transport of ions may be significantly slow within the carbon structure and this is often observed with the presence of micropores. Therefore, AC #1 is

expected to show lower power characteristics than CMPB according to the following equation ($P = V^2/4ESR$). However, its specific capacitance was the highest (around 100 F/g at 20 mV/s) amongst all the examined carbons. Although AC #1 takes a longer time to accumulate and release charge carriers in comparison to CMPB due to the resistive nature of the material, the material (AC #1) is capable of more energy storage. Therefore, AC #1 and CMPB, which were the two best materials in terms of capacitance and resistance respectively, were chosen as active materials for ECs displaying higher energy. Obtained specific capacitances of the different carbons are presented in Table 5.1.

Table 5.1 Specific material capacitance (F/g) of different carbons using symmetrical (balanced) ECs (20 mV/s, 0 to 1V)

	AC #1	CMPB	AC #7	Pineapple	Mango	AC #2	AC #3	Bamboo
*Specific material capacitance (F/g)	94	70	46	38	11	7	5	5

* Material specific capacitance (C_M) should be distinguished from cell specific capacitance (C_{CELL}) (detailed explanation can be found Equation 2.2 (Chapter 2) in this thesis).

5.2. CABOT MONARCH 1300 PIGMENT BLACK (CMPB)

5.2.1. ELECTROCHEMICAL ANALYSIS OF CMPB

Cyclic voltammetry allows the estimation of both the charge consumed for charging the electrical double layer, and the hydrogen adsorption on the surface of CMPB. Carbon materials have long been studied in relation with hydrogen gas evolution, and it was claimed that carbons with smaller

particle and pore sizes would lead to a higher overpotential for hydrogen gas evolution [18]. In this chapter, the results of significantly high hydrogen overpotential using nanoparticles of the CMPB, whose specific surface area is $560 \text{ m}^2/\text{g}$ according to the literature [19- 21], will be presented. In line with the reported value from the literature, further structural studies (SEM, TEM and BET) were carried out for a confirmation purpose and these results are presented with Figure 5.3.

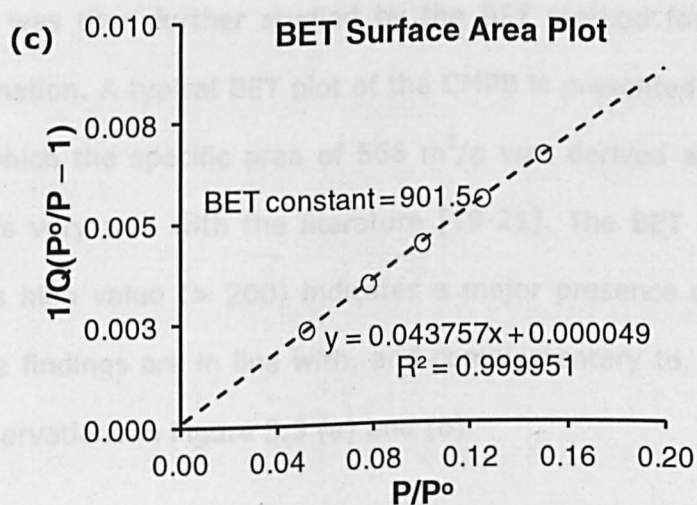
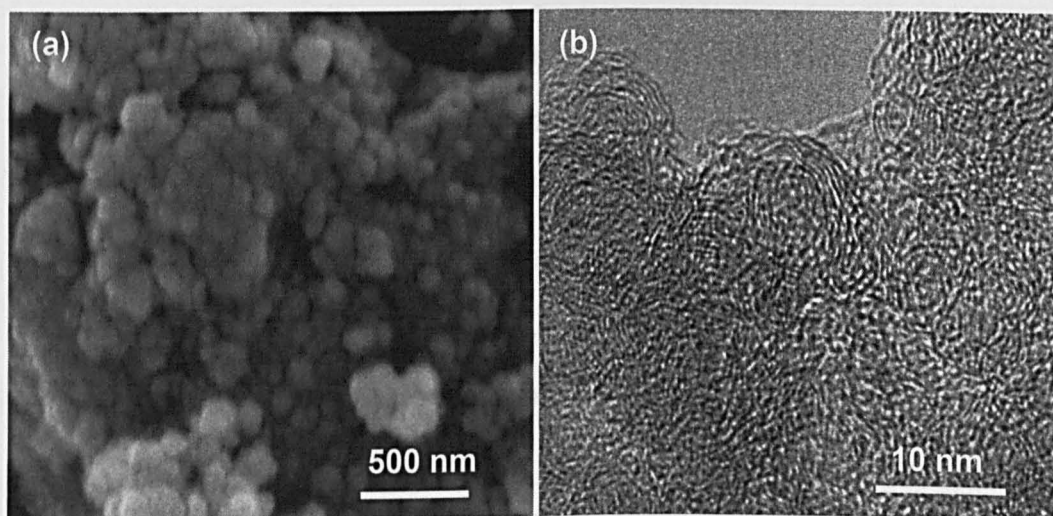


Figure 5.3 (a) SEM, (b) HRTEM images and (c) BET plot for CMPB

The SEM image shown in Figure 5.3 (a) was taken to gain structural information of the CMPB. A lump structure was observed, consisting of aggregated globular carbon nano-particles. It can be seen that the sizes of the globular particles are close to 50 nm. Further inspection of the CMPB by HRTEM revealed that each of the globular particles in Figure 5.3 (a) actually contained even smaller spheres of 10 ± 2 nm in diameter [22]. Figure 5.3 (b) presents a typical HRTEM image of the CMPB, revealing distinct onion-like fringes of the CMPB nano-spheres, which corresponds well with the size information provided by the supplier.

According to the SEM and HRTEM inspections as exemplified in Figure 5.3 (a) and (b), it can be concluded that the CMPB has a three-level hierarchical structure: basic nano-spheres of 10 nm in diameter; the 50 nm globules of closely packed 10 nm spheres; and micrometer sized agglomerates of the 50 nm globules. Such a hierarchical structure implies the presence of micro-pores between the 10 nm spheres in each 50 nm globule, meso-pores between the 50 nm globules in each of the micrometer agglomerates, and macro-pores between the agglomerates. The CMPB was then further studied by the BET method for surface and pore information. A typical BET plot of the CMPB is presented in Figure 5.3 (c) from which the specific area of $566 \text{ m}^2/\text{g}$ was derived and this value corresponds very well with the literature [19-21]. The BET constant was 901.5. This high value (> 200) indicates a major presence of micropores [23]. These findings are in line with, and complementary to, the SEM and HRTEM observations in Figure 5.3 (a) and (b).

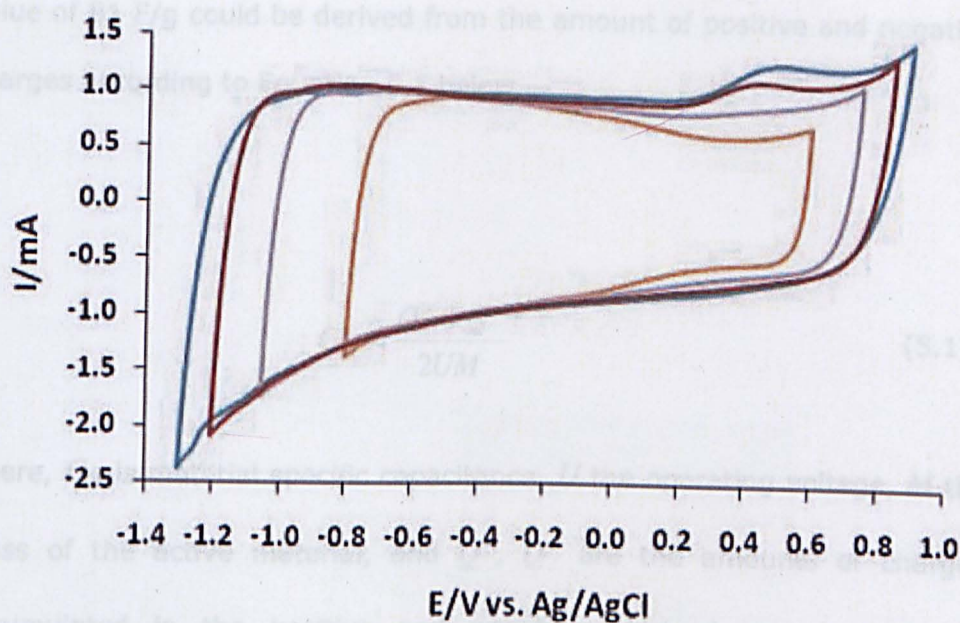


Figure 5.4 CVs of the three-electrode system using CMPB (2.5 mg); Different working potential windows in a neutral aqueous solution of 0.3 mol/L K_2SO_4 at 5 mV/s

Figure 5.4 presents the CVs of the three-electrode system with 0.3 mol/L K_2SO_4 at a scan rate of 5 mV/s. The first cycle was recorded in the narrowest potential range from $E = -0.8$ V to $+0.6$ V vs. Ag/AgCl. The rectangular CVs with comparable positive and negative currents reveal highly capacitive and reversible behaviour, i.e. the positive and negative ions were attracted on the carbon/electrolyte interface by electrostatic forces [1, 24]. The negative current reflects the rate of accumulation of the hydrated cations, H_3O^+ and K^+ , and desorption of anions (SO_4^{2-}) which occur during the negative polarization of carbon, whereas the positive current corresponds to the rates of the desorption of the mentioned cations in the positive electrode and adsorption of hydrated anions. A capacitance

value of 81 F/g could be derived from the amount of positive and negative charges according to Equation 5.1 below,

$$C_M = \frac{Q^+ + Q^-}{2UM} \quad (5.1)$$

where, C_M is material specific capacitance, U the operating voltage, M the mass of the active material, and Q^+ , Q^- are the amounts of charges accumulated in the positive and negative electrodes respectively. A difference in capacitance between the three- (81F/g) and two-electrode systems (70 F/g) was recorded, likely due to the different ranges of electrochemical windows and also different scan rates.

Interestingly, distinctive humps between 0.4 and 0.5 V vs. Ag/AgCl were observed following the potential cycles in which the negative potential limit went below -1.0 V vs. Ag/AgCl. These current humps may be attributed to the electro-oxidation of the so called trapped hydrogen that could form at high negative polarization in an aqueous electrolyte. (Note that the theoretical negative potential limit of water is around -0.8 V vs. SHE, or -1.0 V vs. Ag/AgCl) [18, 25]. The fact that these oxidation current humps were observed at very positive potentials suggests the high irreversibility of the electrochemical formation and removal of the trapped hydrogen. The fast increasing current at potentials near the negative limit was clear evidence of water decomposition. However, the capability of nanoporous carbon to capture hydrogen has been reported [18] and this enables the carbon material to exploit a more negative potential limit than the theoretical value of water decomposition. Although carbon materials have long been known to display significant hydrogen overpotentials, a further

explanation is required to understand the remarkable extension of the potential window up to 2.2 V shown in Figure 5.4, without gas evolution.

5.2.2. ADVANCED DESIGN FOR HIGHER OPERATING VOLTAGE

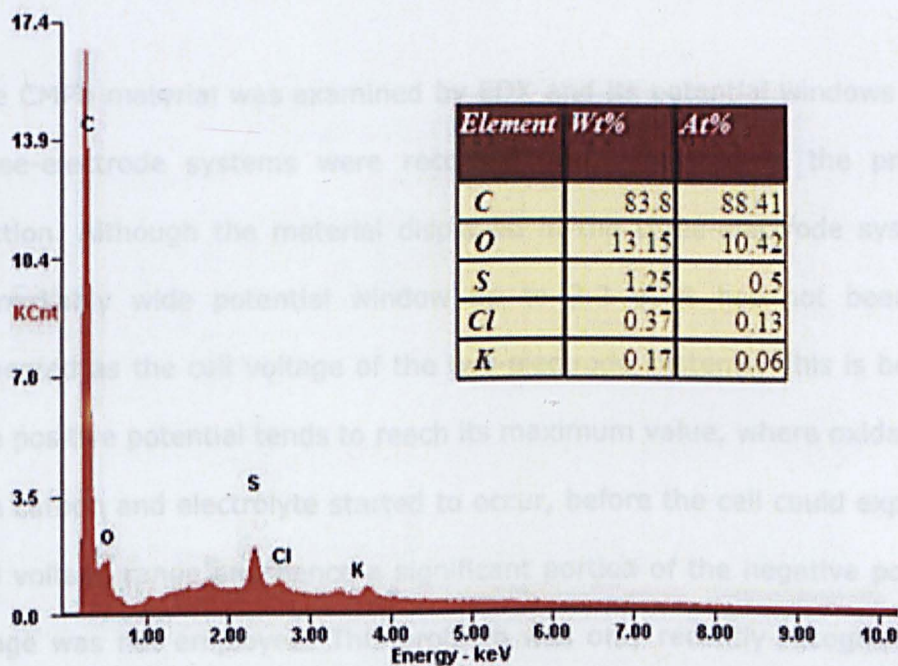


Figure 5.5 EDX spectrum of CMPB

Figure 5.5 displays the EDX spectrum, revealing the elemental composition of CMPB. The detected K (potassium) and Cl (chlorine) were likely impurities gained through incomplete filtration. The spectrum also showed both weight and atomic ratios of oxygen to be over 10 % in the CMPB, suggesting a relatively large portion of the material was consisted of surface functional groups and this may be another contribution to the observed wide range of hydrogen overpotential. The EDX data correspond well with the results claimed by one of the latest papers in which evidence

was provided that the overpotentials for di-hydrogen evolution and carbon oxidation are strongly influenced by the surface functionality [26].

5.2.2. ADVANCED DESIGN FOR HIGHER OPERATING VOLTAGE

The CMPB material was examined by EDX and its potential windows in the three-electrode systems were recorded and evaluated in the previous section. Although the material displayed in the three-electrode system a remarkably wide potential window up to 2.2 V, it has not been fully repeated as the cell voltage of the two-electrode systems. This is because the positive potential tends to reach its maximum value, where oxidation of the carbon and electrolyte started to occur, before the cell could exploit its full voltage range and hence a significant portion of the negative potential range was not employed. This problem was only recently recognised and reported in the recent literature and the highest reported operating voltage so far has been 1.6 V in symmetrical water-based ECs [25, 26]. Due to the operating voltage of ECs being directly related to the overall energy capacity, their narrow potential ranges have hindered their wider potential applications.

Unequalisation (balanced and unbalanced designs are also used in literature, but, for unity with the group's publications, the terminology of equalisation and unequalisation will be used throughout the thesis) of electrode capacitance can result in adjustment of the positive and negative electrode potential windows. This method has been applied to asymmetrical ECs for enhancement of energy capacity in the recent literature [27, 28]. However, the adjusted positive and negative potential windows only play within the fixed potential ranges of the asymmetrical

ECs due to phase changes of active materials. In the case of carbon-carbon ECs in a neutral aqueous electrolyte, this method could be very effective to widen the cell voltage window by utilising the wasted range of negative potential in a symmetrical EC as indicated by the blue arrow in Figure 5.6.

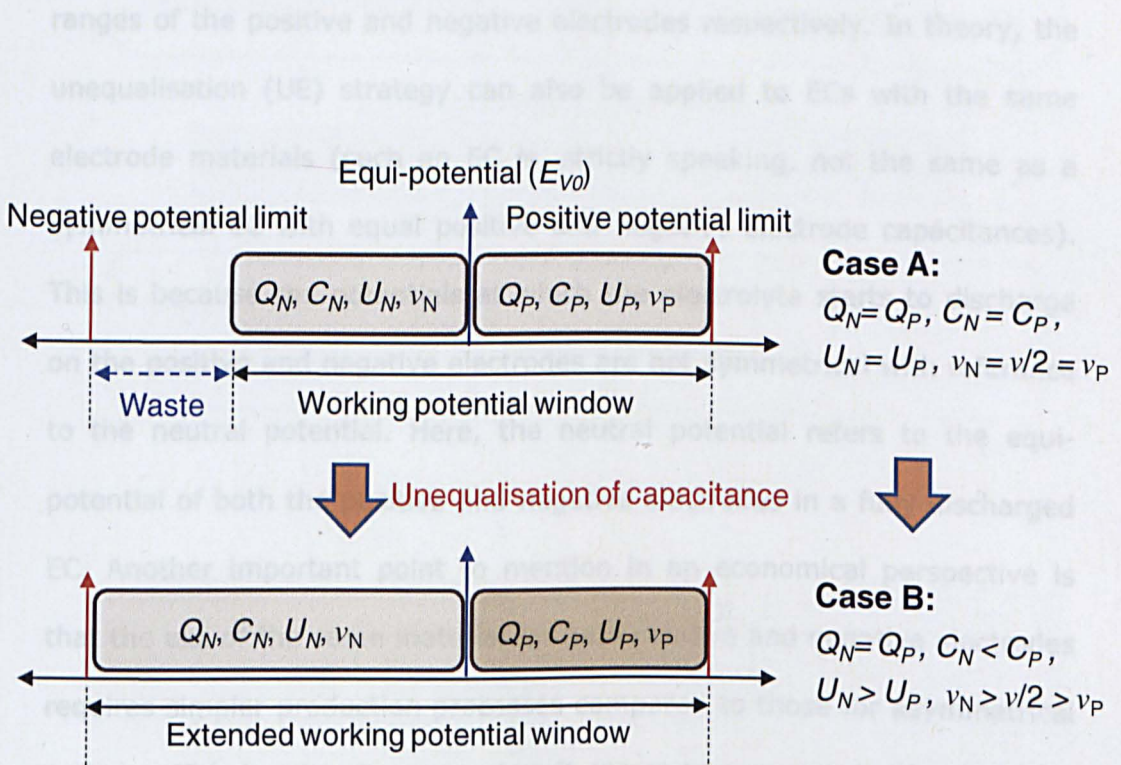


Figure 5.6 A strategy to increase the operating voltage of ECs with the same material for both the positive and negative electrodes via unequialisation (UE) of electrode capacitances, and hence adjustment of positive and negative electrode potential windows. In the drawing, C and Q are the capacitance of, and the charge passed through the cell, or each electrode; U is the window of cell voltage or electrode potential; v is the varying rate of the controlled cell voltage, or the responding electrode potential; The subscripts "P" and "N" indicate positive and negative electrodes, respectively. The darker box (Q_P) in Case B indicates a greater "charge density" than that of the other (Q_N).

This approach utilises the fact that the potential windows of the positive and negative electrodes can be different and governed by the equation, $Q = C_p U_p = C_n U_n$, where Q is the charge passed through the cell, C_p and C_n , and U_p and U_n are the specific capacitance, and the working potential ranges of the positive and negative electrodes respectively. In theory, the unequalisation (UE) strategy can also be applied to ECs with the same electrode materials (such an EC is, strictly speaking, not the same as a symmetrical EC with equal positive and negative electrode capacitances). This is because the potentials at which the electrolyte starts to discharge on the positive and negative electrodes are not symmetrical with reference to the neutral potential. Here, the neutral potential refers to the equipotential of both the positive and negative electrodes in a fully discharged EC. Another important point to mention in an economical perspective is that the use of the same material for both positive and negative electrodes requires simpler production processes compared to those for asymmetrical systems. This is advantageous when it comes to mass production in terms of the manufacturing cost.

As suggested, utilisation of the wider negative potential range due to hydrogen overpotential can increase the overall operating cell voltage of ECs, while the highest positive potential at the highest cell voltage stays within its maximum value. Therefore, the limit of positive potential has to be identified to carry out further investigations. However, tracking either positive or negative electrode potential while the constructed ECs are running within the given operating voltage cannot be done with one potentiostat.

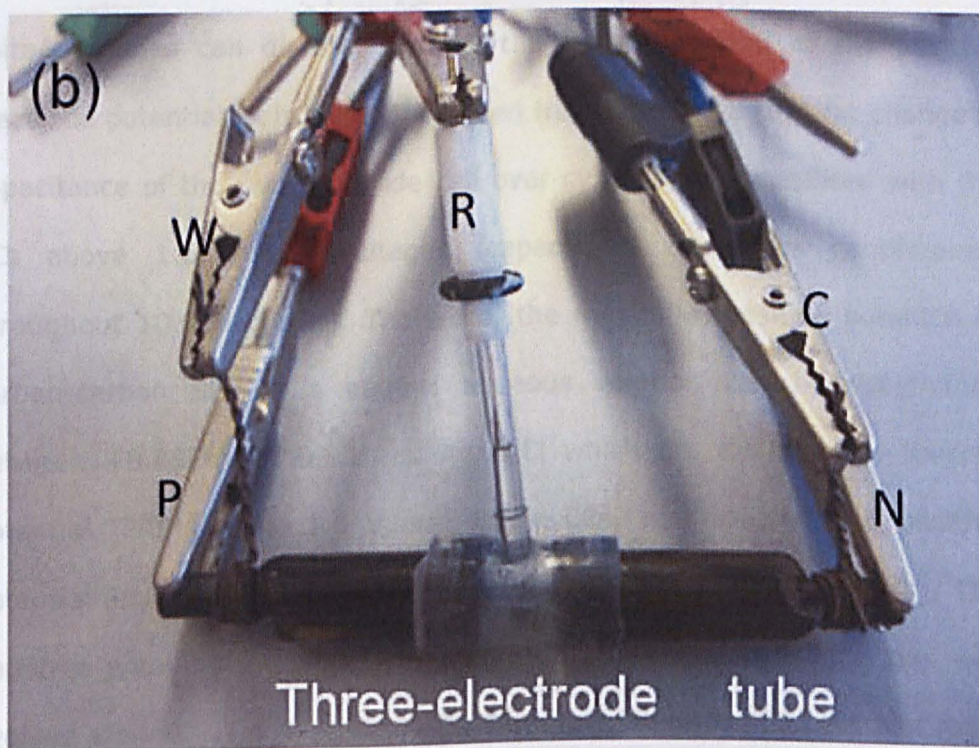
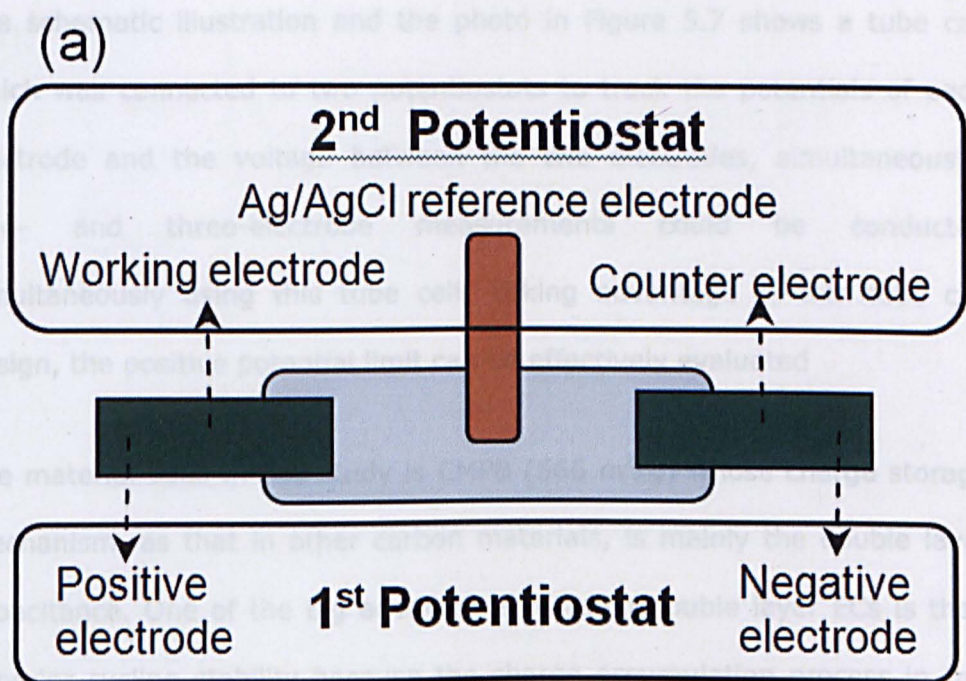


Figure 5.7 Schematic illustration (a) and real image (b) of the electrochemical cell which is able to track a cell voltage and each electrode potential windows simultaneously.

The schematic illustration and the photo in Figure 5.7 shows a tube cell which was connected to two potentiostats to track the potentials of each electrode and the voltage between the two electrodes, simultaneously. Two- and three-electrode measurements could be conducted simultaneously using this tube cell. Taking advantage of this tube cell design, the positive potential limit can be effectively evaluated

The material used in this study is CMPB (566 m²/g) whose charge storage mechanism, as that in other carbon materials, is mainly the double layer capacitance. One of the big advantages of using double layer ECs is their superior cycling stability because the charge accumulation process in this mechanism is purely electrostatic and the material itself is not involved in the chemical reactions. Therefore, tests of cycling stabilities in different cell voltage ranges can directly indicate the maximum limit of the positive electrode potential. It is clearly observed from Figure 5.8 (a) that change in capacitance of the two-electrode cell over cycles is not stabilised with the ECs above 1.6 V cell voltages (capacitance decreases continuously throughout 10,000 cycles). Therefore, the maximum positive potential of carbon-carbon SPs in a neutral aqueous solution can be determined between +0.85 to +0.90 V vs. Ag/AgCl which are the positive reverse potential (PRP) of the 1.6 V and 1.7 V ECs, respectively. The positive potential limit is depicted with the red straight line in Figure 5.8 (b). The negative potential limit was not indicated. However, hydrogen gas was evolved around - 1.4 V vs. Ag/AgCl. Therefore, there is still plenty of room to utilise about 0.6 V in the negative potential range for the 1.6 V single-cell as evidenced by the CV result of the three-electrode system reported previously in Figure 5.4.

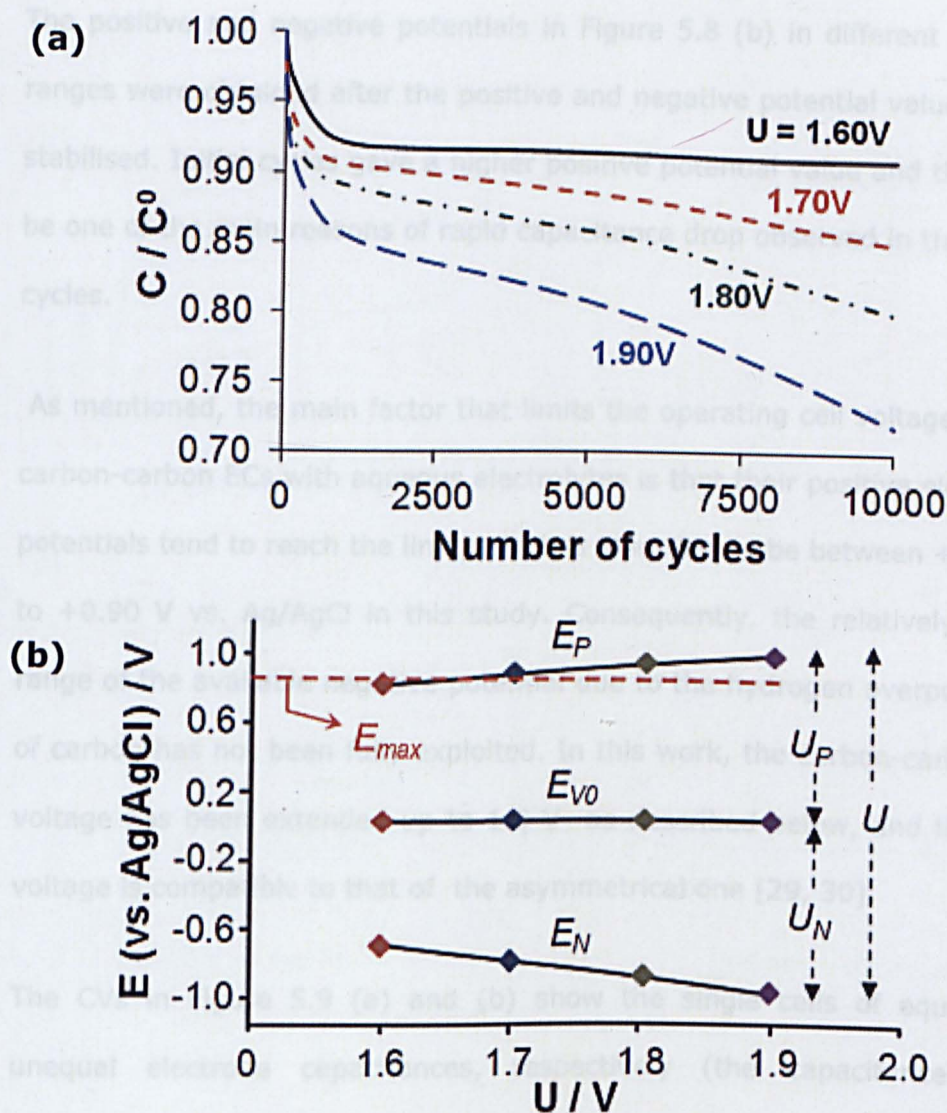


Figure 5.8 (a) Capacitance retention (C_0 and C : Cell capacitance of the first and the following cycles, respectively) of the sandwich type carbon-carbon SPs (40 mg on each electrode) as a function of the number of charge-discharge cycles at the indicated cell voltages. Voltage scan rate: 200 mV s^{-1} . (b) Positive and negative electrode end-potentials (E_P , E_N) measured in the tube cell at different cell voltage limits ($U = 1.60, 1.70, 1.80$ and 1.90 V), and equi-potential (E_{V0}) measured at $U = 0 \text{ V}$ (discharged). The dashed horizontal line indicates the positive potential limit, E_{max} , beyond which unwanted anodic oxidation was observed on CVs.

The positive and negative potentials in Figure 5.8 (b) in different voltage ranges were obtained after the positive and negative potential values were stabilised. Initial cycles gave a higher positive potential value and this may be one of the main reasons of rapid capacitance drop observed in the initial cycles.

As mentioned, the main factor that limits the operating cell voltage of the carbon-carbon ECs with aqueous electrolytes is that their positive electrode potentials tend to reach the limit, which is identified to be between +0.85 V to +0.90 V vs. Ag/AgCl in this study. Consequently, the relatively wider range of the available negative potential due to the hydrogen overpotential of carbon has not been fully exploited. In this work, the carbon-carbon EC voltage has been extended up to 1.9 V as described below, and this cell voltage is compatible to that of the asymmetrical one [29, 30].

The CVs in Figure 5.9 (a) and (b) show the single cells of equal and unequal electrode capacitances, respectively (the capacitance ratio between positive and negative electrodes is 4:3). In the case of the unequal capacitance (UE) design (Figure 5.9 (b)), the potential window is successfully extended towards more negative range while the positive potential window stayed within its positive potential limit. This enables the cell to be charged and discharged up to 10,000 cycles without significant capacitance drop and this can be observed in Figure 5.9 (c). It can also be clearly observed that the equal capacitance single cells at 1.7 V, 1.8 V and 1.9 V in cell voltage showed their positive electrode potential reaching beyond the limit, which consequently could not stabilise their capacitance through 10,000 cycles. The resulting potentials (vs. Ag/AgCl) over cycles with different operating voltage windows were monitored and this is shown in Figure 5.9 (d).

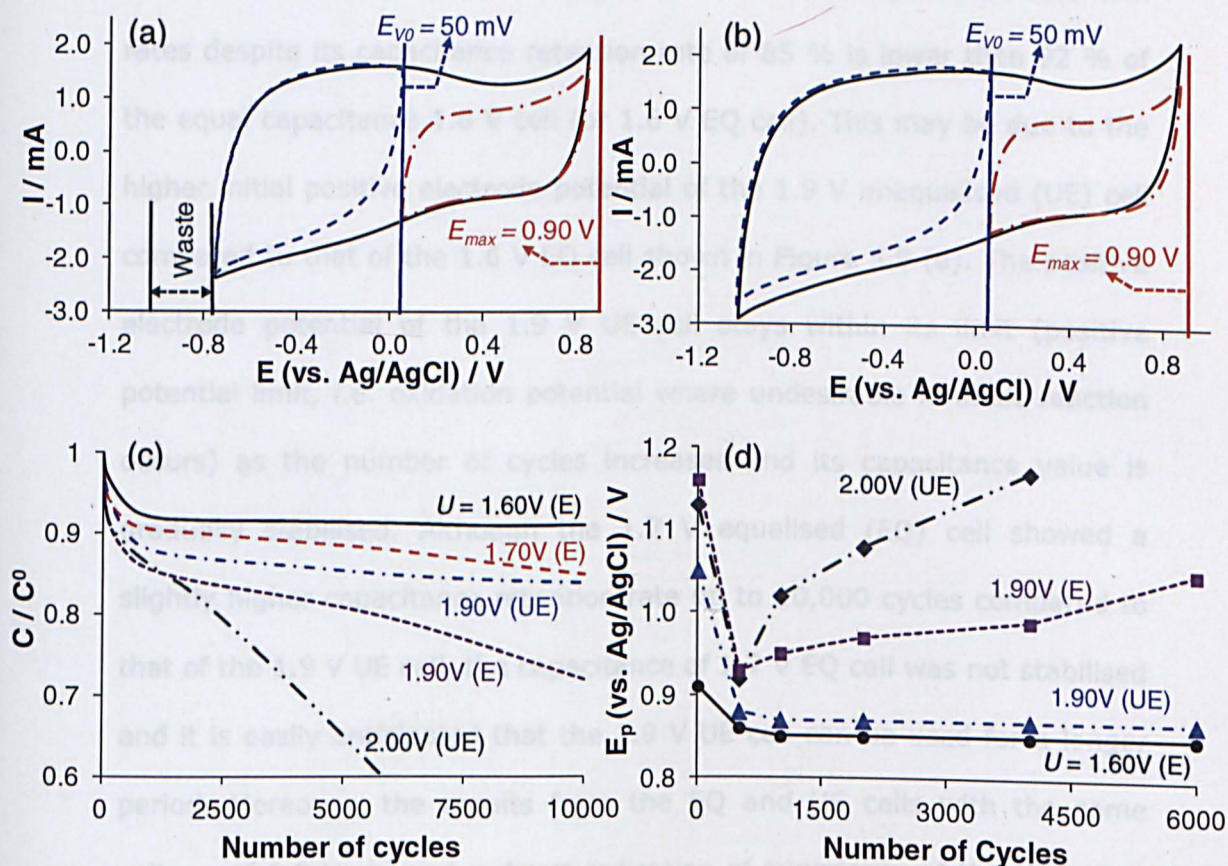


Figure 5.9 (a,b) CVs of CMPB-PTFE (1.0 mg) in the conventional three-electrode cell (0.3 mol L⁻¹ K₂SO₄) with the equi-potential ($E_{V0} = 50$ mV) and potential ranges selected in accordance with the tube cell with (a) equal (EQ) and (b) unequal (UE) electrode capacitances. (c) Capacitance retention (C/C_0) as a function of the number of charge-discharge cycles of sandwich-type SPs with the cell voltage limit indicated. (d) E_p as a function of the number of charge-discharge cycles in the tube cell at indicated cell voltages with equal (EQ) and unequal (UE) electrode capacitances. The C_p/C_N ratios were 4:3 and 3:1 for the UE-cells at 1.90 V and 2.00 V, respectively.

However, the 1.9 V single cell with unequal electrode capacitances (or the 1.9 V UE cell) shows good stability in terms of initial capacitance retention rates despite its capacitance retention rate of 85 % is lower than 92 % of the equal capacitance 1.6 V cell (or 1.6 V EQ cell). This may be due to the higher initial positive electrode potential of the 1.9 V unequalised (UE) cell compared to that of the 1.6 V EQ cell shown in Figure 5.9 (d). The positive electrode potential of the 1.9 V UE cell stays within its limit (positive potential limit, i.e. oxidation potential where undesirable faradaic reaction occurs) as the number of cycles increases and its capacitance value is gradually stabilised. Although the 1.7 V equalised (EQ) cell showed a slightly higher capacitance retention rate up to 10,000 cycles compared to that of the 1.9 V UE cell, the capacitance of 1.7 V EQ cell was not stabilised and it is easily anticipated that the 1.9 V UE cell can be used for a longer period. Moreover, the results from the EQ and UE cells with the same voltage of 1.9 V showed a direct indication of superiority of the UE cell in terms of their initial capacitance retention. The 1.9 V EQ cell displayed a more rapid capacitance decrease as the number of cycles increases. The reason for this will be explained below with Figure 5.10. The achievable maximum cell voltage in the carbon-carbon UE cells is identified at 1.9 V, as the capacitance of the UE 2 V cell decreased rapidly even when the capacitance ratio between the positive and negative electrodes was set to 3:1. This high capacitance ratio should have enabled a lower PRP (positive reverse potential), and also a narrower positive potential range and a wider negative potential range. Disappointingly, this attempt failed and the respect potential windows over cycles in the UE 2 V cell are presented in Figure 5.10.

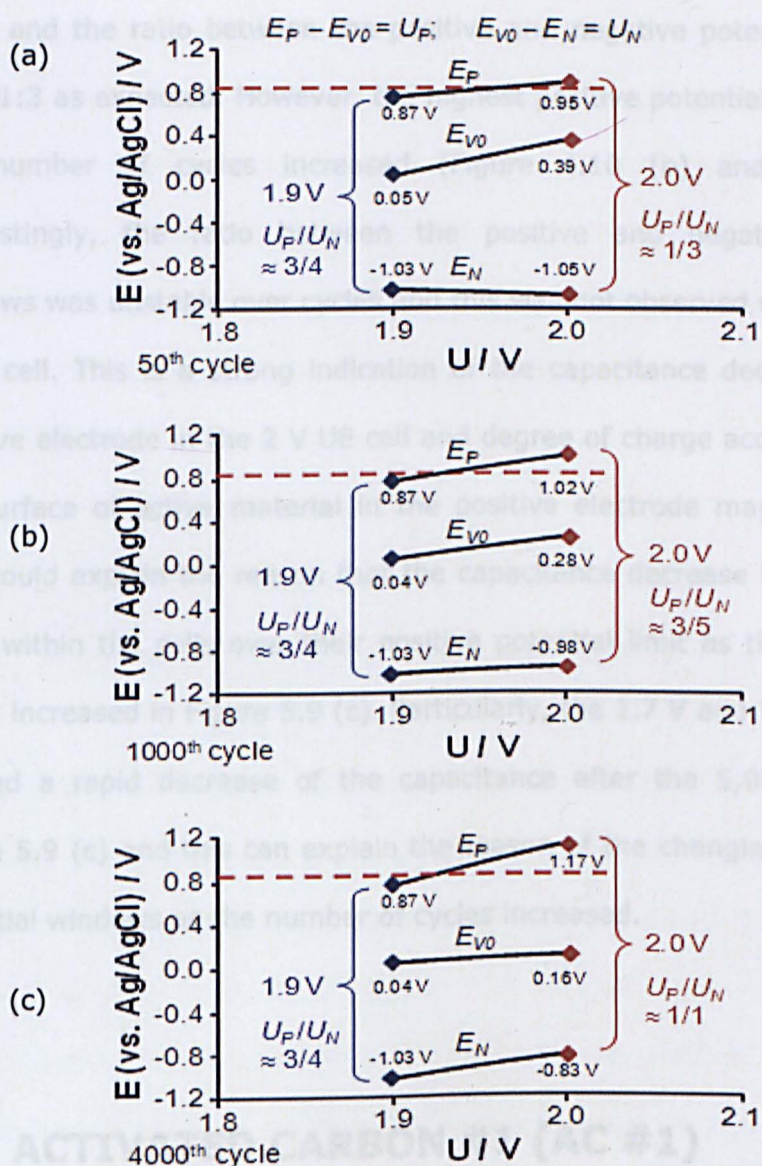


Figure 5.10 End-potentials (E_P , E_N), equi-potentials (E_{V0}), and potential windows (U_P , U_N) of the positive and negative electrodes in the tube cell with unequal electrode capacitances ($C_P/C_N = 4:3$ at 1.9 V, and 3:1 at 2.0 V) measured at cell voltages of 0 V (for E_{V0}), or 1.9 V and 2.0 V (for E_P and E_N), and near the (a) 50th, (b) 1000th, and (c) 4000th charge-discharge cycles.

As Figure 5.10 (a) shows, the highest positive potential value of the 2 V EQ cell is placed slightly over the positive potential limit in the relatively initial

stage and the ratio between the positive and negative potential windows were 1:3 as expected. However, the highest positive potential increased as the number of cycles increased (Figure 4.10 (b) and (c)). More interestingly, the ratio between the positive and negative potential windows was unstable over cycles and this was not observed within the 1.9 V UE cell. This is a strong indication of the capacitance decrease on the positive electrode in the 2 V UE cell and degree of charge accumulation on the surface of active material in the positive electrode may deteriorate. This could explain the reason that the capacitance decrease became more rapid within the cells over their positive potential limit as the number of cycles increased in Figure 5.9 (c). Particularly, the 1.7 V and 1.9 V EQ cells showed a rapid decrease of the capacitance after the 5,000th cycle in Figure 5.9 (c) and this can explain the reason of the changing ratio of the potential windows as the number of cycles increased.

5.3. ACTIVATED CARBON #1 (AC #1)

AC #1 displays the highest specific capacitance value and this can be found in Section 5.1. Energy capacity of ECs is proportional to the capacitance of the electrode material, so it is expected that ECs utilising AC #1 can give highest energy capacity amongst the mentioned carbon materials if the cell voltage is the same. The cell voltage of neutral aqueous ECs using CMPB is successfully increased up to 1.9 V by taking advantage of unequalised electrode capacitances and the fundamentals were explained previously (relevant explanations can be found with Figure 5.5). The idea to increase a cell voltage using AC #1 is the same as the approach mentioned for the CMPB cells. However, some new work and ideas will be introduced to

Increase specific capacitance of the material by reducing resistance. Electrode film made from AC #1 demonstrates resistive behaviour compared to CMPB and an effective approach to reduce its resistance is presented. In addition to the material investigations, an effective method to increase cycling stabilities of the ECs is introduced because cycling behaviour of ECs using AC #1 is different from that of ECs using CMPB due to their relatively high resistance.

5.3.1. ELECTROCHEMICAL ANALYSIS OF AC #1

AC #1 shows the highest specific capacitance (F/g) which is one of the important implications for ECs displaying higher energy. Its resistive behaviour may result in significant sacrifice of the power characteristics. The aim of this study is to design the ECs to improve the energy characteristics while the devices still possess innate merits of their superior kinetics and hence low resistance. Therefore, graphite and CNTs (Multi-walled CNTs, 10–30 nm in diameter and 5–15 μm in length, purchased from Shenzhen Nanotech Port Co., Ltd), were physically mixed with AC #1 to improve the electronic conductivity. When high surface activated carbons are utilised as active film materials, electronic conductivity tends to be low because of presence of more frequent electron hopping resistance at the interface between carbon particles. If electronic conductivity of materials is low, electrons need more energy to jump from one phase to the other and this would cause lower efficiency of systems. Graphite (5 F/g) and CNTs (7-8 F/g) are known as excellent conducting materials [13A-13T]. Thus, these materials are added to enhance conductivity and hence lower resistance.

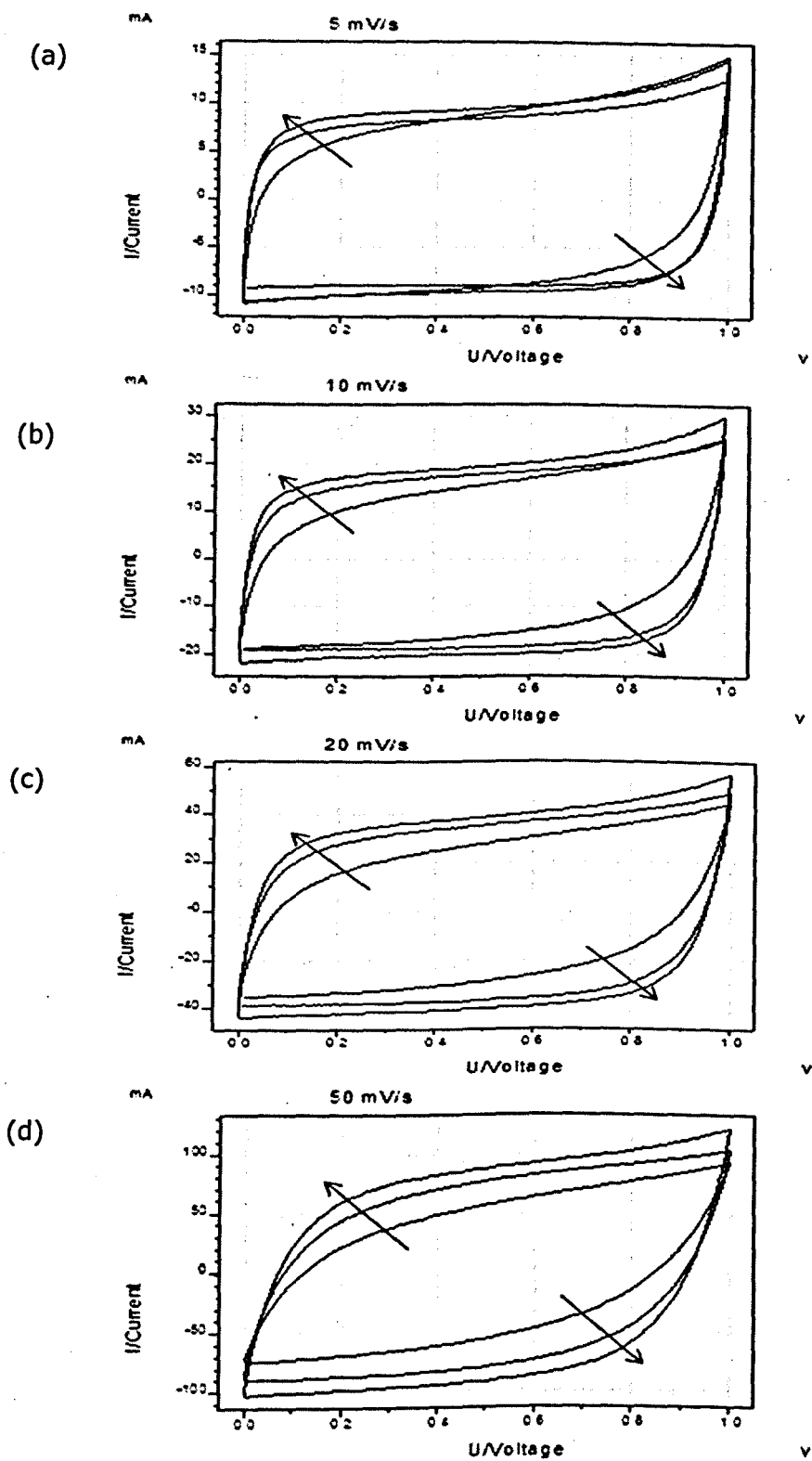


Figure 5.11 CVs of AC #1 (the inner CV trace), AC#1 + 15 wt% graphite and AC #1 (central CV) + 15 wt% CNTs (outer CV) in four different scan rates, (a) 5 mV/s, (b) 10 mV/s, (c) 20 mV/s, (d) 50 mV/s in 3 M KCl, 30 mg per electrode, 60 mg in a cell, a single cell test (two electrode)

AC #1 and its physical mixtures with conducting additives were tested and the results are shown in Figure 5.11. It can be seen that AC #1 alone shows rapid capacitance loss and the shape of CVs deforms to less rectangular as the charging-discharging rate (speed) increases. This can be identified from shape of the inner CVs from Figure 5.11 (a) to (d). Therefore, the rate performance of AC #1 needs to be improved. Addition of conducting agents, i.e. graphite and CNTs, are proven to be very effective in reducing the resistance of AC #1 [31-50]. The difference in specific cell capacitance from the highest to the lowest values at various scan rates is noticeably reduced, from 25 F/g to 18 F/g (material specific capacitance should be four times higher than these values). This is mainly attributed to enhanced electronic conductivity due to the addition of graphite. This value (capacitance gap for different scan rates) is further reduced to 11 F/g when 15 wt% CNTs were added to AC #1. The reason for better result when using CNTs may be found from their unique three dimensional structures [35, 37, 38]. CNTs provide better electronic conductivity to the AC #1 and this is also the case when adding graphite. However, CNTs offer additional passages to the charge carriers (ions), resulting in improvement of ionic conductivity due to their open three dimensional structures [35, 39, 41-50]. Consequently, the highest specific capacitance was obtained in this mixture (AC #1 + 15 wt% CNTs). Detailed capacitance values can be found in Table 5.2. Interestingly, the highest capacitance was achieved at 10 mV/s and this was not the slowest scan rate. This was likely due to the potential step setting of the potentiostat which tends to show higher error at slow scan rates with larger potential steps. According to the author's observations, fewer data points within the same time scale at low scan rates are disadvantageous in terms of accuracy of CV traces.

Table 5.2 Specific capacitance at different scan rates

		5 mV/s	10 mV/s	20 mV/s	50 mV/s	Red - Blue (F/g)
Specific capacitance (F/g)	AC #1	104	102	94	77	25
	AC #1 + 15 wt% Graphite	126	128	119	110	18
	AC #1 + 15 wt% CNTs	130	137	130	126	11

The effect of the amount of conducting additive on specific capacitance of the mixtures is shown in Table 5.3. Weight ratio of the conducting agents is controlled from 0 wt% to 30 wt%. The specific capacitance increased gradually with the addition up to 15 wt% in both graphite and CNTs. However, the capacitance decreased when 30 wt% of conducting agents were added. The best result (amongst four different ratios tested) in terms of capacitance was determined to be 15 wt% physical addition of conducting agents (graphite and CNTs). Since the specific capacitance of the graphite and the CNTs used were individually measured to be about 5 F/g and 15 F/g, respectively, contribution from these two conducting materials towards the specific capacitance of the mixture should have not been significant. However, the additives did contribute to the overall mass of the electrode, resulting in lower specific capacitance as measured against the overall mass of the electrode. Table 5.3 compares the specific capacitance values measured from AC#1 mixed with different amounts of the conducting additives. The results given in Table 5.3 indicate that a

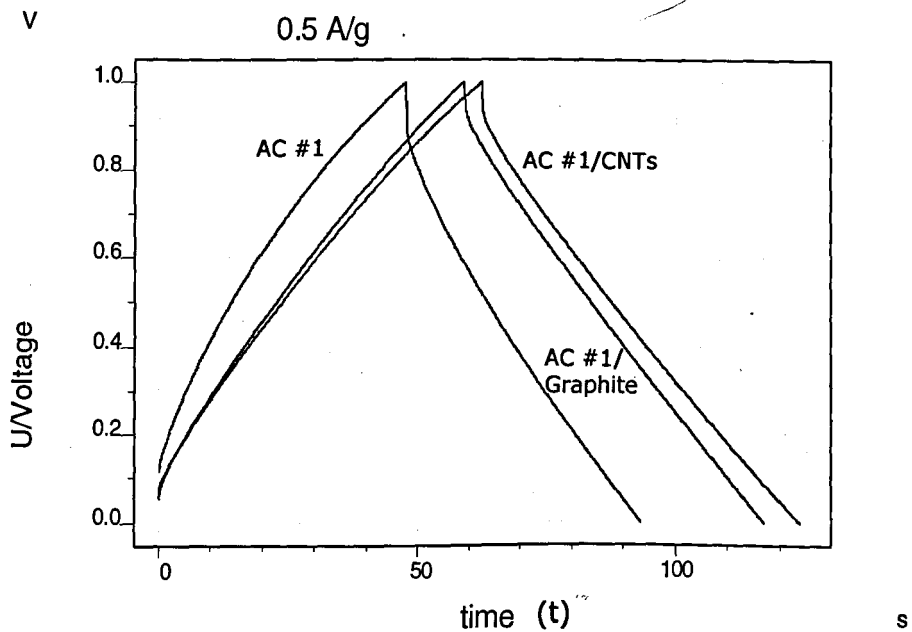
significant amount of surface area (AC #1) was not utilised when it was used on its own, but this drawback could be resolved by adding appropriate ratio of conducting materials (15 wt% of CNTs and graphite shows the best result in terms of capacitance and shape of the CVs recorded). Note that the physical mixture can still bring a positive effect in terms of the material's capacitive behaviour because the additives can enhance the number of active sites which can be exposed to the ions due to the structural advantages with CNTs [41-50].

Table 5.3 Specific capacitance of the mixtures upon amount of addition

		Amount of conducting agent (CNTs, graphite)			
		0 wt %	5 wt%	15 wt%	30 wt%
Specific Capacitance at 10 mV/s (F/g)	AC #1 + graphite	102	110	128	101
	AC #1 + CNTs	102	118	137	125

Cyclic voltammetry is a very powerful method to evaluate electrochemical property of various materials [51-56] (Detailed explanations and fundamentals can be found in Chapter 3). However, its dynamic nature (i.e. the electrode potential changes continuously) may lead to results different from that obtained via measurements under a steady state. Therefore, charging-discharging the electrode with a constant current (i.e. Galvanostatic charging-discharging (GCD)) was introduced to measure the capacitance value.

(a)



(b)

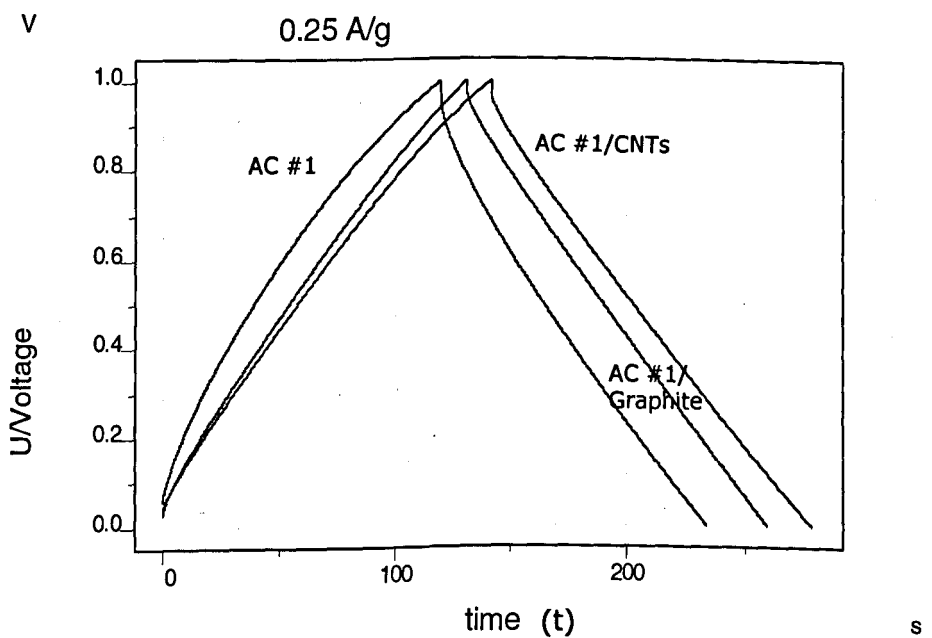


Figure 5.12 Galvanostatic charge-discharge data of AC #1 (the plot placed on the left side), AC#1 + 15 wt% graphite and AC #1 (the one in the middle) + 15 wt% CNTs (right side plot) for differently applied specific current in 3 M KCl, (a) 0.5 A/g, (b) 0.25 A/g

Different electrochemical properties of materials can be obtained from GCD. Figure 5.12 demonstrates the potential and time plots obtained during charging-discharging at different constant currents. When constant current is applied to the cell, the cell voltage increases with time, but not as linear as that of the other two mixtures. Since the charging mechanism for carbon materials mainly relies on non-faradaic charge separation, the cell voltage of an ideal double layer capacitor should display a straight line with time at constant current. Thus, the deviation shown by AC#1 alone indicates that the cell was not ideally polarised due to its high internal resistance. As explained in the previous section, the high resistance of AC#1 and its porous structure may cause incomplete and non-uniform charging along the electrode surface, which may result in faradaic side reactions [57-59].

Table 5.4 Specific capacitance and IR drop

		AC #1	AC #1/ Graphite	AC #1/ CNTs
Specific capacitance (F/g)	0.25 A/g	104	130	138
	0.5 A/g	74	120	126
IR drop (mV)	0.25 A/g	60	33	34
	0.5 A/g	117	60	64

According to Table 5.4, specific capacitance (F/g) drops as specific current increases (A/g). This is directly related with the time period t for ion transport (material utilisation) to polarise the electrode. Relatively shorter time is given for the charge accumulation to achieve certain degree of polarisation with the higher specific current and vice versa with the lower specific current. In the presence of the conducting additive, the resistance

of the cell is reduced almost by half. This explains why the GCD plots show better straight lines in the case of the two mixtures (AC #1/graphite, AC #1/CNTs) compared to that of AC #1 on its own.

5.3.2. EFFECT OF POTENTIAL GRADIENTS ON CYCLING STABILITY

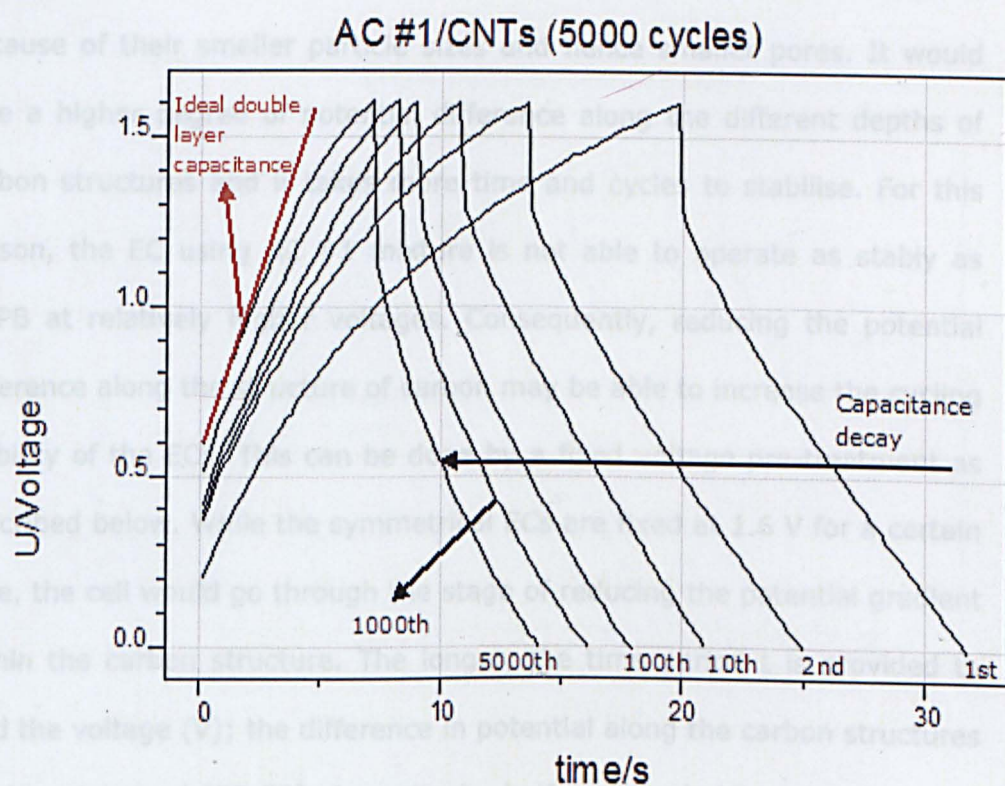
The maximum operating cell voltage of symmetrical ECs in neutral aqueous electrolytes was determined earlier in this chapter to be 1.6 V using CMPB as the film material. The achievable operating voltage could vary, depending on the property of the active material when the other conditions (e.g. electrolytes, current collectors, membranes, geometric area of electrode and so on) remain the same. Different materials have different particle sizes, porous structures, and electronic and ionic conductivities. Therefore, charging efficiency (degree of polarisation) should be different even if the same amount of energy (electrical energy) is provided. Although the maximum operating voltage of symmetrical ECs using CMPB is determined to be 1.6 V, this may not be the case using other materials. AC #1 is expected to possess a different electrochemical stability from CMPB. Thus, the charging efficiency (degree of polarisation) and operating cell voltage should be different. In this study, effective approaches to increase cycling stability are suggested using AC #1 with 15 wt % CNTs since the material shows the best result in terms of specific capacitance and fast current response. Similarly, this mixture (AC #1/CNTs) is expected to display superior energy characteristics compared to other tested materials and their mixtures.

A pre-treatment of constant voltage holding before a cycling test was carried out to examine its effect on EC's cycle life. Two single cells using EQ

and UE designs were pre-treated at the fixed voltages of 1.6 V and 1.9 V for 30 minutes and the other two was tested without the pre-treatment for comparison. After treated at the fixed voltage, the cycling test reveals how effective this method is. These results are presented in Figures 5.13 (1.6 V EQ design) and 5.14 (1.9V UE design).

Although the maximum operating voltage of symmetrical ECs using CMPB is proven to be 1.6 V, AC #1 with CNTs is not able to perform the same, as shown in Figure 5.13 (a). Specific capacitance for the mixture, which can be calculated by $C = I/(dU/dt)$, continuously decreases over 5000 cycles. Moreover, resistance of the ECs increases linearly with the number of cycles, which can be observed from the IR drop at the highest voltage. The type of ECs tested in this study was EDLC which utilised carbon materials. Therefore, the specific capacitance value of these ECs should become stable after a certain number of cycles. However, the ECs using AC #1 with 15 wt % CNTs did not demonstrate a stabilising stage over the given cycles. This feature suggests that some active sites where ions in the electrolyte can access initially became inactive and were no longer able to take a part in charge separation processes. This may be due to the uneven charging process which is normally observed in the initial cycles as already explained previously [57-59]. This effect is more noticeable in the case of AC #1 relative to CMPB because of their smaller particle sizes and hence pores. It would give a higher degree of potential difference along the different depths of carbon structures and it takes more time and cycles to stabilise. This feature suggests that some active sites where ions in the electrolyte can access initially became inactive and were no longer able to take a part in charge separation processes. This may be due to the non-uniform charging process which is normally observed in the initial cycles as already explained previously [57-59].

(a)



(b)

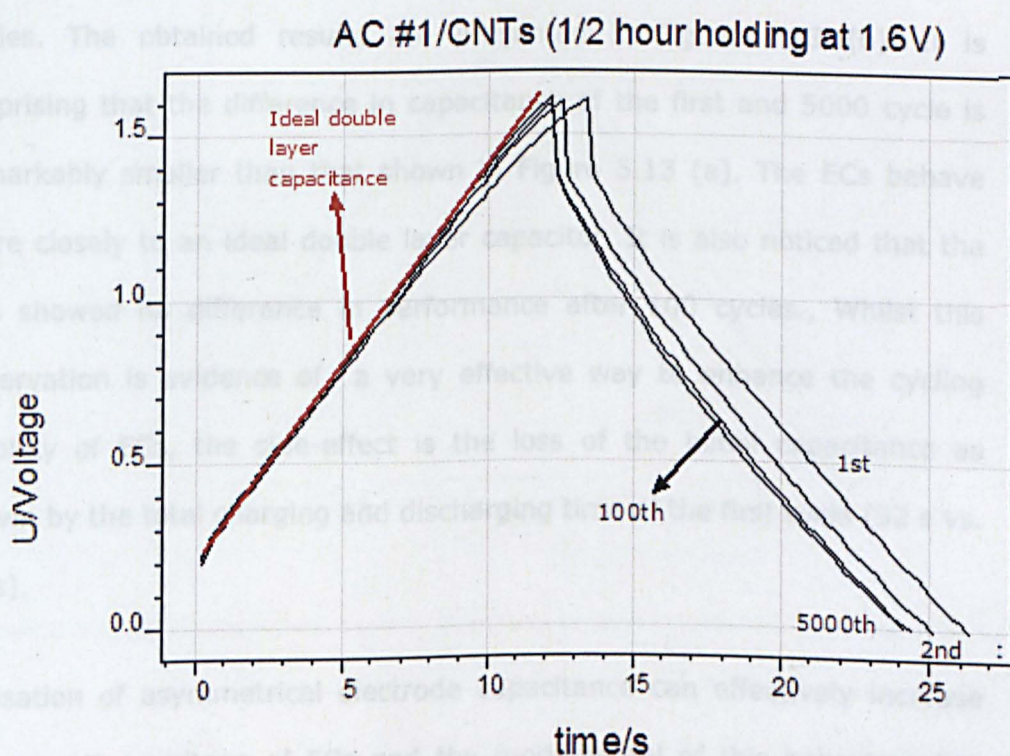
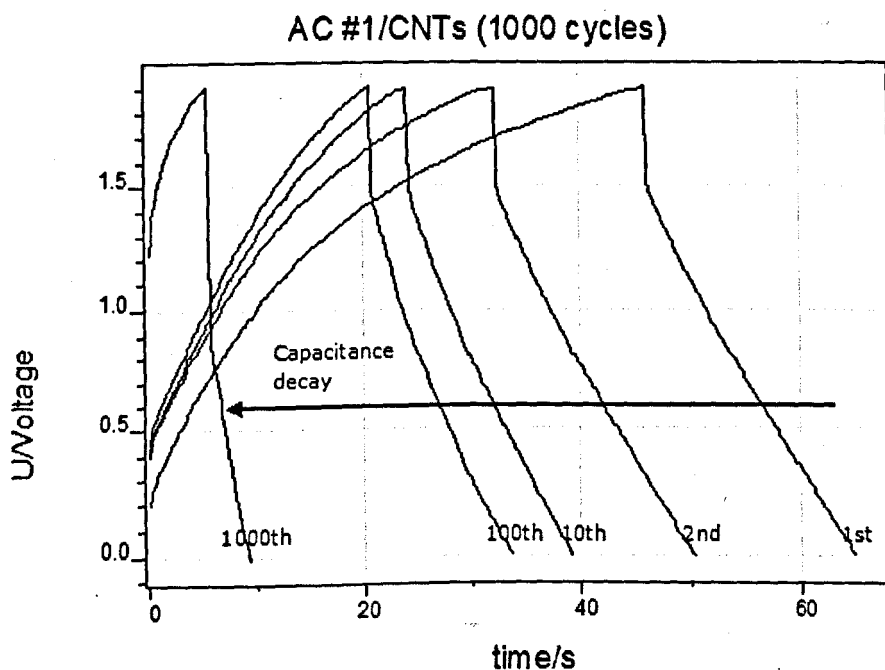


Figure 5.13 Comparison of cycling stabilities of symmetrical ECs using AC #1 with 15 wt % CNTs up to 5000 cycles in 3 mol/L KCl (0 to 1.6 V), (a) without (b) with constant voltage holding

This effect is more noticeable in the case of AC #1 relative to CMPB because of their smaller particle sizes and hence smaller pores. It would give a higher degree of potential difference along the different depths of carbon structures and it takes more time and cycles to stabilise. For this reason, the EC using AC #1 mixture is not able to operate as stably as CMPB at relatively higher voltages. Consequently, reducing the potential difference along the structure of carbon may be able to increase the cycling stability of the ECs. This can be done by a fixed voltage pre-treatment as described below. While the symmetrical ECs are fixed at 1.6 V for a certain time, the cell would go through the stage of reducing the potential gradient within the carbon structure. The longer, the time period t is provided to hold the voltage (V); the difference in potential along the carbon structures will be minimised [57-59]. Accordingly, half an hour holding time at 1.6 V was applied to the ECs using AC #1/CNTs before they went through 5000 cycles. The obtained results are presented in Figure 5.13 (b). It is surprising that the difference in capacitance of the first and 5000 cycle is remarkably smaller than that shown in Figure 5.13 (a). The ECs behave more closely to an ideal double layer capacitor. It is also noticed that the ECs showed no difference in performance after 100 cycles., Whilst this observation is evidence of a very effective way to enhance the cycling stability of ECs, the side-effect is the loss of the initial capacitance as shown by the total charging and discharging time of the first cycle (32 s vs. 26 s).

Utilisation of asymmetrical electrode capacitance can effectively increase the operating voltage of ECs and the fundamental of this behaviour has been explained previously. Therefore, the results from the three-electrode system which demonstrates better utilisation of negative potentials of the carbon materials are omitted to avoid repetition.

(a)



(b)

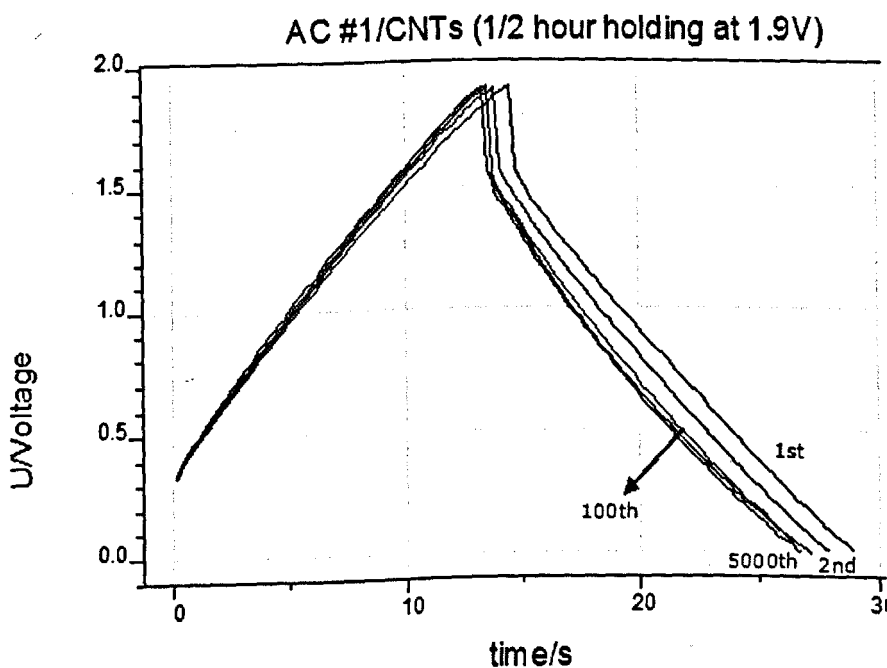


Figure 5.14 Comparison of cycling stabilities of asymmetrical ECs (unequalled electrode capacitance) using AC #1 with 15 wt % CNTs up to 5000 cycles in 3 mol/L KCl (0 to 1.9 V): (a) without (b) with constant voltage holding.

ECs using AC #1 with 15 wt % CNTs have successfully displayed a 1.9 V operating voltage. However, the approach to the result was somewhat different from the ECs using CMPB. Although resistance of the AC #1/CNTs mixture has been reduced dramatically relative to AC #1 on its own, the mixture's resistance is still higher than that of CMPB. This may be the reason that the ECs using the mixture cannot reach up to 1.9 V due to a significant degree of potential gradients within the active material. As shown in the 1.6 V symmetrical ECs, holding the cell at 1.9 V for 30 minutes showed a dramatic change of the cell's long-term cycling behaviour and the results are shown in Figure 5.14. This is indeed very strong evidence that the potential gradients which build along the surface and pores of the active materials caused remarkable effects in terms of cycling stability of ECs. Continuous charging-discharging cycles with uneven potentials noticeably reduce the life span of ECs, most likely because this causes faradaic side reactions [57-59].

Continuous increase of the IR drop over a number of cycles without the constant voltage holding (Figure 5.14 (a)) further supports the argument and this may be the reason of rapid capacitance drop. Conversely, this behaviour of rapid capacitance drop is not observed in the ECs pre-treated by constant voltage holding before the stability test. As explained, the unevenness of potentials built along and within the active materials initially became more uniform through the holding process by redistributing the ions along the carbon structures [57-59].

5.4. ENERGY CAPACITY OF NEUTRAL AQUEOUS ECs

As mentioned previously, the ECs with organic solvent are widely accepted in industry although a number of drawbacks of the device have been reported (more detailed explanations can be found in Chapter 4) [60, 61]. Water-based (aqueous) ECs are less popular due to their lower operating voltage [60]. However, this study suggests that ECs with aqueous electrolytes have a great potential and their characteristics in terms of energy capacity can surpass that of the commercial ECs using organic solvents. Due to a number of advantages of the water-based systems, their potential applications are expected to be huge as long as the ECs display satisfactory energy capacity. Table 5.5 shows the energy characteristics of different carbon materials and their mixtures in neutral aqueous electrolytes.

The highest specific energy amongst the constructed ECs can be found in AC #1 with 15 wt % CNTs. This mixture with asymmetrical design (unequalised electrode capacitances) shows remarkably promising energy characteristics, reaching above 20 Wh/kg. This value is almost three times of that of commercially available ECs with organic solvents. Although the operating cell voltage using neutral aqueous electrolytes is noticeably lower than commercial ECs with organic electrolytes (2.5 to 2.7 V) [61], specific energy (calculated with equation 1) utilising aqueous electrolytes is remarkably higher. This is attributed to optimised cell design and high specific capacitance in aqueous electrolytes since the distance, d , of the electric double layer is, generally speaking, relatively shorter in aqueous electrolytes than in organic solvents [62].

Table 5.4 Performance of ECs with different carbon materials and mixtures

		Cell design S=symmetrical, UE=Unequalisation	Cell specific capacitance (F/g)	Maximum operating voltage (V)	Specific energy (Wh/kg)	ESR (mΩ)	*Ideal operating condition (maximum power)
ECs	CMPB	S	20	1.6	7.1	18	High power (Up to 1 kW/kg)
		UE	17	1.9	8.5		
	AC #1	S	28	1.3	6.6	100	Low power (Up to 100 W/kg)
		UE	24	1.5	7.5		
	AC #1/ graphite	S	38	1.4	10.3	25	Medium power (Up to 600 W/kg)
		UE	32	1.8	14.4		
	AC #1/ CNTs	S	48	1.6	17.1	19	High power (Up to 1 kW/kg)
		UE	41	1.9	20.1		

* The power values were obtained from the ESR from IR drop which were previously presented in this chapter using GCD (3 M KCl). The maximum operating voltages used in maximum power were based on the design with the unequalised capacitance to achieve higher voltage.

Maximum operating voltages in aqueous electrolytes, which are typically known to display around 1 - 1.6 V in the recent literature due to water decomposition [25, 26, 30], has been successfully extended up to 1.9 V using unequalised (UE) electrode capacitances and pre-treatment at the maximum voltage. The asymmetrical design increases the overall cell voltage by utilising more or completely the potential range of the negative electrode due to the high hydrogen overpotential. Moreover, pre-treatment of the ECs at the highest voltage up to 1.9 V before charging-discharging cycling successfully improved their cycling stability. Considering that commercial ECs show usually specific energy between 5 to 8 Wh/kg, the ECs of CMPB and AC #1 in this study demonstrate competitive results. The mixtures of AC#1 and graphite and AC #1-CNTs display far higher specific energy up to 20 Wh/kg. ECs using CMPB and AC #1/CNTs are suitable for both fast and slow rates and this indicates the excellent kinetics of ions (mass) transport within those carbon structures.

References

1. Conway, B. E., *Electrochemical supercapacitors: scientific fundamentals and technological applications*. 1999: Springer, New York.
2. Hulicova, D., Kodama, M. and Hatori, H., *Electrochemical performance of nitrogen-enriched carbons in aqueous and non-aqueous supercapacitors*. Chem. Mater., 2006. **18**(9): p. 2318-2326.
3. Frackowiak, E., *Carbon materials for supercapacitor application*. Phys. Chem. Chem. Phys., 2007. **9**(15): p. 1774-1785.

4. Jin, X., Zhou, W., Zhang, S. and Chen, G. Z., *Nanoscale Microelectrochemical Cells on Carbon Nanotubes*. *Small*, 2007. **3**(9): p. 1513-1517.
5. Wang, Y., Shi, Z., Huang, Y., Ma, Y., Wang, C., Chen, M. and Chen, Y., *Supercapacitor Devices Based on Graphene Materials*. *J. Phys. Chem. C*, 2009. **113**(30): p. 13103-13107.
6. Hu, Z. A., Xie, Y. L., Wang, Y. X., Mo, L. P., Yang, Y. Y. and Zhang, Z. Y., *Polyaniline/SnO₂ nanocomposite for supercapacitor applications*. *Mater. Chem. Phys.*, 2009. **114**(2-3): p. 990-995.
7. Zheng, J. P. and Jow, T. R., *A New Charge Storage Mechanism for Electrochemical Capacitors*. *J. Electrochem. Soc.*, 1995. **142**(1): p. L6-L8.
8. Nagarajan, N. and Zhitomirsky, I., *Cathodic electrosynthesis of iron oxide films for electrochemical supercapacitors*. *J. Appl. Electrochem.*, 2006. **36**(12): p. 1399-1405.
9. Chang, K. H., Hu, C. C., Huang, C. M., Liu, Y. L. and Chang, C. I., *Microwave-assisted hydrothermal synthesis of crystalline WO₃-WO₃·0.5 H₂O mixtures for pseudocapacitors of the asymmetric type*. *J. Power Sources*, 2011. **196**: p. 2387-2392.
10. Gujar, T. P., Shinde, V. R., Lokhande, C. D. and Han S. H., *Electrosynthesis of Bi₂O₃ thin films and their use in electrochemical supercapacitors*. *J. Power Sources*, 2006. **161**(2): p. 1479-1485.
11. Rajeswari, J., Kishore, P. S., Viswanathan, B. and Varadarajan, T. K., *One-dimensional MoO₂ nanorods for supercapacitor applications*. *Electrochem. Commun.*, 2009. **11**(3): p. 572-575.

12. Lee, H. Y. and Goodenough, J. B., *Ideal supercapacitor behavior of amorphous $V_2O_5 \cdot nH_2O$ in potassium chloride (KCl) aqueous solution.* J. Solid State Chem., 1999. **148**(1): p. 81-84.
13. Choi, D., Blomgren, G. E. and Kumta, P. N., *Fast and Reversible Surface Redox Reaction in Nanocrystalline Vanadium Nitride Supercapacitors.* Adv. Mater., 2006. **18**(9): p. 1178-1178.
14. Liu, T. C., Pell, W. G., Conway, B. E. and Roberson, S. L., *Behavior of molybdenum nitrides as materials for electrochemical capacitors.* J. Electrochem. Soc., 1998. **145**: p. 1882-1888.
15. Snook, G. A. and Chen, G. Z., *The measurement of specific capacitances of conducting polymers using the quartz crystal microbalance.* J. Electroanal. Chem., 2008. **612**(1): p. 140-146.
16. Du Pasquier, A., Plitz, I., Menocal, S. and Amatucci, G. A *comparative study of Li-ion battery, supercapacitor and nonaqueous asymmetric hybrid devices for automotive applications.* J. Power Sources, 2003. **115**(1): p. 171-178.
17. Burke, A., *Ultracapacitors: why, how, and where is the technology.* J. Power Sources, 2000. **91**(1): p. 37-50.
18. Jurewicz, K., Frackowiak, E. and Béguin, F., *Towards the mechanism of electrochemical hydrogen storage in nanostructured carbon materials.* Appl. Phys. A: Mater. Sci. Proc., 2004. **78**(7): p. 981-987.
19. McBreen, J., Olender, H. and Srinivasan, S., *Carbon supports for phosphoric acid fuel cell electrocatalysts: alternative materials and methods of evaluation.* J. Appl. Electrochem., 1981, **11**: p. 787-796

20. Haacke, G., Longordo, E., Andrawes, F. F. and Campbell, B. H., Interactions between light stabilizers and pigment particles in polymeric coatings., *Progress in organic coatings*, 1997, **34**(1-4): p. 75-83
21. Haacke, G., Longordo, E., Brinen, J. S, Andrawes, F. F. and Campbell, B. H., Chemisorption and physical adsorption of light stabilizer on pigment and ultrafine particles in coatings., *Journal of Coating Technology*, 1999, **71**(888): p. 87-94
22. Zhou, X., Peng, C. and Chen, G. Z., 20 V stack of aqueous supercapacitors with carbon (-), titanium bipolar plates and CNT-polypyrrole composite (+). *AIChE Journal*, 2012, **58**: p. 974-983.
23. Sing, K. S. W., Everett, D. H., Haul, R. A. W., Moscou, L., Pierotti, R. A. and Rouquerol, J., Reporting physisorption data for gas/solid systems with special reference to the determination of surface area and porosity. *Pure and Applied Chemistry*, 1985, **57**: p. 603-619.
24. Simon, P. and Burke, A., Nanostructured carbon; double-layer capacitance and more., *Electrochem. Soc. Interface*, 2008, **17**: p. 38 - 43.
25. Demarconnay, L., *A symmetric carbon/carbon supercapacitor operating at 1.6 V by using a neutral aqueous solution*. *Electrochem. Commun.*, 2010. **12**(10): p. 1275-1278
26. Bichat, M. P., Raymundo-Piero, E. and Béguin, F., *High voltage supercapacitor built with seaweed carbons in neutral aqueous electrolyte*. *Carbon*, 2010. **48**(15): p. 4351-4361.

27. Peng, C., Zhang, S., Zhou, X. and Chen, G. Z., *Unequalisation of electrode capacitances for enhanced energy capacity in asymmetrical supercapacitors*. *Energ. Environ. Sci.*, 2010. **3**(10): p. 1499-1502.
28. Demarconnay, L., Raymundo-Pinero, E. and Beguin, F., *Adjustment of electrodes potential window in an asymmetric carbon/MnO₂ supercapacitor*. *J. Power Sources*, 2011. **196**(1): p. 580-586.
29. Khomenko, V., Raymundo-Piñero, E. and Béguin, F., *Optimisation of an asymmetric manganese oxide/activated carbon capacitor working at 2 V in aqueous medium*. *J. Power Sources*, 2006. **153**(1): p. 183-190.
30. Khomenko, V., Raymundo-Pinero, E., Frackowiak, E. and Beguin, F., *High-voltage asymmetric supercapacitors operating in aqueous electrolyte*. *Appl. Phys. A: Mater. Sci. Proc.*, 2006. **82**(4): p. 567-573.
31. Wang, Y., Shi, Z., Huang, Y., Ma, Y., Wang, C., Chen, M. and Chen, Y., *Supercapacitor devices based on graphene materials*. *J. Phys. Chem. C*, 2009. **113**(30): p. 13103-13107.
32. Liu, C., Yu, Z., Neff, D., Zhamu, A. and Jang, B. J., *Graphene-based supercapacitor with an ultrahigh energy density*. *Nano Lett.*, 2010. **10**: p. 4863-4868.
33. Stankovich, S., Dikin, D. A., Piner, R. D., Kohlhaas, K. A., Kleinhammes, A., Jia, Y., Wu, Y., Nguyen, S. T. and Ruoff, R. S., *Synthesis of graphene-based nanosheets via chemical reduction of exfoliated graphite oxide*. *Carbon*, 2007. **45**(7): p. 1558-1565.

34. Zhang, Y., Li, H., Pan, L. and Sun, T. L., *Capacitive behavior of graphene-ZnO composite film for supercapacitors*. J. Electroanal. Chem., 2009. **634**(1): p. 68-71.
35. Frackowiak, E., Khomenko, V., Jurewicz, K., Lota, K. and Beguin, F., *Supercapacitors based on conducting polymers/nanotubes composites*. J. Power Sources, 2006. **153**(2): p. 413-418.
36. Wang, D. W., Li, F. Zhao, J., Ren, W., Chen, Z. G., Tan, J., Wu, Z. S., Gentle, I., Lu, G. Q. and Cheng, H. M., *Fabrication of graphene/polyaniline composite paper via in situ anodic electropolymerization for high-performance flexible electrode*. ACS Nano, 2009. **3**(7): p. 1745-1752.
37. Zhang, J., Kong, L. B., Wang, B., Luo, Y. C. and Kang, L., *In-situ electrochemical polymerization of multi-walled carbon nanotube/polyaniline composite films for electrochemical supercapacitors*. Synth. Met., 2009. **159**(3-4): p. 260-266.
38. Yu, M. F., Lourie, O., Dyer, M. J., Moloni, K. Kelly, T. F. and Ruoff, R. S., *Strength and breaking mechanism of multiwalled carbon nanotubes under tensile load*. Science, 2000. **287**(5453): p. 637-640.
39. Poncharal, P., Wang, Z. L., Ugarte, D. and De Heer, W. A., *Electrostatic deflections and electromechanical resonances of carbon nanotubes*. Science, 1999. **283**(5407): p. 1513-1516.
40. Saito, R., Fujita, M., Dresselhaus, G. and Dresselhaus, M. S., *Electronic structure of graphene tubules based on C₆₀*. Am. Phys. Soc., 1992. **46**(3): p. 1804-1811.

41. Ebbesen, T. W., Lezec, H. J., Hiura, H., Bennett, J. W., Ghaemi, H. F. and Thio, T., *Electrical conductivity of individual carbon nanotubes*. Nature, 1996. **382**(6586): p. 54-56.
42. Kang, Y. J., Kim, B., Chung, H. and Kim, W., *Fabrication and characterization of flexible and high capacitance supercapacitors based on MnO₂/CNT/papers*. Synth. Met., 2010. **160**(23-24): p. 2510-2514.
43. Du, C., Yeh, J. and Pan, N., *High power density supercapacitors using locally aligned carbon nanotube electrodes*. Nanotechnology, 2005. **16**: p. 350.
44. Talapatra, S., Kar, S., Pal, S. K., Vajtai, R., Ci, L., Victor, P., Shaijumon, M. M., Kaur, S., Nalamasu, O. and Ajayan, P. M., *Direct growth of aligned carbon nanotubes on bulk metals*. Nat. Nanotech., 2006. **1**(2): p. 112-116.
45. Fan, Z., Chen, J. H., Zhang, B., Liu, B., Zhong, X. X. and Kuang, Y. F., *High dispersion of r-MnO₂ on well-aligned carbon nanotube arrays and its application in supercapacitors*. Diamond Relat. Mater., 2008. **17**(11): p. 1943-1948.
46. Gao, F., Zhang, L. and Huang, S., *Fabrication horizontal aligned MoO₂/single-walled carbon nanotube nanowires for electrochemical supercapacitor*. Mater. Lett., 2010. **64**(4): p. 537-540.
47. Park, J. H., Ko, J. M. and Park, O. O., *Carbon nanotube/RuO₂ nanocomposite electrodes for supercapacitors*. J. Electrochem. Soc., 2003. **150**(7): p. A864-A867.

48. Qian, D., Dickey, E. C., Andrews, R. and Rantell, T., *Load transfer and deformation mechanisms in carbon nanotube-polystyrene composites*. *Appl. Phys. Lett.*, 2000. **76**: p. 2868-2890.
49. Andrews, R., Jacques, D., Qian, D. and Rantell, T., *Multiwall carbon nanotubes: synthesis and application*, *Ace. Chem. Res*, 2002. **35**: p. 1008-1017.
50. Cochet, M., Maser, W. K., Benito, A. M., Callejas, M. A., Martinez, M. T., Benoit, J. M., Schreiber, J. and Chauvet, O., *Synthesis of a new polyaniline/nanotube composite: "in-situ" polymerisation and charge transfer through site-selective interaction*. *Chem. Commun.*, 2001. **2001(16)**: p. 1450-1451.
51. Compton, R. G. and Banks, C. E., *Understanding Voltammetry*, 2007, World Scientific Publishing Co. Pte. Ltd., Singapore
52. Bard, A. J. and Faulkner, L. R., *Electrochemical Methods: Fundamentals and Applications*, 2000, 2nd ed., Wiley, New York.
53. Kissinger, P. T. and Heineman, W. R., *Cyclic voltammetry*. *J. Chem. Educ.*, 1983. **60(9)**: p. 702.
54. Zoski, C. G., *Handbook of Electrochemistry.*, 2007, Elsevier Science, Oxford.
55. Krause, S., *Impedance methods; Encyclopedia of Electrochemistry*. 2003: Wiley-VCH.
56. Albery, W. J., Chen. Z., Horrocks, B.R., Mount, A.R., Wilson, P.J., Bloor, D., Monkman, A.T. and Elliott, C.M., *Spectroscopic and*

- electrochemical studies of charge transfer in modified electrodes.* Faraday Discuss. Chem. Soc., 1989. **88**: p. 247-259.
57. Black, J. and Andreas, H. A., *Effect of charge redistribution on self-discharge of electrochemical capacitors.* Electrochim. Acta, 2009, **54**: p. 3568-3574
58. Kaus, M., Kowal, J. and Sauer, D. U. *Modelling the effect of charge redistribution during self-discharge of supercapacitors.* Electrochim. Acta, 2010, **55**: p. 7516-7523
59. Graydon, J. W., Panjehshahi, M. and Kirk, D. W. *Charge redistribution in electrochemical capacitors.* Electrochem. Soc., 2010, 218th ECS Meeting: Abstract # 424
60. Zhang, L. L. and Zhao, X. S., *Carbon-based materials as supercapacitor electrodes.* Chem. Soc. Rev., 2009, 38: p. 2520 - 2531
61. Simon, P. and Burke, A., *Nanostructured carbon; Double-layer capacitance and more.* Electrochem. Soc. Interface, 2008, **17**: p. 38 - 43.
62. Sillars, F. B., Fletcher, S. I., Mirzaeian, M. and Hall, P. J. *Variation of electro-chemical capacitor performance with room temperature ionic liquid electrolyte viscosity and ion size.* Phys. Chemist. Chem. Phys., 2012, **14**: p. 6094-6100.

CHAPTER 6 MnO₂-CARBON ASYMMETRICAL ECs

In this chapter, the characteristics of MnO₂ nanocomposites synthesised with CNTs will be discussed. As mentioned, CNTs offer a number of advantages due to their unique properties. Therefore, the materials are very widely used as a backbone structure to support other nano materials such as transition metal oxides and conducting polymers. MnO₂ is one of the most popular materials in this research topic and often synthesised with CNTs to overcome shortcomings of MnO₂, particularly electrical conductivity. Therefore, the electrochemical characteristics of the materials were investigated with application of other analytical methods such as SEM, TEM and XRD. It should be pointed out that most of the nanocomposite materials in this study were based on acid treated CNTs, unless otherwise specified. The difference in performance between raw CNTs and the treated CNTs will be discussed in this chapter. Moreover, general structural characteristics, electrochemical properties of the binary composite (MnO₂/CNTs) and its synthesis from KMnO₄ as an oxidising agent are also presented. Using this composite and CMPB, an asymmetrical EC was constructed. Electrochemical analysis of the EC in terms of its rate performance, operating voltage and cycling stability was also carried out. Detailed explanation with the relevant data will be presented in this chapter.

6.1. ACID TREATED CNTS

6.1.1. BRIEF DESCRIPTION OF ACID TREATMENT

Most of the experiments based on CNTs utilised acid treated CNTs. The advantages of using the acid pre-treatment will be explained in this chapter. A brief introduction of the treatment procedure is as below.

A desirable amount of raw commercial CNTs (Multi-walled CNTs, 10–30 nm in diameter and 5–15 μm in length, were purchased from Shenzhen nanotech Port Co., Ltd) was measured and placed in a round flask. Then, concentrated sulphuric (98.0 %, Fluka Analytica) and nitric (> 69.0 %, Sigma-Aldrich) acids in the ratio 3:2 v/v are added to the flask and mixed well for a better contact between the solid CNTs particles and acidic liquid. The mixture of the CNTs and concentrated acids is boiled at a refluxing temperature of 105 °C for 20 minutes and enough time was given for the mixture to cool to room temperature. Once, the temperature reached the room temperature, the CNTs mixture with concentrated acids is diluted by adding deionised water and the acid treated CNTs were filtered and washed several times using both acetone and deionised water. After thorough washing and filtering processes, the wet product of pre-treated CNTs was dried at 60 °C for at least 24 hours. The final product was pulverised into fine powder using an agate pestle and mortar. Finally, the desired pre-treated CNTs were ready to use. These procedures are illustrated in Figure 6.1. Relevant literature regarding the procedure (acid pre-treated CNTs) can be found [1-3].

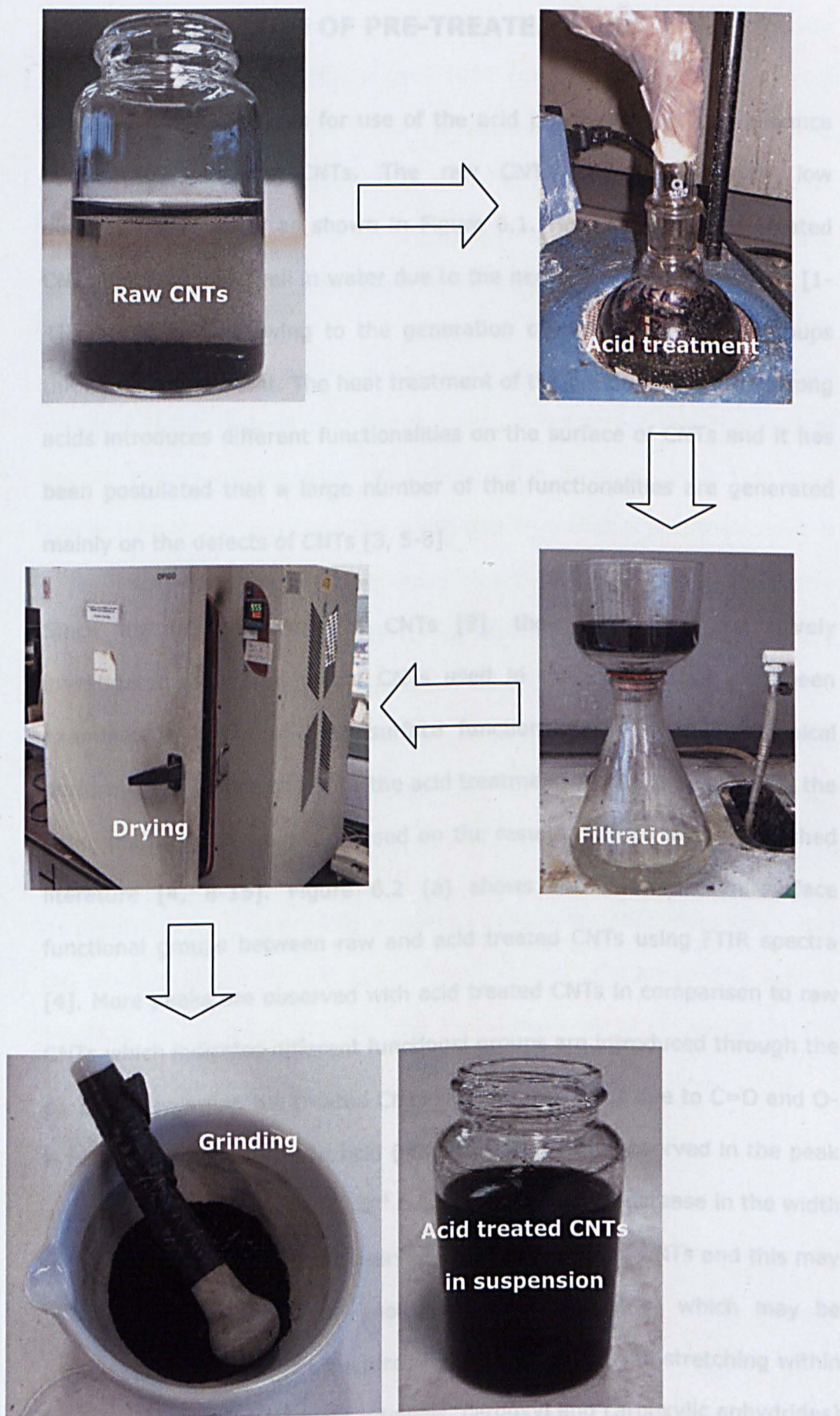


Figure 6.1 Brief procedures for the acid pre-treatment of CNTs [1-3]

6.1.2. DISCUSSION OF PRE-TREATED CNTs

One of the main reasons for use of the acid pre-treatment is to enhance hydrophilicity of the CNTs. The raw CNTs show significantly low dispersibility in water as shown in Figure 6.1. However, the acid treated CNTs disperse very well in water due to the negatively charged surface [1-4]. This is largely owing to the generation of surface functional groups through the treatment. The heat treatment of the pristine CNTs with strong acids introduces different functionalities on the surface of CNTs and it has been postulated that a large number of the functionalities are generated mainly on the defects of CNTs [3, 5-8].

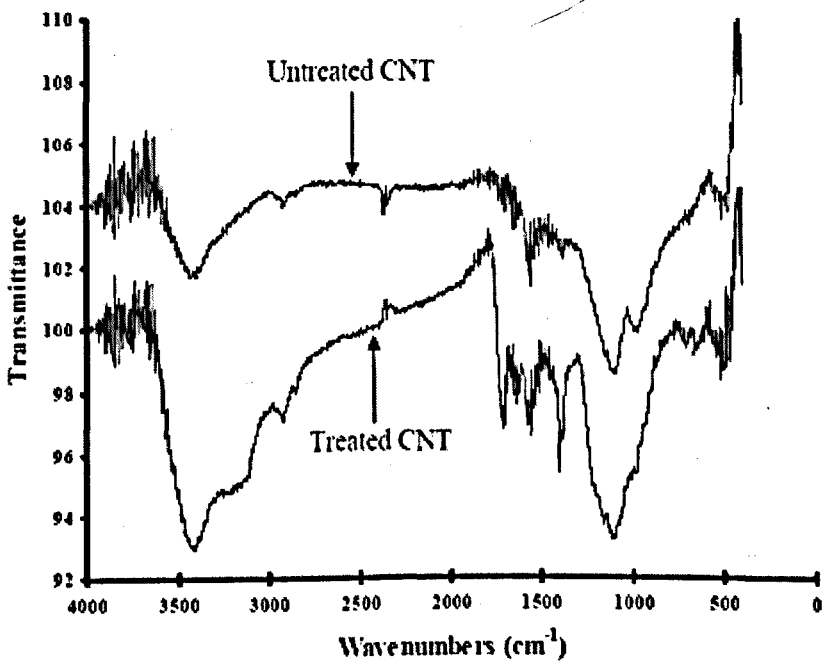
Since the first discovery of CNTs [9], they have been extensively investigated. The commercial CNTs used in this study have also been examined in terms of their surface functionalities and electrochemical performances before and after the acid treatment. A brief discussion on the same material will be given based on the results claimed in the published literature [4, 8-15]. Figure 6.2 (a) shows the difference in surface functional groups between raw and acid treated CNTs using FTIR spectra [4]. More peaks are observed with acid treated CNTs in comparison to raw CNTs which indicates different functional groups are introduced through the process. Regarding the treated CNTs, absorption bands due to C=O and O-H bending in the carboxylic acid (-COOH) group were observed in the peak around 1710 cm^{-1} and 1400 cm^{-1} respectively [4, 10]. Increase in the width of the broad peak was also observed in the acid treated CNTs and this may be attributed to the water molecules (O-H stretching) which may be trapped within the CNTs structures [8, 11, 12]. C-O bond stretching within the oxygen functional groups (phenols, carboxyl and carboxylic anhydrides) was also evidenced by the peak around 1200 cm^{-1} [4, 13, 14]. The FTIR

spectra also provided structural information for the CNTs before and after treatment. More specifically, a peak (981 cm^{-1}) observed in the pristine CNTs, which was thought to be due to structural defects of the CNTs, no longer existed in the treated CNTs and this is an evidence of successful modification of the defects through the process [4]. These structural defects are known to improve the oxidation of the surfaces of CNTs [15].

The acid treatment shows a significant influence on electrochemical property of the material and this is shown in Figure 6.2 (b). The level of specific current response in the treated CNTs displays about 5-6 times higher than that of pristine CNTs which directly indicates that the former is capable of storing significantly more energy. Moreover, the distinctive humps along the cycle (a_1 , a_2 , c_1 , c_2) indicate the presence of surface functional groups. These clearly show that the acid treatment provides surface functionalities which enhance hydrophilicity of the material and also extra capacity of energy storage due to redox reactions (pseudocapacitance) within the functional groups [4].

As previously mentioned, only a short discussion has been given to explain the effect of acid treatment since a large amount of study on this topic is available in literature [1-15]. The main focus of this chapter is the MnO_2/CNTs composite material.

(a)



(b)

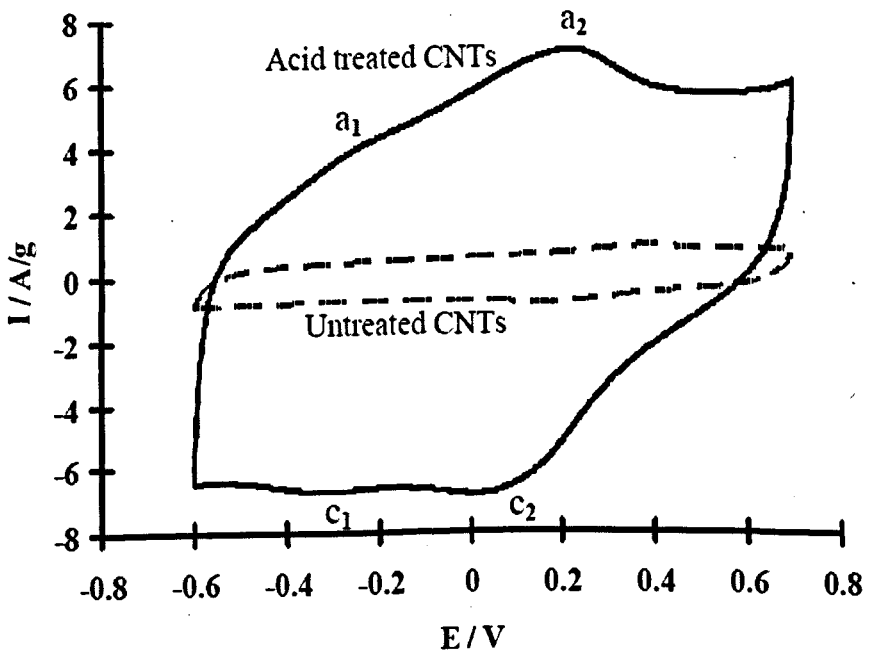


Figure 6.2 Comparison of raw and acid treated CNTs, (a) FTIR spectra, (b) CVs at 100 mV/s [4]

6.2. MnO₂/CNTs COMPOSITE

6.2.1. MATERIAL SYNTHESIS

A number of benefits use CNTs coated with metal oxides and conducting polymers, and many promising results have been reported in the literature [16-18, 19-24]. Especially, MnO₂ is one of the most widely investigated metal oxide as a positive electrode material in ECs [16, 17, 21, 22, 24-28]. Typically, MnO₂, which is one of the most popular semiconductor materials in this research area, can be produced by simply mixing Mn(VII) and Mn(II) [29-31]. However, this method is disadvantageous to synthesise the MnO₂/CNTs binary composite because the produced MnO₂ from the redox reactions of Mn(VII) and Mn(II) can form randomly on their own without CNTs. Therefore, an alternative synthetic method for the binary composite was suggested using KMnO₄ precursor as an oxidising agent [3]. Using the method, reduction of the Mn(VII) can take place mainly on the surface of CNTs and hence higher MnO₂ contents within the binary composite can be synthesised.

The natural colour of KMnO₄ solution is purple. In this work, once the Mn(VII) species were reduced completely to MnO₂, the colour of the solution changed to transparent light brown as shown in Figure 6.3. Although the natural colour of MnO₂ is brown, the produced composite displayed black due to the presence of CNTs. Complete consumption of the precursor (KMnO₄) can be indicated from this colour change of the solution (purple → transparent light brown).

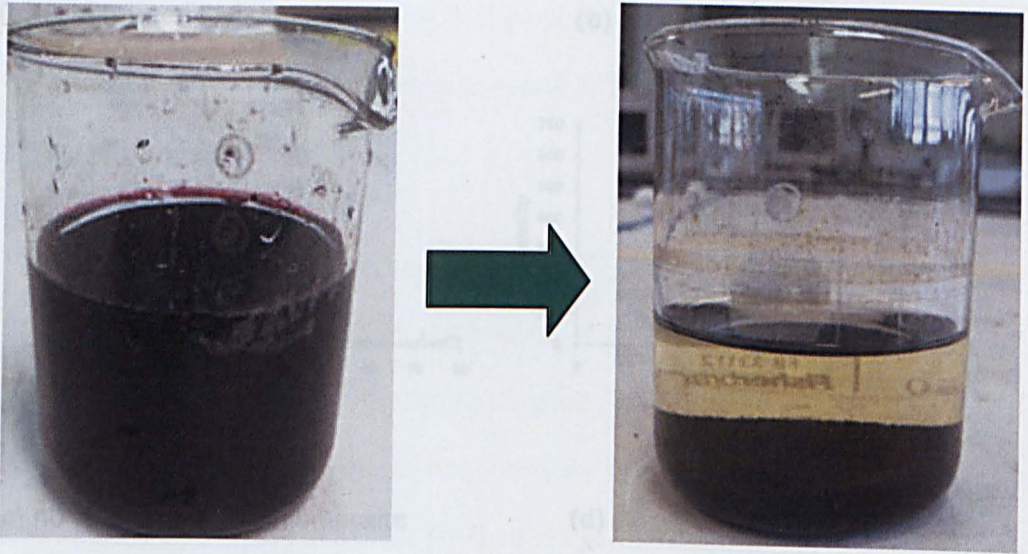
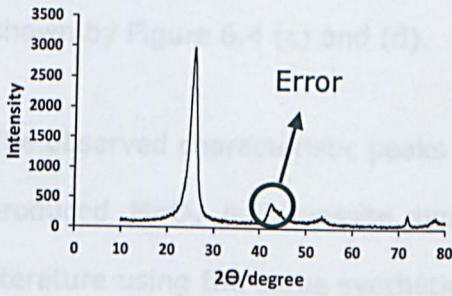


Figure 6.3 From KMnO_4 and CNTs solution to MnO_2/CNTs solution

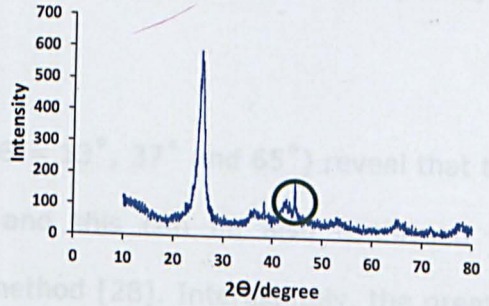
6.2.2. X-ray diffraction (XRD)

XRD examines the crystallinity of a material. Different materials have unique orientations of crystalline structures and it is possible to identify these materials using this technique. Before examining the MnO_2/CNTs binary composite, it is important to discuss CNTs. In this study, most of the composite materials were based on the acid treated CNTs. Figure 6.4 shows the XRD patterns of acid treated CNTs and of the 20 wt% MnO_2/CNTs composite. The diffraction peak at $2\theta = 26.2^\circ$ (graphite-like peak) presents the main features of the CNTs in the XRD pattern [28]. Evaluation of the optimum level in acid treatment is very important because the degree of crystallinity is directly related to both conductivity and physical strength of CNTs, resulting in significantly different characteristics for the composite materials.

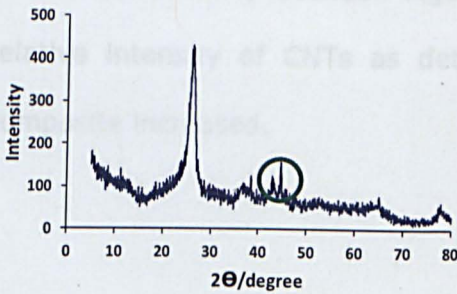
(a) Acid treated CNTs



(b) 20 wt% MnO₂/CNTs composite



(c) 40 wt% MnO₂/CNTs composite



(d) 70 wt% MnO₂/CNTs composite

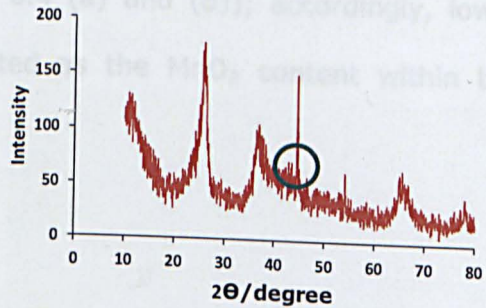


Figure 6.4 XRD data for (a) acid treated CNTs, (b) 20 wt %, (c) 40 wt% and (d) 70 wt% MnO₂/CNTs binary composites; Note that the peak shown at 42-44 degree is due to the error of the experimental device (Indicated as green circle in the figure)

Interestingly, the XRD pattern of the 20 wt% MnO₂/CNTs composite displayed broader and less clear features compared to that of the CNTs (Figure 6.4 (b)), indicating the presence of a significant proportion of amorphous (MnO_x) and disordered (CNTs) regions. This can be attributed to two reasons. Firstly, a large part of the produced MnO₂, which is mainly placed on both the outer and inner surfaces of the multi-wall CNTs [3], is amorphous. Secondly, the precursor (KMnO₄) oxidises the surfaces of acid-treated CNTs further, so there is a more disordered structure within the

back-bone CNTs. The degree of the broad and unclear features within XRD data becomes greater with more content of MnO_x within the composite, as shown by Figure 6.4 (c) and (d).

The observed characteristic peaks ($2\theta = 13^\circ$, 37° and 65°) reveal that the produced MnO_x is birnessite type and this can be also confirmed by literature using the same synthetic method [28]. Interestingly, the greater the MnO_x content is, the lower the intensity of the carbon peak at 26° due to the successful deposition of MnO_2 onto the surface of CNTs (differences in relative intensity between Figure 6.4 (a) and (d)); accordingly, lower relative intensity of CNTs as detected as the MnO_2 content within the composite increased.

6.2.3. EM ANALYSIS (SEM, TEM)

Scanning electron microscopy (SEM) and transmission electron microscopy (TEM) provide useful information about morphology and structure of materials. Although the purpose of the two devices is different (SEM mainly focuses on surface morphology, whereas TEM provides more information on the structure of materials), they are complementary to each other in many occasions when examining structures of materials.

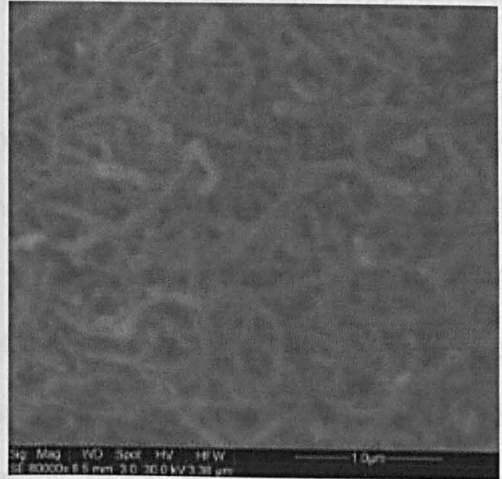
6.2.3.1. SEM DATA

SEM images were taken to examine and compare the surface morphologies of four different samples. The results are shown in Figure 6.5.

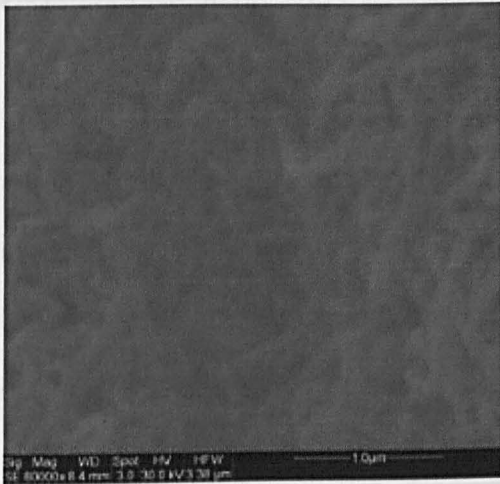
(a) 0 wt%



(b) 20 wt%



(c) 40 wt%



(d) 70 wt%

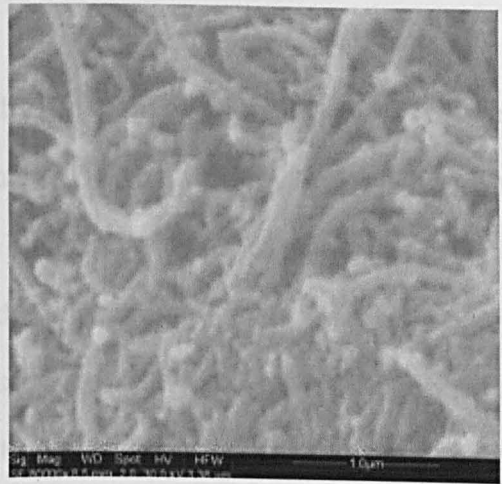


Figure 6.5 SEM images of four different samples, (a) acid treated CNTs, (b) 20 wt%, (c) 40 wt% and (d) 70 wt% MnO_2/CNTs binary composites

The SEM image of acid treated multi-walled CNTs (10 - 30 nm in diameter, Shenzhen Nanotech Port Co., Ltd.) is provided in Figure 6.5 (a) for a comparison purpose. The image reveals that the sizes of CNTs are very uniform and they do not lose their unique three dimensional structures even after the acid pre-treatment [32]. The three dimensional structure of acid treated CNTs are clearly observed and this unique feature of CNTs

significantly increases the amount of channels in various sizes, which enhances ion transfer within the structures (enhanced ionic conductivity). Moreover, the SEM image of the acid treated CNTs indicates their excellent electronic conductivity (cylindrical shaped continuous structure, the ratio between diameter and length is high). Better kinetics and electronic conductivity within the structures of materials are important for electrode materials for ECs. In particular, materials displaying pseudo-capacitance such as MnO_2 are able to show enhanced faradaic process, which is a key charge storage mechanism of transition metal oxides (more details in chapter 2.1.2. PSEUDO-CAPACITANCE), due to the better electronic and ionic conductivities.

Figure 6.5 (b), (c) and (d) show the images of the MnO_2/CNTs binary composites with different contents of MnO_2 (the weight % for MnO_2 and CNTs were determined by using thermogravimetric analysis (TGA)). Although the SEM Images provide the morphology focusing only on the surface, the difference in thicknesses of the individual CNT with the three different MnO_2 contents can be easily distinguished (the thickness of the individual CNT deposited 70 wt% MnO_2 is noticeably thicker than 20 wt% one). As the content of the MnO_2 deposition increased from 20 wt% to 70 wt%, the materials became more densely packed and closely located to each other. In addition, less clear images compared to the image of CNTs reveals the binary composites lost conductivity significantly due to the MnO_2 deposition. Therefore, lower ionic and electronic conductivities are expected as the MnO_2 contents increase and these are surely disadvantageous for utilisation of this particular binary composite as the positive electrode materials of ECs. This will be discussed later in seeking to overcome this potential problem.

6.2.3.2. TEM DATA

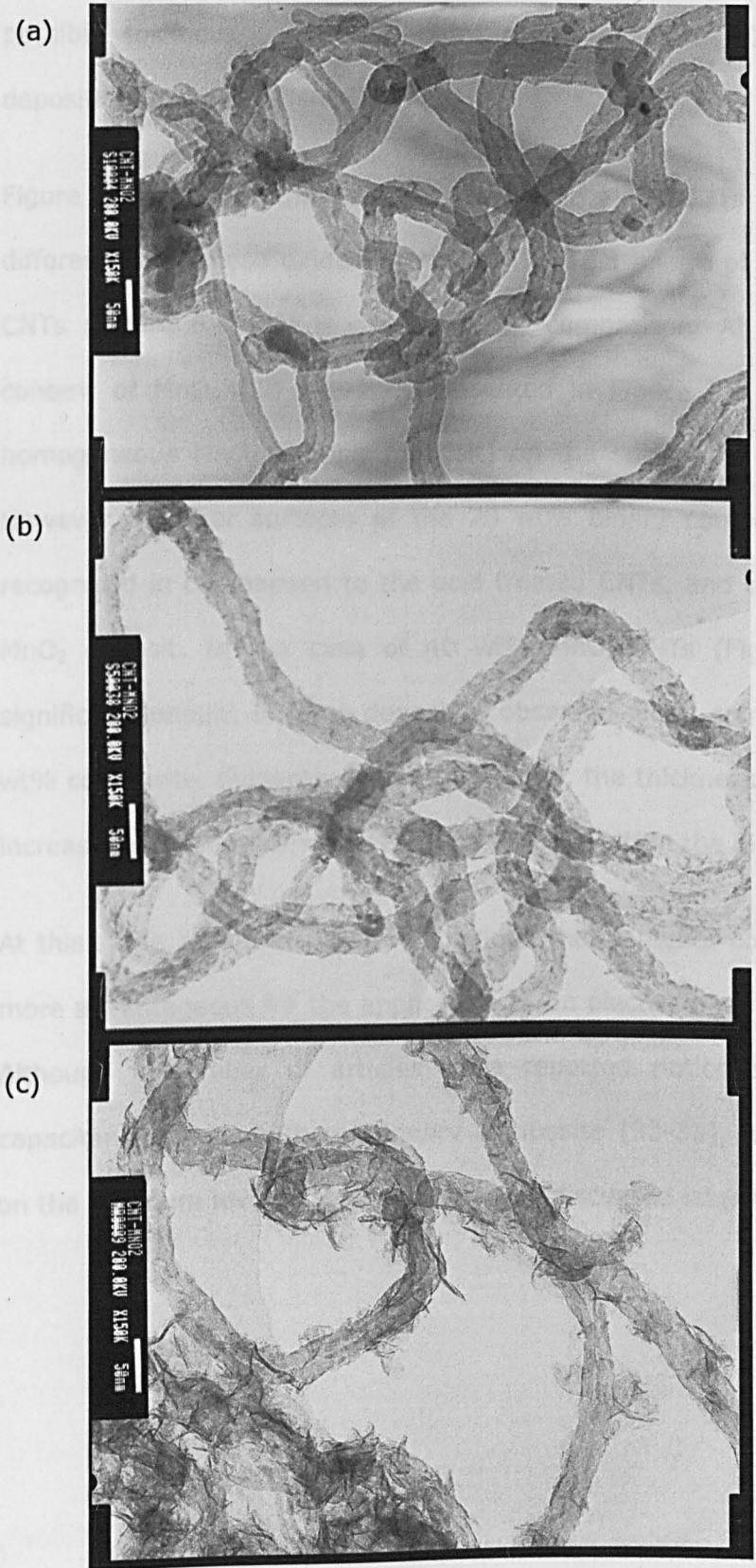


Figure 6.6 TEM images of (a) acid treated CNTs (b) 20 wt% and (c) 40 wt% of MnO₂/CNTs binary composites in MnO₂ contents

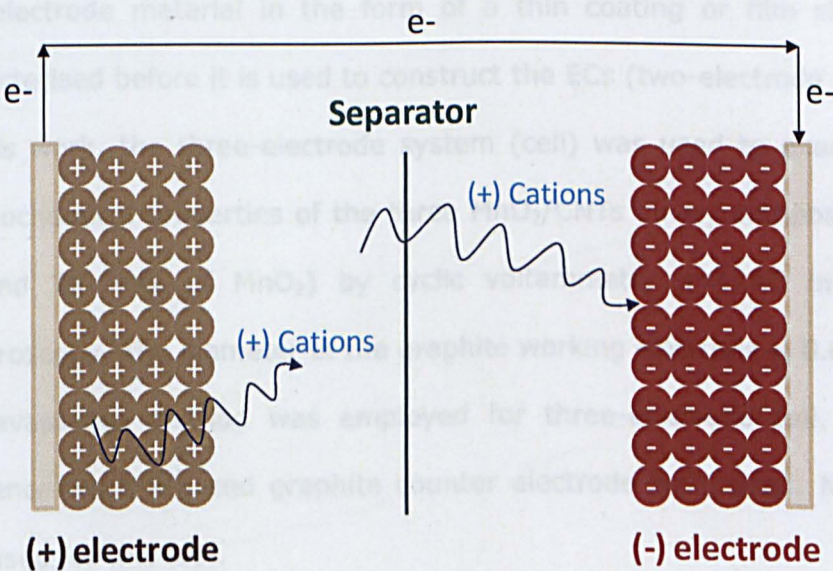
TEM can provide structural information of the materials, which is different from SEM that mainly focuses on surface of materials. Using TEM, it is possible to focus on the structure of an individual CNT and various deposition features of MnO_2 .

Figure 6.6 provides the TEM images of the MnO_2/CNTs composites with different manganese oxides contents. The TEM image of the acid treated CNTs (Figure 6.6 (a)) is presented for comparison. At a relatively low content of MnO_2 (20 wt%) as presented in Figure 6.6 (b), a thin and homogeneous MnO_2 coating (deposit) on the surface of CNTs is formed. However, rougher surfaces of the 20 wt% binary composites are easily recognised in comparison to the acid treated CNTs, and this is due to the MnO_2 deposit. In the case of 40 wt% MnO_2/CNTs (Figure 6.6 (c)), a significant amount of lump deposit is observed when compared to the 20 wt% composite. Evidently, and as expected, the thickness of MnO_2 coating increased with increasing the content of MnO_2 within the binary composite.

At this stage, it is premature to conclude that a higher content of MnO_2 is more advantageous for the application as an electrode material in the ECs. Although a number of articles have reported noticeably high specific capacitance values with this binary composite [33-35], few have focused on the optimum level of MnO_2 . This will be discussed later in this Chapter.

6.2.4. ELECTROCHEMICAL PROPERTY OF MnO₂/CNTs

In this section, electrochemical properties of the MnO₂/CNTs binary composites are examined for the application as a positive electrode material in asymmetrical ECs. The performance of various MnO₂/CNTs composites will be evaluated in terms of specific capacitance (F/g), resistance (Ω), electrochemical windows (V) and, eventually, specific energy of the asymmetrical supercapacitor using MnO₂/CNTs (+) and CMPB (-). Before the obtained results are introduced, their respective mechanism (positive and negative electrode) should be demonstrated briefly and this is shown in Figure 6.7.



*Pseudo capacitance (faradaic reaction)

- Amorphous structure (surface storage): $[(\text{MnO}_2)\text{-C}^+]\text{surface} \leftrightarrow (\text{MnO}_2)\text{surface} + \text{C}^+ + \text{e}^-$
- Crystalline structure (bulk storage): $[(\text{MnOO})\text{-C}^+] \text{ (intercalation)} \leftrightarrow (\text{MnO}_2) + \text{C}^+ + \text{e}^-$

C⁺: positive cations

* Double layer capacitance

- + hydrogen storage (high voltage)

Figure 6.7 Mechanisms of the positive (MnO₂) and negative (activated carbon) electrodes within an asymmetrical EC; combination of pseudo and double layer capacitances

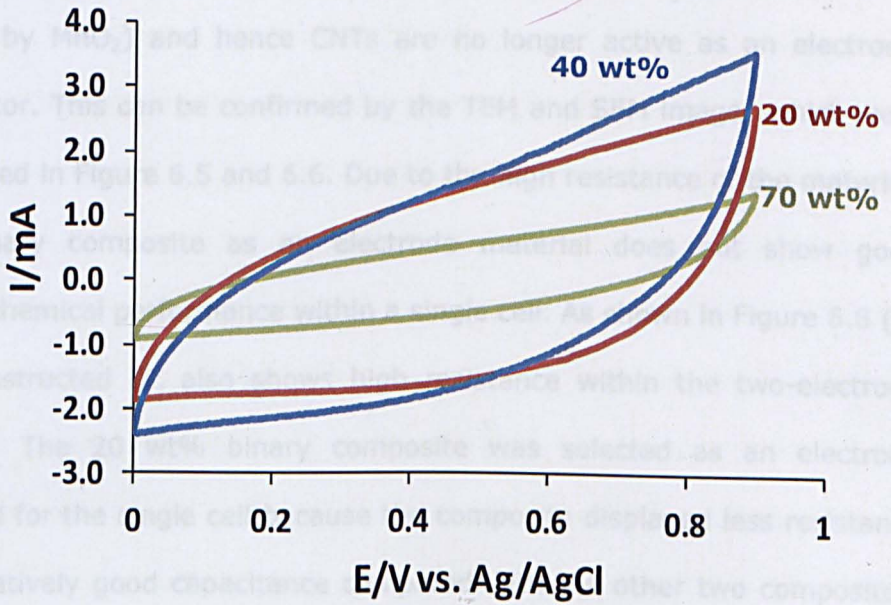
MnO₂ is one of the main focuses as a positive electrode in this thesis. Figure 6.7 demonstrates asymmetrical EC combining MnO₂ (+) and carbon (-) and the charge storage mechanism of MnO₂ is different from carbon materials. In particular, MnO₂ kicks out cations instead of attracting anions and gives out electrons through the external circuit when they are positively charged (higher oxidation state). When the EC is discharged, the MnO₂ material take electrons back to become a lower oxidation state and attract cations to achieve electro neutrality.

6.2.4.1. ELECTROCHEMICAL ANALYSIS OF MnO₂/CNTs

The electrode material in the form of a thin coating or film should be characterised before it is used to construct the ECs (two-electrode system). In this work, the three-electrode system (cell) was used to examine the electrochemical properties of the three MnO₂/CNTs binary composites (20, 40 and 70 wt% of MnO₂) by cyclic voltammetry and AC impedance spectroscopy. The diameter of the graphite working electrode is 0.6 cm and cast-evaporate method was employed for three-electrode cell. Ag/AgCl reference electrode and graphite counter electrode were used. No binder was used for this test.

As discussed previously, the incorporation of CNTs was expected to enhance both the ionic and electronic conductivity within the structures of the binary composite due to their unique, innate properties. However, the material still showed very resistive behaviour according to the CV data shown in Figure 6.8. Due to the low conductivity of MnO₂ coating, the overall shape of CVs is not quite close to rectangular and this is observed with all the three samples (20, 40, 70 wt% binary composites).

(a) Three-electrode system



(b) Symmetrical EC (Two-electrode system)

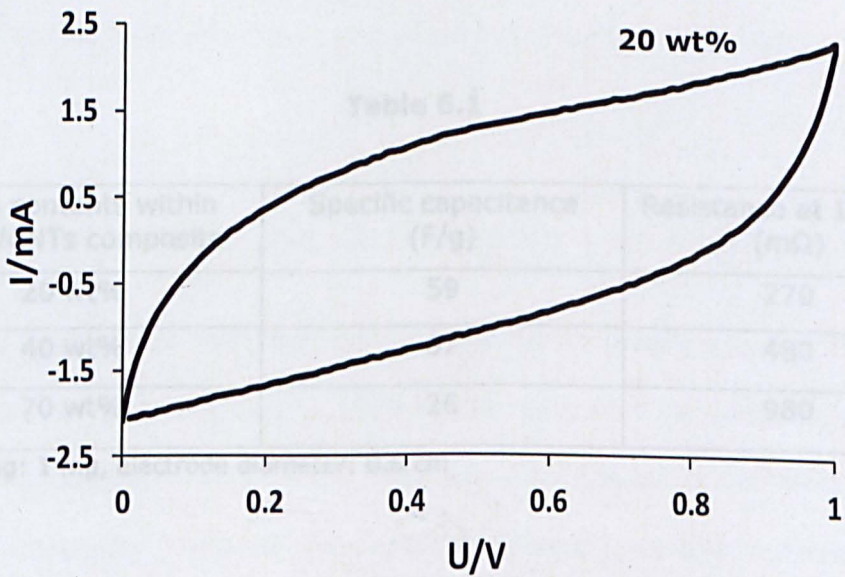


Figure 6.8 CVs at 20 mV/s of (a) 20, 40 and 70 wt % MnO₂/CNTs binary composites in the three-electrode system; electrode loading: 1 mg, (b) 20 wt% MnO₂/CNTs binary composite in the two electrode system; total loading: 5 mg (2.5 mg on each electrode)

The high resistance observed within the materials may be due to a consumption of CNTs' surfaces (most of the CNTs' surfaces is oxidised and coated by MnO₂) and hence CNTs are no longer active as an electronic conductor. This can be confirmed by the TEM and SEM images which were presented in Figure 6.5 and 6.6. Due to the high resistance of the material, the binary composite as an electrode material does not show good electrochemical performance within a single cell. As shown in Figure 6.8 (b), the constructed EC also shows high resistance within the two-electrode system. The 20 wt% binary composite was selected as an electrode material for the single cell because the composite displayed less resistance and relatively good capacitance compared with the other two composites. Detailed information in terms of specific capacitance (F/g) and resistive behaviour is presented in Table 6.1.

Table 6.1

MnO ₂ contents within MnO ₂ /CNTs composite	Specific capacitance (F/g)	Resistance at 10 mHz (mΩ)
20 wt%	59	270
40 wt%	67	480
70 wt%	26	980

* Loading: 1 mg, electrode diameter: 0.6 cm

It should be pointed out that the lowest specific capacitance is observed with the composite of highest MnO₂ contents. MnO₂ is well known to show pseudo-capacitive behaviour. Therefore, it was expected that higher contents of MnO₂ would be more advantageous to achieve higher values of specific capacitance. However, the result revealed that more contents of MnO₂ within the binary composite are not necessarily beneficial. Although

the specific capacitance value with the 40 wt% composite was slightly higher than that of 20 wt%, the difference in the capacitance is not significant considering the remarkable difference in their MnO₂ contents. As mentioned, this may be due to the high resistance of the composite and CNTs may not be able to carry out the role as an electronic conductor. Therefore, electrons cannot move through the structure smoothly and hence noticeably slow current response, which is evidenced by the non-rectangular CV in Figure 6.8. The drastic decrease in the specific capacitance from the 40 wt% to the 70 wt% composite indicates that a significant amount of dead volume with the 70 wt% composite was not electrochemically active and hence relatively less active sites were available for redox reactions. Therefore, an alternative approach should be considered to utilise the dead volume in the MnO₂/CNTs composite coating. Physical addition of electronic conductors is one of the often used methods to resolve this issue and this is presented in the following section.

6.2.4.2. ELECTROCHEMICAL ANALYSIS OF MnO₂/CNTs + ELECTRONIC CONDUCTOR

Physical addition of electronic conductor such as graphite and CNTs was found to be very effective to resolve the resistance problem within the system in Chapter 5.3.1. This method was also applied to the MnO₂/CNTs binary composite because the material showed resistive behaviour as demonstrated in Figure 6.7. Both graphite and CNTs were added as the electronic conductor. Accordingly, CNTs addition was found to be more effective and only the result with CNTs addition will be presented in this thesis (Comparison between graphite and CNTs as conducting additives can be found in Chapter 5.3.1).

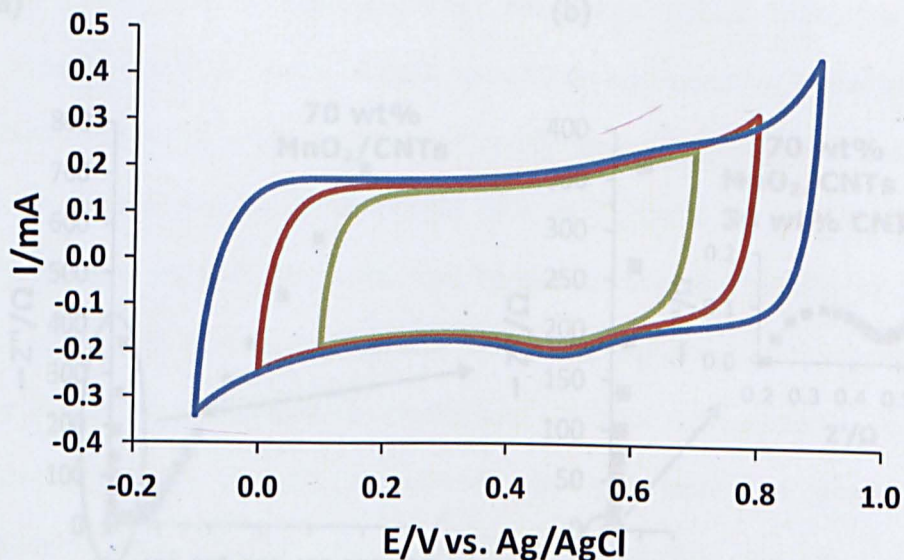


Figure 6.9 CVs at 20 mV/s of the 70 wt% MnO₂/CNTs composite with 30 wt% physical addition of CNTs to boost electronic conductivity; electrode loading: 250 μg

According to Figure 6.8, physical addition of acid treated CNTs dramatically resolves the resistance problem within the composite materials. The 70 wt% MnO₂/CNTs composite, which had the highest MnO₂ content amongst the three prepared samples, was selected to examine the effectiveness of the addition of CNTs. Due to the relatively thicker MnO_x coating on individual CNTs, which was evidenced by SEM and TEM images (Figure 6.5 and 6.6), the 70 wt% composite displayed highest resistance compared to the other two samples with lower MnO₂ contents. Even with the sample displaying the highest resistance, the shape of the CVs becomes very close to rectangular over positive ranges of potential up to 0.9 V vs. Ag/AgCl. Compared to the CVs shown in Figure 6.7, the addition of CNTs as an electronic conductor significantly reduces the resistance of the composite material.

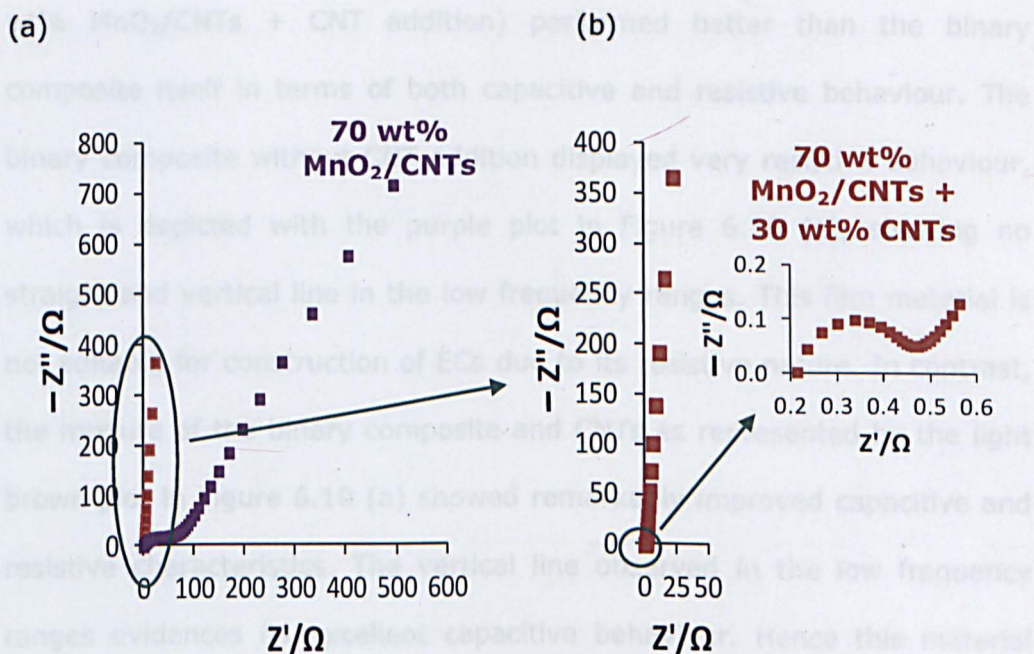


Figure 6.10 AC impedance spectroscopy data of (a) direct comparison between the size of 70 wt% MnO₂/CNTs composite and the mixture of 30 wt% CNTs to the 70 wt% composite, (b) magnified AC impedance data of the mixture (30 wt% CNTs + 70 wt% MnO₂/CNTs); a single cell design, total loading: 3 mg, frequency range: 100 kHz to 10 mHz, applied voltage: 0 V

6.2.5. CONSTRUCTION OF ASYMMETRICAL ECs

In the above section, the binary composite (MnO₂/CNTs) was shown to be a good electrode material for ECs. Previously, the physical mixture of CNTs and MnO₂/CNTs was proven to show noticeably better capacitive behaviour, with significantly smaller resistance in comparison to the composite without addition of CNTs. This was evidenced by the more rectangular CVs in Figure 6.9.

More detailed information of the material's capacitive and resistive behaviour is discussed below with reference to Figure 6.9. AC impedance spectroscopy was employed for this study. A direct comparison is made between the 70 wt% binary composite and its mixture with the CNTs. The result is shown in Figure 6.9 (a). It is straightforward that the mixture (70

wt% MnO_2/CNTs + CNT addition) performed better than the binary composite itself in terms of both capacitive and resistive behaviour. The binary composite without CNT addition displayed very resistive behaviour, which is depicted with the purple plot in Figure 6.10 (a), showing no straight and vertical line in the low frequency ranges. This film material is not suitable for construction of ECs due to its resistive nature. In contrast, the mixture of the binary composite and CNTs as represented by the light brown plot in Figure 6.10 (a) showed remarkably improved capacitive and resistive characteristics. The vertical line observed in the low frequency ranges evidences its excellent capacitive behaviour. Hence this material can be utilised as an electrode film material for ECs. Moreover, significantly smaller resistance (R) was observed with the mixture and this is evident in the size of semi-circles (charge transfer resistance) and the lengths of 45° line (diffusion resistance).

6.2.5. CONSTRUCTION OF ASYMMETRICAL ECs

In the above section, the binary composite (MnO_2/CNTs) was shown to have very resistive characteristics. Physical addition of CNTs to boost electronic conductivity within the material's structure was proven to be an effective approach. According to the electrochemical analysis, the mixture is suitable for use as a positive electrode material in an asymmetrical EC. In this study, electrochemical data of the asymmetrical EC fabricated from the mixture as a positive electrode and CMPB as a negative electrode will be presented.

6.2.5.1. MnO₂/CNTs + CNT MIXTURE AS A POSITIVE ELECTRODE

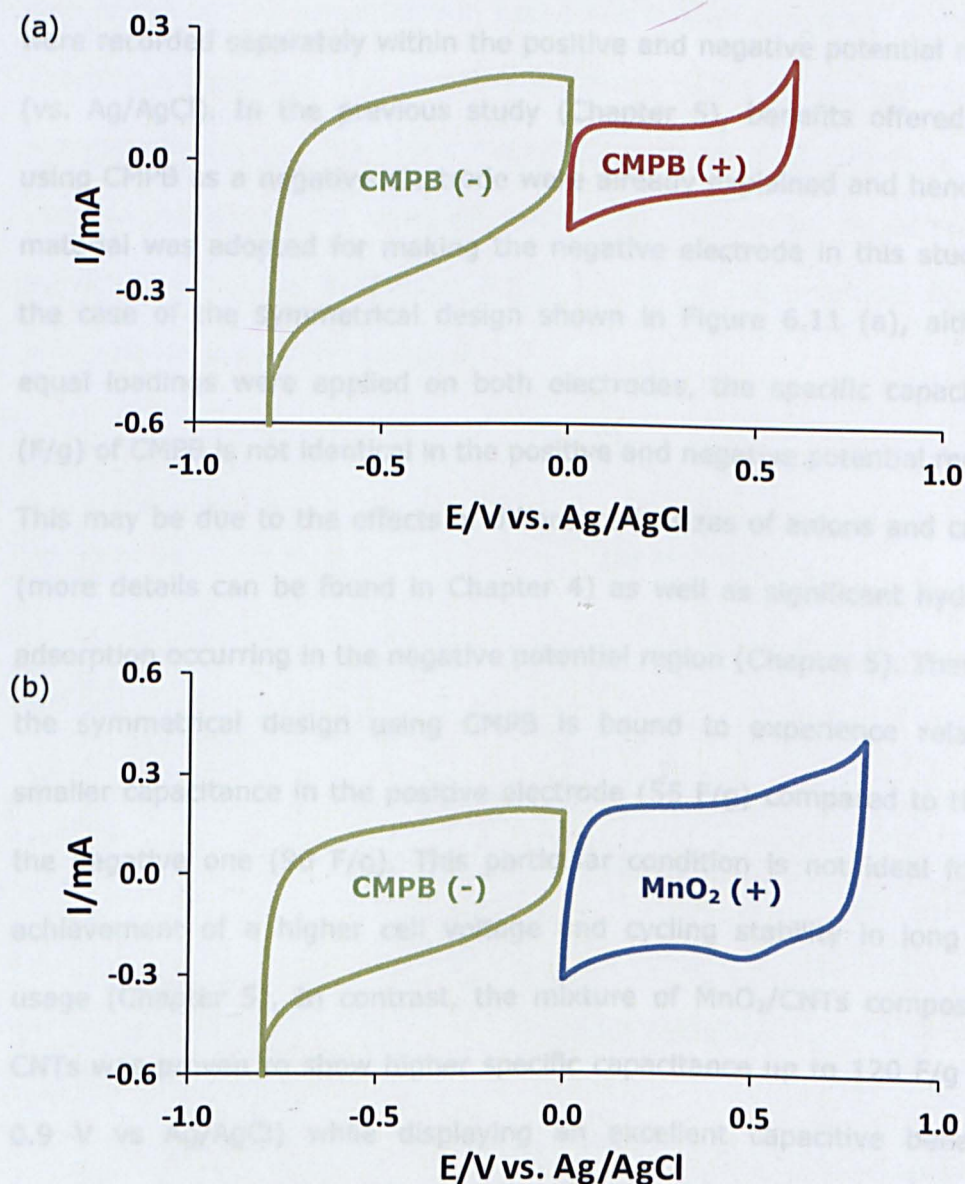


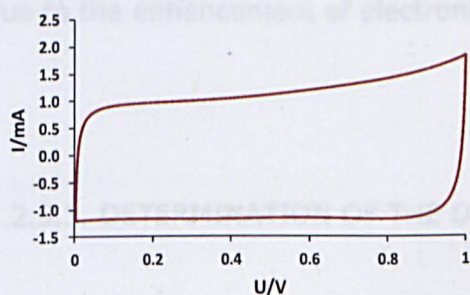
Figure 6.11 CVs recorded the positive and negative potential windows separately with (a) symmetrical design EC using CMPB for both the positive and negative electrodes (C-C supercapacitor, specific capacitances of the material are different at the positive and negative potential windows), (b) asymmetrical design EC using the 40 wt% MnO₂/CNTs composite with CNT addition as a positive electrode and CMPB as a negative electrode; equal amount loading applied on the positive and negative electrodes

Several advantages of employing an asymmetrical design are demonstrated in Figure 6.11. The CVs for both (a) and (b) in Figure 6.11 were recorded separately within the positive and negative potential ranges (vs. Ag/AgCl). In the previous study (Chapter 5), benefits offered from using CMPB as a negative electrode were already explained and hence the material was adopted for making the negative electrode in this study. In the case of the symmetrical design shown in Figure 6.11 (a), although equal loadings were applied on both electrodes, the specific capacitance (F/g) of CMPB is not identical in the positive and negative potential regions. This may be due to the effects of difference in sizes of anions and cations (more details can be found in Chapter 4) as well as significant hydrogen adsorption occurring in the negative potential region (Chapter 5). Therefore, the symmetrical design using CMPB is bound to experience relatively smaller capacitance in the positive electrode (55 F/g) compared to that of the negative one (90 F/g). This particular condition is not ideal for the achievement of a higher cell voltage and cycling stability in long term usage (Chapter 5). In contrast, the mixture of MnO₂/CNTs composite + CNTs was proven to show higher specific capacitance up to 120 F/g (0 to 0.9 V vs Ag/AgCl) while displaying an excellent capacitive behaviour (Figure 6.11 (b)). Therefore, combination of the two materials as the positive and negative electrodes in construction of the asymmetrical EC is worthwhile examining. Various testing results for the asymmetrical EC such as rate performance, operating voltage and cycling stability will be presented in the following sections.

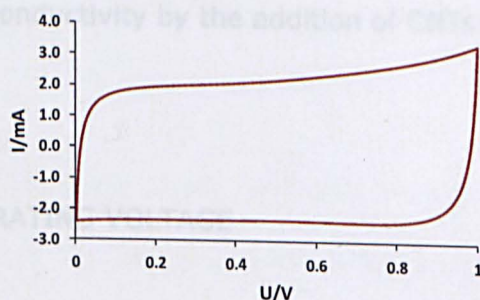
6.2.5.2. RATE PERFORMANCE OF THE ASYMMETRICAL EC

One of the advantages of carbon based ECs is their capability of very fast charging-discharging. This is mainly attributed to the double layer charge-storage mechanism. For redox materials, such as MnO_2 which is widely used in batteries, the charging-discharging mechanism is different as previously explained in Chapter 6.2.4. Hence the asymmetrical EC's rate performance should be examined.

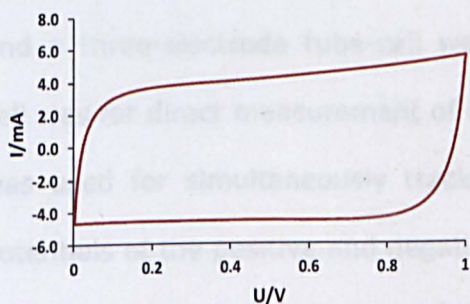
(a) 50 mV/s



(b) 100 mV/s



(c) 200 mV/s



(d) 500 mV/s

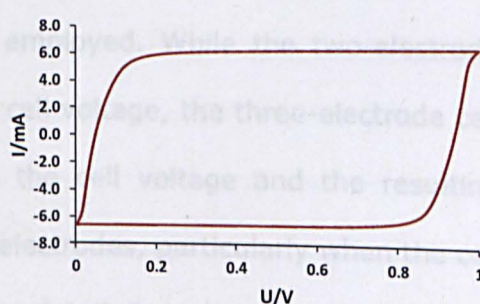


Figure 6.12 CVs of the asymmetrical EC at different scan rates in 3 M KCl from 50 to 500 mV/s within 1 V; 40 wt% MnO_2/CNTs + 15 wt% CNTs (+) and CMPB (-), geometric area of electrode film: 1 cm^2 , equal capacitance, 500 μg per each electrode

The asymmetrical EC displays excellent rate performance. As shown in Figure 6.12, the EC shows a rectangular shape of CV even in extremely fast scan rate of 500 mV/s. The cell does not show significant capacitance drop up to 200 mV/s (less than 7 %) and it shows about 20 % capacitance drop at 500 mV/s compared to that of 50 mV/s. Due to the limitation of ion transfer kinetics, the capacitance drop observed at relatively fast scans is inevitable. A more important finding about this design is that the EC was still capable of showing an excellent capacitive behaviour at an extremely high sweep rate (7 % and 20 % drop in terms of specific capacitance under 4 and 10 times higher rates respectively). The relatively slow response of the MnO₂ positive electrode was not problematic in this design, apparently due to the enhancement of electronic conductivity by the addition of CNTs.

6.2.5.3. DETERMINATION OF THE OPERATING VOLTAGE

In this section, more experimental results are presented to assist evaluation of the asymmetrical EC discussed in section 6.2.5.2 in term of its operating voltage (V). Both a sandwich type two-electrode single-cell and a three-electrode tube-cell were employed. While the two-electrode cell was for direct measurement of the cell voltage, the three-electrode cell was used for simultaneously tracking the cell voltage and the resulting potentials of the positive and negative electrodes, particularly when the cell was fully charged and discharged. More detailed explanation of these two cells and their operations can be found in Chapter 5.

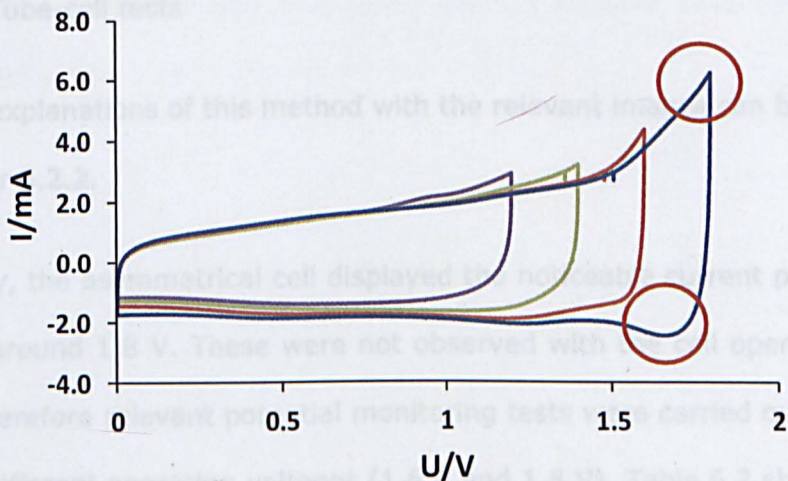


Figure 6.13 CVs at 50 mV/s of the asymmetrical EC within different operating voltages from 1.2 V to 1.8 V, 3 M KCl; the red circles are the indications of faradaic reaction

CVs of the asymmetrical EC (the two-electrode single-cell) were recorded up to different voltages from 1.2 to 1.8 V. The results are presented in Figure 6.13. These CVs show good capacitive features until the voltage was increased to beyond 1.6 V when significant increase in current occurred as highlighted with the red circles in Figure 6.13. The dramatic increase in current at the highest voltage is the indication of undesired faradaic reaction, i.e. gas evolution in particular, within the cell. At this point, it is not clear what the cause was. Due to the remarkably high over-potential of carbon for hydrogen evolution, the current peak at high voltages shown in the charging sweep should have not been due to the reduction on the negative CMPB electrode. In other words, the peak was due to the oxidation of either the electrode material (MnO_2/CNTs) or the electrolyte. For further explanations to examine the reaction above 1.6 V, the tube-cell (more details in Chapter 5.2.2) was adopted to simultaneously monitor the cell voltage and the potentials of the positive and negative electrodes.

- Tube-cell tests

Detailed explanations of this method with the relevant images can be found in Chapter 5.2.2.

Previously, the asymmetrical cell displayed the noticeable current peaks on the CVs around 1.8 V. These were not observed with the cell operating at 1.6 V. Therefore relevant potential monitoring tests were carried out within the two different operating voltages (1.6 V and 1.8 V). Table 6.2 shows the resulting potentials of the two different electrodes.

Table 6.2 Limiting potentials and equi-potential of the positive and negative electrodes at different maximum cell voltages of the tube cell of

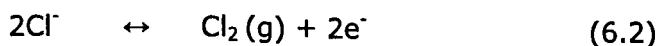
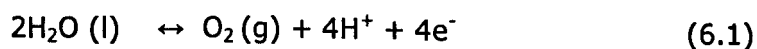


Cell voltage (U)	(+) potential vs. Ag/AgCl	(-) potential vs. Ag/AgCl	Equi-potential vs. Ag/AgCl
1.6 V	0.9 V	- 0.7 V	0.25 V
1.8 V	1.05 V	-0.75 V	0.3 V

*Equi-potential is the electrode potential where the EC is fully discharged (the positive and negative electrode potential at 0 V)

Three different potentials were measured while the cell was operating within two different voltages (1.6 and 1.8 V). The limiting potential of the positive electrode, which is highlighted in green, should be examined to explain the cause of the observed peaks shown in Figure 6.12. As explained above, the potential of the negative electrode should be limited by proton reduction which has, however, remarkably high overpotentials on carbon (CMPB). Thus, the current peaks in Figure 6.13 were unlikely to be due to negative electrode reactions. The following chemical reactions are

the possible reactions that may occur on the positive electrode of the asymmetrical EC.



The limiting potential of the positive electrode measured within the 1.8 V cell was 1.05 V vs. Ag/AgCl. The oxidation potential of the water molecule is known to be 1.019 V vs. Ag/AgCl [36]. Accordingly, the potential of the positive electrode within the 1.8 V cell exceeds the oxidation potentials of $\text{H}_2\text{O (l)}$ and forms $\text{O}_2\text{(g)}$. Chlorine gas from oxidation of chloride anions forms at 1.15 V vs. Ag/AgCl [36] and this potential is higher than the potential of the positive electrode of the 1.8 V asymmetrical cell. However, this theoretical potential values are based on 1 M solutions. In this experiment, 3 M KCl was used as the electrolyte and the concentrations of chemical species also changed due to the redox reactions shown in Equation 6.1 and 6.2. The shift of oxidation potential has to be considered to evaluate the system and this can be done in the Nernst equation [37, 38].

$$E = E^0 - \frac{RT}{nF} \ln \frac{[\text{Red}]}{[\text{Ox}]} \quad (6.3)$$

Where, E is cell potential, E^0 is standard cell potential, R is universal gas constant (8.31447215 J/K mol), T is absolute temperature, n is the number of moles of electrons transferred in the cell reaction or half reaction, F is the Faraday constant (the number of coulombs per mole of electrons:

$9.64853399 \times 10^4 \text{ C/mol}$) and [Red], [Ox] are the activities or concentrations of reduced and oxidised chemical species respectively.

Using the Nernst equation, the oxidation and reduction potential shifts of different chemical species within the cell can be estimated after the concentration of chemical species changes. As a result, the calculated $\text{O}_2(\text{g})$ evolution potential was determined to be 0.93 V vs. Ag/AgCl and the oxygen evolution was identified as the main reason for the sharp current peak observed in the 1.8 V CV data provided in Fig. 6.13. To avoid oxidation of water, use of an alkaline solution with 3 M KCl could extend the positive potential limit in the case of the asymmetrical EC. However, increase in pH of the electrolyte results in narrow potential window as previously discussed in Chapter 4.1.1. Therefore, the optimum pH level for alkaline solution should be examined (future work).

For the optimum design of the asymmetrical EC, the highest potential of the positive electrode should remain below 0.9 V vs. Ag/AgCl due to the evolution of oxygen gas. This is the main reason for the difference in CV shapes between 1.6 V and 1.8 V ECs shown in Figure 6.13. The 1.6 V asymmetrical EC shows a better CV than 1.8 V CV because the highest positive potentials of the two different operating voltages were 0.9 V (under the oxidation potential of water) and 1.05 V (higher than the water oxidation potential) vs. Ag/AgCl respectively. Therefore, the former did not display a significant indication of faradaic reaction (current surge) and the later did.

The limiting potentials and the potential windows of the positive and negative electrodes, and their equi-potentials observed with the 1.6 V asymmetrical EC are depicted in Figure 6.14.

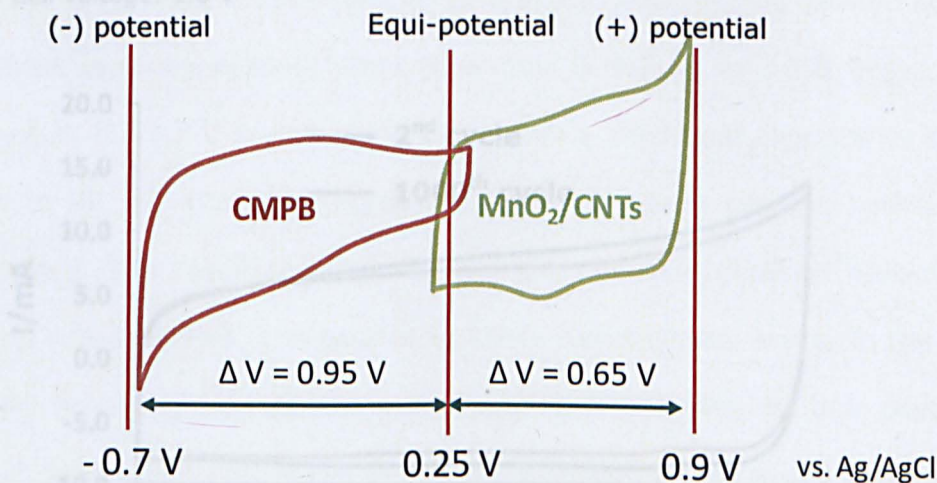
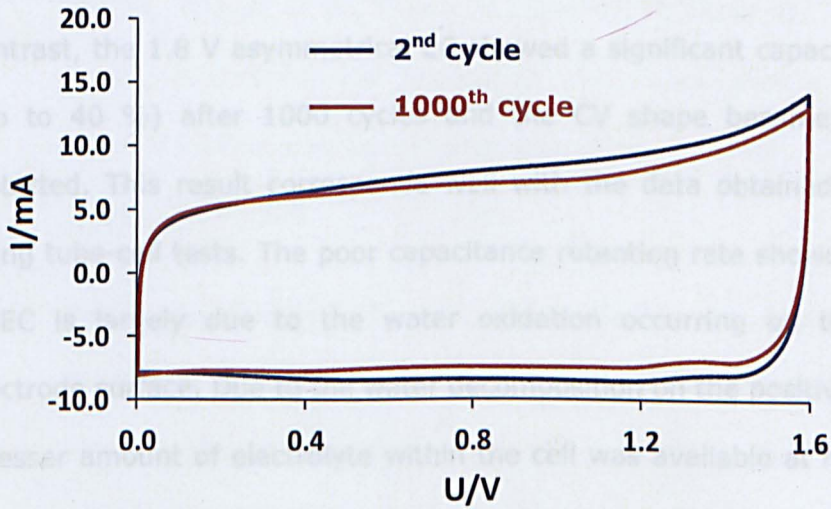


Figure 6.14 Determination of the positive and negative potential windows using the 1.6 V asymmetrical EC and these data were obtained from the tube cell experiments.

6.2.5.4. LONG-TERM CYCLING STABILITY OF THE ASYMMETRICAL EC

The asymmetrical ECs' operating voltage was evaluated using cyclic voltammogram data obtained from both the two- and three-electrode cells. These tests provided information about the stable electrochemical windows for the system for both the positive and negative electrodes. However, the maximum operating voltage of ECs cannot be determined accurately until the cycling stability test is carried out although the cyclic voltammograms provided useful information about the cell. Since the potentials change over charge/discharge cycles (more details can be found in Chapter 5), the capacitance retention rate should be examined by cycling test. For evaluation of the cycling performance, the sandwich type single cells (two-electrode test) were tested. These results are presented in Figure 6.15.

(a) Cell voltage: 1.6 V



(b) Cell voltage: 1.8 V

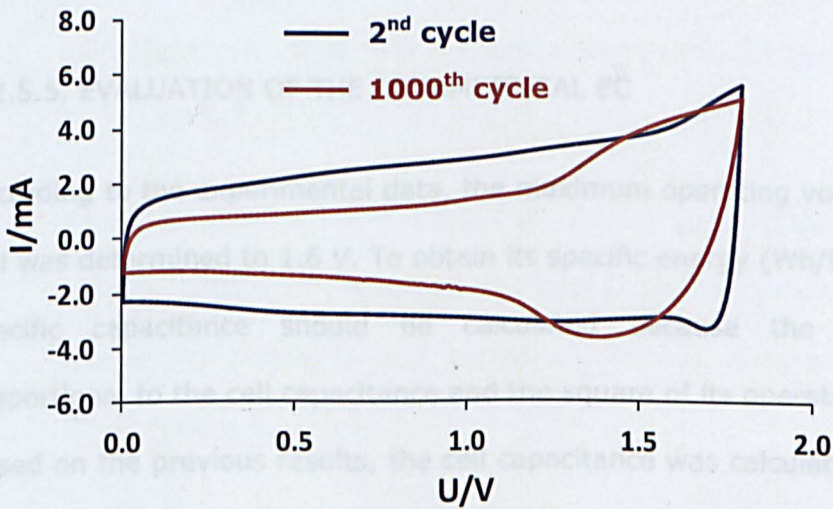


Figure 6.15 Long-term cycling stability tests of (a) 1.6 V operating voltage (total applied loading is 3 mg), (b) 1.8 V operating voltage (total applied loading is 1.5 mg); a single cell test, scan rate: 100 mV/s, electrolyte: 3 M KCl

The CVs shown in Figure 6.15 confirm the previous observations (Figure 6.13 and Table 6.2). As expected, the asymmetrical EC with a 1.6

operating voltage window displayed a more ideal cycling performance, without rapid capacitance drop (less than 5 %) up to 1000 cycles. In contrast, the 1.8 V asymmetrical EC showed a significant capacitance drop (up to 40 %) after 1000 cycles and the CV shape became noticeably distorted. This result corresponds well with the data obtained previously using tube-cell tests. The poor capacitance retention rate shown in the 1.8 V EC is largely due to the water oxidation occurring on the positive electrode surface. Due to the water decomposition on the positive electrode, a lesser amount of electrolyte within the cell was available at higher cycle numbers. This may result in a lower current response and the distorted CV at the 1000th cycle compared to the initial one.

6.2.5.5. EVALUATION OF THE ASYMMETRICAL EC

According to the experimental data, the maximum operating voltage of the cell was determined to 1.6 V. To obtain its specific energy (Wh/kg), the cell specific capacitance should be calculated because the energy is proportional to the cell capacitance and the square of its operating voltage. Based on the previous results, the cell capacitance was calculated to be 25 F/g. The asymmetrical EC performed at 9 Wh/kg in terms of specific energy while it still showed excellent power characteristics due to the low cell resistance. Although the energy value is lower than that of the unequalised (unbalanced) design using carbon materials reported in Chapter 5, it is still higher than most commercial ECs using organic solvents.

References

1. Wu, M., Snook, G. A., Gupta, V., Shaffer, M., Fray, D. J. and Chen, G. Z., *Electrochemical fabrication and capacitance of composite films of carbon nanotubes and polyaniline*. J. Mater. Chem., 2005, **15**: p. 2297-2303
2. Snook, G., Chen, G. Z., Fray, D. J., Hughes, M. and Shaffer, M., *Studies of deposition of and charge storage in polypyrrole-chloride and polypyrrole-carbon nanotube composites with an electrochemical quartz crystal microbalance*. J. Electroanal. Chem. 2004, **568**: p. 135-142
3. Jin, X., Zhou, W., Zhang, S. and Chen, G. Z., *Nanoscale microelectrochemical cells on carbon nanotubes*. Small, 2007. **3**(9): p. 1513-1517.
4. Peng, C., Jin, J, and Chen, G. Z., *A comparative study on electrochemical co-deposition and capacitance of composite films of conducting polymers and carbon nanotubes*. Electrochim. Acta, 2007. **53**(2): p. 525-537.
5. Shaffer, M. S. P., Fan, X, and Windle A. H., *Dispersion and packing of carbon nanotubes*. Carbon, 1998. **36**(11): p. 1603-1612.
6. Mawhinney, D. B., Naumenko, V., Kuznetsova, A., Yates Jr, J. T., Liu, J. and Smalley, R. E., *Surface defect site density on single walled carbon nanotubes by titration*. Chem. Phys. Lett., 2000. **324**(1): p. 213-216.
7. Hu, H., Bhowmik, P., Hamon, M. A., Itkis, M. E. and Haddon, R. C., *Determination of the acidic sites of purified single-walled carbon*

- nanotubes by acid-base titration.* Chem. Phys. Lett., 2001. **345**(1): p. 25-28.
8. Kim, U. J., Furtado, C. A., Liu, X., Chen, G. and Eklund, P. C., *Raman and IR spectroscopy of chemically processed single-walled carbon nanotubes.* J. Am. Chem. Soc., 2005. **127**(44): p. 15437-15445.
 9. Futaba, D., Hata, K., Yamada, T., Mizuno, K., Yumura, M. and Iijima, S., *Kinetics of water-assisted single-walled carbon nanotube synthesis revealed by a time-evolution analysis.* 2005, Phys. Rev. Lett., **95** (5): p. 56104
 10. Goyanes, S., Rubiolo, G. R., Salazar, A., Jimeno, A., Corcuera, M. A. and Mondragon, I. *Carboxylation treatment of multiwalled carbon nanotubes monitored by infrared and ultraviolet spectroscopies and scanning probe microscopy.* Diamond Relat. Mater., 2007. **16**(2): p. 412-417.
 11. Reddy, A. L. M. and Ramaprabhu, S., *Nanocrystalline metal oxides dispersed multiwalled carbon nanotubes as supercapacitor electrodes.* J. Phys. Chem. C, 2007. **111**(21): p. 7727-7734.
 12. Holzinger, M., Vostrowsky, O., Hirsch, A., Hennrich, F., Kappes, M., Weiss, R. and Jellen, F. *Sidewall functionalization of carbon nanotubes.* Angew. Chem. Int. Ed., 2001. **40**(21): p. 4002-4005.
 13. Kuznetsova, A., Mawhinney, D. B., Naumenko, V. Yates Jr. J. T., Liu, J. and Smalley, R. E., *Enhancement of adsorption inside of single-walled nanotubes: opening the entry ports.* Chem. Phys. Lett., 2000. **321**(3): p. 292-296.

14. Shanmugam, S. and Gedanken, A., *Generation of hydrophilic, bamboo-shaped multiwalled carbon nanotubes by solid-state pyrolysis and its electrochemical studies*. J. Phys. Chem. B, 2006. **110**(5): p. 2037-2044.
15. Monthieux, M., Smith, B. W., Burtiaux, B., Claye, A., Fischer, J. E. and Luzzi, D. E. *Sensitivity of single-wall carbon nanotubes to chemical processing: an electron microscopy investigation*. Carbon, 2001. **39**(8): p. 1251-1272.
16. Gao, F., Zhang, L. and Huang, S., *Fabrication horizontal aligned MoO₂/single-walled carbon nanotube nanowires for electrochemical supercapacitor*. Mater. Lett., 2010. **64**(4): p. 537-540.
17. Yan, J., Fan, Z. Wei, T. Cheng, J. Shao, B., Wang, K., Song, L. and Zhang, M., *Carbon nanotube/MnO₂ composites synthesized by microwave-assisted method for supercapacitors with high power and energy densities*. J. Power Sources, 2009. **194**(2): p. 1202-1207.
18. Sivakkumar, S. R., Ko, J. M., Kim, D. Y., Kim, B. C. and Wallace, G. G., *Performance evaluation of CNT/polypyrrole/MnO₂ composite electrodes for electrochemical capacitors*. Electrochim. Acta, 2007. **52**(25): p. 7377-7385.
19. Frackowiak, E., Khomenko, V., Jurewicz, K., Lota, K. and Beguin, F., *Supercapacitors based on conducting polymers/nanotubes composites*. J. Power Sources, 2006. **153**(2): p. 413-418.
20. Zhang, J., Kong, L. B., Wang, B., Luo, Y. C. and Kang, L., *In-situ electrochemical polymerization of multi-walled carbon*

nanotube/polyaniline composite films for electrochemical supercapacitors. Synth. Met., 2009. 159(3-4): p. 260-266.

21. Kang, Y. J., Kim, B., Chung, H. and Kim, W., *Fabrication and characterization of flexible and high capacitance supercapacitors based on MnO₂/CNT/papers. Synth. Met., 2010. 160(23-24): p. 2510-2514.*
22. Fan, Z., Chen, J. H., Zhang, B., Liu, B., Zhong, X. X. and Kuang, Y. F., *High dispersion of r-MnO₂ on well-aligned carbon nanotube arrays and its application in supercapacitors. Diamond Relat. Mater., 2008. 17(11): p. 1943-1948.*
23. Cochet, M., Maser, W. K., Benito, A. M., Callejas, M. A., Martinez, M. T., Benoit, J. M., Schreiber, J. and Chauvet, O., *Synthesis of a new polyaniline/nanotube composite: "in-situ" polymerisation and charge transfer through site-selective interaction. Chem. Commun., 2001. 2001(16): p. 1450-1451.*
24. Yan, J., Fan, Z. Wei, T. Cheng, J. Shao, B., Wang, K., Song, L. and Zhang, M., *Carbon nanotube/MnO₂ composites synthesized by microwave-assisted method for supercapacitors with high power and energy densities. J. Power Sources, 2009. 194(2): p. 1202-1207.*
25. Wei, J., Nagarajan, N. and Zhitomirsky, I., *Manganese oxide films for electrochemical supercapacitors. J. Mater. Process. Technol., 2007. 186(1-3): p. 356-361.*

26. Reddy, R. N. and Reddy, R. G., *Sol-gel MnO₂ as an electrode material for electrochemical capacitors*. J. Power Sources, 2003. **124**(1): p. 330-337.
27. Donne, S. W., Lawrance, G. A. and Swinkels, D. A. J. *Redox processes at the manganese dioxide electrode*. J. Electrochem. Soc., 1997. **144**: p. 2949.
28. Ng, K. C., Zhang, S. and Chen, G. Z. *An asymmetrical supercapacitor based on CNTs/SnO₂ and CNTs/MnO₂ nanocomposites working at 1.7 V in aqueous electrolyte*. ECS Transactions, 2008. **16**(1): p. 153-162.
29. Fei, J. Cui, Y., Yan, X., Qi, W., Yang, Y., Wang, K., He, Q. and Li, J., *Controlled preparation of MnO₂ hierarchical hollow nanostructures and their application in water treatment*. Adv. Mater., 2008, **20**: p. 452-456
30. Chen, K., Noh, Y. D., Lin, S., Komarneni, S. and Xue, D. *Crystallization of MnO₂ for lithium-ion battery and supercapacitor*. Mater. Focus, 2013, **2**(3): p. 195-200
31. Song, Z., Liu, W., Zhao, M., Zhang, Y., Liu, G., Yu, C. and Qiu, J. *A facile template-free synthesis of α-MnO₂ nanorods for supercapacitor*. J. Alloy. Compd., 2013, **560**: p. 151-155
32. Zhang, S., *Carbon nanotube based composites for electricity storage in supercapacitors*. The University of Nottingham, PhD thesis, 2010. U. K.

33. Lee, S. W., Kim, J. Chen, S., Hammond, P.T. and Shao-Horn, Y., *Carbon nanotube/manganese oxide ultrathin film electrodes for electrochemical capacitors*. ACS Nano, 2010. **4**(7): p. 3889-3896.
34. Fan, Z., Chen, J. H., Zhang, B., Liu, B., Zhong, X. X. and Kuang, Y. F., *High dispersion of r-MnO₂ on well-aligned carbon nanotube arrays and its application in supercapacitors*. Diamond Relat. Mater., 2008. **17**(11): p. 1943-1948.
35. Zhang, L. L., Wei, T., Wang, W. and Zhao, X. S., *Manganese oxide-carbon composite as supercapacitor electrode materials*. Microporous Mesoporous Mater., 2009. **123**(1-3): p. 260-267.
36. Fischer, A. C., *Electrode dynamics*. Oxford University Press, 1996., U.K.
37. Bard, A. J. and Faulkner, L. R., *Electrochemical Methods: Fundamentals and Applications*, 2000, 2nd ed., Wiley, New York.
38. Compton, R. G. and Banks, C. E., *Understanding Voltammetry*, 2007, World Scientific Publishing Co. Pte. Ltd., Singapore

Chapter 7 BIPOLAR STACK

The carbon-carbon and pseudo-capacitive oxide-carbon ECs which were presented in Chapters 5 and 6 displayed promising results. However, they were tested on a relatively small lab scale. Obviously, ECs constructed in smaller scales using thin electrode films are often more advantageous due to faster electrolyte impregnation within the electrode and this results in better and faster material utilisation. Therefore, the smaller-scaled ECs using the thin electrode often display better performance mainly in terms of power [1-5]. The main challenge of scale-up is to build the significantly larger system which is able to perform similarly to the smaller scale one in terms of specific energy and comparable power.

The construction of stacked ECs using bipolar plates which have to be mechanically strong is remarkably challenging because a less-performing single cell within an EC stack affects the performance of the whole stack [6-8]. Therefore, individual cells should be designed identically (electrode, electrolyte, separator and current collectors) to maximise the individual cell performance and hence the stack performance.

Based on the data collected from CMPB and pseudo-capacitive material (Chapters 5 and 6), three different stacks using neutral aqueous electrolyte (KCl, K_2SO_4) were constructed. Equal and unequal electrode capacitance designs were employed to build the stacks using CMPB (rolling method). A pellet press was used to produce electrodes containing pseudo-capacitive material. Their performance will be compared to those of smaller scaled ECs adopting the same design. Moreover, their results will also be compared with the 20 V stack previously built within the group [7].

7.1. EFFECTIVE DESIGN OF BIPOLAR STACK

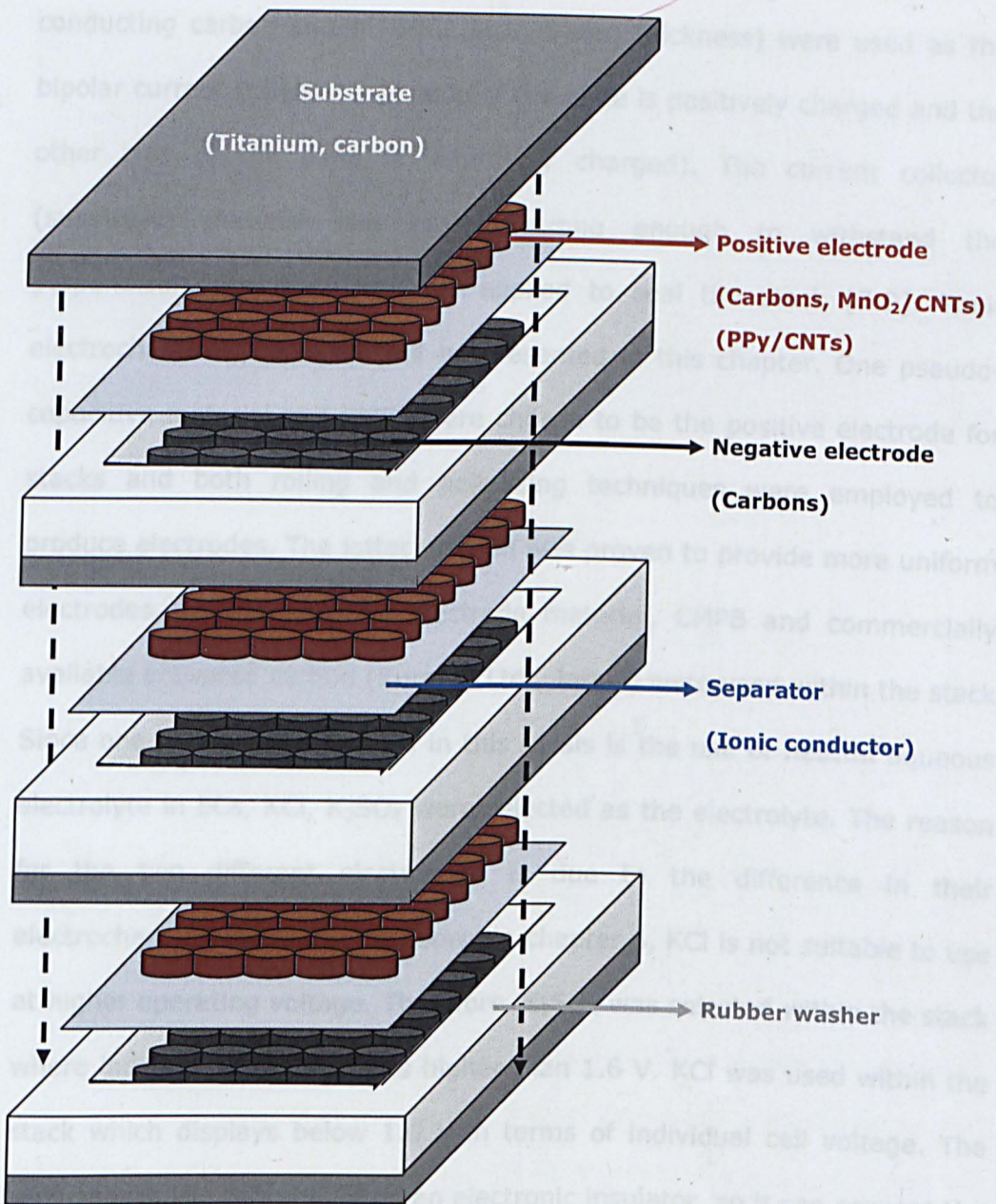


Figure 7.1 Three-dimensional design of supercapattery stack; three cells are connected in series by using two bipolar plates and two end plates, current collector (substrate): Titanium or conducting carbon plates, positive electrode: MnO_2/CNTs , PPy/CNT or CMPB carbons, negative electrode: CMPB carbons, electrolytes: neutral aqueous electrolytes (KCl , K_2SO_4), separator: filter papers, polymer membrane (should be an ionic conductor, but electronic insulator)

Figure 7.1 shows the schematic image of a bipolar stack. Metal titanium plates (99.6 %, Goodfellow Cambridge Ltd., 0.1 mm thickness) and conducting carbon plates (BAC2 Ltd., 5 mm thickness) were used as the bipolar current collector (one side of the plate is positively charged and the other side of the plate is negatively charged). The current collector (substrate) material has to be strong enough to withstand the perpendicular pressure which is applied to seal the stack [7-9]. Their electrochemical properties will be presented in this chapter. One pseudo-capacitive material and CMPB were chosen to be the positive electrode for stacks and both rolling and pelletizing techniques were employed to produce electrodes. The latter method was proven to provide more uniform electrodes. As the negative electrode material, CMPB and commercially available activated carbon (Kuraray Ltd., Japan) were used within the stack. Since one of the main focuses in this thesis is the use of neutral aqueous electrolyte in ECs, KCl, K_2SO_4 were selected as the electrolyte. The reason for the two different electrolytes is due to the difference in their electrochemical durability. As shown in chapter 6, KCl is not suitable to use at higher operating voltage. Therefore, K_2SO_4 was selected within the stack where individual cell voltage is higher than 1.6 V. KCl was used within the stack which displays below 1.6 V in terms of individual cell voltage. The separator in the ECs should be an electronic insulator, so it can prevent the direct current flow (short-circuit) from one electrode to the other (more detailed explanations can be found in chapter 2). More importantly, it has to be an ionic conductor [1, 8, 10]. Two different separators were selected and one was a commercially available membrane (Celgard Ltd, 25 μ m thickness) and the other one was a filter paper (Schleicher & Schuell, Germany). A rubber gasket (1.5 mm and 3 mm) was used to seal the stack to prevent electrolyte loss.

7.2. SYMMETRICAL STACK (EQUAL CAPACITANCE)

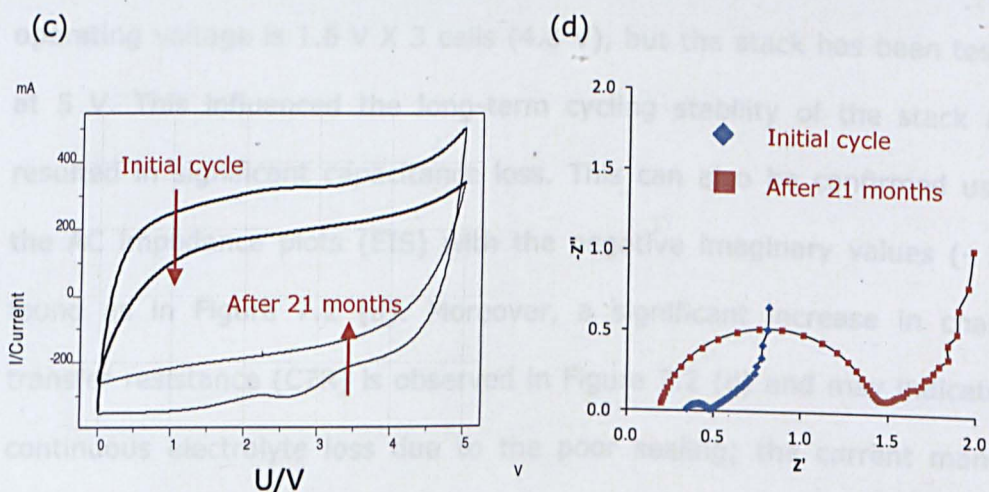
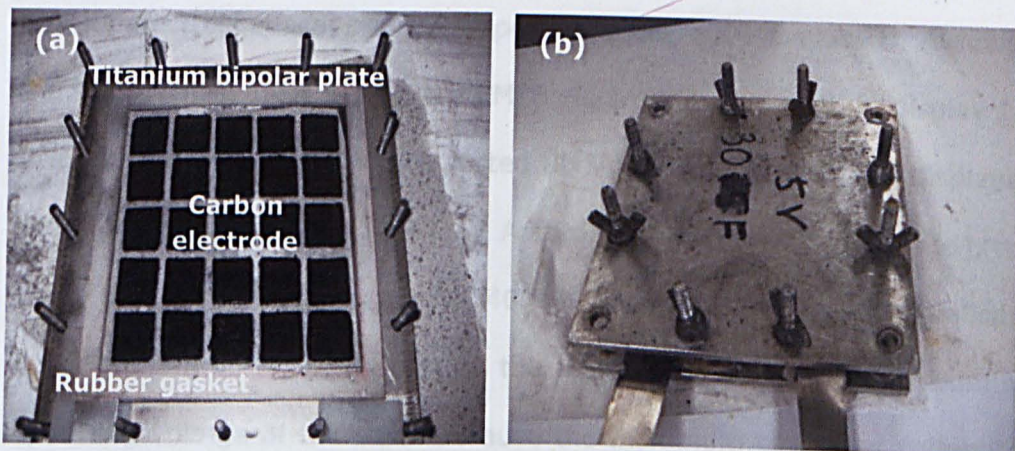


Figure 7.2 (a) and (b) Images of 30 F stack in which three cells are connected in series, Performance of 5 V stack (three cells connected in series), (c) CVs of initial and after 21 months (1500 cycles) at 10 mV/s, (d) AC impedance plots of initial and after 21 months (100 kHz to 10 mHz); Individual cell voltage: 1.67 V, electrolyte: 0.3 M K_2SO_4 , electrode material: CMPB, metal current collector (substrate): titanium, separator: Celgard membrane, plates geometric area of the electrode: 36 cm^2 , geometric capacitance: 4.2 F/cm^2 in the initial cycle, equalised capacitances in positive and negative electrodes

The first symmetrical stack (CMPB for the both electrodes with equal capacitance) was constructed (see the images in Figure 7.2 (a) and (b)) and its electrochemical and cyclic performances were evaluated. Although the symmetrical design using the CMPB electrode was proven to display 1.6 V in chapter 5, the stack was tested at 5 V in which each cell displayed slightly higher than 1.6 V (1.67 V). According to Figure 7.2 (c) and (d), the stack lost its capacitance up to 40 %. The reasons for the significant capacitance drop is mainly due to the higher voltage than the maximum operating voltage of the stack because the maximum operating voltage of each cell is 1.6 V in the equalised capacitance design and the maximum operating voltage is 1.6 V X 3 cells (4.8 V), but the stack has been tested at 5 V. This influenced the long-term cycling stability of the stack and resulted in significant capacitance loss. This can also be confirmed using the AC impedance plots (EIS) with the negative imaginary values ($-Z''$) found as in Figure 7.2 (d). Moreover, a significant increase in charge transfer resistance (CTR) is observed in Figure 7.2 (d) and may indicate a continuous electrolyte loss due to the poor sealing; the current manual process has to be improved. Decrease in ESR may be due to installation of a docking station (better contact between the stack and the potentiostat). Due to the abuse of the stack by applying higher voltage (5 V) than its maximum operating voltage (4.8 V), the stack lost significant capacitance and hence energy storage.

At the time of constructing the first stack, the maximum operating voltage of the symmetrical single cell using CMPB was not identified (studies in chapter 5 carried out later than the construction of this stack). Based on this data with the study in chapter 5, another stack was constructed and the results are presented in chapter 7.3.

7.3. ASYMMETRICAL STACK (UNEQUAL CAPACITANCE)

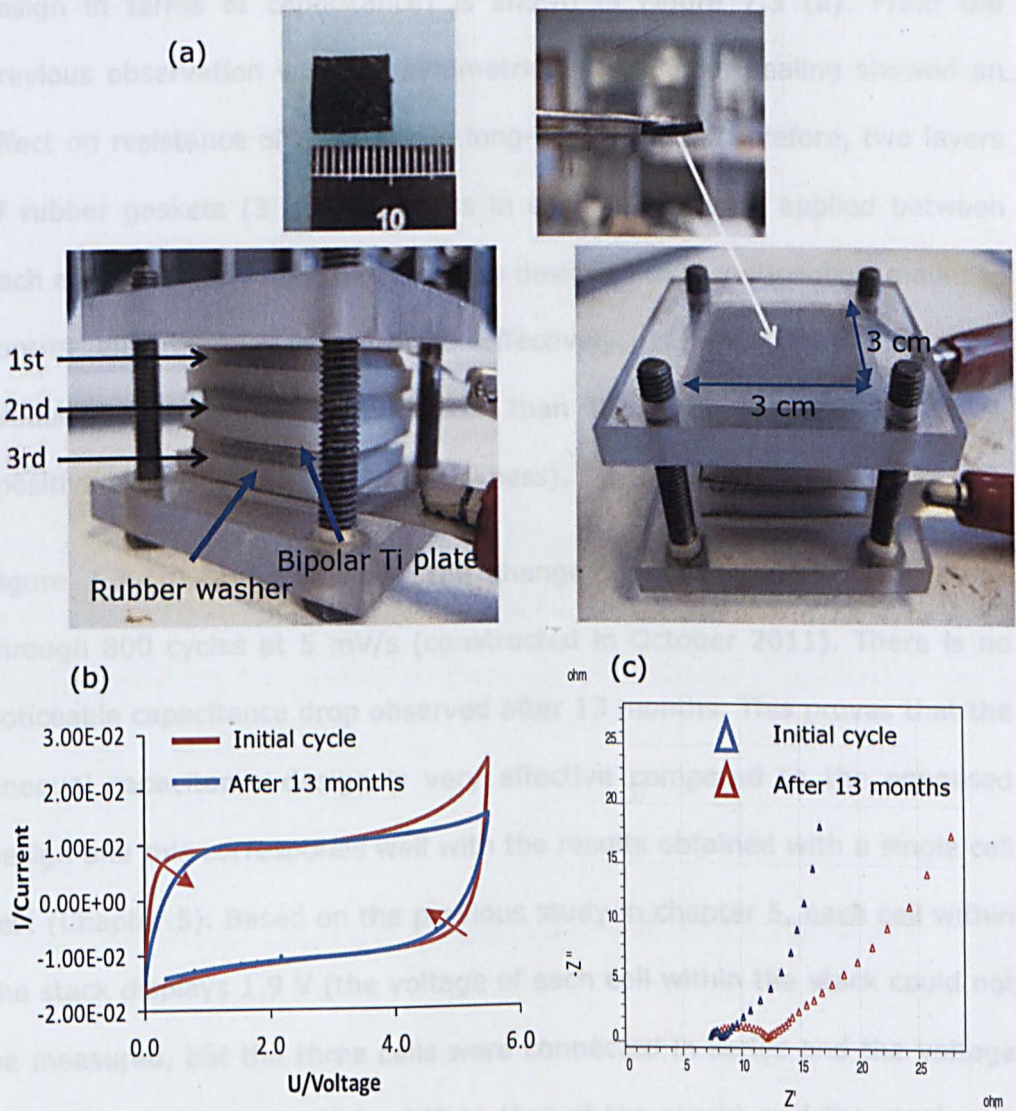


Figure 7.3

(a) Images of bipolar stack employing the unequal electrode capacitance, performance of 5.7 V stack, (b) CVs of initial and after 13 months (800 cycles) at 5 mV/s, (c) AC impedance plots of initial and after 13 months (100 kHz to 10 mHz at 0 V); Electrode material: CMPB, metal substrate: titanium plates, separator: Celgard membrane, sealing: rubber gasket (3 mm X 2 in the individual cell), electrolyte: 0.3 M K_2SO_4 , thickness of the electrode films: 5 mm (+) and 2.4 mm(-), amount of Loading of the electrodes: 400 mg (+) and 170 mg (-), geometric area of the electrode: 1 cm^2 , unequalised capacitances in positive and negative electrodes (capacitance ratio = 4:3)

The images of the stack (CMPB for the both electrode, but asymmetrical design in terms of capacitance) is shown in Figure 7.3 (a). From the previous observation with the symmetrical stack, poor sealing showed an effect on resistance of the stack in long-term usage. Therefore, two layers of rubber gaskets (3 mm thickness in each layer) were applied between each electrode plate and the stack was designed to be noticeably smaller to control electrolyte leakage more effectively. However, the electrodes produced were significantly thicker than those of the previous stack (positive electrode was 5 mm in thickness).

Figure 7.3 (b) and (c) shows the change in performance of the stack through 800 cycles at 5 mV/s (constructed in October 2011). There is no noticeable capacitance drop observed after 13 months. This proves that the unequal capacitance design is very effective compared to the equalised design and this corresponds well with the results obtained with a single cell test (Chapter 5). Based on the previous study in chapter 5, each cell within the stack displays 1.9 V (the voltage of each cell within the stack could not be measured, but the three cells were connected in series and the voltage from the each cell should be 1/3 to that of the stack) and the stack was tested at 5.7 V and this is significantly higher than that of the equalised EC (as presented previously, that three cell stack could not perform in long term at 5 V, e.g. 40 % drop in terms of capacitance and energy). Due to the thick film fabrication (positive electrode is 5 mm), the geometric capacitance per each electrode was measured 12.5 F/cm² (initial cycle) and 12 F/cm² (after 13 months). This is remarkably higher than that of the symmetrical stack (4.2 F/cm² at the initial cycle). The main problem of thick films is less effective utilisation (slower electrolyte impregnation) of the electrode material [4, 5]. However, the stack shows a specific capacitance at 65 F/g at slow scan rates and this value is comparable to

the material specific capacitance of CMPB. Therefore, the stack is suitable for slow scan rate applications. However, it is not ideal for the fast rate applications due to remarkably high resistance due to the thickness of film. As presented in Figure 7.3 (c), the stack shows noticeably high diffusion resistance and this can be confirmed by the AC impedance data (length of 45 ° angle region) [1, 11]. Moreover, significant increase in charge transfer resistance is observed with the plot after 13 months. ESR does not show any changes. The increase in resistance in both charge transfer and diffusion resistances results in a less rectangular shape of CV trace, as shown in Figure 7.4 (a). Increase in charge transfer resistance should be examined further. No significant capacitance drop after 800 cycles is confirmed by the AC impedance plots via the imaginary impedance value (Z'') at the low frequency ranges.

7.4. BIPOLAR STACK (PSEUDO-CAPACITANCE)

In contrast to the previous studies in this thesis, conducting carbon plates (BAC2 Ltd.) were used as bipolar plates in the third stack. Moreover, pseudo-capacitive material (conducting polymer) was employed as a positive electrode prepared using a pellet press. Properties of the different carbon plates in terms of their structural morphology, electronic conductivity and electrochemical characteristics were examined in comparison to titanium plate which was used as a current collector throughout this study. Furthermore, the biggest stack in terms of weight and volume was successfully constructed using the carbon bipolar plates and its performance as an energy storage device was also evaluated in terms of energy and power characteristics.

7.4.1. CONDUCTING CARBON PLATES

Use of conducting carbon plates within a bipolar stack has been reported [8]. Five different samples of a conducting carbon plate were provided from BAC2 Ltd and different tests (conductivity, structural study, electrochemical properties) were carried out to identify the most suitable carbon plate for the use as a bipolar plate within the stack.

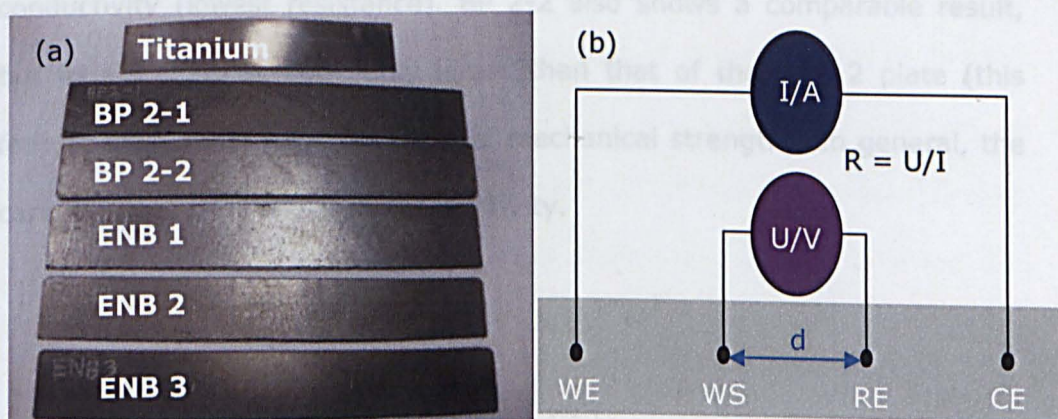


Figure 7.4 (a) Images of five different carbon samples and one titanium plate (BP 2-1, ENB 1, 2 and 3 are roughly 1 mm in thickness and BP2-2 is 2 mm in thickness) and (b) schematic image of four point measurement to examine conductivity of the different plates (R: resistance, U: voltage, I: current, WE: working electrode, WS: working sensor, RE: reference electrode, CE: counter electrode)

The resistance of the five different carbon plates and one titanium plate were tested by four point measurement [12, 13] and their images are shown in Figure 7.4. Using this technique, the resistance R of the each plate can be obtained from the equation of $R = U/I$ and hence their conductivity can also be evaluated. The testing result is shown in Table 7.1.

Table 7.1 Conductivity measurement of conducting carbon plates

Sample	Thickness, L (mm)	Area, A (mm ²)	Measured resistance, R (m Ω)	ρ (m Ω ·mm)
Titanium	0.11	100	1.92	1745.45
BP2-1	1.15	100	5.46	474.78
BP2-2	2.02	100	4.86	240.59
ENB-1	1.05	100	5.76	548.57
ENB-2	1.15	100	2.33	202.61
ENB-3	1.06	100	4.14	390.57

According to conductivity tests, the ENB 2 plate shows the highest conductivity (lowest resistance). BP 2-2 also shows a comparable result, but its thickness is noticeably larger than that of the ENB 2 plate (this feature may be beneficial in term of mechanical strength). In general, the carbon plates show excellent conductivity.

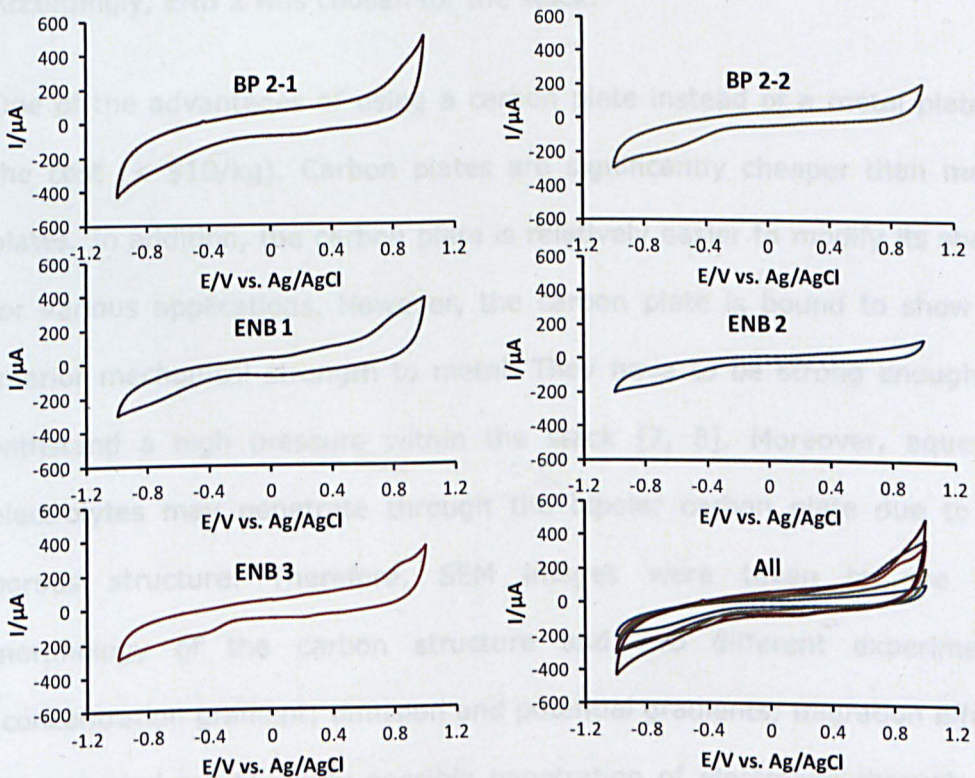


Figure 7.5 Electrochemical stability of the different carbon plates in neutral aqueous electrolyte (1M Na₂SO₄)

Electronic conductivity of the bipolar plate contributes to the overall resistance of the stack, so the plate showing higher conductivity would be beneficial for a better performance which is directly related to power characteristics [1, 3, 6-8]. Another crucial feature to consider is the stack's electrochemical performance. If the substrate is not electrochemically stable within the operating voltage of the stack, the innate properties (i.e. conductivity and surface morphology) of a carbon plate will gradually change over repeated charge/discharge cycles. One of the clear indications of these changes is a current surge beyond (or below) a certain potential [14-16]. This dramatic increase (or decrease) in current is due to faradaic reactions (oxidation or reduction) and this electrochemical reaction, in many cases, changes the material's electrochemical properties [17-19]. According to the cyclic voltammograms in Figure 7.5, ENB 2 shows the most stable results within the 2 V potential window (-1 to 1 V vs. Ag/AgCl). Accordingly, ENB 2 was chosen for the stack.

One of the advantages of using a carbon plate instead of a metal plate is the cost (< \$10/kg). Carbon plates are significantly cheaper than metal plates. In addition, the carbon plate is relatively easier to modify its shape for various applications. However, the carbon plate is bound to show an inferior mechanical strength to metal. They have to be strong enough to withstand a high pressure within the stack [7, 8]. Moreover, aqueous electrolytes may penetrate through the bipolar carbon plate due to its porous structure. Therefore, SEM images were taken to see the morphology of the carbon structure and two different experiments (concentration gradient; diffusion and potential gradients; migration effect) were carried out to study possible penetration of electrolyte through the carbon structure.

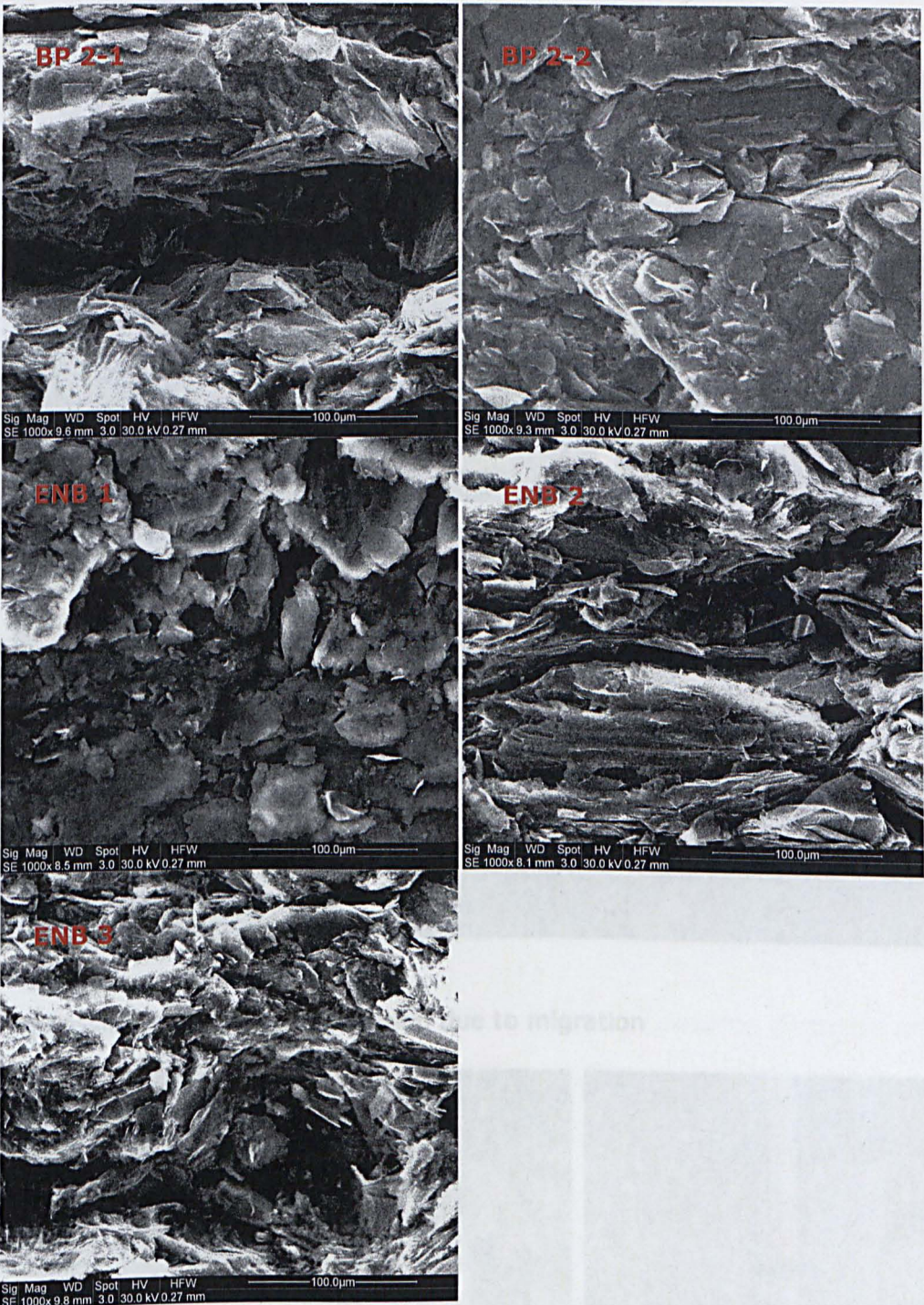
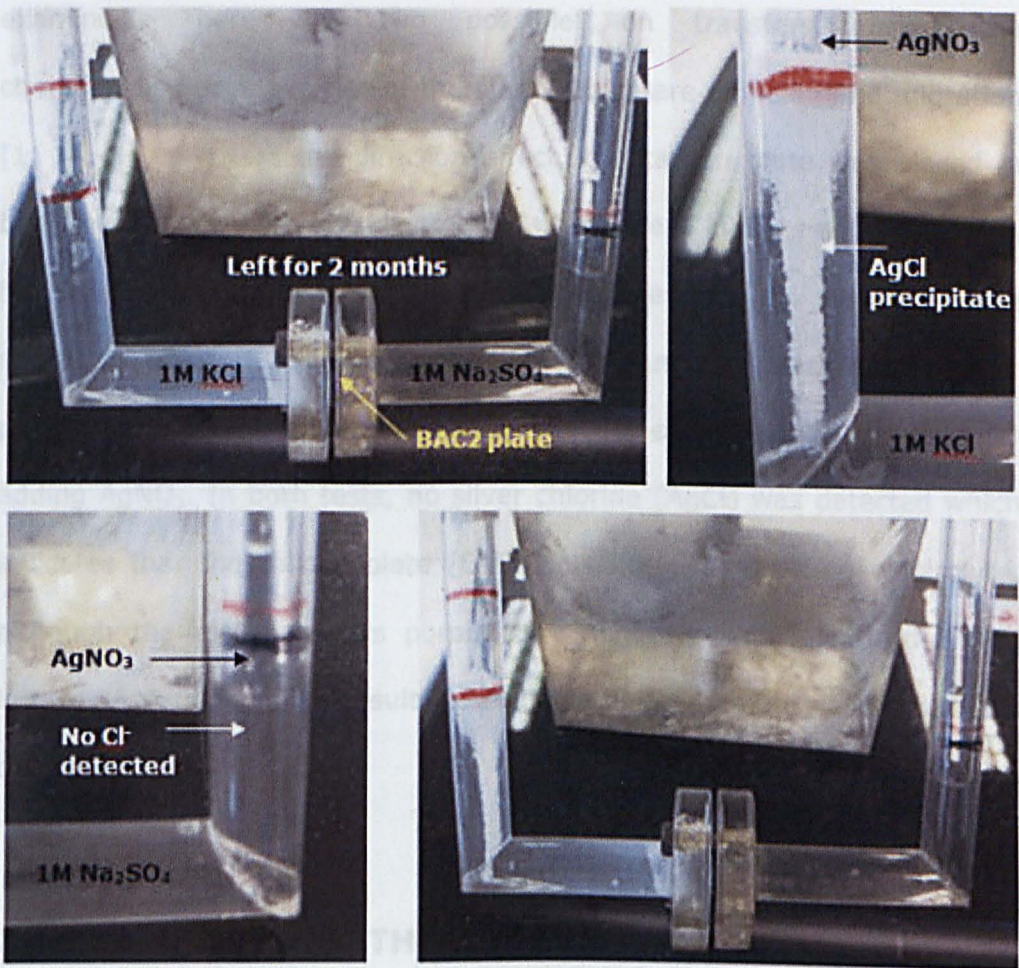


Figure 7.6 SEM images of the five different carbon plates

Figure 7.6 shows the SEM images of the different carbon plates; they are all porous. Permeability tests were carried out to see if electrolyte can penetrate through the porous carbon plate (ENB 2).

(a) Possible electrolyte penetration due to diffusion



(b) Possible electrolyte penetration due to migration

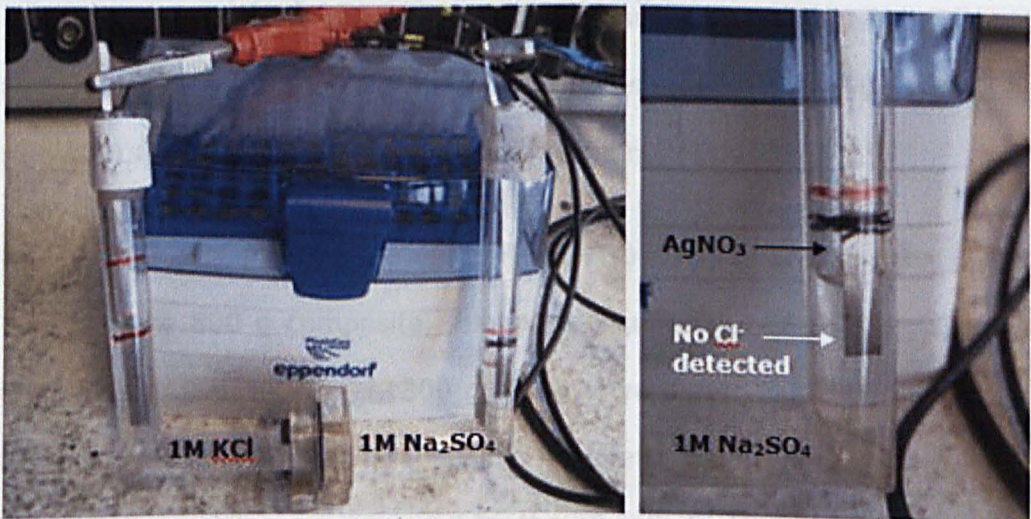


Figure 7.7 Permeability test of ENB 2 carbon plate due to (a) diffusion (two month penetration time), (b) migration; under applied voltage: 1.2 V for 20 hours

Possible electrolyte penetration through the carbon plate (ENB2) was examined. There are two possible ion transfers during the charging/discharging cycles of the stack, which are diffusion and migration [1, 14, 15]. To test the diffusion effect, the carbon plate was placed in between the two different electrolytes which are 1 M KCl and 1 M Na₂SO₄ for two months and this is shown in Figure 7.6 (a). Regarding the migration effect, 1.2 V was applied for 20 hours, so possible electrolyte penetration, if any, from one column to the other can be detected by adding AgNO₃. In both tests, no silver chloride (AgCl) was detected which indicates that the carbon plate (ENB 2) is not permeable to electrolyte, although the plate appears porous as previously shown with the SEM images. According to the result, no evidence for electrolyte penetration has been observed.

7.4.2. SCALE UP SYNTHESIS OF ELECTRODE MATERIALS

A polypyrrole (PPy)/CNTs composite was used as a positive electrode and commercially available activated carbon (Kuraray Ltd, Japan) was selected as a negative electrode. The material synthesis for the positive electrode (PPy/CNTs) can be found in the recent literatures [7].

Briefly, 800 g of positive material (PPy/CNTs) was required for the stack. To make the 800 g composite, minimum requirement of acid pre-treated CNTs was 160 g. Moreover, 300 g of negative material (activated carbon with 5 wt% binder) was prepared. Procedures below describe how the electrode materials were prepared for the 10 cell-stack.

- Acid pre-treatment of 200 g raw CNTs

50 g of raw commercial CNTs (C-NANO) was placed in a 5 L round flask. Then, 1.2 L concentrated sulphuric (98.0 %, Fluka Analytica) and 0.8 L nitric (> 69.0 %, Sigma-Aldrich) acids were added into the flask and mixed well for a better dispersion of CNTs particles in the acid mixture. The mixture of the CNTs and concentrated acids was heated at a refluxing temperature of 105 °C for 20 minutes and enough time was given to cool down the mixture before the filtration. The cooled solution was filtered and washed several times using deionised water until the pH of the discharged solution became neutral pH. After thorough washing and filtering processes, the wet product was dried at 60 °C for at least 24 hours. The final product was pulverised into fine powder using an agate pestle and mortar. Higher than 90% yield was achieved.

- Synthesis of CNT/PPy composite (positive electrode)

12.00 g (180 mmol) of pyrrole monomers and 3 g of CNTs (CNTs solution should be sonicated at least 15 minutes beforehand) were added into 4 L deionised water in 5 L beaker. The mass ratio between pyrrole and CNT should be controlled at 4:1. The mixture was continuously stirred until the pyrrole monomers are fully dissolved and kept in ice basket to lower the temperature of the pyrrole/CNTs solution (below 5 °C). When the temperature reached below 5 °C, 60 g (263 mmol) ammonium persulphate (APS) solution in 500 mL water was slowly added to the pyrrole and CNTs solution (the APS solution should be cooled (<5 °C) before being added to the CNT solution). The polymerisation is exothermic. Therefore the temperature of the solution will increase up to 10 °C (this temperature can

be lowered by adding the oxidising agent more slowly). Reaction time was controlled at 30 minutes. The product was washed with deionised water and ethanol, and filtered using vacuum filtration using 4# (100 – 200 µm) sintered filter until the solution becomes closer to neutral (pH 5-6). Then, the product was dried in a vacuum oven at 40 °C overnight. The final yield is 15 g - 20 g. This process was continuously repeated until 800 g of the positive material was synthesised.

- Preparation of the negative electrode (AC + 5 wt% PTFE)

PTFE-binder (Sigma Aldrich) was mixed with AC in a mortar. The ratio between active material and PTFE was 19 : 1 (5 wt%). Ethanol was added (about 10 ml on 1 g active material) to disperse PTFE suspension within the active material and obtained a homogeneous slurry. When mixing, ethanol evaporated and finally a thick paste-like material was collected. The collected material was placed in the oven and dried for 4 h at 150 °C. About 30 g of material could be made per batch. This process was continuously repeated until 300 g of the negative material was prepared.

7.4.3. CONSTRUCTION OF THE 10 CELL-STACK

The positive and negative electrode material, were prepared and each procedure was described previously. Actual construction of the stack will be described and its performance will be evaluated.

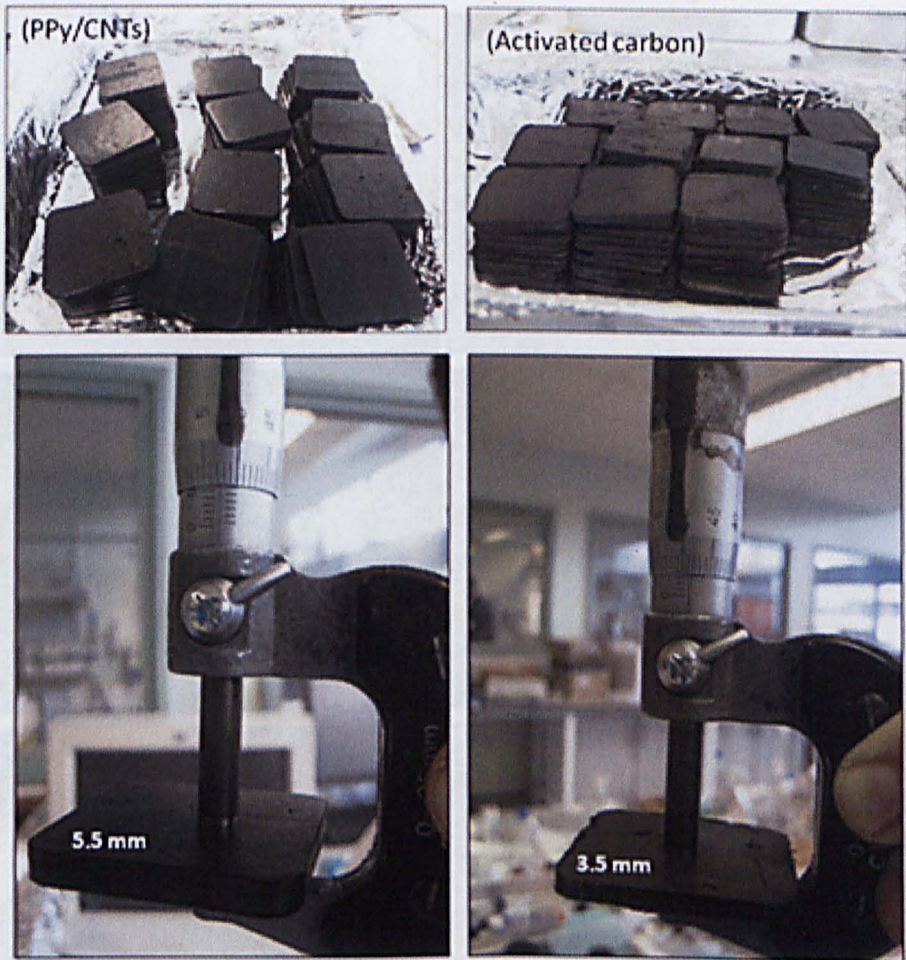


Figure 7.8 Images of 198 pellets of the positive and negative electrodes ($4 \times 4 \text{ cm}^2$) and their thickness; applied pressure: 25 tonnes, weight of electrodes: 8 g and 3 g for the positive and negative electrodes respectively, thickness of electrodes: 5.5 mm and 3.5 mm for the positive and negative electrodes respectively

A total of 198 pellets (99 pellets for the positive and the other 99 pellets for the negative electrode) were pressed by the pellet press at 25 tonnes. The geometric area of the pellet was $4 \times 4 \text{ cm}^2$ and the loading of the two electrodes was strictly controlled at 8g and 3 g to adjust the capacitance ratio at 3:1. As shown in Figure 7.8, the thickness of the electrode was measured at 5.5 mm for the positive and 3.5 mm for the negative electrode respectively.

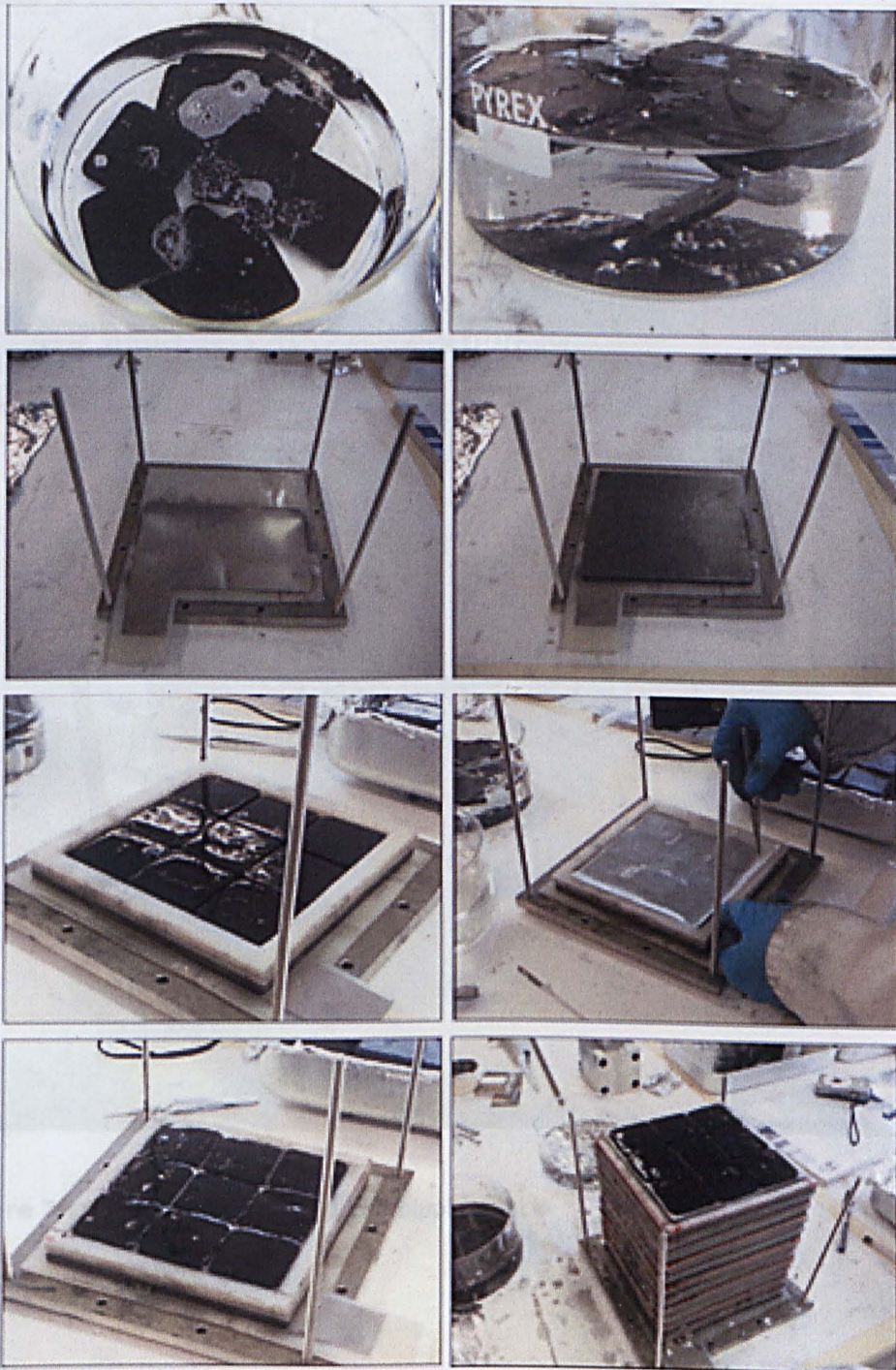


Figure 7.9 Construction of 10-cell stack

Each steps for the construction is described with images in Figure 7.9. Before placing the pellets on the carbon plate, they have to go through thorough a wetting process (first two images on top in Figure 7.9).

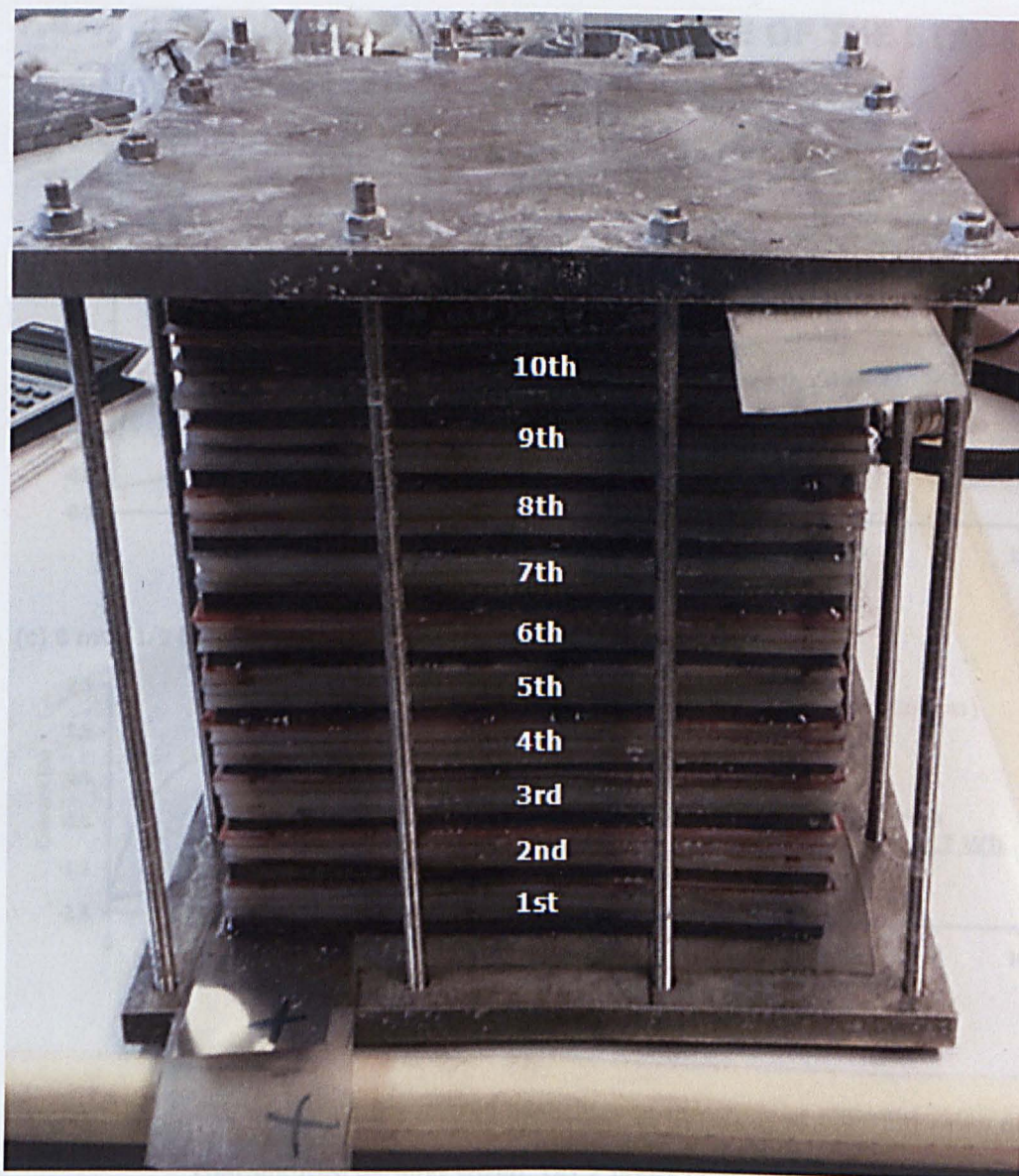


Figure 7.10 Completion of 10-cell bipolar stack

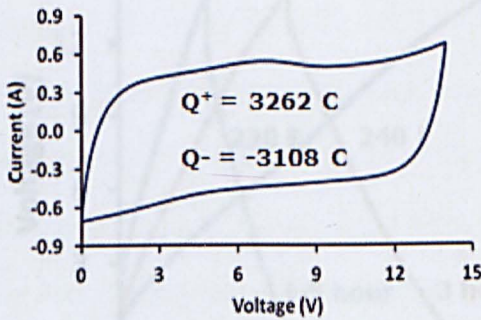
A 10-cell bipolar stack was successfully constructed and the image of the stack is shown in Figure 7.10.

- Volume: $20 \times 20 \times 17 \text{ cm}^3$ ($15 \times 15 \times 15 \text{ cm}^3$ without two end plates)
- Weight: 11.2kg (two stainless steel end plates: 6.6 kg, 11 carbon plates: 2.1 kg, 180 pellets: 1 kg, rubber gasket: 600 g)

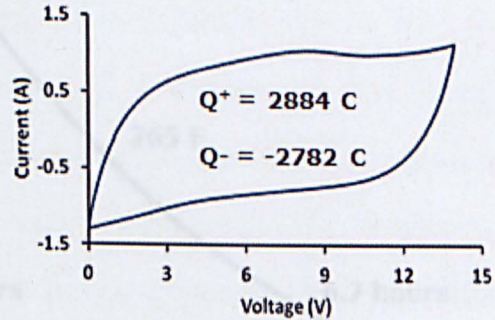
7.4.4. ELECTROCHEMICAL PERFORMANCE OF THE STACK

- Cyclic voltammetry at 14 V

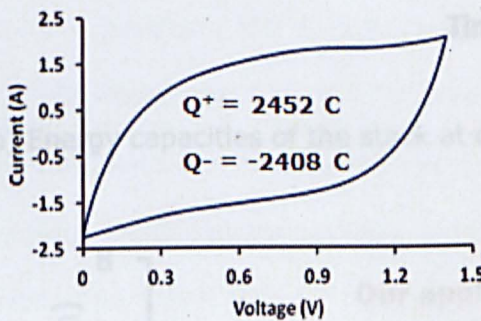
(a) 2 mV (2 hours charging)



(b) 4 mV (1 hour charging)



(c) 8 mV (1/2 hour charging)



(d)

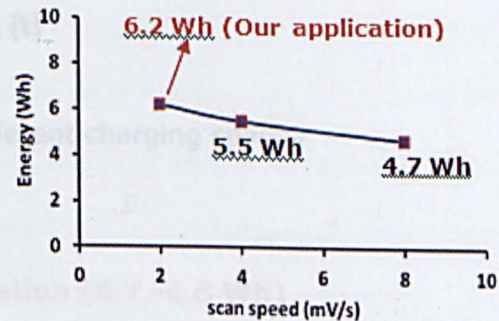
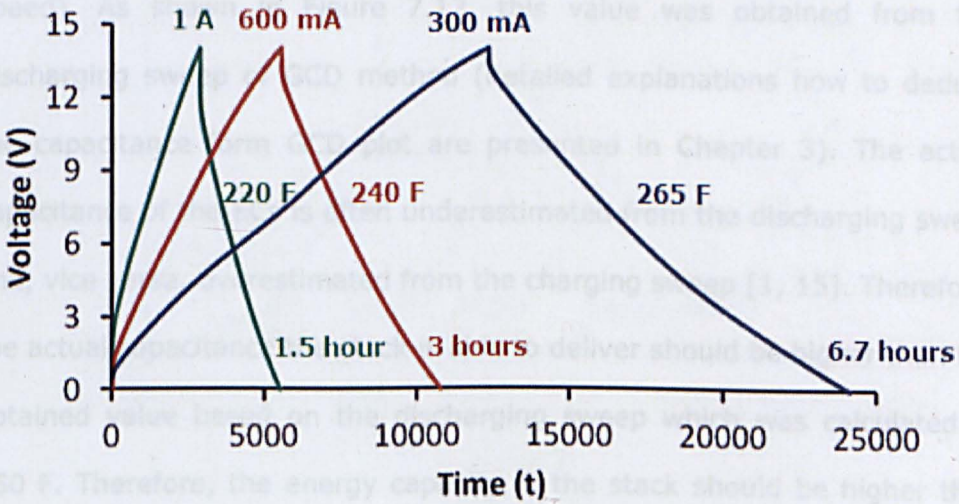


Figure 7.11 CVs and resulting energy capacities of the stack at different rates of charging/discharging speed. (a) 2 hours charging/discharging speed (total 4 hours) at 2 mV/s, (b) 1 hour charging/discharging speed (total 2 hours) at 4 mV/s, (c) ½ hour charging/discharging speed (total 1 hour) at 8 mV/s, (d) Total energy capacity of the stack at different scan rates

The highest voltage was set at 14 V for this test (maximum voltage of this stack is around 15 V), but this can go up to 16 V if the individual cells can be identically balanced. Due to the nature of cyclic voltammetry, capacitance of the stack is often measured lower than the actual value compared to GCD [1, 14, 15].

- Galvanostatic charge-discharge (GCD) up to 14 V

(a) GCD plots at different currents from 300 mV to 1 A



(b) Energy capacities of the stack at different charging speeds

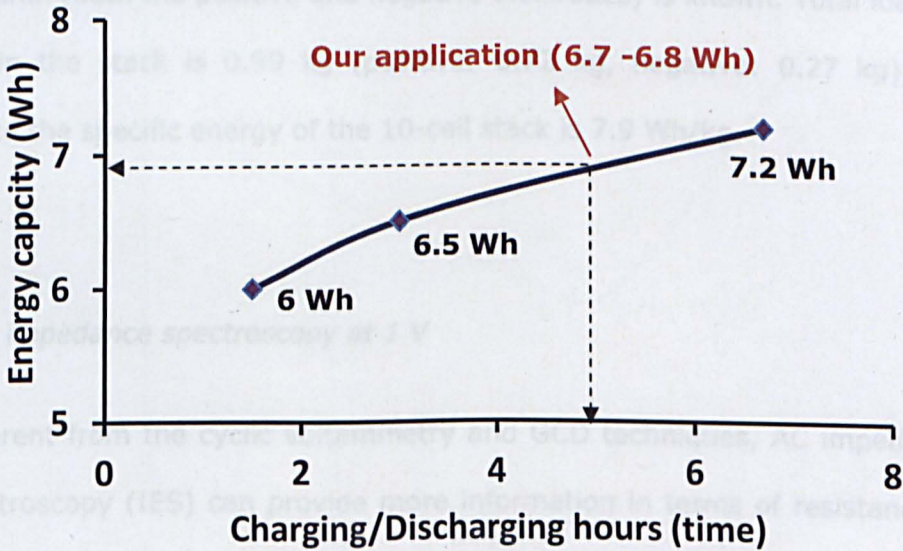


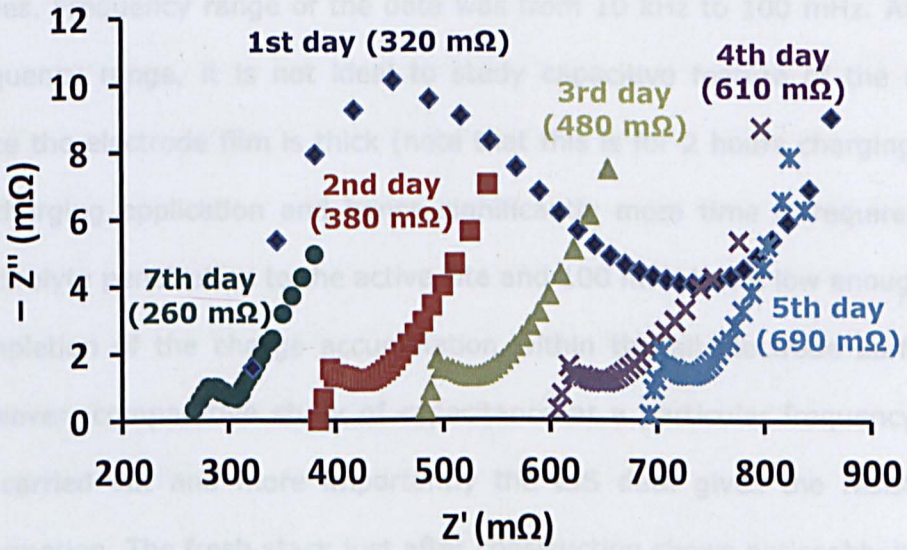
Figure 7.12 GCD plots and energy capacities of the stack at the different charging/discharging speed. (a) GCD plots at the three different charging/discharging speeds from 0.3 to 1 A (stack capacitance values were calculated based on the discharging sweep after the IR drop region), (b) Total energy capacity of the stack at the different scan rates

At 15 V, the energy capacity at a total of 4 hours charging/discharging speed can show around 7.8 Wh based on 250 F (this value was estimated from the two plots which is 3 hours and 6.7 hours charging/discharging speed). As shown in Figure 7.12, this value was obtained from the discharging sweep of GCD method (detailed explanations how to deduce the capacitance from GCD plot are presented in Chapter 3). The actual capacitance of the ECs is often underestimated from the discharging sweep and, vice versa, overestimated from the charging sweep [1, 15]. Therefore, the actual capacitance the stack is able to deliver should be higher than the obtained value based on the discharging sweep which was calculated at 250 F. Therefore, the energy capacity of the stack should be higher than 7.8 Wh. Moreover, the specific capacitance of the stack which is based on the unit mass can be also calculated since the total loading of the electrode material (both the positive and negative electrodes) is known. Total loading within the stack is 0.99 kg (positive: 0.72 kg, negative: 0.27 kg) and hence the specific energy of the 10-cell stack is 7.9 Wh/kg.

- AC impedance spectroscopy at 1 V

Different from the cyclic voltammetry and GCD techniques, AC impedance spectroscopy (IES) can provide more information in terms of resistance of the system at various equilibrium time (frequencies) [1, 11, 15]. Of course, the technique also gives capacitance information at low frequency regions. Although the resistance can be calculated from IR drop by GCD (often mixture of ESR and resistance due to dynamics), IES can provide more detailed information of different resistance elements (ESR, charge transfer and diffusion resistances) and they are directly related to the power characteristics of the stack [1].

(a) AC impedance data from 1st to 7th days



(b) Maximum power of the stack over time (days)

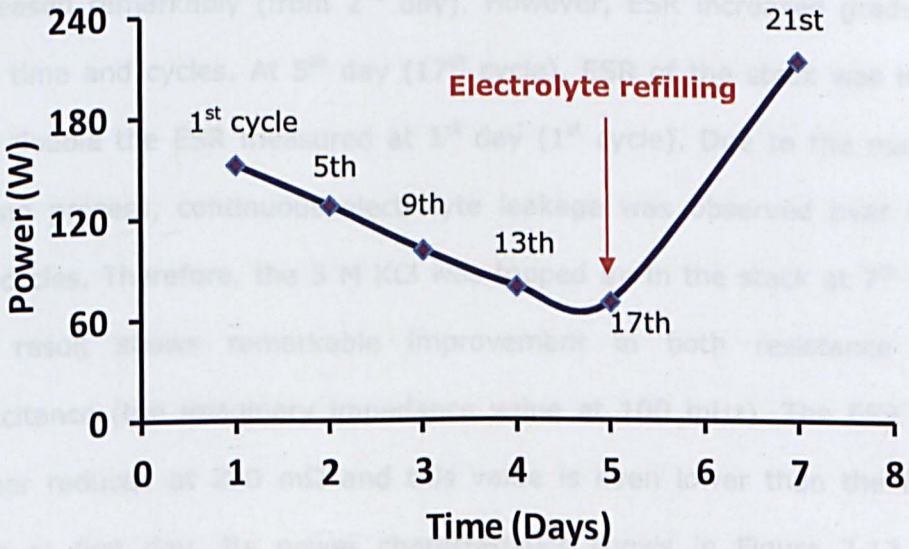


Figure 7.13 Impedance plots and power characteristics of the stack over time, (a) Impedance plots measured from day 1 to day 7 from 10 kHz to 100 mHz, (b) The maximum power of the stack based on ESR values at different days; electrolyte (3 M KCl) was refilled after 17th cycles at 5th day

EIS data were obtained at different days and cycle numbers. Figure 7.13 (a) shows how ESR and charge transfer resistance change over time and cycles. Frequency range of the data was from 10 kHz to 100 mHz. At this frequency range, it is not ideal to study capacitive feature of the stack since the electrode film is thick (note that this is for 2 hours charging and discharging application and hence significantly more time is required for electrolyte penetration to the active site and 100 mHz is not low enough for completion of the charge accumulation within the all electrode surface). However, comparative study of capacitance at a particular frequency can be carried out and more importantly the EIS data gives the resistance information. The fresh stack just after construction shows noticeably higher charge transfer resistance (CTR) and its ESR was measured at 310 mΩ. This is due to the incompleteness of wetting. After several cycles, CTR decreased remarkably (from 2nd day). However, ESR increased gradually over time and cycles. At 5th day (17th cycle), ESR of the stack was more than double the ESR measured at 1st day (1st cycle). Due to the manual sealing process, continuous electrolyte leakage was observed over time and cycles. Therefore, the 3 M KCl was topped up in the stack at 7th day. The result shows remarkable improvement in both resistance and capacitance (the imaginary impedance value at 100 mHz). The ESR was further reduced at 260 mΩ and this value is even lower than the fresh stack at first day. Its power characteristics shows in Figure 7.13 and significant increase were observed in terms of power at day seven (after refilling electrolyte). From this observation, the increase in ESR of the stack over time and cycle is due to the gradual loss of electrolyte. The sealing of the bipolar stack has to be improved for further development of this design.

7.5. EVALUATION

The stack using the design of unequal electrode capacitance performed very promisingly. Each cell displayed up to 1.9 V and this is significantly higher than our previous 20 V stack in which each cell demonstrate at 1.1 V. To build a 20 V stack, the unequal capacitance design only need 11 cells connected in series and this will be more economical in terms of the manufacturing cost. Moreover, the thicker electrode films resulted in remarkably high geometric capacitance of 12 F/cm^2 based on a single electrode. In terms of specific energy of the stack, our previous stack, which is consisted of CMPB negative electrode and PPy/CNTs composite as the positive electrode, displayed 3.64 Wh/kg [7] and the unequal capacitance stack showed 8.2 Wh/kg . A 10-cell stack was also constructed using thick pellet electrode. PPy/CNTs and activated carbon were used for positive and negative electrodes respectively. Energy capacity of the stack was measured at 7.8 Wh and its specific energy was about 8 Wh/kg . Using a thicker electrode, the geometric capacitance based on a single electrode was 40 F/cm^2 in average between the both electrodes (positive electrode only will give higher than 40 F/cm^2). However, the applications of those stacks using thin and thick electrodes should be different. Due to the thick film utilisation, it suffers from a relatively high diffusion resistance and hence it only operates in relatively slow rate applications (maximum power of 10-cell stack is about 210 W and this value will drop significantly in practical use). In contrast, the 20 V stack is able to work within extremely fast charging/discharging conditions (tested up to 1000 mV/s) due to its lower resistance owing to the use of thin electrode films [7].

References

1. Conway, B. E., *Electrochemical Supercapacitors: Scientific Fundamentals and Technological Applications*. 1999: Kluwer Academic/Plenum Publishers. New York.
2. Talapatra, S., Kar, S., Pal, S. K., Vajtai, R., Ci, L., Victor, P., Shaijumon, M. M., Kaur, S., Nalamasu, O. and Ajayan, P. M. , *Direct growth of aligned carbon nanotubes on bulk metals*. *Nat. Nanotech.*, 2006. **1**(2): p. 112-116.
3. Yan, J., Fan, Z. Wei, T. Cheng, J. Shao, B., Wang, K., Song, L. and Zhang, M., *Carbon nanotube/MnO₂ composites synthesized by microwave-assisted method for supercapacitors with high power and energy densities*. *J. Power Sources*, 2009. **194**(2): p. 1202-1207.
4. Lee, S. W., Kim, J. Chen, S., Hammond, P. T. and Shao-Horn, Y., *Carbon nanotube/manganese oxide ultrathin film electrodes for electrochemical capacitors*. *ACS Nano*, 2010. **4**(7): p. 3889-3896.
5. Gujar, T. P., Shinde, V. R., Lokhande, C. D. and Han S. H., *Electrosynthesis of Bi₂O₃ thin films and their use in electrochemical supercapacitors*. *J. Power Sources*, 2006. **161**(2): p. 1479-1485.
6. Ng, K. C., Zhang, S. Peng, C. and Chen, G. Z., *Individual and bipolarly stacked asymmetrical aqueous supercapacitors of CNTs/SnO and CNTs/MnO nanocomposites*. *J. Electrochem. Soc.*, 2009. **156**: p. A846-A853.

7. Zhou, X., Peng, C. and Chen, G. Z, *20 V stack of aqueous supercapacitors with carbon (-), titanium bipolar plates and CNT-polypyrrole composite (+)*, *AIChE Journal*, 2011, **58**(2): p. 974 – 983
8. Burke, A., *Ultracapacitors: why, how, and where is the technology*. *J. Power Sources*, 2000. **91**(1): p. 37-50.
9. Zhag, S., Peng, C., Ng, K. C. and Chen, G. Z, *Nanocomposites of manganese oxides and carbon nanotubes for aqueous supercapacitor stacks*, *Electrochim. Acta*, 2010, 55(25): p. 7447 – 7453
10. Zhang, S. W. and Chen, G. Z., *Manganese oxide based materials for supercapacitors*. *Energ. Mater.: Mater. Sci. Eng. Energ. Syst.*, 2008. **3**(3): p. 186-200.
11. Krause, S., *Impedance methods; Encyclopedia of Electrochemistry*. 2003: Wiley-VCH.
12. Choi, T. Y., Poulikakos, D., Tharian, J. and Sennhauser, U., *Measurement of the thermal conductivity of individual carbon nanotubes by the four-point three- ω method*. *Nano Lett*, 2006, **6**(8): p. 1589-1593
13. Shiraki, I., Tanabe, F., Hobara, R., Nagao, T. and Hasegawa, S., *Independently driven four-tip probes for conductivity measurements in ultrahigh vacuum*. *Surface Sci*, 2001, **493**(1-3): p. 633-643
14. Compton, R. G. and Banks, C. E., *Understanding Voltammetry*, 2007, World Scientific Publishing Co. Pte. Ltd., Singapore

15. Bard, A. J. and Faulkner, L. R., *Electrochemical Methods: Fundamentals and Applications*, 2000, 2nd ed., Wiley, New York.
16. Kissinger, P. T. and Heineman, W. R., *Cyclic voltammetry*. J. Chem. Educ., 1983. **60**(9): p. 702.
17. Bichat, M. P., Raymundo-Piero, E. and Béguin, F., *High voltage supercapacitor built with seaweed carbons in neutral aqueous electrolyte*. Carbon, 2010, **48**(15), p. 4351-4361.
18. Khomenko, V., Raymundo-Pinero, E., Frackowiak, E. and Beguin, F., *High-voltage asymmetric supercapacitors operating in aqueous electrolyte*. Appl. Phys. A: Mater. Sci. Proc., 2006. **82**(4): p. 567-573.
19. Demarconnay, L., Raymundo-Pinero, E. and Béguin, F., *A symmetric carbon/carbon supercapacitor operating at 1.6 V by using a neutral aqueous solution*. Electrochem. Commun., 2010. **12**(10): p. 1275-1278.

Chapter 8 CONCLUSIONS AND FUTURE WORK

In this chapter, a brief summary of Chapter 4 to 7 is provided. More detailed explanations can be found in the relevant results chapters. Overall, various studies were carried out to suggest an optimum design of the neutral aqueous ECs. Different neutral electrolytes were examined in terms of their ionic size, concentration and temperature. In addition, the freezing temperature of the aqueous electrolyte was successfully depressed down to $-20\text{ }^{\circ}\text{C}$. Regarding electrode materials, different carbon materials and MnO_2/CNTs composites were studied. Moreover, symmetrical and asymmetrical designs of the ECs were constructed using such materials. Based on the results obtained from laboratory scale ECs, stacked ECs were constructed and tested.

Moreover, lists of future work for the further development of the aqueous ECs will be discussed later in this chapter.

8.1. CONCLUSIONS

8.1.1. NEUTRAL AQUEOUS ELECTROLYTES

One of the main focuses in this study is the utilisation of neutral aqueous electrolytes in ECs. Although many commercial ECs are based on organic solvents due to their wider potential windows, this study suggests that water-based systems are also able to display comparable potential windows by using pH-neutral aqueous solutions such as KCl and K_2SO_4 . The neutral aqueous electrolytes displayed almost twice as wide potential

windows with the carbon electrode material (CMPB) than those with acid and basic aqueous electrolytes. Moreover, a number of benefits offered by the aqueous electrolytes are identified, which are non-flammability, low toxicity and environmental impact, ease of maintenance, cost effectiveness and large specific heat capacity, can be beneficial in EC's applications.

8.1.2. SIZE EFFECT OF IONS

Different results were obtained using differing anions and cations. The hydrated radii showed great influences on the material's capacitive behaviour. The hydrated radii of different cations are different from their crystal radii. In this study, the carbon electrode with the K^+ cation (whose crystal radii is bigger than those of Na^+ and Li^+) showed the highest capacitance responses.

Crystal radii: $Li^+ < Na^+ < K^+$

Hydrated radii: $Li^+ > Na^+ > K^+$

Kinetics and capacitance: $Li^+ < Na^+ < K^+$

Diffusivity and migration rate, which are directly related with the capacitive performance of the EC, are hugely influenced by the size of hydrated ions. In the case of anions, the result corresponded well with the result obtained from the cations. The EC with Cl^- performed better than that with SO_4^{2-} . As expected, the reason is that the size of the monoatomic Cl^- ion is far smaller than the polyatomic SO_4^{2-} ion.

Hydrated radii: $\text{Cl}^- < \text{SO}_4^{2-}$

Kinetics and capacitance: $\text{Cl}^- > \text{SO}_4^{2-}$

8.1.3. EFFECT OF ION CONCENTRATION AND TEMPERATURE

Different concentrations were also found to show a great influence on capacitive behaviour of the EC system. In particular, difference concentration of the electrolyte resulted in remarkable changes in terms of the rate performance of the EC. The EC with the higher molar concentration was proven to display superior rate performance and higher capacitance at faster charging/discharging rates. Similarly, the EC performed differently at different temperatures. The cell at a higher temperature was found to be more advantageous than that at a lower temperature in terms of the rate performance and capacitance. The temperature and molar concentration resulted in different activities (higher kinetic energy) at the solid (carbon electrode)/liquid (aqueous electrolyte) interface and the EC with the higher molar concentration and higher temperature showed higher energy storage and charge rate at a given voltage.

8.1.4. FREEZING POINT DEPRESSION

One of the biggest challenges for a wider application of the aqueous ECs is their freezing point because pure water solidifies at 0°C . However, the freezing point of water can be lowered down to certain degrees by adding

salts. This is due to the interaction between water molecules and ions which disturb the formation of hydrogen bonds between water molecules at temperatures below 0 °C (slower kinetics). Differing concentrations of the electrolytes resulted in different degrees of freezing point depression. In particular, 5 M NaCl did not show any ice formation down to -20 °C. This proved the potential for applications of the aqueous system below 0 °C.

8.1.5. ADVANCED DESIGN OF CARBON-CARBON ECs

Eight different carbon materials were tested as potential candidates of the electrode materials in ECs. CMPB displayed excellent capacitive and conductive behaviour. Using this material, successful extension of the EC's operating voltage was achieved by taking advantage of the advanced cell design which used unequal capacitances between the positive and negative electrodes. By controlling the capacitance ratio of the electrodes at 4:3 (positive: negative), the operating voltage of the EC increased up to 1.9 V without showing significant capacitance drop. It is commonly believed that the aqueous ECs could only operate within cell voltage of 1.23 V due to thermodynamic limit (water decomposition). However, the 1.9 V operating voltage was successfully achieved owing to remarkably high hydrogen over-potential at the carbon negative electrode and the advanced design of the EC. Specific energy of the EC was obtained at 8.5 Wh/kg. This value is higher than some commercial ECs using organic solvents.

Carbon sample #1 displayed higher capacitance than CMPB, but the material showed a noticeably more resistive nature. Physical addition of CNTs was found to be very effective to resolve the issue. The mixture performed significantly better than the carbon sample without CNTs. A 1.9

V EC was also constructed using the carbon/CNTs mixture. Cycling stability of the EC was enhanced by adding CNTs as an electronic conductor. The specific energy was measured at 20 Wh/kg and this value is comparable to that of the Pb-acid battery.

8.1.6. MnO₂/CNTs COMPOSITE AND ITS MIXTURE

MnO₂/CNTs binary composites were successfully synthesised in the KMnO₄ (aq) (precursor) + CNTs suspension. Structural analyses of the composites were carried out using XRD, SEM and TEM. XRD revealed that the produced MnO₂ was the birnessite-type according to the distinctive 2 θ peaks observed at 13°, 37°, 65°. In addition, the thickness of the MnO₂ deposit clearly increased in the composites with higher MnO₂ contents. This was perceptible in both SEM and TEM images. However, the composite was not suitable as the positive electrode of ECs due to its relatively high resistance. This issue was resolved by mixing CNTs with the electrode materials, and the result was very promising. The MnO₂/CNTs + CNTs mixture displayed excellent capacitive and conductive behaviour with excellent rate performance up to 500 mV/s. This improvement can be attributed to the increased electronic and ionic conductivities of the composite + CNTs.

8.1.7. CONSTRUCTION OF ASYMMETRICAL ECs

Asymmetrical ECs were constructed using the MnO₂/CNTs + CNTs positive electrode and CMPB negative electrode. Unequal capacitances were also applied to obtain a higher operating voltage. Using a tube-cell, the highest positive potential was obtained while the cell was operating at different

voltages from 1.2 to 1.8 V. At 1.6 V, the measured potential was 0.9 V and oxygen and chlorine gases from the electrolyte (3 M KCl) could have been generated at this potential. Therefore, the maximum cell voltage of the asymmetrical EC was determined to be 1.6 V. This result corresponds well with the data obtained from the cycling stability test. The 1.6 V cell performed well without showing a significant capacitance loss and the CV shape remained rectangular without distortion after 1000 cycles. In contrast, the 1.8 V cell displayed 40 % loss in capacitance after 1000 cycles compared to the initial cycle. The specific energy of the asymmetrical EC was measured at 9 Wh/kg at 1.6 V.

8.1.8. SCALE-UP

Three stacked ECs were constructed and were all based on the carbon (CMPB) electrode. The first one was a symmetrical EC and the positive and negative electrode had equal capacitances. This stacked EC consisted of three single cells connected in series with Ti bipolar plate (current collector). Each cell performed up to 1.6 V and the stacked EC could not operate at 5 V in the long term. The stacked EC has been operating for two years with more than 4000 cycles. It showed about 40 % loss in capacitance and one of the reasons must be electrolyte loss (poor sealing); that was evidenced by the significant increase in charge transfer resistance. In addition, another stacked EC was built, but this EC was designed to have different electrode capacitances between the positive and negative electrodes. This stack consisted of three single cells, but it displayed up to 5.8 V due to its unequalled capacitance design. This stacked cell was working after 12 months, still without showing significant capacitance loss.

However, the charge-transfer resistance increased significantly and this may be also due to the sealing of the cell being insufficient to prevent evaporation of water from the electrolyte. Lastly, a 10-cell bipolar stack (7.8 Wh) using conducting carbon plates was constructed and this was the biggest stack of this type. The carbon plates (ENB2 type) were proven to be a suitable substrate material. The maximum operating voltage of the stack is 15 V (each cell displays up to 1.5 V), but balancing between the individual cells is required. Sealing has to be improved to maintain the power level (continuous electrolyte loss). This stack works ideally for a 2 hour charge and another 2 hour discharge rate.

8.2. FUTURE WORK

8.2.1. FULL UTILISATION OF POTENTIAL WINDOWS

The operating voltage of the aqueous ECs in this thesis is often smaller than the sum of the positive and negative potential windows measured in the three-electrode cell. This is normally because of the undesirable faradaic reaction (oxidation) occurred at the positive electrode and hence the full range of the negative electrode potential could not be utilised. Since fine carbon materials, which are commonly used as the negative electrode in the ECs, show remarkably high hydrogen over-potential, the overall EC's operating voltage can be still expanded. It is anticipated that if the full potential windows of the negative electrode can be entirely utilised, and a 2.3 V aqueous EC is therefore achievable.

8.2.2. NOTICEABLE INCREASE IN CHARGE-TRANSFER RESISTANCE

The constructed single-cell ECs and the stacked ECs displayed a significant increase in charge transfer resistance as the number of charge-discharge cycles increase. At present, the cause of the phenomenon is not clear and more studies need to be carried out. One of the possible scenarios is continuous depletion of the electrolytes. All the EC's constructions in this work were done manually and it was difficult to build the cell with a completely sealed structure. Continuous evaporation of water from the aqueous electrolytes might be the reason for the remarkable increase in charge transfer resistance. Another possible cause might be the formation of metal oxide layer on the surface of the titanium current collector. At the very first layer of the Ti plate, the oxide layer might be formed beyond the certain potential. The AC impedance data in Figure 4.7 supports this argument. However, it is still premature to conclude if the mentioned phenomena are the exact causes for the increase in charge transfer resistance. More investigations should be carried out.

8.2.3. ELECTRODE MATERIALS AND COMPOSITES

Carbon is one of the most widely used materials for making the electrode in ECs and many commercial products are available in the market. Moreover, MnO_2 is a rigorously investigated material for the research in ECs. Therefore, these two materials were focused in this thesis. However, many promising results have been reported in the literature using different materials such as conducting polymers, other metal oxides, metal nitrides and the relatively new carbon forms known as graphene. A wide range material should be examined for the development of the advanced aqueous

ECs. It should be pointed out that most research attention in ECs in terms of materials is on the positive electrode because the carbon materials perform excellently as the negative electrode material. However, extra effort should be made to find other potential materials as the EC's negative electrode. Fe_2O_3 , WO_3 , Bi_2O_3 and SnO_2 are all potential negative electrode materials and they need to be studied in same depth.

8.2.4. VARIOUS METHODS OF ELECTRODE FILM FABRICATIONS

Different methods to fabricate the electrode films were used in this work. The cast-evaporate method was used in various materials for the three-electrode test. However, it was very challenging to fabricate thicker films for a higher loading with this technique. Therefore, most results obtained from the three electrode cell had to be based on relatively smaller loading and likely caused a greater error due to inaccurate estimations. In the two-electrode single cell, either rolling or pellet-pressing methods were used. Although the electrode films of the ECs with rolling method provided reasonable data, it could be problematic to construct larger scale stacked ECs. It is hard to manually control the thickness of film uniformly and the amount of loading with this method. In contrast, it is relatively less challenging using a pellet press, and this is ideal to produce thick electrode by simply adding material and pressing at the required pressure. However, many electrodes need to be produced (180 pellets for the 10-cell stack) and hence the method is time consuming if carried out manually in laboratory. For larger scaled ECs, it is worth examining other fabrication methods such as screen printing or spray methods (mainly thin electrode film fabrications which are able to give devices with high power but low energy).

8.2.5. BINDER EFFECT

Most electrodes in this thesis contain 5 wt% binder (PTFE). However, it is known that the use of binder within the electrode film influences its capacitive and conductive behaviour because the binder is normally non-conducting and non-active (also often known to be hydrophobic in nature and this feature will reduce a significant portion of active site within the electrode). Therefore, it would be more advantageous to keep the ratio of the binder within the electrode material as low as possible. An optimum ratio between the binder and electrode material should be evaluated.

8.2.6. SELF-DISCHARGE TEST

Once the charge storage devices (ECs, batteries) are fully charged, self-discharging always takes place. According to thermodynamics, the system spontaneously moves to the lower energy state than the higher charged energy state. Therefore, continuous self-discharge occurs over the time and this is not an ideal situation to use the devices. Accordingly, it will be preferable to control the self-discharge rate as low as possible. Indeed, basic self-discharge phenomenon with lab-scale cells were evaluated in this thesis and the results can be found in Figure 2.8 (although presented in the literature review, the data are solely the author's own work). However, self-discharge of the constructed ECs in larger scale were not studied. More investigations should be undertaken in terms of understanding and reducing self-discharge rate because it will show huge impact on the aqueous EC's future applications and their market potential.

8.2.7. CONSTRUCTION OF MnO₂/CNTs (+)-AC (-) STACK

Three stacked ECs were constructed in this study. One was a stack of three symmetrical cells, displaying a total operating voltage of 4.8 V (1.6 V for each cell) using CMPB electrode. The other three-cell stack displayed a total voltage of 5.7 V (1.9 V each cell) with unequal electrode capacitances using the same carbon material. Both ECs showed a good consistency with the smaller scale ECs in terms of performance. Further, a pseudo capacitive composites (PPy/CNTs) were used for the stack. Combined with activated carbon as a negative electrode, the asymmetrical 10-cell bipolar stack performs promisingly. However, the EC using MnO₂/CNTs (positive electrode) and CMPB (negative electrode) or activated carbon was only tested at small scale and the stacked EC using those materials was not constructed. Bigger asymmetrical ECs using the MnO₂/CNTs composite need to be constructed and their performance should be evaluated. Moreover, carbon sample #1 with addition of CNTs should also be examined as the negative electrode material instead of CMPB at the bigger scale. It is expected that the mixture (-) combined with MnO₂/CNTs (+) will display improved energy characteristics than CMPB (-) with MnO₂/CNTs (+) based on the result of single cells.

8.2.8. FUTHER SCALE UP (30 cm X 20 cm)

Based on the promising results with the 10-cell bipolar stack, an even bigger stack are to be constructed. The size of the new carbon plates will be 20 X 30 cm². It is expected to show lower resistance (higher power), due to the larger geometric area where the current can flow more smoothly, and greater energy stored (more material can be loaded in each cell).

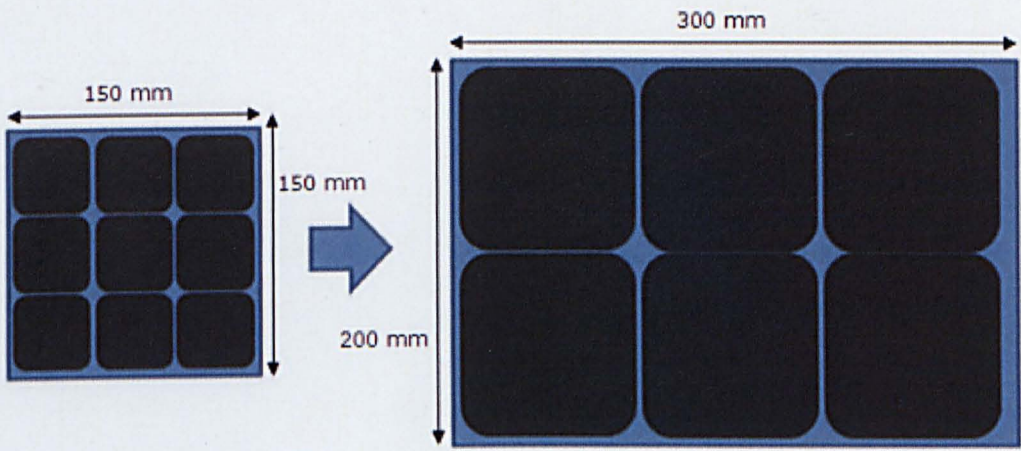


Figure 8.1 Further scale up from 150 X 150 mm² to 200 X 300 mm²

Figure 8.1 shows one of author's future studies. The current 4 X 4 cm² pellet electrode (pressed at 25 tonnes) will be increased to 9 X 9 cm² (130 tonnes pressing). Six of the 9 X 9 cm² pellets will be placed on the 20 X 30 cm² carbon plates. A single cell with the bigger plate will display 8400 F which is about 3.5 times higher than the current design (and so 3.5 time higher energy stored). Conversely, the resistance of the cell will be 3.5 times lower.